From Supramolecular Chemistry to Nanotechnology: Assembly of 3D Nanostructures

This research has been supported by the Council for Chemical Sciences of the Netherlands Organization for Scientific Research (NWO-CW), in the Vernieuwingsimpuls programme (Vidi grant 700.52.423 to Jurriaan Huskens).

ISBN: 978-90-365-2716-3

FROM SUPRAMOLECULAR CHEMISTRY TO NANOTECHNOLOGY: ASSEMBLY OF 3D NANOSTRUCTURES

PROEFSCHRIFT

ter verkrijging van
de graad van doctor aan de Universiteit Twente,
op gezag van de rector magnificus,
prof. dr. W.H.M. Zijm,
volgens besluit van het College voor Promoties
in het openbaar te verdedigen
op vrijdag 24 oktober 2008 om 13.15 uur

door

Xing Yi Ling

geboren op 30 mei 1979
te Pahang, Malaysia

Dit proefschrift is goedgekeurd door:

Promotoren: Prof. dr. ir. J. Huskens
Prof. dr. ir. D. N. Reinhoudt

This thesis is dedicated to grandma, my family and In Yee

Table of Contents

Chapter 1 General introduction 1

Chapter 2 Chemically directed self-assembly of nanoparticle structures on surfaces 5

2.1. Introduction 6

2.2. Chemical nanoparticle assembly on non-patterned surfaces 7

2.2.1 Covalent bonding 7

2.2.2 Noncovalent interactions 9

2.2.2.1 Electrostatic interactions 9

2.2.2.2 Metal-ligand coordination 11

2.2.2.3 Hydrogen bonding 14

2.2.2.4 Host-guest interactions 15

2.2.2.5 Biomolecular interactions 16

2.3. Chemical nanoparticle assembly on patterned surfaces 17

2.3.1 Patterning by photolithography 18

2.3.2 Patterning by soft lithography 21

2.3.3 Patterning by nanoimprint lithography 25

2.3.4 Patterning by scanning probe lithography 26

2.4. Conclusions 28

2.5. References 28

Chapter 3 Ferrocenyl-functionalized silica nanoparticles: preparation, characterization and molecular recognition at interfaces 33

3.1. Introduction 34

3.2. Results and discussion 35

3.3. Conclusions 45

3.4. Experimental 45

3.5. Acknowledgements 47

3.6. References and notes 47

Chapter 4 **An *in situ* study of the adsorption behavior of functionalized particles on self-assembled monolayers via different chemical interactions** **51**
4.1. Introduction 52
4.2. Results and discussion 54
4.2.1 Preparation and characterization of PS-COOH and PS-CD particles 54
4.2.2 Assembly of particles on non-patterned flat surfaces 58
4.2.3 Assembly of particles on nanoimprint lithography (NIL) patterned substrates 68
4.3. Conclusions 70
4.4. Experimental 70
4.5. Acknowledgements 72
4.6. References and notes 72

Chapter 5 **Reversible attachment of nanostructures at molecular printboards through supramolecular glue** **75**
5.1. Introduction 76
5.2. Results and discussion 77
5.3. Conclusions 83
5.4. Experimental 84
5.5. Acknowledgements 85
5.6. References 85

Chapter 6 **Supramolecular layer-by-layer assembly of 3D multicomponent nanostructures via multivalent molecular recognition interactions** **87**
6.1. Introduction 88
6.2. Results and discussion 89
6.3. Conclusions 95
6.4. Experimental 96
6.5. Acknowledgements 97
6.6. References 97

Chapter 7 **The formation and transfer printing of stable and ordered 3D supramolecular nanoparticle structures** **99**
7.1. Introduction 100
7.2. Results and discussion 101
7.3. Conclusions 111
7.4. Experimental 112
7.5. Acknowledgements 113
7.6. References 113

Chapter 8 **Free-standing nanoparticle bridges and hollow capsule ribbons of supramolecular materials** **117**
8.1. Introduction 118
8.2. Results and discussion 119
8.3. Conclusions 129
8.4. Experimental 130
8.5. Acknowledgements 132
8.6. References 132

Summary **135**

Samenvatting **139**

Acknowledgements **143**

About the author **147**

List of publications **149**

Chapter 1

General introduction

The advancements of nanotechnology have provided a variety of nanostructured materials with highly controlled, interesting and exceptional properties. Among these materials, nanoparticles sized between 1 ~ 1000 nm elicit an intense interest because of their unique optical, electronic, magnetic, catalytic and other physical properties arising from the core material and the nanometer dimensions.

The ability to attach nanoparticles onto planar surfaces in a well-defined, controllable, and reliable manner is an important prerequisite for the fabrication of micro- or nanostructured devices suitable for the application in the field of (bio)nanotechnology. The stability and ordering of these nanoparticle structures are the utmost important features of such structures in order to achieve function for long term applications.

In general, there are two approaches to assemble nanostructured materials, namely physical assembly and chemical assembly. Physical assembly techniques are based on the assembly of non-functionalized nanoparticles on surfaces by physical forces, such as convective or capillary assembly,[1] spin coating,[2] and sedimentation.[3] The physical assembly of nanoparticles generally results in relatively simple close-packed 2D or 3D particle arrays with limited stabilities.

Hence, coupling chemistries are being incorporated to direct and control the deposition of nanoparticles with surface functionalities onto a functionalized substrate. Control over functional groups at the surface of nanoparticles allows tailoring of the nanostructures in a predictable manner, resulting in the formation of functional, more complex nanostructured architectures on surfaces to meet the needs for specific applications such as in molecular electronics and biosensing.[4] Various chemical interaction strategies, *e.g.* covalent bonding,[5] electrostatic forces,[6] and host-guest interactions[7] have been employed to chemically govern the self-assembly of nanoparticles onto surfaces. Crosslinking of the neighboring particles with chemical forces by selective binding can further enhance the stability of nanoparticle assemblies.[8] These methods are anticipated to directly control the

spatial distribution of nanoparticles across a large area in more complex patterns when combined with nanopatterning schemes.

The integration of particles into devices usually requires placing them in specific positions on surfaces. Top-down (nano)fabrication techniques, *e.g.* microcontact printing,[9] transfer printing,[10] nanoimprint lithography,[11] and photolithography[12] have been combined with the self-assembly of nanoparticles in creating structures of nanoparticles with desired geometries and dimensions.

The work in this thesis integrates nanotechnology and supramolecular chemistry to control the self-assembly of 2D and 3D receptor-functionalized nanoparticles. The aim is to generate stable and ordered 3D nanoparticle structures while using molecular recognition, both for establishing stability and order as well as creating a functionality of the resulting structure. The host-guest complexation of β-cyclodextrin (CD) and its guest molecules, *e.g.* adamantane and ferrocene, are applied in this thesis to assist the nanoparticle assembly. Direct adsorption of supramolecular guest- and host-functionalized nanoparticles onto (patterned) CD self-assembled monolayers (SAMs) *via* multivalent host-guest interactions and layer-by-layer (LbL) assembly are demonstrated and characterized using a variety of techniques. The control over the reversibility and fine-tuning of the nanoparticle-surface binding strength in this supramolecular assembly scheme are extensively examined. Furthermore, the supramolecular nanoparticle assembly has been integrated with top-down nanofabrication schemes to generate stable and ordered 3D nanoparticle structures, with controlled geometries and sizes, on surfaces, other interfaces, and as free-standing structures.

Chapter 2 provides a literature review regarding the recent developments of chemically directed self-assembly of nanoparticle structures on surfaces that are essential in the fabrication of nanoparticle structures of various kinds to accommodate the need for device applications. Particular attention is paid to the chemical interactions used to direct the assembly of nanoparticles on surfaces and a few major top-down patterning techniques employed in combination with chemical nanoparticle assembly in manufacturing 2D and 3D nanoparticle structures.

Chapter 3 describes the preparation of ferrocenyl-functionalized silica (SiO_2-Fc) nanoparticles. The aim is to synthesize nanoparticles with guest moieties such that nanoparticles can be directly assembled on CD SAMs *via* specific adsorption. The supramolecular recognition properties of the ferrocenyl-functionalized nanoparticles towards complementary CD host surfaces and nanoparticles are studied in solution and at interfaces.

In Chapter 4, the formation of particle monolayers by convective assembly is studied with three different kinds of particle-surface interactions: adsorption onto native surfaces, using additional electrostatic interactions, and using supramolecular host-guest interactions. The adsorption and desorption behavior of particles onto and from these surfaces is demonstrated *in situ* using a horizontal deposition setup. The resulting packing density and order of the adsorbed particle lattices are compared.

Chapter 5 illustrates the reversible attachment of nanostructures of CD-functionalized nanoparticles of different core materials and sizes onto and from stimuli-responsive, pre-adsorbed, ferrocenyl-functionalized poly(propylene imine) dendrimers at a CD SAM. Electrochemical oxidation of the ferrocenyl endgroups is employed to induce desorption of the nanostructures from the CD SAMs. The regenerability of the surface after multiple electrochemical modifications and the local desorption of nanoparticles is demonstrated.

In Chapter 6, the supramolecular layer-by-layer assembly of 3D multicomponent nanostructures of nanoparticles on nanoimprint lithographic (NIL) patterns is demonstrated. Supramolecular nanoparticles of various sizes and materials are assembled onto the complementary surface *via* multivalent host-guest interactions. The effects of the nanoparticle assembly steps from large to small nanoparticles and small to large nanoparticles on the ordering, and the control over the thickness of the supramolecular hybrid nanostructures are studied.

Chapter 7 introduces a sequential process to construct highly stable and crystalline supramolecular nanoparticle crystals by convective nanoparticle assembly and supramolecular chemistry. The transfer printing technique is incorporated into the process, such that supramolecular nanoparticle crystals, the size of which is controlled by the geometry and size of the poly(dimethylsiloxane) (PDMS) stamps, can be transferred onto a target surface. 3D free-standing nanoparticle composite bridges on topographically patterned substrates are formed by strengthening the cohesion of the nanoparticle crystals by supramolecular LbL assembly of guest- and host-functionalized supramolecular glues within the nanoparticle crystals. The 3D receptor behavior of the nanoparticle crystal for the further assembly of complementary molecules is studied as well.

In Chapter 8, an approach is described to form stable and ordered free-standing hollow capsule ribbons by using a release-and-transfer technique that involves the self-assembly of nanoparticles, templating and supramolecular LbL assembly. The geometry of the entire capsule structures can be designed by the geometry and size of the underlying NIL-

patterned template. The ability of the hollow capsules for storing organic fluorescent molecules is investigated.

REFERENCES

1. Denkov, N. D.; Velev, O. D.; Kralchevsky, P. A.; Ivanov, I. B.; Yoshimura, H.; Nagayama, K. *Nature* **1993**, *361*, 26.
2. Ozin, G. A.; Yang, S. M. *Adv. Funct. Mater.* **2001**, *11*, 95.
3. Wijnhoven, J.; Vos, W. L. *Science* **1998**, *281*, 802.
4. Lahav, M.; Shipway, A. N.; Willner, I.; Nielsen, M. B.; Stoddart, J. F. *J. Electroanal. Chem.* **2000**, *482*, 217.
5. Paraschiv, V.; Zapotoczny, S.; de Jong, M. R.; Vancso, G. J.; Huskens, J.; Reinhoudt, D. N. *Adv. Mater.* **2002**, *14*, 722.
6. Decher, G. *Science* **1997**, *277*, 1232.
7. Crespo-Biel, O.; Dordi, B.; Reinhoudt, D. N.; Huskens, J. *J. Am. Chem. Soc.* **2005**, *127*, 7594.
8. Zirbs, R.; Kienberger, F.; Hinterdorfer, P.; Binder, W. H. *Langmuir* **2005**, *21*, 8414.
9. Park, J. I.; Lee, W. R.; Bae, S. S.; Kim, Y. J.; Yoo, K. H.; Cheon, J.; Kim, S. *J. Phys. Chem. B* **2005**, *109*, 13119.
10. Meitl, M. A.; Zhu, Z. T.; Kumar, V.; Lee, K. J.; Feng, X.; Huang, Y. Y.; Adesida, I.; Nuzzo, R. G.; Rogers, J. A. *Nat. Mater.* **2006**, *5*, 33.
11. Maury, P.; Escalante, M.; Reinhoudt, D. N.; Huskens, J. *Adv. Mater.* **2005**, *17*, 2718.
12. Yin, Y. D.; Lu, Y.; Gates, B.; Xia, Y. N. *J. Am. Chem. Soc.* **2001**, *123*, 8718.

Chapter 2

Chemically directed self-assembly of nanoparticle structures on surfaces*

ABSTRACT. This chapter describes the recent developments of chemically directed self-assembly of nanoparticle structures on surfaces. The first part focuses on the chemical interactions used to direct the assembly of nanoparticles on surfaces. The second part highlights a few major top-down patterning techniques employed in combination with chemical nanoparticle assembly in manufacturing 2D or 3D nanoparticle structures. The combination of top-down and bottom-up techniques is essential in the fabrication of nanoparticle structures of various kinds to accommodate the need for device applications.

---

* This chapter has been submitted as a book chapter: X. Y. Ling, D. N. Reinhoudt, J. Huskens, "Chemically directed self-assembly of nanoparticle structures on surfaces" in *Supramolecular Chemistry of Organic-Inorganic Hybrid Materials* (Edited by K. Rurack), Wiley-VCH: Weinheim, **2008**.

2.1. INTRODUCTION

The self-assembly of ordered nanostructures consisting of nanoparticles with sizes between 1 - 1000 nm has attracted a lot of attention owing to their unique optical, electronic, magnetic, catalytic and other physical properties.[1] The ability to attach nanoparticles onto planar surfaces in a well-defined, controllable, and reliable manner is an important prerequisite for the fabrication of micro- or nanostructured devices suitable for the application in the field of nano(bio)technology.[2]

In general, there are two approaches to assemble nanostructured materials, namely physical assembly and chemical assembly. Physical assembly techniques are based on the assembly of non-functionalized nanoparticles on surfaces by physical forces, which include convective or capillary assembly,[3,4] spin coating,[5] and sedimentation.[6] The physical assembly of nanoparticles generally results in relatively simple close-packed 2D or 3D particle arrays. In addition, the physically assembled nanoparticle structures lack long-term stability because they were deposited at relatively low surface pressures.[7]

Chemical assembly utilizes coupling chemistries to direct and control the deposition of nanoparticles with surface functionalities onto a functionalized substrate. The control over the surface functionalities of nanoparticles allows tailoring of the nanostructures in a predictable manner and thus the formation of functional, more complex nanostructured architectures on surfaces to meet the needs for specific applications such as molecular electronics and biosensing.[8] Various chemical interaction types, *e.g.* covalent bonding,[9] electrostatic forces,[10] and host-guest interactions,[11] have been employed to chemically govern the self-assembly of nanoparticles onto surfaces. Crosslinking of the neighboring particles with chemical forces by selective binding further enhanced the stability of nanoparticle assemblies.[12] These methods are anticipated to directly control the spatial distribution of nanoparticles across a large area in more complex patterns when combined with nanopatterning schemes.

In this chapter, the recent developments of chemically directed self-assembly of nanoparticle structures on surfaces are described. The first part focuses on the chemical interactions used to direct the assembly of nanoparticles on surfaces. The second part highlights a few major top-down patterning techniques employed in combination with chemical nanoparticle assembly in manufacturing 2D or 3D nanoparticle structures. The combination of top-down and bottom-up techniques is essential in the fabrication of nanoparticle structures of various kinds to accommodate the need for device applications.

2.2. CHEMICAL NANOPARTICLE ASSEMBLY ON NON-PATTERNED SURFACES

Recent advances in nanotechnology have led to well-defined nanoparticles and self-assembled monolayers (SAMs) with desired surface functionalities. The chemically directed assembly of functionalized nanoparticles onto SAMs utilizes the specific binding affinity between organic head groups of the SAMs with the surface functional groups of the nanoparticles. In this section, the use of covalent bonding[13] and noncovalent interactions, including electrostatic interactions, metal coordination,[14] hydrogen bonding,[12] host-guest interactions[12] and biomolecular interactions,[15] for the construction of functional nanoparticle architectures is discussed.

2.2.1 Covalent bonding

The coupling chemistries that have been widely used in organic chemistry for producing chemical bonds have been applied to form irreversible and stable nanoparticle arrays on surfaces. Eychmuller *et al.* used the carbodiimide coupling chemistry to covalently assemble carboxylate-functionalized CdTe nanocrystals (NCs) onto amino-terminated glass surfaces, which resulted in densely covered nanoparticle films.[13] The same principle was also applied to coat SiO_2 microparticles by CdTe NCs.

The assembly of monolayer of alkylbromide-functionalized Co nanoparticles onto amino-terminated silicon surfaces through direct nucleophilic substitution was reported by Kim *et al.*[16] The nanoparticle density on the surface can be controlled by changing the immersion time of the silicon surface in the nanoparticle solution. Directed assembly of nanoparticles was observed on a chemically patterned surface.

Yang *et al.* utilized the diazo-nucleophile covalent bonding to assemble poly(methacrylic acid) (PMAA)-capped Fe_3O_4 nanoparticles onto 2-nitro-*N*-methyl-4-diazonium-formaldehyde resin (NDR) in a layer-by-layer (LbL) manner to form a multilayered photosensitive precursor film.[17] The assembly was initiated by the electrostatic attraction between the negatively charged carboxylate groups of the PMAA surface and the cationic diazoresin of NDR. The multilayer films formed *via* electrostatic interactions are less stable in polar solvents or aqueous electrolyte solutions, which limits their application range. To circumvent the limited stability of the electrostatic LbL multilayer films, a photo-crosslinking reaction between the diazoresin and carboxylate groups was performed by UV irradiation to convert the ionic bonds to covalent bonds. The stability of the LbL films was

evaluated by solvent etching in a mixture of polar solvents, which indicated stable films with no obvious desorption of nanoparticles.

Sun *et al*. extended the diazo-carboxylate covalent bonding to the assembly between diazo-resins and gold nanoparticles.[18] The ionic LbL assembly was first achieved by using diazo-resins and citrate-capped gold nanoparticles. Under UV irradiation, diazonium groups decomposed to phenyl cations that reacted with the nucleophilic carboxylate groups on the gold nanoparticles *via* an S_N1 reaction.

p-Aminothiophenol-capped cadmium sulfide (CdS) nanoparticles were electrochemically crosslinked onto p-aminothiophenol-functionalized Au electrode surfaces.[19] The covalent LbL assembly of nanoparticles to the electrode was monitored by electrochemistry and AFM imaging, which revealed a random and densely packed CdS nanoparticle array, with a surface coverage of 65% of the theoretical coverage of a dense monolayer of nanoparticles. The dianiline-bridged CdS nanoparticles assembled on the Au electrode revealed highly efficient photoelectrochemical properties in the presence of triethanolamine as a sacrificial electron donor.

Huskens and Reinhoudt *et al.* demonstrated a functionalized surface with local isolated functional groups (Scheme 2.1).[9] Au nanoparticles (d ~ 3 nm) stabilized with propanethiol and monofunctionalized with (mercaptopropyl)methyldimethoxysilane (MPMD) were first prepared by a place-exchange reaction. The Au nanoparticles were covalently assembled onto the surface *via* a single methyldimethoxysilane unit by reaction with Si-OH surface groups. AFM images revealed the attachment of Au nanoparticles to the surface in a dense but disordered fashion. The Au nanoparticles were then removed to set free the single functional units, spaced by a minimum distance governed by the nanoparticle size. This allowed reattachment of the other entities, but the subsequent attachment of nanoparticles *via* thiol place-exchange was found to be much slower than the initial covalent assembly reaction.

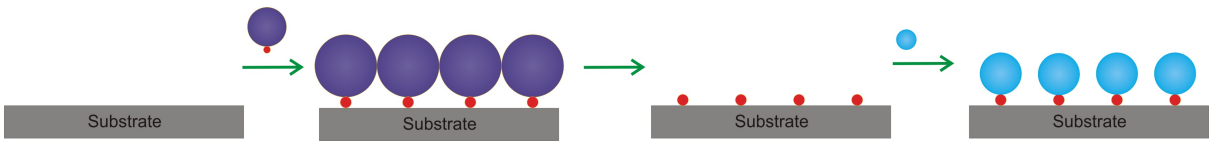

Scheme 2.1. The preparation of surfaces with spaced single functional groups and (re)attachment of entities to these functional groups *via* specific interactions.

2.2.2 Noncovalent interactions

Despite the high stability of the covalently bound nanoparticle films, the order is often lacking. This is attributed to the rapid and strong chemical reaction that occurs between the functional groups of the nanoparticles and SAMs, leading to irreversible anchoring of the nanoparticles onto the surface. Hence, fine-tuning of the coupling chemistry is needed to obtain a balance between the ordering and the stability of the nanoparticle array.

The use of noncovalent interactions has been exploited for the synthesis of *e.g.* receptor-functionalized nanoparticles and/or SAMs with molecular recognition abilities at the interface. The advantage of noncovalent interactions over covalent bonding is that the former offer the possibility for error correction.[20]

2.2.2.1 Electrostatic interactions

Electrostatic assembly, which involves attractive forces between two oppositely charged entities (polymers, nanoparticles, and substrates), has been proposed in the pioneering work of Iler for the assembly of 2D and 3D structures.[21] The LbL assembly of charged polyelectrolytes was later reported by Decher *et al.* for the fabrication of multilayer films of polyelectrolytes. Their technique is based on the consecutive adsorption of polyanions and polycations from dilute aqueous solutions onto a charged substrate (Scheme 2.2).[10,22]

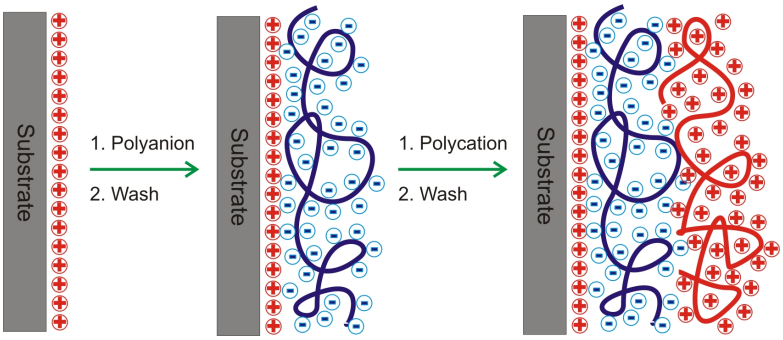

Scheme 2.2. Layer-by-layer (LbL) assembly of polyelectrolyte films.[10]

Owing to its simplicity, the LbL assembly of multilayer films by electrostatic interactions has been widely extended to the assembly of chemically functionalized particles onto surfaces. The LbL assembly of multilayer nanoparticle films of metallic,[23,24] semiconductor,[25,26] inorganic[27] and polymeric nanoparticles[27-29] has been demonstrated by using polyelectrolytes as a sandwich layer between the nanoparticles. Sandwich structures of

negatively charged CdS, and TiO_2 nanoparticles and positively charged polyelectrolytes have been fabricated (Scheme 2.3).[25] The fluorescence emission intensity was found to increase linearly with increasing number of polyelectrolyte-CdS bilayers. Composite films of (polyelectrolyte-TiO_2-polyelectrolyte-CdS) behave like a n-type semiconductor upon irradiation.[25]

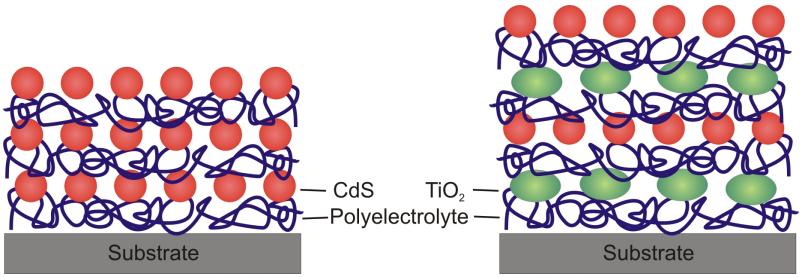

Scheme 2.3. The assembly of CdS nanoparticles and CdS-TiO_2 composite films.[25]

Similar methodologies were adopted by others. For instance, Akashi *et al.*[30] and Kunitake *et al.*[31] studied, independently, the adsorption of multilayers of nanoparticles and polyelectrolytes onto surfaces and its kinetics. Their studies revealed that the LbL films of nanoparticles and polyelectrolytes were molecularly flat after each bilayer assembly. However, both reports highlight the requirement of achieving an adsorption and desorption balance of the polyelectrolytes at the solid/liquid interface. The growth and properties of the multilayer films are sensitive to chemical factors such as polyelectrolyte and nanoparticle concentrations, ionic strength, pH, and hydrogen-bonding, more pronounced than observed in the LbL assembly of polyelectrolytes. In particular, an increase in ionic strength enhanced not only the extent of adsorption but also the nanoparticle-polyelectrolyte mass ratio per adsorption cycle, as a result of excess and free cationic sites on the polyelectrolytes. Murray *et al.* noticed the formation of multiple layers of poly(styrene sulfonate) and arylamine-functionalized nanoparticles incorporated during a single adsorption cycle in a LbL process, implying looping/entanglement of charged polymer chains with charged nanoparticles.[32] Quantized double layer charging in a LbL assembled film was observed, indicating a substantial microscopic mobility of both the polyelectrolytes and the nanoparticles within the film. These observations indicated the structural differences between LbL films of pure polyelectrolytes and of polyelectrolytes and nanoparticles. The differences in size, morphology, and effective charge density between nanoparticles and polyelectrolytes significantly affect their adsorption behavior.

The direct LbL assembly of oppositely charged nanoparticles, which did not involve polyelectrolytes, was also examined. Sastry *et al.* demonstrated the formation of alternating layers of gold and silver nanoparticles *via* sequential electrostatic assembly.[29] In the absence of polyelectrolytes, the effective charging of gold and silver nanoparticle was accomplished by the adsorption of 4-aminothiophenol and 4-carboxythiophenol molecules on the nanoparticle surfaces, respectively. The multilayer films were stable up to 100 ^{o}C.

Willner *et al.* demonstrated three-dimensional networks of Au, Ag and mixed composites of Au and Ag nanoparticles assembled on a conductive (indium-doped tin oxide) glass support by stepwise LbL assembly with *N,N*'-bis(2-aminoethyl)-4,4'-bipyridinium as a redox-active crosslinker.[8,33] The electrostatic attraction between the amino-bifunctional crosslinker and the citrate-protected metal particles led to the assembly of a multilayered composite nanoparticle network. The surface coverage of the metal nanoparticles and bipyridinium units associated with the Au nanoparticle assembly increased almost linearly upon the formation of the three-dimensional (3D) network. A Coulometric analysis indicated an electroactive 3D nanoparticle array, implying that electron transport through the nanoparticles is feasible. A similar multilayered nanoparticle network was later used in a study on a sensor application by using a bis-bipyridinium cyclophane as a crosslinker for Au nanoparticles and as a molecular receptor for π-donor substrates.[8]

2.2.2.2 Metal-ligand coordination

Metal coordination chemistry enables ligand-bearing components to be assembled into supramolecular structures using appropriate metal or metal ions. The strong coordinative bonding between sulfur groups and transition metal surfaces, *e.g.* gold[29,34] and silver,[35] has been exploited in the assembly of thiol-functionalized nanoparticles onto surfaces. Fitzmaurice *et al.* studied the thiol-based self-assembly of TiO_2 NCs on a substrate by two related methods.[36] In the first method, bare TiO_2 NCs were self-assembled on a thiol-functionalized gold substrate, forming a NC SAM. In a second method, thiol-functionalized TiO_2 NCs were assembled on annealed gold surfaces.

Brust *et al.* adapted an LbL approach to form a 3D multilayered nanoparticle assembly.[37,38] A substrate with free thiols was subjected to a gold nanoparticle solution. After washing, the substrate was rinsed with a dithiol solution, providing new surface thiol groups for attachment of additional layers of particles, forming multilayered Au nanoparticle films (Scheme 2.4). Their study indicated a linear relationship between the number of adsorption

layers and the apparent thickness of the nanoparticle assemblies.[37] Optical investigation of the Au nanoparticle films revealed that the individual nanoparticles did not fuse into larger units because of the protection by the dithiol ligand shells. Study of the optical and electronic properties of LbL films of 6-nm Au nanoparticles and dithiols revealed nonmetallic properties.[37] The temperature dependence of the conductivity of the nanoparticle films predicted that conduction occurred *via* an electron hopping mechanism.

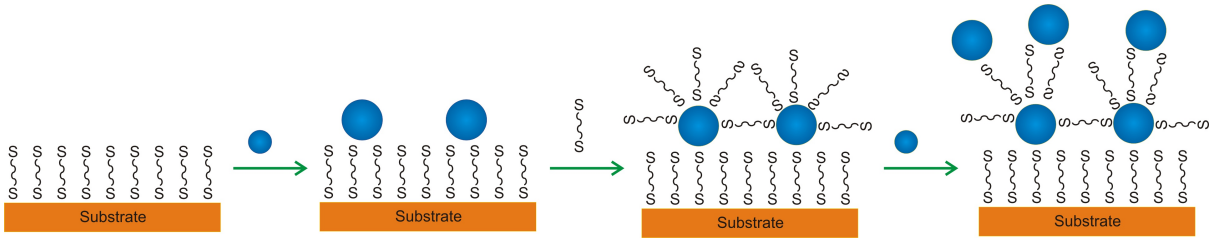

Scheme 2.4. The construction of nanomaterials from LbL assembly of Au nanoparticles and dithiol ligands.[37]

Further characterization of 3D Au and Ag nanoparticle multilayered films, with a short dithiol as a crosslinker, was studied by Natan *et al.*[39,40] They confirmed the porous, discontinuous morphology of the LbL films. Changes in electrical and optical film properties were reported when bifunctional dithiols of different lengths were used. Multilayer films assembled from more than six LbL cycles exhibited high conductivity and resembled bulk Au. In contrast, films of similar particle coverage generated using a longer cross-linker (1,6-hexanedithiol) exhibited a higher transmission in the near-infrared region and showed a reduced conductivity. The presence of conductive and insulating regions consistent with the metal-insulator transition was observed. On conducting substrates, Au or Ag monolayers were electrochemically addressable and behaved like a collection of closely spaced microelectrodes.[39] Dithiols have been further reported as crosslinkers for the multilayer fabrication of CdS nanoparticles[26] and alternating layers of Pt and CdS nanoparticles[41] on gold substrates.

Bharathi *et al*. reported the construction of an electrochemical interface with a tunable kinetic barrier by a mercaptopropyltrimethoxysilane-modified silica network. The thiol served as a matrix for the encapsulation of gold nanoparticles.[42] The silica network without Au nanoparticles exhibited a kinetic barrier for the electron transfer between the electrode surface and the electroactive species (ferrocyanide) in solution. However, with increasing immersion time of the silica network in a Au nanoparticle solution, the voltammetric

response of ferrocyanide was gradually restored. This illustrated that the gold nanoparticles provided a conductive pathway to facilitate normal electron transfer. Wang *et al.* utilized a similar gold nanoparticle-modified electrode to inhibit the adsorption of cytochrome *c* onto a bare electrode and to act as a bridge for electron transfer between protein and electrode.[43]

Rubinstein *et al.* constructed monolayers and multilayers (*via* LbL assembly) of bishydroxamate-functionalized Au nanoparticles onto bishydroxamate disulfide SAMs using Zr^{4+} as binding ions (Scheme 2.5).[14] The thickness of the densely packed Au nanoparticle layers increased regularly with the number of nanoparticle layers assembled, indicating a LbL growth of a monolayer of nanoparticles at a time, as a result of the highly specific metal coordination binding. Controlled spacing of nanoparticle layers from the surface was accomplished by binding of the Au nanoparticles to an organic multilayer spacer. The spacer comprised of a Zn^{2+}-coordinated monolayer of a bishydroxamate disulfide ligand on gold and multilayers of branched hexahydroxamate ligands. The electrical behavior of the coordinated nanoparticle layers spaced from the Au substrate by the organic spacer showed an ohmic resistance that increased with the number of nanoparticle layers, with a larger resistance observed when an organic multilayer spacer was used.

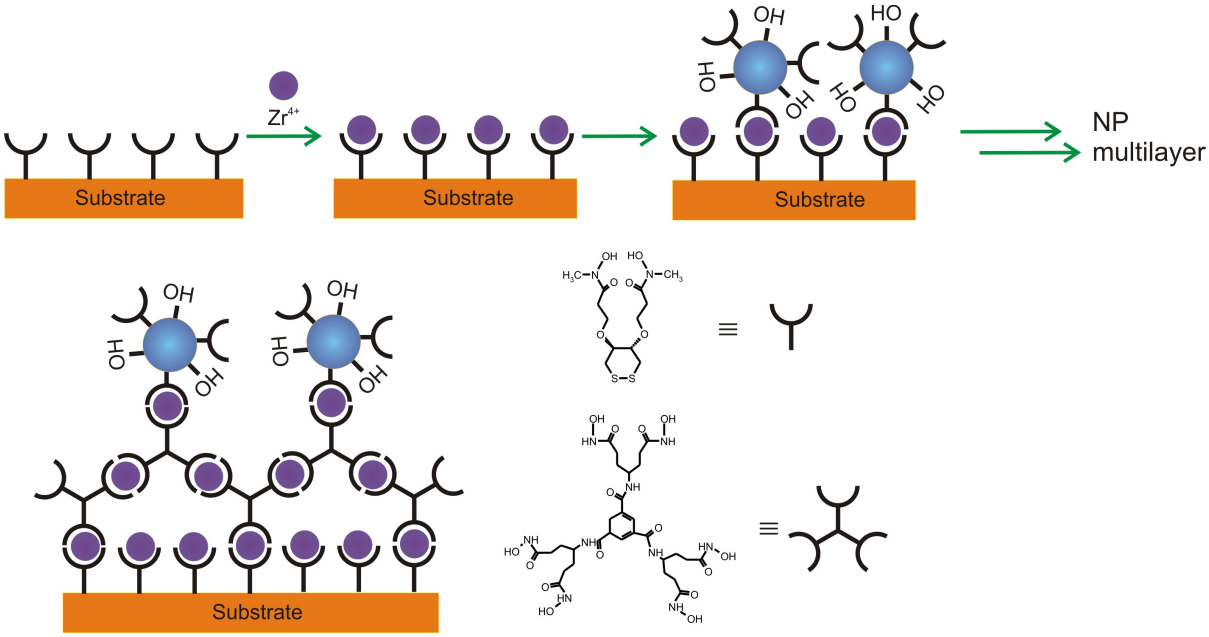

Scheme 2.5. LbL assembly of bishydroxamate-functionalized Au nanoparticles onto the bishydroxamate disulfide SAMs by Zr^{4+} as binding ions (top). Controlled spacing of nanoparticle layer was achieved using multilayer of branched hexahydroxamate ligands (bottom).[14]

Murray *et al.* developed Cu^{2+}- and Zn^{2+}-carboxylate linker chemistry to prepare monolayer and multilayer films of Au alkanethiolate-monolayer-protected clusters (MPCs) onto a mercaptoundecanoic acid monolayer.[44] [(2-Mercaptopropanoyl)amino]acetic acid-(tiopronin-)functionalized Au MPCs were subsequently attached *via* Cu^{2+}-carboxylate chemistry. Quantized double-layer charging was observed in these films.[44] Attachment of additional layers of tiopronin-MPCs was demonstrated by repeating adsorption cycles of Cu^{2+} ions and tiopronin-MPCs, resulting in a high yield surface attachment. The Cu^{2+}-carboxylate chemistry was also used to induce the reversible formation of transient soluble tiopronin-MPC aggregates. The aggregation was controlled by changing the pH of the Cu^{2+} solution, with increased aggregation at lower pH. The reversible formation of transiently soluble alkanethiolate- and tiopronin-MPCs was demonstrated by treatment with sodium acetate solution or concentrated acetic acid. In conclusion, the use of highly specific coordination chemistry offers a convenient tool for the construction of multilayer and multicomponent nanostructures on surfaces.

2.2.2.3 Hydrogen bonding

Assembling nanoparticles onto surfaces by means of hydrogen bonding was reported by Binder *et al.*[12] On a monolayer of Hamilton-type receptors with an intrinsic binding strength of $\sim 10^5$ M^{-1}, barbituric acid-functionalized Au nanoparticles were selectively adsorbed. The density of the receptors on the surface was varied by adjusting the receptor concentration during preparation. In addition, the Hamilton receptors were incorporated into one block of microphase-separated block copolymer thin films.[12] Highly selective binding of barbituric acid-functionalized Au nanoparticles onto the specific block copolymer phases on the surfaces was observed.

Lian *et al.* reported hydrogen bonding-based routes for LbL assembly of polymer/Au nanoparticle multilayer thin films.[45] Au nanoparticles modified with carboxylate or pyridine groups, were adsorbed onto poly(4-vinylpyridine) (PVP) and carboxylate-functionalized Au nanoparticle surfaces, respectively. Alternating deposition of poly(acrylic acid) (PAA) and Au nanoparticles with pyridine groups resulted in a multilayer buildup, which showed a linear increase of the film thickness with the number of adsorbed Au nanoparticle layers. FTIR spectroscopy verified the hydrogen bonding between the pyridine and carboxylate groups, which is the driving force for the formation of the polymer/Au multilayer thin films.

Similar polymer/Au nanoparticle multilayer thin films were made by Wu *et al.* in a study of pH-sensitive dissociation behavior of poly(3-thiophene acetic acid) (PTAA) and

PAA in a LbL film (of 8 bilayers).[46] Unlike the pure polymer LbL film, the Au nanoparticles-containing LbL films were difficult to be released from the substrate by varying the pH. It was suggested that the gold particles act as a crosslinker in between the multilayers, thus further enhancing the stability of the LbL films.

Barbiturate-triaminodiazine hydrogen bonding was used to assemble CdS nanoparticles and gold/CdS nanoparticle hybrids onto gold surfaces.[47] A CdS nanoparticle-modified electrode generated a light-induced photocurrent in the system. A 2.6-fold enhancement in photocurrent was observed for the gold/CdS composite-modified electrode. The enhancement was attributed to the charge separation of the electron-hole pair that is generated upon the photochemical excitation of the CdS nanoparticles.

2.2.2.4 Host-guest interactions

Host-guest chemistry involves the complexation of two or more molecules that are held together in a unique structure via specific interactions, *e.g.* hydrophobic interactions, Van der Waals forces, or hydrogen bonding. Cyclodextrin is an interesting host molecule because it is a natural receptor that forms stable and specific inclusion complexes with a variety of organic guest molecules in aqueous media.[48,49] The bond between hosts and guests are continuously broken and formed. Hence, the use of molecules with multiple binding sites is used to enhance the binding affinities (multivalency).[50]

Different cyclodextrin monolayers have been synthesized and their surface properties have been characterized. Kaifer and Stoddart *et al.* prepared per-6-thiol-cyclodextrins, and described the interfacial monovalent ferrocene complexation at the monolayer.[51] Mittler-Neher *et al.* studied the kinetics of the adsorption of mono- and multithiolate-functionalized β-cyclodextrin (CD) SAMs.[52,53] Huskens and Reinhoudt *et al.* introduced the concept of 'molecular printboards', *i.e.* CD SAMs on gold or silicon oxide substrates, onto which complementary multivalent guest-functionalized dendrimer molecules were adsorbed, resulting in the formation of kinetically stable supramolecular assemblies.[54-57] With the aid of adamantyl- or ferrocenyl-functionalized poly(propylene imine) dendrimers as a noncovalent supramolecular glue, CD-functionalized nanoparticles were assembled onto CD SAMs (Scheme 2.6).[11,58] Ferrocenyl-functionalized silica nanoparticles were also directly adsorbed onto CD SAMs *via* host-guest complexation. All of these host- or guest-functionalized nanoparticle layers bind strongly at the interface owing to the formation of multivalent interactions.[59]

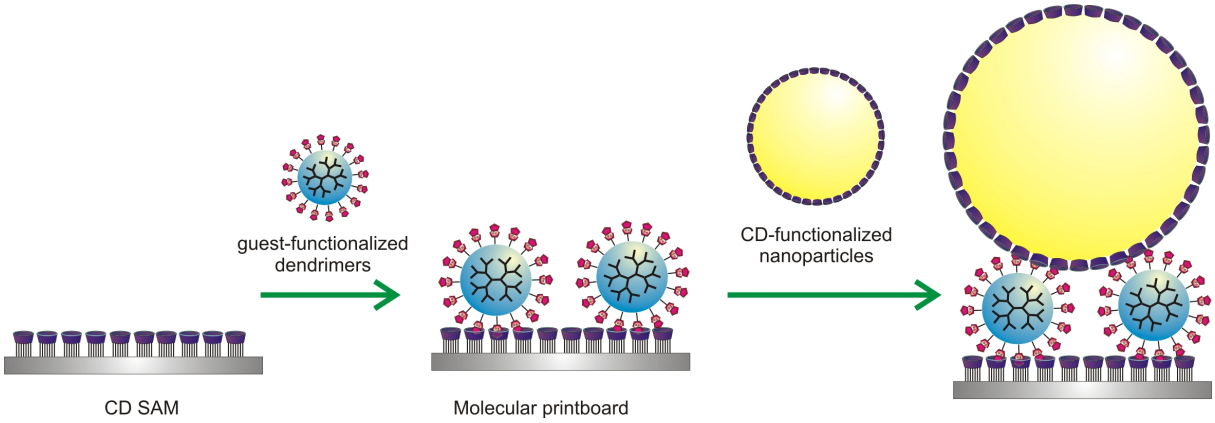

Scheme 2.6. The adsorption of multivalent guest-functionalized dendrimers onto a CD SAM and the subsequent assembly of complementary CD-functionalized nanoparticles.

The stepwise construction of self-assembled organic/inorganic multilayers based on multivalent supramolecular interactions between guest-functionalized dendrimers and nanoparticles and host-modified gold nanoparticles has been developed, yielding supramolecular LbL assembly.[11] Multilayer thin films composed of CD-functionalized gold nanoparticles and adamantyl-terminated dendrimers have been prepared on CD SAMs, whereby the thickness was controlled at the nm level.

2.2.2.5 Biomolecular interactions

In recent years, there has been a lot of research in the utilization of biomolecule-functionalized nanoparticles for the formation of hybrid nanostructures. While much effort was spent on solution systems, there are some examples which exploit the binding specificity of the biomolecules, *e.g.* proteins, peptides, and DNA to assemble nanoparticles on surfaces.

The strong and specific biotin-streptavidin binding was used to assemble biomolecule-functionalized nanoparticles in multilayered structures.[60] Application of an electrical field allowed the assembly of multilayer structures by using extremely low concentrations of nanoparticles with minimal nonspecific binding. A microelectrode array was used to facilitate the rapid parallel electrophoretic transport and binding of biotin- and streptavidin-functionalized fluorescent nanoparticles to specific sites. By controlling the current, voltage, and activation time at each nanoparticle adsorption step, the directed assembly of more than 50 layers of nanoparticles was accomplished within an hour.

Mirkin *et al.* used gold nanoparticles functionalized with thiol-modified oligonucleotides to detect the presence of the complementary sequence hybridized on a transparent substrate (Scheme 2.7).[15] In comparison to conventional fluorophore probes, this

technique is three times more sensitive in discriminating an oligonucleotide sequence with a single basepair mismatch. In addition, signal amplification by reduction of silver ions on the nanoparticles drastically increased the sensitivity of this detection system, exceeding that of the fluorophore system by two orders of magnitude.

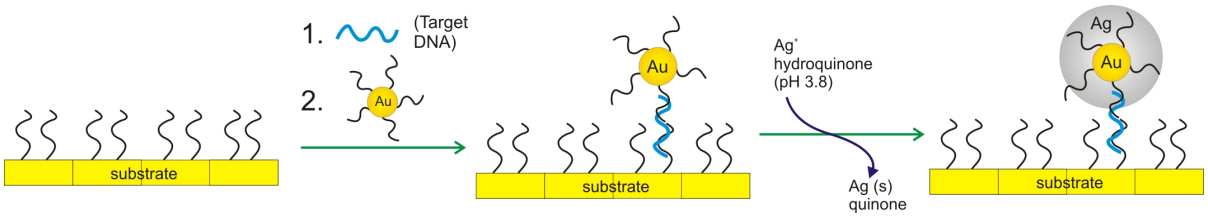

Scheme 2.7. The assembly of oligonucleotide-functionalized Au nanoparticles on a Au surface via DNA hybridization and signal enhancement by reduction of silver ions on the nanoparticles for DNA array detection.[15]

Alternatively, a DNA array based on electrical detection was reported to detect a target oligonucleotide at a concentration as low as 500 fM. Oligonucleotide-functionalized gold nanoparticles were locally and specifically assembled between an electrode gap, functionalized with complementary oligonucleotides. The silver deposition on these nanoparticles resulted in conductivity changes, which allow the detection of target oligonucleotides.[61]

2.3. CHEMICAL NANOPARTICLE ASSEMBLY ON PATTERNED SURFACES

In device fabrication, the location of functional materials is as important as their properties. The integration of solid particles into devices usually requires placing them in specific positions. Hence, the combination of top-down patterning techniques and bottom-up self-assembly is crucial in obtaining (submicron) patterned functional nanostructures on surfaces.

The introduction of SAMs on localized areas of a substrate allows straightforward further functionalization and directed assembly of nanoparticles. By using chemistry, specific binding can be introduced, allowing the control of nanoparticle assembly onto lithographic patterns. Wet-chemical self-assembly of nanoparticles is particularly attractive for the fabrication of nanoparticle-based nanostructures because of its compatibility with various kinds of substrates with complex shapes. In this section, conventional and non-conventional patterning techniques for the chemical assembly of nanoparticles will be highlighted.

2.3.1 Patterning by photolithography

Conventional patterning techniques, *e.g.* photolithography and electron beam lithography are frequently used for the fabrication of patterned substrates owing to their capability to produce nanometer features with remarkable perfection. However, the slow process of electron beam lithography has limited most of its application fabricating high-end devices.[62,63]

Photolithography is one of the most widely implemented fabrication techniques. It involves an exposure of a resist on an inert surface to an irradiation source (*e.g.* UV, X-ray) through a mask with a pre-fabricated pattern to induce chemical changes to the exposed areas of the substrate, yielding a replica of the pattern of the mask.[64] Development of the exposed resist, *e.g.* by chemical etching, results in topographically or chemically patterned substrates. In general, chemical patterns with different wettability, owing to the relative simplicity, have been most widely employed for the assembly of multicomponent and 3D nanoparticle crystals.

Heath *et al.* exploited photolithography to generate chemical patterns for the assembly of different nanocrystals (Scheme 2.8).[65] Organic monolayers of an adsorbate-functionalized with the photolabile protection group nitroveratryloxycarbonyl (NVOC) were deprotected locally by UV exposure through a mask, resulting in spatially and chemically distinct areas on the substrate. On patterns of an adsorbate functionalized with the photolabile NVOC and amino-functionalized regions, multiple types of metal and semiconductor nanocrystals were produced. The adsorption of amine-functionalized CdSe/CdS core-shell nanocrystals, Au, and Pt nanoparticles onto the pattern was achieved by the ligand exchange of the amino groups of the nanocrystals by the substrate-bound amino groups. A wide range of fluorescence intensities (from 100/1 to 8/1 signal-to-noise ratio) of the CdSe/CdS core-shell nanocrystals on the surface was observed, indicating that the binding selectivity of the nanocrystals is dependent on the type of particle, the particle concentration, the chemical composition of the NC solution, and the immersion time of the pattern in the particle solution. The assembly of nanocrystals is characterized by strong interparticle and particle–substrate dispersion interactions that scale geometrically with the size of the particle. Such interactions can compete effectively with ligating particle–substrate interactions, and thus decrease the binding selectivity.

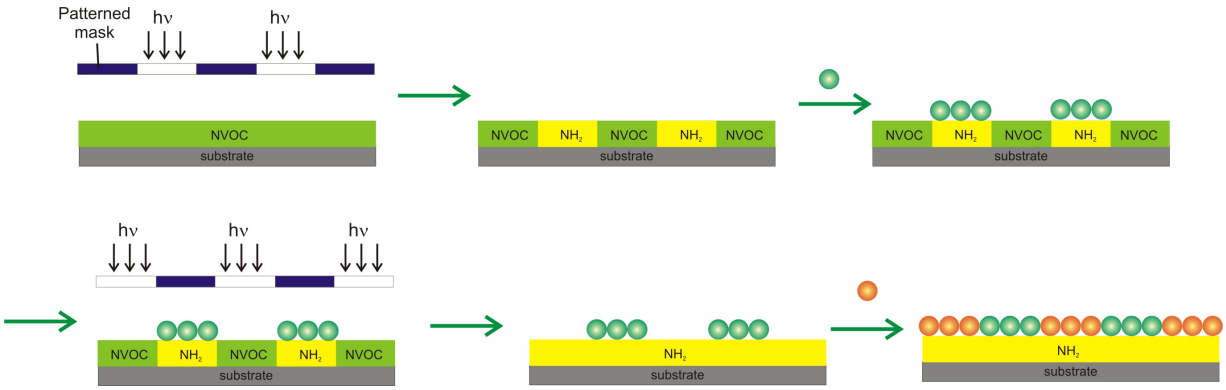

Scheme 2.8. Reaction scheme for the stepwise preparation of multicomponent particle arrays by photolithography, employing NVOC as protection groups.[65]

Similar NVOC deprotection chemistry was used by Jonas *et al.* to study the selective assembly of polybutylmethacrylate particles onto chemically patterned silane layers *via* electrostatic interactions.[66] Substrates functionalized with triethoxysilane with photoprotected NVOC amino groups were patterned by photolithography. Site-specific nanoparticle adsorption was observed on the photo-deprotected layers after local conversion to amino groups. A three-step mechanism was suggested for the site-selective particle adsorption. The positioning and adhesion of the nanoparticles in liquid suspension are controlled by electrostatic attraction and polar interactions (*e.g.* hydrogen bonding) between the substrate and the particle surfaces. They depend on the solution pH that governs the pK_a of the carboxylic acid on the nanoparticles. Capillary forces between particles and the surface laterally rearrange the particles during the drying process. Thirdly, an irreversible reorganization of the particle-substrate interface occurs after complete evaporation.

Rotello *et al.* patterned silica substrates with thymine (Thy-PS) and positively charged *N*-methylpyridinium (PVMP) polymers by photolithography.[67] By using the the triple hydrogen bonding diamidopyridine-thymine motif and pyridinium-carboxylate electrostatic interactions, selective self-assembly of diaminopyridine-functionalized polystyrene and carboxylate-derivatized CdSe/ZnS core-shell nanoparticles onto the complementary domains of the patterned substrate was observed. Owing to the specificity and selectivity of the interactions involved, the recognition-directed orthogonal self-assembly of multicomponent nanoparticle arrays can be performed in one step.

The combination of patterning and chemical assembly has also been extended to the formation of patterned 3D nanoparticle crystals. Parikh *et al.* fabricated patterned substrates with different chemical functionalities and wettability by photolithography (Scheme 2.9).[68] A

concentrated nanoparticle solution was injected into the gap between the patterned substrate and a hydrophilic glass substrate. After solvent evaporation, the structure was peeled off, leaving cleaved face-centered cubic nanoparticle crystals on each of the two surfaces, corresponding to the substrate hydrophilicity. The crystal thickness was controlled by the spacing between the substrates, and by the amount and concentration of the nanoparticle solution. The measured photonic stop gaps for the nanoparticle crystals were slightly lower than the theoretically predicted values, probably due to nanoparticle shrinking as a result of dehydration.

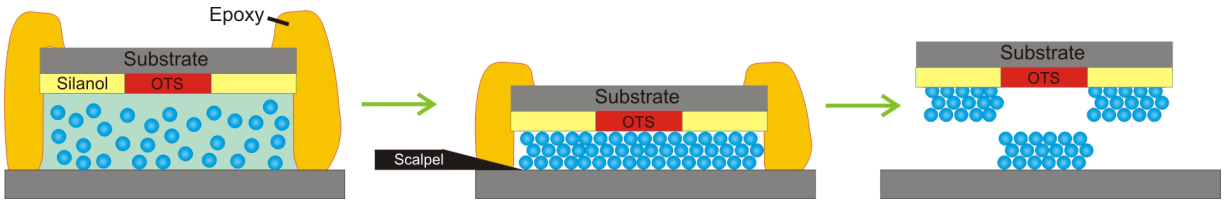

Scheme 2.9. The patterning of nanoparticle crystals by combination of photolithography and surface wettability.[68]

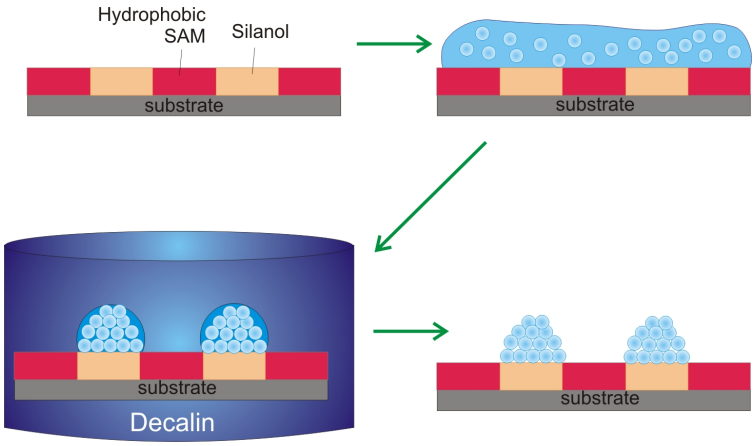

Scheme 2.10. The preparation of spherically shaped nanoparticle crystals.[69]

In addition to the manipulation of wettability of the patterned substrate, Masuda *et al.* utilized the dynamic interactions between particles, substrate and solution, and the shrinkage of nanoparticle droplets to form spherical particle assemblies (Scheme 2.10).[69,70] A droplet of a SiO_2 nanoparticle solution in methanol was placed on photolithographically patterned hydrophilic and hydrophobic SAMs. The substrate was then immersed in decalin. The nanoparticles selectively contacted the hydrophilic regions and bound to the droplet interfaces by surface tension of the emulsified droplets. The water in the particle droplets

slowly dissolved into the hexane, resulting in reduction of the droplet size and rearrangement of the nanoparticles resulting in close-packed spherical particle assemblies.

The selective adsorption of catalytic nanoparticles onto patterned substrates has been demonstrated by Akamatsu *et al.* to allow direct metallization on insulating substrates.[71] TiO_2 nanocrystals were selectively adsorbed onto a hydrophobic region of lithographically patterned glass substrate *via* electrostatic interactions. TiO_2 nanocrystals, known for their strong oxidizing ability, were used as a photocatalyst to oxidize methanol in solution to produce formic acid. This led to the reduction of copper ions to produce metallic copper films. The thickness of the deposited copper films was controlled by varying the irradiation time and power, and by the initial concentration of methanol as a hole scavenger. The deposited copper thin films exhibited electrical conductivity slightly lower than bulk copper, probably due to the formation of relatively large grains of copper that were loosely connected to each other.

2.3.2 Patterning by soft lithography

Unconventional patterning techniques, such as soft lithography (*e.g.* microcontact printing), nanoimprint lithography, and scanning probe lithography, are increasingly used for the cost-effective fabrication of nanostructures. They are particularly attractive because they can be performed (even) without cleanroom facilities.

Microcontact printing (μCP) utilizes an elastomeric stamp that can be molded from a patterned substrate pre-fabricated by photolithography or e-beam lithography.[29,72] The elastomeric stamp, most commonly made of poly(dimethylsiloxane) (PDMS), is employed for transferring and fabricating features at the intended target surface in a non-destructive manner, making it particularly suitable for the patterning of SAMs, nanoparticles, biomolecules, and nanostructures.

There are two μCP methodologies for the assembly of nanoparticles into patterned nanoparticle arrays on surfaces, *i.e.* (1) the direct use of nanoparticles as the 'ink' in μCP and thus the transfer of the nanoparticle ink to the substrate by the stamp, and (2) the preparation of patterned monolayers on a substrate to direct the adsorption of nanoparticles from solution. Whitesides and co-workers pioneered the μCP of SAMs and nanostructures. In their earlier work, micropatterns of palladium nanoparticles were prepared by μCP, which served as a catalyst for electroless deposition of copper (Scheme 2.11).[73] A PDMS stamp was soaked in a Pd nanoparticle solution and stamped onto amino-functionalized substrates. The electroless

deposition of copper only occurred at the patterned Pd nanoparticle regions. Printing on curved substrates and the fabrication of free-standing copper and multilevel metal structures with variable thickness in different regions were also demonstrated.

Andres *et al.* demonstrated the μCP of densely packed alkanethiolate-functionalized Au nanoparticle arrays in monolayer and multilayer structures.[74,75] Dense and hexagonally packed monolayers of nanoparticles were first assembled on a water surface. By using the Langmuir-Schäfer technique, the Au nanoparticle monolayer was transferred to a PDMS stamp, and printed onto a substrate. Multilayers were prepared by repeating the printing process in a LbL scheme, in which subsequent particle layers may be made up of the same or different types of particles. Similarly, the assembly of irregular, densely packed monolayers of polystyrene nanoparticles on μCP substrates *via* carbodiimide coupling was reported.[76] The conformal contact of the carbodiimide-functionalized polystyrene particles resulted in the covalent attachment of the nanoparticles at a carboxylate-functionalized surface.

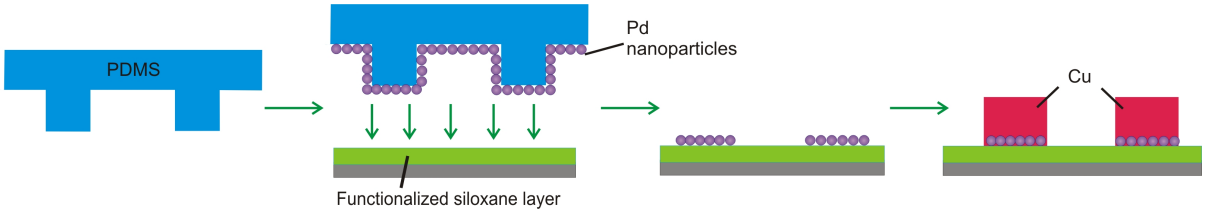

Scheme 2.11. The μCP of Pd nanoparticles on an amino-functionalized substrate and the subsequent electroless deposition of copper.[73]

Owing to the flexibility of PDMS stamps, nanocomposites could also be printed. Wang *et al.* reported the μCP of a polymeric/inorganic nanocomposite of hydrolyzed poly(styrene-*alt*-maleic anhydride) (HSMA) and TiO_2 on substrates from a dispersion of TiO_2 nanoparticles in a HSMA solution. The printed composite layers had a dish shape, with more nanoparticles accumulated in the periphery of the dishes. The size of the rim and the thickness of the printed dish depended on the TiO_2 particle concentration. Calcination of the composite dishes removed the polymer and resulted in nanostructured TiO_2 layers. In addition, Bittner *et al.* reported the μCP of CdS/dendrimer nanocomposites on hydroxy-terminated silicon surfaces.[77] Dendrimers were used as hosts for CdS nanoparticles, and facilitated the adsorption of the nanoparticles to the surface *via* electrostatic forces, hydrogen bonds and/or Van der Waals interactions.

Recently, Wolf *et al.* introduced the self-assembly, transfer and integration (SATI) of nanoparticles with high placement accuracy.[78,79] By convective assembly, silica and polymer nanoparticles were positioned on a PDMS stamp (Scheme 2.12). By controlling the printing temperature or by using a thin polymer layer as an adhesion layer, nanoparticles of different shapes and sizes were printed onto the target substrate. By convective assembly of nanoparticles, they have demonstrated the printing of a 60-nm Au nanoparticle array with single-particle resolution.[35]

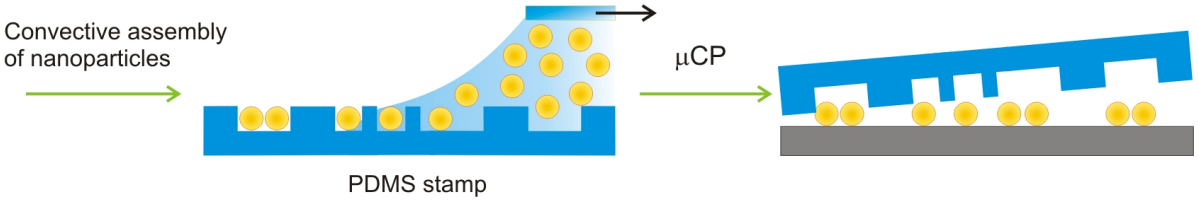

Scheme 2.12. The use of convective assembly to control the arrangement of nanoparticles on a patterned PDMS stamp and the subsequent printing of the nanoparticles with single-particle resolution.[35]

Huskens *et al.* exploited host-guest interactions between dendritic guest molecules and CD-modified nanoparticles for the formation of organic/metal nanoparticle multilayers on a PDMS stamp (Scheme 2.13).[80] The multilayer stacks were transferred to a complementary host surface, while no materials remained on the protruding areas of the PDMS stamp. These multilayers showed a well-defined thickness control of 2 nm per bilayer.

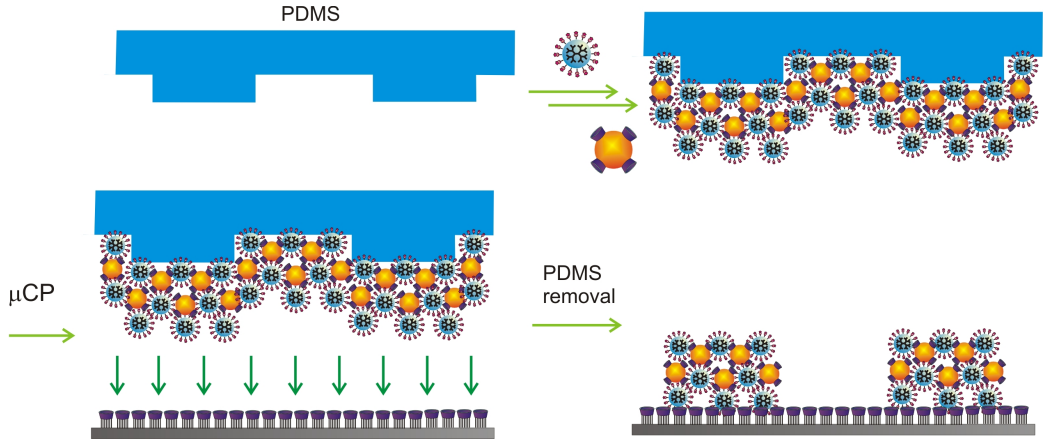

Scheme 2.13. The preparation of a multilayered supramolecular nanostructure on PDMS and transfer printing onto a CD SAM.

In the indirect printing approach, organic molecules were first printed onto substrates. The μCP of organic adsorbates serves to direct the assembly of nanoparticles for the formation of ordered 2D arrays of particles. Whitesides *et al.* prepared patterned surfaces with grids of hydrophobic (CH_3-terminated) and hydrophilic (COOH-terminated) SAMs of alkanethiols on a gold substrate.[81] The nanoparticle solution wetted exclusively the hydrophilic regions of surface by controlling the substrate withdrawing speed from the nanoparticle solution. The dimensions of these particle patterns can be controlled by the concentration and composition of the solution, and shape and area of the hydrophilic regions.

Hammond *et al.* reported the self-organization of SiO_2 and polystyrene nanoparticles on a μCP-patterned polyelectrolyte substrate (Scheme 2.14).[27] The multicomponent nanoparticle assembly was driven by spatial electrostatic and hydrophobic interactions between the nanoparticles and the polyelectrolyte substrate. The surface charge density was modulated by pH, ionic strength and effective surface charge of the polyelectrolyte.[82] However, only a moderate packing density was achieved due to the repulsive forces between the particles. In addition, a balance between the interactions involved during the nanoparticle assembly is needed to obtain an optimum adsorption strength and deposition selectivity.

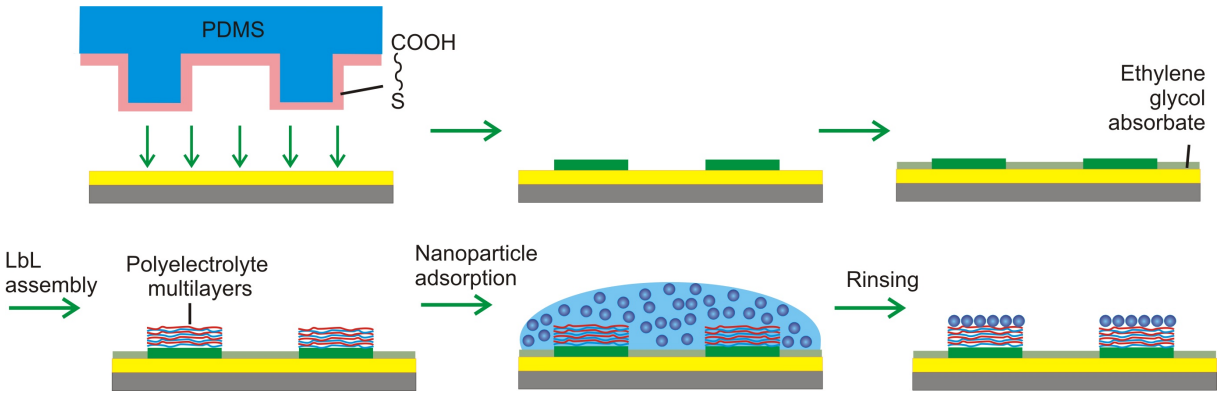

Scheme 2.14. Chemical patterning by μCP, LbL assembly of polyelectrolytes and nanoparticle assembly.[27]

Kang and Klenerman *et al.* studied the selective LbL assembly of NCs on microcontact printed carboxylate-functionalized SAMs.[83] The LbL assembly was achieved by alternating adsorption of NCs functionalized with hydrophobic trioctylphosphine oxide and 2-mercaptoethanesulfonic acid, and positively charged linear poly(ethyleneimine) (LPEI). By adsorption of 11-mercaptoundecylhexa(ethylene glycol) in the non-contacted areas,

nonspecific interactions were minimized. A uniform and linear growth of the polymer-NC layers were observed.

Combinatorially selected peptides and peptide–organic conjugates were used as linkers to direct the attachment of NCs on a microcontact printed carboxylate SAM.[84] The use of genetically engineered peptides (GEPIs) allowed control over conformations during the nanoparticle assembly. In addition, the spatial configurations of the NCs at the surface were varied by tailoring GEPIs with π-conjugated functional molecules. An increase in the average NC attachment density was observed when peptide–organic conjugates were employed in the formation of hybrid nanostructures.

2.3.3 Patterning by nanoimprint lithography

Nanoimprint lithography (NIL) is an embossing method for fabricating patterns by mechanical deformation of an imprint resist. Unlike μCP, it offers three-dimensional patterning with high resolution features down to 6 nm,[85] making it a low cost, high throughput, and high resolution technique. Two general methods are used to pattern the imprint resist, *i.e.* hot embossing of a thermoplastic polymer and UV imprint lithography of a photocurable monomer.

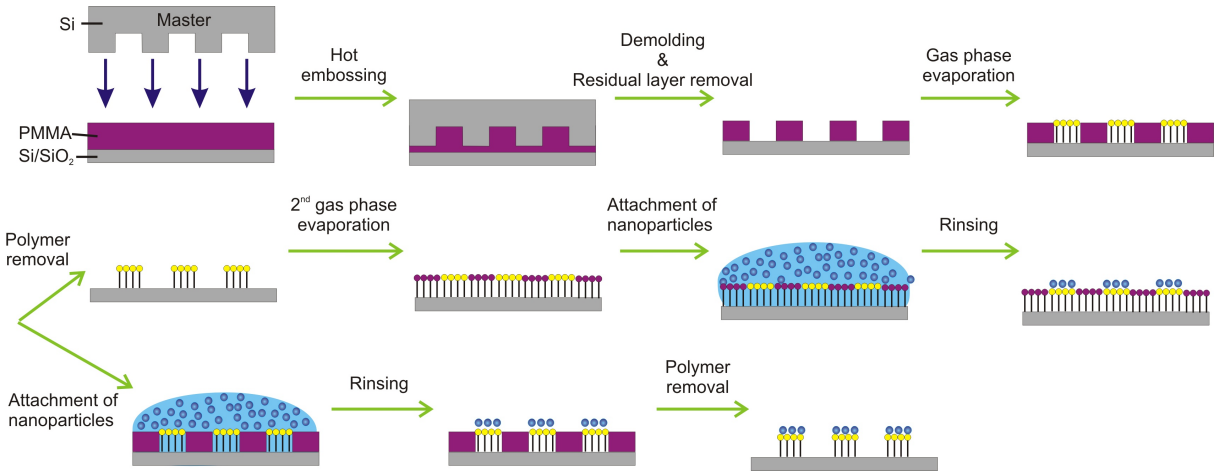

Scheme 2.15. The NIL process and nanoparticle assembly.

Huskens *et al.* utilized NIL as a tool to pattern SAMs on silicon substrates.[86] As shown in Scheme 2.15, a pre-fabricated silicon wafer with a pattern was pressed against a thin layer of PMMA on a silicon substrate above the glass transition temperature. The system was then cooled and the thin polymer residual layer was removed. SAMs of aminoalkylsilanes were formed on the uncovered regions. Carboxylate-functionalized

polystyrene nanoparticles were electrostatically attached to the amino-functionalized surface. Alternatively, chemical patterns were created by removing the patterned polymer layers, and adsorbing a second silane on the remaining areas. Selective attachment of carboxylate-functionalized silica nanoparticles on complementary amino regions was observed in this case.

NIL patterns were also used for the assembly of nanoparticles *via* supramolecular host-guest interactions.[87] The NIL-patterned substrate was functionalized with CD SAMs via a three-step synthesis process. The fabrication of 3D nanostructures was achieved by the alternating assembly of multivalent guest-functionalized dendrimers and CD-functionalized Au nanoparticles.[80]

2.3.4 Patterning by scanning probe lithography

The application of scanning probe lithography (SPL) has been widespread owing to its ability to modify substrates with very high resolution and ultimate pattern flexibility.[88] Dip-pen nanolithography (DPN),[89] high contact force atomic force microscopy (AFM),[90] and constructive nanolithography[91] are some of the most commonly employed techniques, all of which aim to control the position and directed assembly molecules and nanoparticles.

DPN is a scanning probe nanopatterning technique developed by Mirkin and co-workers.[89] An AFM tip is used to deliver molecules to a surface through a water meniscus, which naturally forms in ambient atmosphere. DPN can also be used to generate many customized templates from the same or different chemical inks. Making use of this idea, Mirkin *et al.* employed their DPN-based strategy for generating charged chemical templates to study the assembly of single particles into 2D lattices (Scheme 2.16). They used 16-mercaptohexadecanoic acid (MHDA) to make templates, and positively charged protonated amino-modified polystyrene particles (d ~ 930 nm) were then electrostatically assembled onto the MHDA surface.[92] The non-patterned regions were passivated by a hydrophobic alkanethiol, which prevented undesired particle diffusion. They also extended the DPN-driven nanoparticle assembly to magnetic nanoparticles (*e.g.* Fe_2O_3, $MnFe_2O_4$).[93] Detailed experimental studies showed that the size of the nanoparticle dots or lines correlated with the size of the dots or lines of the MHDA patterns generated by DPN. The template dot diameter could be controlled by tuning the tip-substrate contact time, whereas the line width could be controlled by adjusting the scan speed.

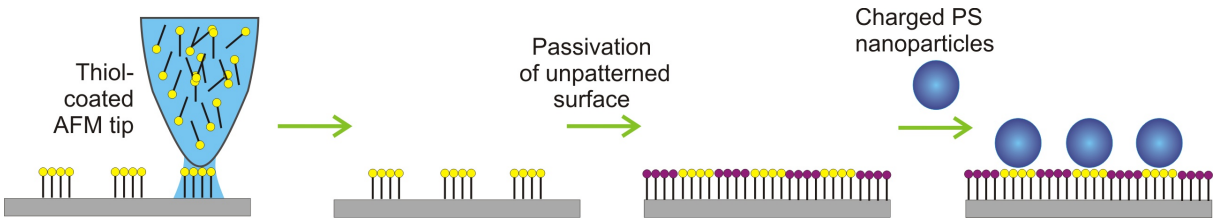

Scheme 2.16. DPN-based particle assembly.

Sagiv *et al.* introduced 'constructive nanolithography', a surface patterning process utilizing conductive AFM tips as nanoelectrochemical 'pens'.[91] The top surface of an organosilane monolayer on silicon was electrochemically transformed and inscribed by electrical pulses delivered *via* a conductive AFM tip. Further surface chemical derivatization and guided self-assembly resulted in hierarchical LbL assembly. Utilizing this strategy, they reported the assembly of Au clusters on patterned silicon substrates. As shown in Scheme 2.17, alkylsilane monolayer regions were electrochemically transformed to carboxylate-functionalized monolayers.[94,95] Subsequent exposure to nonadecenyltrichlorosilane (NTS) resulted in patterned monolayers with terminal vinyl groups (-CH=CH_2). Photochemical radical addition of H_2S to these vinyl moieties and further reduction (with BH_3.THF) of a fraction of the disulfide groups produced a thiol-functionalized layer. Phosphine ligands on Au clusters were partially lost due to the exchange process during gold cluster attachment to the thiol-coated surface.

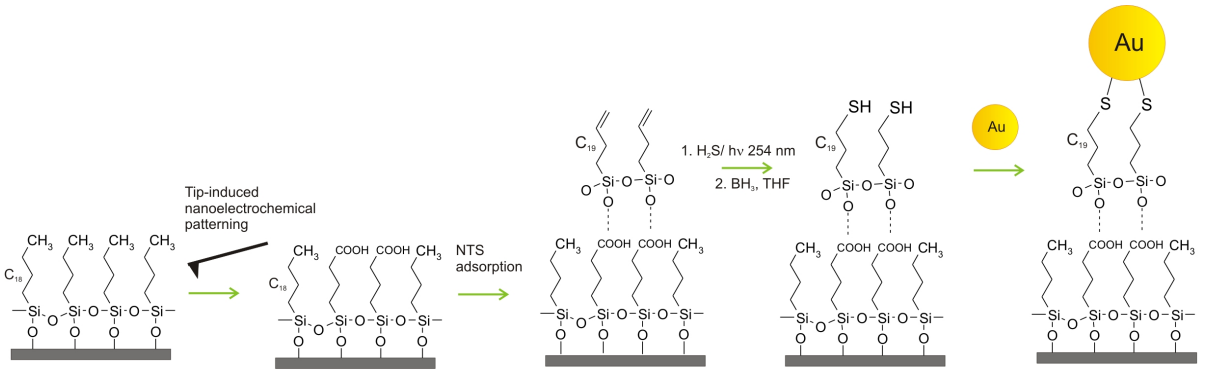

Scheme 2.17. The template-directed self-assembly of Au clusters on silicon substrate patterned by constructive nanolithography.

Liu *et al.* utilized AFM-based nanooxidation to fabricate Au nanoparticle arrays on silicon substrates.[90] An octadecyltrichlorosilane (OTS) monolayer on silicon was first subjected to localized chemical oxidation by using a conductive AFM tip to form silicon

oxide. The oxide region was then further modified to an amino-terminated silane monolayer *via* selective chemical adsorption. The patterned substrate was exposed to negatively charged Au nanoparticles which resulted in the formation of nanoparticle arrays *via* electrostatic interactions in the amino-terminated silane regions. By optimizing the humidity, applied voltage and the pulse duration of the system, oxidized areas as small as 15 nm were fabricated. A very regular nanoparticle array, with only one nanoparticle per oxide dot was obtained.[90] However, the assembly efficiency of nanoparticles onto the guiding templates was not perfect (70 %), and showed a decrease in efficiency when the oxide dots were smaller. The authors attributed this to smaller effective areas to adsorb nanoparticles compared to the actual geometrical areas. The difference in effective areas and geometrical areas were attributed to imperfectness of the AFM nanooxidation process.

2.4. CONCLUSIONS

Parallel advances in the development of the self-assembly of nanoparticles by chemical means and of different patterning strategies have enabled the creation of 2D and 3D nanoparticle crystals. In particular, the use of noncovalent chemistry for the directed assembly of functionalized nanoparticles onto desired patterned substrates has resulted in highly specific assembly of nanoparticles with controlled affinity and reversibility. However, it is clear that the reported nanoparticle crystals are still relatively simple in structure, and that the intriguing properties of the nanoparticle structures have not been extensively studied. Hence, the development of the integration of self-assembly of nanoparticles into nanofabrication schemes still requires more efforts to fully extend its potential to the fabrication of devices that target specific applications. It is anticipated, using chemically-directed self-assembly as a nanofabrication tool, that more ordered and complex arrays of chemically, optically and geometrically tunable nanostructured building blocks can be realized. These will one day be of benefit for the development of novel technologies, such as optical data processing, molecular electronics, and quantum computing.

2.5. REFERENCES

1. Daniel, M. C.; Astruc, D. *Chem. Rev.* **2004**, *104*, 293.
2. Arsenault, A.; Fournier-Bidoz, S.; Hatton, B.; Miguez, H.; Tetreault, N.; Vekris, E.; Wong, S.; Yang, S. M.; Kitaev, V.; Ozin, G. A. *J. Mater. Chem.* **2004**, *14*, 781.
3. Denkov, N. D.; Velev, O. D.; Kralchevsky, P. A.; Ivanov, I. B.; Yoshimura, H.; Nagayama, K. *Nature* **1993**, *361*, 26.

4. Malaquin, L.; Kraus, T.; Schmid, H.; Delamarche, E.; Wolf, H. *Langmuir* **2007**, *23*, 11513.
5. Ozin, G. A.; Yang, S. M. *Adv. Funct. Mater.* **2001**, *11*, 95.
6. Wijnhoven, J.; Vos, W. L. *Science* **1998**, *281*, 802.
7. Chen, S. *Langmuir* **2001**, *17*, 2878.
8. Lahav, M.; Shipway, A. N.; Willner, I.; Nielsen, M. B.; Stoddart, J. F. *J. Electroanal. Chem.* **2000**, *482*, 217.
9. Paraschiv, V.; Zapotoczny, S.; de Jong, M. R.; Vancso, G. J.; Huskens, J.; Reinhoudt, D. N. *Adv. Mater.* **2002**, *14*, 722.
10. Decher, G. *Science* **1997**, *277*, 1232.
11. Crespo-Biel, O.; Dordi, B.; Reinhoudt, D. N.; Huskens, J. *J. Am. Chem. Soc.* **2005**, *127*, 7594.
12. Zirbs, R.; Kienberger, F.; Hinterdorfer, P.; Binder, W. H. *Langmuir* **2005**, *21*, 8414.
13. Shavel, A.; Gaponik, N.; Eychmuller, A. *ChemPhysChem* **2005**, *6*, 449.
14. Wanunu, M.; Popovitz-Biro, R.; Cohen, H.; Vaskevich, A.; Rubinstein, I. *J. Am. Chem. Soc.* **2005**, *127*, 9207.
15. Taton, T. A.; Mirkin, C. A.; Letsinger, R. L. *Science* **2000**, *289*, 1757.
16. Park, J. I.; Lee, W. R.; Bae, S. S.; Kim, Y. J.; Yoo, K. H.; Cheon, J.; Kim, S. *J. Phys. Chem. B* **2005**, *109*, 13119.
17. Zhang, H.; Wang, R.; Zhang, G.; Yang, B. *Thin Solid Films* **2003**, *429*, 167.
18. Bai, Y.; Zhao, S.; Zhang, K.; Sun, C. *Colloid Surface A* **2006**, *281*, 105.
19. Granot, E.; Patolsky, F.; Willner, I. *J. Phys. Chem. B* **2004**, *108*, 5875.
20. Reinhoudt, D. N.; Crego-Calama, M. *Science* **2002**, *295*, 2403.
21. Iler, R. K. *J. Colloid Interf. Sci.* **1966**, *21*, 569.
22. Decher, G.; Hong, J. D.; Schmitt, J. *Thin Solid Films* **1992**, *210*, 831.
23. Ostrander, J. W.; Mamedov, A. A.; Kotov, N. A. *J. Am. Chem. Soc.* **2001**, *123*, 1101.
24. Malikova, N.; Pastoriza-Santos, I.; Schierhorn, M.; Kotov, N. A.; Liz-Marzan, L. M. *Langmuir* **2002**, *18*, 3694.
25. Kotov, N. A.; Dekany, I.; Fendler, J. H. *J. Phys. Chem.* **1995**, *99*, 13065.
26. Nakanishi, T.; Ohtani, B.; Uosaki, K. *J. Phys. Chem. B* **1998**, *102*, 1571.
27. Zheng, J. W.; Zhu, Z. H.; Chen, H. F.; Liu, Z. F. *Langmuir* **2000**, *16*, 4409.
28. Maury, P.; Escalante, M.; Reinhoudt, D. N.; Huskens, J. *Adv. Mater.* **2005**, *17*, 2718.
29. Meitl, M. A.; Zhu, Z. T.; Kumar, V.; Lee, K. J.; Feng, X.; Huang, Y. Y.; Adesida, I.; Nuzzo, R. G.; Rogers, J. A. *Nature Mater.* **2006**, *5*, 33.
30. Serizawa, T.; Takeshita, H.; Akashi, M. *Langmuir* **1998**, *14*, 4088.
31. Lvov, Y.; Ariga, K.; Onda, M.; Ichinose, I.; Kunitake, T. *Langmuir* **1997**, *13*, 6195.
32. Hicks, J. F.; Seok-Shon, Y.; Murray, R. W. *Langmuir* **2002**, *18*, 2288.
33. Blonder, R.; Sheeney, L.; Willner, I. *Chem. Commun.* **1998**, 1393.

34. C. J. Kiely, J. F., J. G. Zheng, M. Brust, D. Bethell, D. J. Schiffrin *Adv. Mater.* **2000**, *12*, 640.
35. Sellers, H.; Ulman, A.; Shnidman, Y.; Eilers, J. E. *J. Am. Chem. Soc.* **1993**, *115*, 9389.
36. Rizza, R.; Fitzmaurice, D.; Hearne, S.; Hughes, G.; Spoto, G.; Ciliberto, E.; Kerp, H.; Schropp, R. *Chem. Mater.* **1997**, *9*, 2969.
37. Kiely, C. J.; Fink, J.; Zheng, J. G.; Brust, M.; Bethell, D.; Schiffrin, D. J. *Adv. Mater.* **2000**, *12*, 640.
38. Joseph, Y.; Besnard, I.; Rosenberger, M.; Guse, B.; Nothofer, H. G.; Wessels, J. M.; Wild, U.; Knop-Gericke, A.; Su, D.; Schlogl, R.; Yasuda, A.; Vossmeyer, T. *J. Phys. Chem. B* **2003**, *107*, 7406.
39. Freeman, R. G.; Grabar, K. C.; Allison, K. J.; Bright, R. M.; Davis, J. A.; Guthrie, A. P.; Hommer, M. B.; Jackson, M. A.; Smith, P. C.; Walter, D. G.; Natan, M. J. *Science* **1995**, *267*, 1629.
40. Musick, M. D.; Keating, C. D.; Lyon, L. A.; Botsko, S. L.; Pena, D. J.; Holliway, W. D.; McEvoy, T. M.; Richardson, J. N.; Natan, M. J. *Chem. Mater.* **2000**, *12*, 2869.
41. Sarathy, K. V.; Thomas, P. J.; Kulkarni, G. U.; Rao, C. N. R. *J. Phys. Chem. B* **1999**, *103*, 399.
42. Bharathi, S.; Nogami, M.; Ikeda, S. *Langmuir* **2001**, *17*, 1.
43. Wang, L.; Wang, E. *Electrochem. Commun.* **2004**, *6*, 49.
44. Templeton, A. C.; Zamborini, F. P.; Wuelfing, W. P.; Murray, R. W. *Langmuir* **2000**, *16*, 6682.
45. Hao, E. C.; Lian, T. Q. *Chem. Mater.* **2000**, *12*, 3392.
46. Jiang, Y.; Shen, Y.; Wu, P. Y. *J. Colloid Interface Sci.* **2008**, *319*, 398.
47. Baron, R.; Huang, C. H.; Bassani, D. M.; Onopriyenko, A.; Zayats, M.; Willner, I. *Angew. Chem. Int. Ed.* **2005**, *44*, 4010.
48. Rekharsky, M. V.; Inoue, Y. *Chem. Rev.* **1998**, *98*, 1875.
49. Connors, K. A. *Chem. Rev.* **1997**, *97*, 1325.
50. Mulder, A.; Huskens, J.; Reinhoudt, D. N. *Org. Biomol. Chem.* **2004**, *2*, 3409.
51. Rojas, M. T.; Koniger, R.; Stoddart, J. F.; Kaifer, A. E. *J. Am. Chem. Soc.* **1995**, *117*, 336.
52. Weisser, M.; Nelles, G.; Wohlfart, P.; Wenz, G.; MittlerNeher, S. *J. Phys. Chem.* **1996**, *100*, 17893.
53. Nelles, G.; Weisser, M.; Back, R.; Wohlfart, P.; Wenz, G.; MittlerNeher, S. *J. Am. Chem. Soc.* **1996**, *118*, 5039.
54. Beulen, M. W. J.; Bügler, J.; Lammerink, B.; Geurts, F. A. J.; Biemond, E.; van Leerdam, K. G. C.; van Veggel, F.; Engbersen, J. F. J.; Reinhoudt, D. N. *Langmuir* **1998**, *14*, 6424.
55. Huskens, J.; Deij, M. A.; Reinhoudt, D. N. *Angew. Chem. Int. Ed.* **2002**, *41*, 4467.

56. Auletta, T.; Dordi, B.; Mulder, A.; Sartori, A.; Onclin, S.; Bruinink, C. M.; Peter, M.; Nijhuis, C. A.; Beijleveld, H.; Schonherr, H.; Vancso, G. J.; Casnati, A.; Ungaro, R.; Ravoo, B. J.; Huskens, J.; Reinhoudt, D. N. *Angew. Chem. Int. Ed.* **2004**, *43*, 369.
57. Nijhuis, C. A.; Huskens, J.; Reinhoudt, D. N. *J. Am. Chem. Soc.* **2004**, *126*, 12266.
58. Mahalingam, V.; Onclin, S.; Peter, M.; Ravoo, B. J.; Huskens, J.; Reinhoudt, D. N. *Langmuir* **2004**, *20*, 11756.
59. Ludden, M. J. W.; Reinhoudt, D. N.; Huskens, J. *Chem. Soc. Rev.* **2006**, *35*, 1122.
60. Dehlinger, D. A.; Sullivan, B. D.; Esener, S.; Heller, M. J. *Small* **2007**, *3*, 1237.
61. Park, S. J.; Taton, T. A.; Mirkin, C. A. *Science* **2002**, *295*, 1503.
62. Moon, J. H.; Ford, J.; Yang, S. *Polymers for Advanced Technologies* **2006**, *17*, 83.
63. Ito, T.; Okazaki, S. *Nature* **2000**, *406*, 1027.
64. Xia, Y.; Rogers, J. A.; Paul, K. E.; Whitesides, G. M. *Chem. Rev.* **1999**, *99*, 1823.
65. Vossmeyer, T.; Jia, S.; DeIonno, E.; Diehl, M. R.; Kim, S. H.; Peng, X.; Alivisatos, A. P.; Heath, J. R. *J. Appl. Phys.* **1998**, *84*, 3664.
66. Fustin, C. A.; Glasser, G.; Spiess, H. W.; Jonas, U. *Langmuir* **2004**, *20*, 9114.
67. Xu, H.; Hong, R.; Lu, T.; Uzun, O.; Rotello, V. M. *J. Am. Chem. Soc.* **2006**, *128*, 3162.
68. Brozell, A. M.; Muha, M. A.; Parikh, A. N. *Langmuir* **2005**, *21*, 11588.
69. Masuda, Y.; Itoh, T.; Koumoto, K. *Adv. Mater.* **2005**, *17*, 841.
70. Masuda, Y.; Itoh, T.; Koumoto, K. *Langmuir* **2005**, *21*, 4478.
71. Akamatsu, K.; Kimura, A.; Matsubara, H.; Ikeda, S.; Nawafune, H. *Langmuir* **2005**, *21*, 8099.
72. Gates, B. D.; Xu, Q. B.; Stewart, M.; Ryan, D.; Willson, C. G.; Whitesides, G. M. *Chem. Rev.* **2005**, *105*, 1171.
73. Hidber, P. C.; Helbig, W.; Kim, E.; Whitesides, G. M. *Langmuir* **1996**, *12*, 1375.
74. Santhanam, V.; Liu, J.; Agarwal, R.; Andres, R. P. *Langmuir* **2003**, *19*, 7881.
75. Santhanam, V.; Andres, R. P. *Nano Letters* **2004**, *4*, 41.
76. Himmelhaus, M.; Takei, H. *Physical Chemistry Chemical Physics* **2002**, *4*, 496.
77. Austin, M. D.; Ge, H. X.; Wu, W.; Li, M. T.; Yu, Z. N.; Wasserman, D.; Lyon, S. A.; Chou, S. Y. *Appl. Phys. Lett.* **2004**, *84*, 5299.
78. Kraus, T.; Malaquin, L.; Delamarche, E.; Schmid, H.; Spencer, N. D.; Wolf, H. *Adv. Mater.* **2005**, *17*, 2438.
79. Kraus, T.; Malaquin, L.; Schmid, H.; Riess, W.; Spencer, N. D.; Wolf, H. *Nat. Nanotechnol.* **2007**, *2*, 570.
80. Crespo-Biel, O.; Dordi, B.; Maury, P.; Peter, M.; Reinhoudt, D. N.; Huskens, J. *Chem. Mater.* **2006**, *18*, 2545.
81. Qin, D.; Xia, Y. N.; Xu, B.; Yang, H.; Zhu, C.; Whitesides, G. M. *Adv. Mater.* **1999**, *11*, 1433.
82. Zheng, H. P.; Lee, I.; Rubner, M. F.; Hammond, P. T. *Adv. Mater.* **2002**, *14*, 569.

83. Zhou, D. J.; Bruckbauer, A.; Abell, C.; Klenerman, D.; Kang, D. J. *Adv. Mater.* **2005**, *17*, 1243.
84. Zin, M. T.; Munro, A. M.; Gungormus, M.; Wong, N. Y.; Ma, H.; Tamerler, C.; Ginger, D. S.; Sarikaya, M.; Jen, A. K. Y. *J. Mater. Chem.* **2007**, *17*, 866.
85. Guo, L. J. *Adv. Mater.* **2007**, *19*, 495.
86. Maury, P.; Peter, M.; Mahalingam, V.; Reinhoudt, D. N.; Huskens, J. *Adv. Funct. Mater.* **2005**, *15*, 451.
87. Maury, P.; Peter, M.; Crespo-Biel, O.; Ling, X. Y.; Reinhoudt, D. N.; Huskens, J. *Nanotechnology* **2007**, *18*, 044007.
88. Wouters, D.; Schubert, U. S. *Angew. Chem. Int. Ed.* **2004**, *43*, 2480.
89. Rosi, N. L.; Mirkin, C. A. *Chem. Rev.* **2005**, *105*, 1547.
90. Garno, J. C.; Yang, Y.; Amro, N. A.; Cruchon-Dupeyrat, S.; Chen, S.; Liu, G. Y. *Nano Lett.* **2003**, *3*, 389.
91. Maoz, R.; Cohen, S. R.; Sagiv, J. *Adv. Mater.* **1999**, *11*, 55.
92. Demers, L. M.; Mirkin, C. A. *Angew. Chem. Int. Ed.* **2001**, *40*, 3069.
93. Liu, X. G.; Fu, L.; Hong, S. H.; Dravid, V. P.; Mirkin, C. A. *Adv. Mater.* **2002**, *14*, 231.
94. Liu, S. T.; Maoz, R.; Sagiv, J. *Nano Lett.* **2004**, *4*, 845.
95. Liu, S. T.; Maoz, R.; Schmid, G.; Sagiv, J. *Nano Lett.* **2002**, *2*, 1055.

Chapter 3

Ferrocenyl-functionalized silica nanoparticles: preparation, characterization and molecular recognition at interfaces*

ABSTRACT. Ferrocenyl-functionalized silica nanoparticles (SiO_2-Fc, **6a** - **6c**) of about 60 nm with supramolecular 'guest' properties were prepared. Nanoparticles **6a** – **6c** differed by the addition of different molar ratios of starting compounds during the functionalization step, i.e., 1:0, 1:10, and 1:90 of 2-ferrocenyl amidoethoxyethanol and diethylene glycol for **6a, 6b**, and **6c**, respectively. X-ray photoelectron spectroscopy (XPS) proved the presence of ferrocenyl groups on the surfaces of **6a** - **6c**, whereas the elemental analysis revealed an iron content of particles **6a** - **6c** of 0.10 - 0.16 %. Dynamic light scattering (DLS) results showed that, compared with **6a**, **6b** dispersed well in aqueous media, possibly due to the presence of diethylene glycol at the surfaces of **6b** that significantly increases its overall hydrophilicity. Cyclic voltammetry of **6b** indicated a totally irreversible system and a "mixed" diffusion-adsorption behavior, which is attributed to sluggish electron transfer. The shifted $|I_{p,C}/I_{p,A*}|$ ratio showed that the ferrocenyl groups are robustly attached to the nanoparticle surface within the experimental potential range. The supramolecular recognition of SiO_2-Fc nanoparticles at interfaces was verified by their adsorption on β-cyclodextrin (CD) self-assembled monolayers, as monitored by surface plasmon resonance (SPR) spectroscopy. The ability of the SiO_2-Fc nanoparticles to form host-guest interactions was also demonstrated by the attachment of CD-functionalized Au nanoparticles (3 nm) onto the SiO_2-Fc surfaces, when mixed in solution.

---

* This chapter has been published in X. Y. Ling, D. N. Reinhoudt, J. Huskens, Ferrocenyl-functionalized silica nanoparticles: preparation, characterization, and molecular recognition at interfaces, *Langmuir* **2006**, *22*, 8777.

3.1 INTRODUCTION

Recent advances in nanotechnology have provided a variety of nanostructured materials with highly controlled, interesting and exceptional properties. Among these materials, nanoparticles sized between 1 ~ 1000 nm elicit an intense interest because of their unique optical, electronic, magnetic, catalytic and other physical properties.[1] Apart from the properties arising from the core material and its nanometer dimensions, control over nanoparticles' surface functionalities is equally important. As a result, one can control and tailor the properties of nanostructures in a very predictable manner to better suit their integration to the formation of functional, more complex nanostructured architectures on surfaces or in solution and to meet the needs of a specific application in molecular electronics, biosensors, etc.

Various interaction types (e.g., covalent bonds,[2] electrostatic forces,[3] host-guest interactions[4]) have been employed to govern the assembly of nanoparticles on surfaces. These methods are anticipated to directly control the spatial distribution of nanoparticles across a large area and in more complex patterns and more reliable submicron nanofabrication schemes, where physical assembly of non-functionalized nanoparticles is not possible. Covalent binding of particles onto substrates was reported to form strong and stable particle arrays, however, in irregular patterns. This is due to the fact that self-correction is impossible in this case.[2] Electrostatic assembly, which involves electrostatic interactions between oppositely charged nanoparticles and substrates,[3] has also been further extended to the assembly of 2D and 3D nanostructures.[5,6,7,8] The self-assembly of thiol-functionalized nanoparticles via strong coordinative bonds to transition metal surfaces was also extensively studied.[9,10] Noncovalent interactions are attractive to assemble receptor-functionalized nanoparticles onto functional self-assembled monolayers (SAMs) with controllable molecular recognition abilities at the interface, and thus with the possibility for self-correction.[11] Recently, the idea of 'molecular printboards', i.e. β-cyclodextrin (CD) SAMs on gold or silicon oxide substrates that possess supramolecular host properties has been introduced.[12,13] On these CD SAMs, complementary multivalent adamantyl- or ferrocenyl-terminated dendrimer molecules were adsorbed and, as a result, kinetically stable supramolecular assemblies were formed.[14,15] In addition, desorption of ferrocenyl-terminated dendrimers from the molecular printboards was stimulated efficiently by electrochemical oxidation of the ferrocenyl groups to ferrocenium cations.[16,17] With the aid of adamantyl- or ferrocenyl-terminated dendrimers as a noncovalent glue, CD-functionalized gold and silica nanoparticles have been assembled onto CD SAMs.[4,18]

The surface properties and assembly behavior of ferrocenyl- (guest-) functionalized nanoparticles are also potentially interesting for the assembly into more complex architectures. In fact, ferrocenyl-functionalized nanoparticles have already been reported earlier.[19,20,21] Most of them describe gold nanoparticles of smaller than 10 nm, where ferrocenyl thiols were assembled onto the Au surface via ligand place exchange. The reported ferrocenyl-functionalized gold nanoparticles are only soluble in organic solvents, which limit the range of conditions for molecular recognitions studies.[21] Aoki *et al.* synthesized vinylferrocenyl polystyrene nanoparticles that are dispersed in aqueous suspension.[22] The effects of particle size on voltammetric electroactivity were extensively studied. However, the potential supramolecular guest properties of these ferrocenyl polystyrene nanoparticles were not examined.

In this chapter, the preparation of ferrocenyl-functionalized silica (SiO_2-Fc) nanoparticles is described. The aim is to synthesize nanoparticles with a controllable interface, i.e., tunable and specific adsorption and possibly (stimulated) desorption. Specific assembly is also anticipated to extend to buildup of supramolecular nanostructures via layer-by-layer assembly. The scope of this chapter is the synthesis, characterization and basic host-guest properties of the nanoparticles. The surface properties of the nanoparticles were characterized by X-ray photoelectron spectroscopy (XPS), elemental analysis, dynamic light scattering (DLS), zeta potential and electrochemistry. The supramolecular recognition properties of the ferrocenyl-functionalized nanoparticles in solution and at interfaces were studied by surface plasmon resonance (SPR) spectroscopy and scanning and transmission electron microscopy (SEM, TEM).

3.2 RESULTS AND DISCUSSION

Scheme 3.1 shows the multi-step synthesis and functionalization routes of ferrocenyl-functionalized silica nanoparticles (SiO_2-Fc). Silica particles with silanol surface groups (**1**) were prepared by using a modified Stöber method, as reported previously.[18,23] Particles were then grafted with 3-aminopropyl triethoxysilane (APTES), which resulted in amino-functionalized nanoparticles (**2**). The amino groups of **2** were functionalized by *N,N'*-disuccinimidyl carbonate (DSC) to form particles **3**. 2-Ferrocenyl amidoethoxyethanol (**4**) was added, forming particles **6a**. In the cases of particles **6b** and **6c**, diethylene glycol (**5**) was mixed with the precursor **4** during the functionalization process. This was done to vary and control the density of ferrocenyl groups on the particle surface, such that complexation with CD is effective. Moreover, grafting of diethylene glycol chains onto the particle surface is

also anticipated to improve the hydrophilicity of particles **6b** and **6c** compared to **6a**, and thus to increase their solubility in aqueous medium.

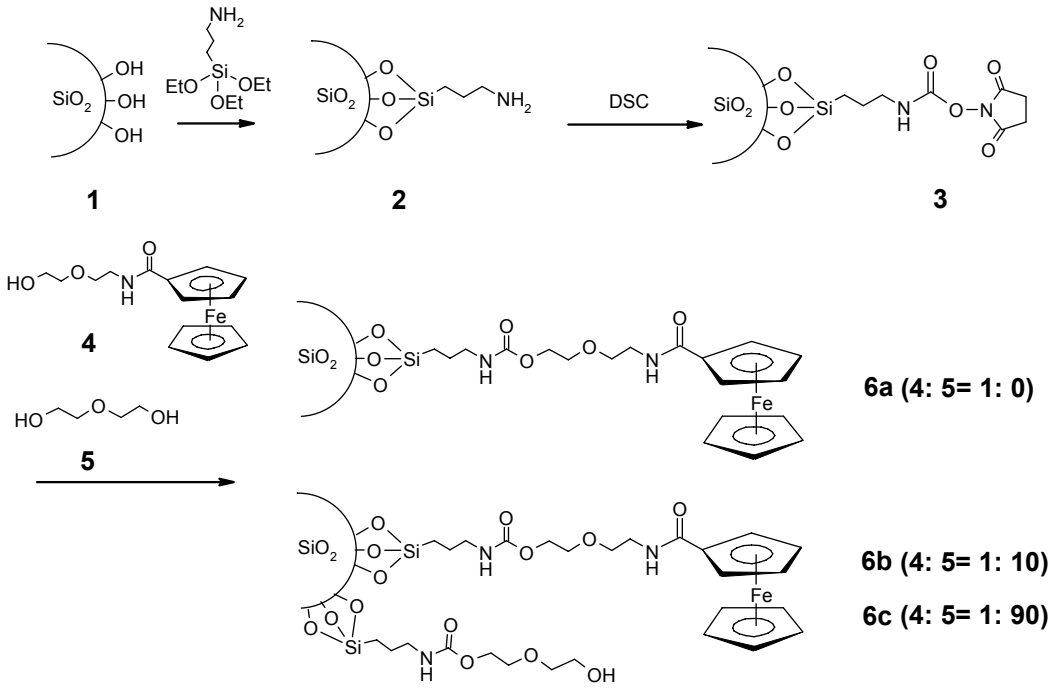

Scheme 3.1. Functionalization routes towards ferrocenyl-functionalized silica nanoparticles, with indicated ratio of 2-ferrocenyl amidoethoxyethanol (**4**) and diethylene glycol (**5**).

The conversion of **2** to **6a - 6c** was qualitatively examined by Fourier Transform Infrared (FT-IR) spectroscopy (Figure 3.1). The spectrum of **2** shows a sharp -NH stretch and a small primary NH_2 deformation at ~3400 cm^{-1} and ~1635 cm^{-1}, respectively. For **6a**, the primary amine peak was smaller and another peak appeared at ~1650 cm^{-1}, indicating the formation of the newly formed amide group. The fact that the primary amine peak did not completely disappear indicates that not all **4** added to the reaction is incorporated onto the surface of **6**, possibly due to incomplete functionalization in the preceding step leading to **3**. For **6b** and **6c**, the amide peak remained and the amine peak became less apparent. These spectra also show a drastic broadening of the peak at ~3400 cm^{-1}, indicating the presence of OH groups at the surface of these nanoparticles. It was impossible to identify the ether stretch vibrations as they overlap with the more dominant Si-O-Si antisymmetric stretching. The ring breathing vibration of ferrocene was not observed in all **6a** – **6c** as the concentration of ferrocene was in all cases far below the detection limit.

Particles **6a - 6c** were made from the same batch of **1.** Hence, the size and size distribution of **6b** were measured to represent all batches of **6a - 6c**. SEM showed that the

average particle diameter distribution of **6b** was 59 ± 11 nm. The dried particles, after repeated purification by centrifugation and freeze drying, displayed a yellowish color, indicating the presence of ferrocene.

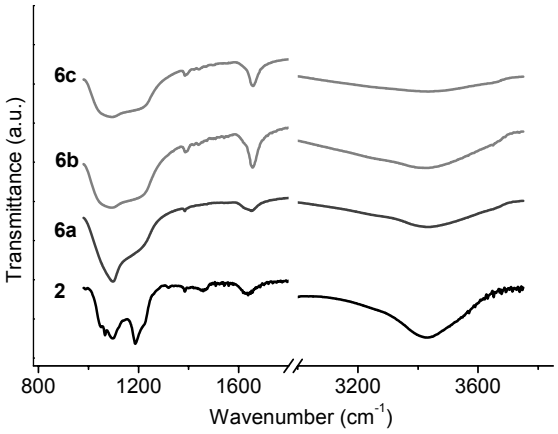

Figure 3.1. FT-IR spectra of **2** and **6a** - **6c**.

X-ray photoelectron spectroscopy (XPS) was used to determine the surface composition of ferrocene on the silica nanoparticles. The high-resolution Fe 2p scans for the starting compound (**4**) and **6a** - **6c** are given in Figure 3.2. All elemental scans show two peaks at ~ 722.3 eV and at ~ 709.0 eV, with intensities of approximately 1 : 2 ratio, corresponding to the Fe $2p_{1/2}$ and Fe $2p_{3/2}$, which is in agreement with control compound **4**. These features clearly demonstrate the presence of ferrocenyl groups on the nanoparticles.

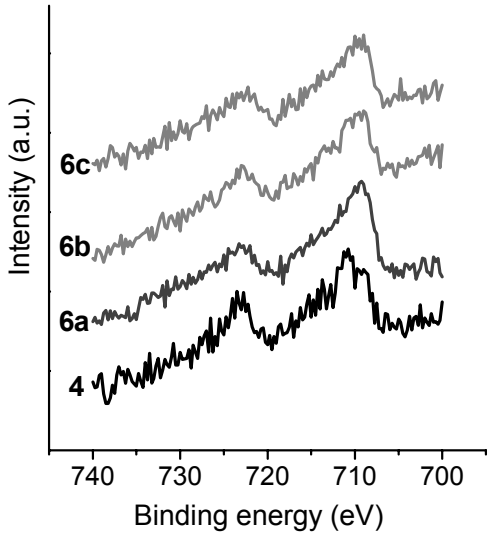

Figure 3.2. High-resolution XPS Fe 2p spectra of **4** and **6a** - **6c**.

Knowing the density of ferrocenyl groups is crucial for control of the host-guest interactions. Table 3.1 compares the iron to nitrogen (Fe/N) atomic ratios and weight percentages of iron on nanoparticle **6a** - **6c**, as obtained from XPS and elemental analysis, respectively. The Fe/N ratio decreased from 0.09 to 0.04 for particles **6a** to **6c**, with decreasing amounts of ferrocenyl groups taking part in the reactions. These ratios are lower than the theoretical maximum Fe/N value of 0.33, when assuming that the surface is fully functionalized with **4** (see Scheme 3.1.).[24,25,26] In the case of **6a**, this indicates that the functionalization of amino groups to carbamates and/or further to ferrocenyl was incomplete. In other words, there are unfunctionalized amino groups present on the surface of the nanoparticles. The relative similarity of the Fe/N ratios for **6a** - **6c**, especially when taking into account the large excess of **5** relative to **4** employed in the case of **6b** and, even more so, **6c**, indicate a more efficient functionalization and/or a higher reactivity of the ferrocenyl precursor (**4**) compared to diethylene glycol (**5**).

Table 3.1. The atomic Fe/N ratios and Fe weight percentages for **6a** - **6c**, as obtained from XPS and elemental analysis, respectively.

Sample	Fe/N atomic ratio (XPS)	Fe wt/wt % (elem. anal.)
6a	0.09	0.20
6b	0.05	0.13
6c	0.04	0.14

The iron weight percentages of nanoparticles **6a** - **6c** were 0.20 %, 0.13 % and 0.14 %, respectively. In general, elemental analysis is useful to approximate the molecular formula from weight percentages of carbon, nitrogen, hydrogen, and oxygen. However, in this case, due to excessively large amounts of silica in each sample, it is not appropriate to estimate ratios of ferrocenyl and diethylene glycol chains from such elements data.

The results from elemental analyses were recalculated to numbers of ferrocenyl groups per nanoparticle. The theoretical maximum number of ferrocenyl groups that can occupy the surface of a SiO_2 nanoparticle of average 59 nm in diameter, is about 32000.[24] Based on the elemental analysis data, the experimental average numbers of ferrocenyl groups per nanoparticle for **6a - 6c** were approximately 5000, 3200, and 3350,[27] which correspond to 16 %, 10 %, and 11 % of the maximal geometrical occupancy, respectively. These occupancies reveal that the ferrocenyl moieties are widely dispersed over the silica surface and hence have sufficient freedom to exhibit host-guest interactions with CD molecules. In

fact, the geometrical percentages can also be directly compared to the Fe/N ratios obtained by XPS. Taking **6a** as an example, 16 % surface coverage by ferrocenyl groups implies that ~ 8 % of the amino groups of **3** reacted with **4**,[24] which indicates an Fe/N ratio after functionalization of 0.07, which compares well to the experimental value (0.09). By using the same approach, Fe/N ratios of 0.05 was estimated for both **6b** and **6c.** These calculations again nicely correlated with the experimental Fe/N ratios. Due to the high similarity between **6b** and **6c**, only **6b** was further compared to **6a** in the experiments described below.

The average hydrodynamic diameter, d_{av}, which reveals the nanoparticle dispersity or aggregation behavior in different buffer solutions (either in the presence or absence of 10 mM native CD) was studied by dynamic light scattering (DLS), as shown in Table 3.2. All DLS data showed considerably higher d_{av} values as compared to those measured with SEM. This is because the hydrodynamic diameter depends on the nanoparticle shape (conformation) as well as the molecular mass. Small amounts of aggregates in the solution will distinctly influence the overall average size. Therefore, it is not surprising that the hydrodynamic size differs significantly from the true physical size.[28] As shown in Table 3.2, nanoparticle **6a** was unable to disperse well in buffers of any pH. The dispersity slightly improved in the presence of 10 mM CD at pH 2.0 or pH 9.5. Conversely, nanoparticle **6b** showed much better dispersity in all buffers. Only a slight increase in d_{av} was observed in water (pH 5.7) and HEPES buffer (pH 7.0). In buffer with native CD, the dispersity of **6b** at pH 5.7 and 7.0 actually worsened as compared to buffer without native CD, while at pH 2.0 or 9.5, the nanoparticles remained reasonably dispersed.

Table 3.2. Average hydrodynamic diameters, d_{av}, of particles **4** and **5** in the absence and presence of 10 mM CD as a function of pH of the buffer solution.

	6a		**6b**	
pH	d_{av} in buffer (nm)	d_{av} in buffer with CD (nm)	d_{av} in buffer (nm)	d_{av} in buffer with CD (nm)
2.0 (aq. HCl)	>1000	390.8	163.9	164.3
4.0 (acetate buffer)	>1000	980.5	177.4	216.5
5.7 (water)	>1000	>1000	234.9	>1000
7.0 (HEPES buffer)	>1000	>1000	269.4	495.7
9.5 (carbonate buffer)	>1000	294.2	179.1	220.2

It is not surprising that **6a** did not disperse well in aqueous buffer at any pH, considering a large fraction of its surface is functionalized with hydrophobic ferrocenyl groups. Its solubility improved in the presence of 10 mM β-CD at pH 9.5 and at pH 2.0, which indirectly indicates that ferrocene complexes with native β-CD in solution. In contrast, **6b** has much a better dispersity. This can be rationalized by the presence of hydrophilic diethylene glycol chains and by a lower coverage of hydrophobic ferrocenyl groups.

The surface charges of **6a** and **6b** over this pH range as assessed by zeta potential measurements (Figure 3.3) provided further support of the DLS data. The zeta potentials in pure buffer solutions and in the presence of CD were comparable at all pH values (data not shown). **6a** and **6b** exhibited comparable surface charges over the whole pH range. Both exhibited positive surface charges at pH 2.0, which inversed with increasing pH. At pH 9.5, the nanoparticles possessed clearly negative surface charges. We interpret these data as follows: at low pH, the protonation of unreacted amino groups creates positive charges at the surface of the nanoparticles.[29] Both nanoparticle dispersions revealed an isoelectric point at pH 7, which explains the aggregation of nanoparticles around this pH. The charge reversal to negative charge, which is typical for unfunctionalized silica nanoparticles,[30] is probably caused by binding of (hydroxyl) anions to the surface silanol groups of the nanoparticles at high pH. This conveys stability to the nanoparticle dispersion in the case of **6b**. As for **6a**, negative charges were insufficient to improve its dispersity, possibly because of the domination of the hydrophobicity of the ferrocenyl groups on the surface.

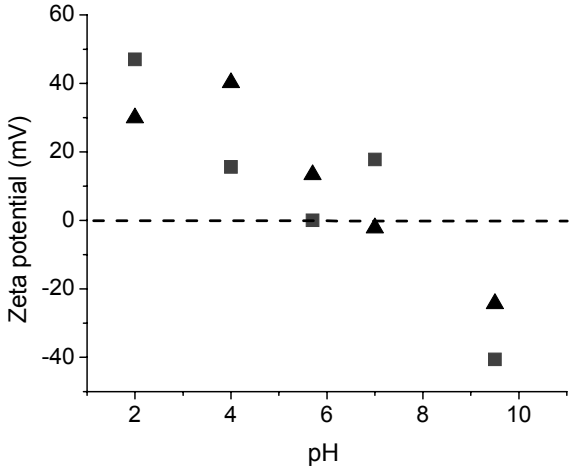

Figure 3.3. Zeta potentials of dispersions of **6a** (■) and **6b** (▲) as a function of the pH of the buffer solution.

For solubility reasons, we continued further electrochemistry and assembly experiments with **6b** only. Electrochemistry was performed in a solution of **6b** (0.25 wt %) in 0.1 M aqueous K_2SO_4, with 10 mM carbonate buffer, pH 9.5, to obtain its best dispersity. The electrochemistry of **4** in 0.1 M K_2SO_4 solution was investigated as a control experiment.

The formal potentials (E_o), as measured by differential pulse voltammetry, of **4** and **6b** were 0.44 V (versus Ag/AgCl) and 0.27 V, respectively (data not shown). Both formal potentials fall into the typical formal potential range of ferrocene, which again proves the presence of ferrocenyl groups on the surface of **6b**.[31] The slightly lower formal potential of **6b** compared to **4** can be attributed to a different solution environment as influenced by the surface immobilization, different pH, surface charging, etc.

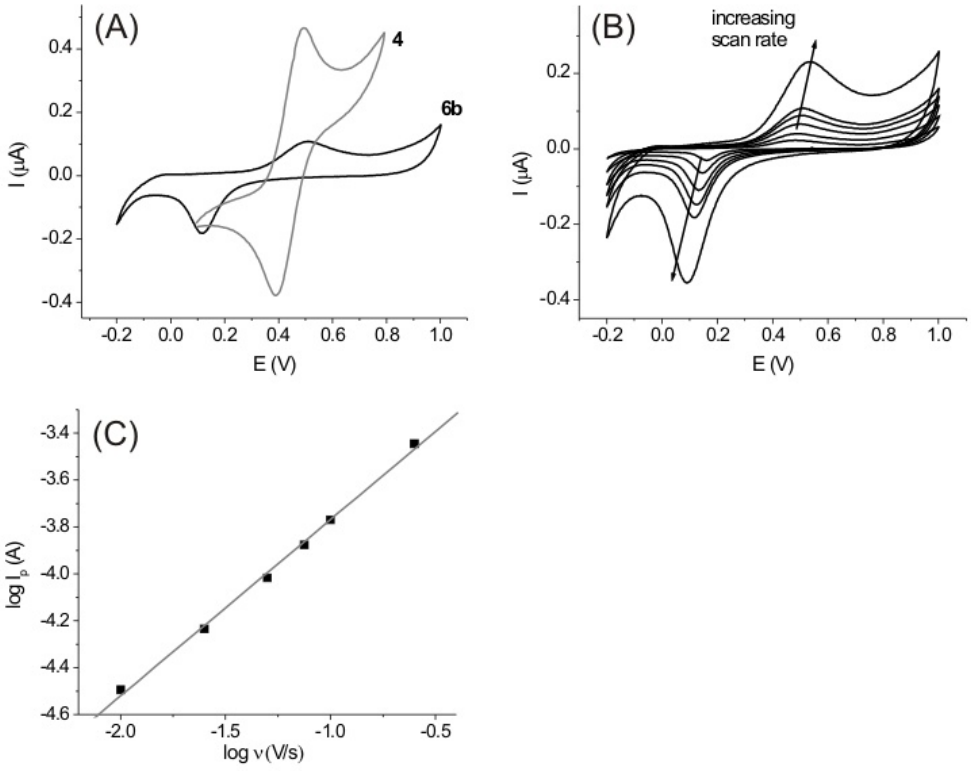

Figure 3.4. (A) Cyclic voltammograms (vs. Ag/AgCl) of **4** and **6b**, in 0.1 M K_2SO_4 at 0.1 V/s. The pH of the solution of **6b** was adjusted to 9.5 by using a carbonate buffer. (B) Cyclic voltammograms of **6b** at scan rates varying from 0.01 V/s to 0.25 V/s. (C) Plot of the oxidation peak current, $I_{p,}$ vs. scan rate, ν.

The cyclic voltammograms (CVs) of **4** and solutions of **6b** are shown in Figure 3.4A. The solution of **4** showed a typical reversible electrochemical reaction, with an oxidation

peak at 0.49 V. For the ferrocenyl-functionalized silica nanoparticles **6b**, a single distinctive oxidation peak occurred at 0.52 V, while its reduction peak at 0.12 V was well separated. The observed single oxidation wave suggests that all ferrocenyl groups within electrode proximity are electrochemically equivalent. The appearance of the reduction peak at a lower potential compared to **4** indicates that, for **6b**, the current responds more sluggishly to the applied voltage compared to the reversible system of **4**. In addition, the anodic and cathodic peaks are fully separated. The combined observations strongly indicate that the electrochemistry of **6b** is that of a totally irreversible system.[32]

Figure 3.4B illustrates the CVs of **6b** as a function of scan rate. The peak potentials shifted to more positive and more negative for the anodic and cathodic peaks, respectively, with increasing scan rates. This indicates a slow electron transfer process with respect to the time scale of the experiment.[32] In general the cathodic scans displayed narrower reduction peaks, which can be attributed to adsorption of **6b** on the electrode as ferrocenium-functionalized particles (Fc^{+}-SiO_2).

The absolute shifted ratio of the cathodic to anodic peak currents ($|I_{p,C}/I_{p,A*}|$) was examined.[33] If the redox reaction would be coupled to chemical reactions, e.g., carbamate bond dissociation leading to ferrocene removal from the nanoparticle surface, the peak current of the reverse scan would be affected, resulting in non-unity $|I_{p,C}/I_{p,A*}|$ ratios. At all scan rates, the $|I_{p,C}/I_{p,A*}|$ ratios were close to 1, demonstrating that no chemical reaction was involved during CV. Thus we conclude that the ferrocenyl groups remain robustly attached to the nanoparticle surface within the experimental potential range.

The electron transfer kinetics of **6b** was determined by plotting the peak current, I_p vs. the scan rate, ν (Figure 3.4C). A linear relationship was obtained, with a slope of 0.75. This is an intermediate value between diffusion-controlled kinetics (0.5) and surface-confined kinetics (1.0), suggesting a "mixed" diffusion-adsorption behavior.[32] This could be due to the sluggish electron transfer kinetics between ferrocenyl groups on the nanoparticle surface and the electrode. Also, mass transport limitation may be involved as the 60 nm ferrocenyl-functionalized nanoparticles are comparatively large and therefore diffuse slowly.[34]

The adsorption behavior of **6b** in 10 mM carbonate buffer at pH 9.5 was monitored by surface plasmon resonance (SPR) spectroscopy on CD and 1-mercapto-11-undecyl-tetra(ethylene glycol) (PEG) SAMs. The SPR reflectivity (R) changes upon injection of an aqueous solution of **6b** are shown in Figure 3.5. The adsorption was followed for 50 min followed by rinsing of the cell with the same buffer solution. The adsorption of **6b** onto the CD SAM was clearly observed, while insignificant adsorption was seen on a PEG SAM. This

provides strong evidence that CD-ferrocene host-guest interactions mediate the adsorption of **6b** onto the CD SAM. The absence of desorption upon rinsing after adsorption indicated that the nanoparticles had formed stable assemblies on the surface of CD SAM.

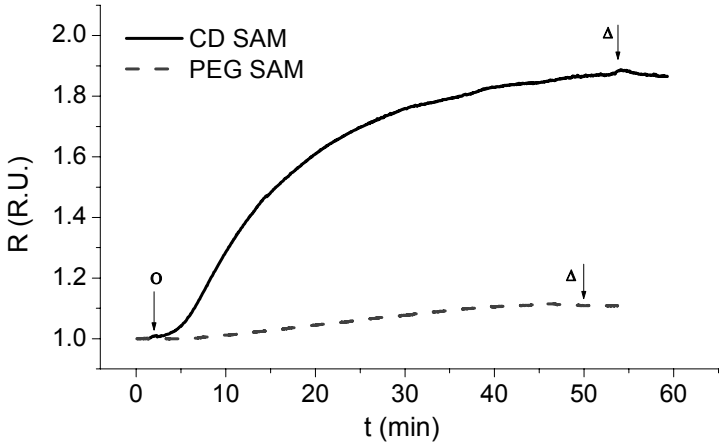

Figure 3.5. SPR sensorgrams of the adsorption of **6b** on CD and PEG SAMs. Symbol 'o' indicates the addition of 0.25 wt % of **6b** solution in a carbonate buffer, pH 9.5; symbol 'Δ' indicates the onset of rinsing with the same carbonate buffer.

The supramolecular specificity of the ferrocenyl-functionalized silica nanoparticles at interfaces was also visualized by SEM. The experiments were done by drop casting a solution of **6b** on surfaces with different self-assembled monolayers for 10 min. The substrates were then rinsed extensively with native CD solution and sonicated in Milli-Q water to remove any non-specifically bound nanoparticles. Figure 3.6 shows SEM micrographs of nanoparticles **6b** on a CD SAM, an amino-terminated SAM and a freshly cleaned silicon substrate with silanol groups, respectively. The images in Figure 3.6 show that nanoparticles were successfully adsorbed onto the CD SAM, whereas hardly any nanoparticle was absorbed onto the amino and silica surfaces. These observations provide a visual proof of the specificity of the host-guest interactions between CD and ferrocenyl-functionalized silica nanoparticles on the CD SAM. The fact that the nanoparticles remain attached on the CD SAM, even after sonication in water, indicates a strong interaction between the nanoparticles and the surface, likely owing to the formation of multivalent interactions.[35]

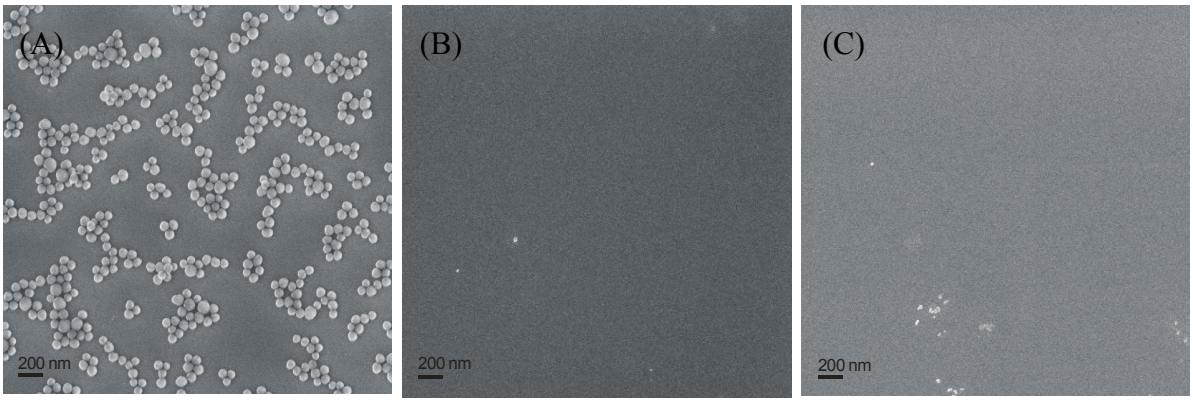

Figure 3.6. SEM micrographs of the adsorption (10 min) of **6b** (0.25 wt %, in a carbonate buffer, pH 9.5) on a CD SAM (A), an amino-terminated SAM (B), and a freshly oxidized silicon substrate (C).

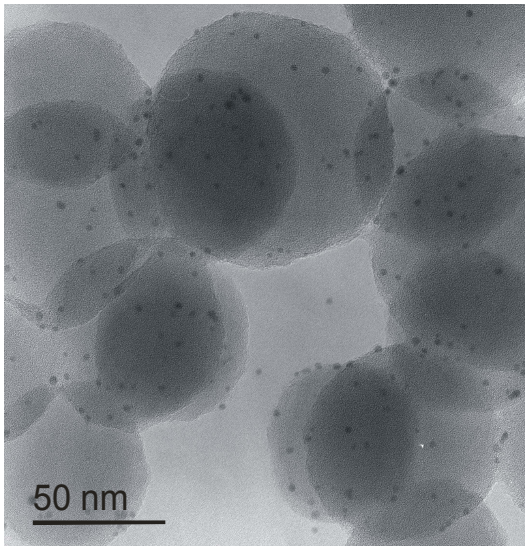

Figure 3.7. TEM picture of 60 nm ferrocenyl-functionalized silica particles, decorated with ~3-nm CD-functionalized gold nanoparticles via specific host-guest interactions.

As a step towards making more complex structures on surfaces, we take advantage of the highly specific supramolecular recognition properties by decorating the surfaces of the ferrocenyl-functionalized silica nanoparticles with CD-functionalized gold nanoparticles of ~3 nm.[4] This was done by adding the gold nanoparticles to the solution of **6b**, where the molar ratio of CD to Fc was set to 1:10. The TEM picture in Figure 3.7 shows that most gold nanoparticles were attached onto the surfaces of SiO_2-Fc nanoparticles. Only a few gold nanoparticles remained unattached. For each touching silica nanoparticle pair, there was at least one gold nanoparticle present at the interface, indicating that larger binary nanostructures had already formed as well.

3.3 CONCLUSIONS

The preparation, characterization and molecular recognition at interfaces of ferrocenyl-functionalized silica nanoparticles were presented in this chapter. These nanoparticles displayed specific molecular recognition properties towards complementary host surfaces and nanoparticles. The strategy of employing chemically driven assembly of functionalized nanoparticles on functionalized substrates is an attractive option for fabricating nanoparticle arrays. In particular, implementation of simple structures into potentially useful, complex ones, on submicron scales, where tunable surface properties are favorable, is of importance for future nanotechnological developments.

3.4 EXPERIMENTAL

Chemicals. Tetraethyl orthosilicate, 3-aminopropyl triethoxysilane (APTES), concentrated ammonium hydroxide, *N,N'*-disuccinimidyl carbonate (DSC), 2-(*N*-morpholino)-ethanesulfonic acid (MES), 4-(2-hydroxyethyl)piperazine-1-ethanesulfonic acid (HEPES), 11-mercapto-1-undecanol and *N*-[3-(trimethoxysilyl)propyl)]ethylenediamine were obtained from commercial sources. Milli-Q water with a resistivity greater than 18 MΩ.cm was used in all our experiments. CD heptamine,[36] CD heptathioether[12] and 1-mercaptoundec-11-yl-tetra(ethylene glycol)[37] were synthesized as described before. NMR spectra were recorded on a Varian AMX400 spectrometer. FAB-MS spectra were recorded with a Finnigan MAT 95 spectrometer.

Synthesis of 2-ferrocenyl amidoethoxyethanol, 4. A solution of 2-(2-aminoethoxy)ethanol in CH_2Cl_2 was added to 1-(chlorocarbonyl)-ferrocene[38] (1.0 g, 4.0 mmol) in CH_2Cl_2. After stirring overnight at room temperature, the reaction mixture was washed with saturated $NaHCO_3$, 0.1 M HCl and saturated NaCl, respectively and dried over $MgSO_4$. The product was purified by column chromatography over silica, using MeOH/CH_2Cl_2: 3/97 as eluent solution, and isolated as dark red/ orange crystals. ^{1}H NMR (400 MHz, DMF-d_7) δ (ppm): 7.80 (t, 1H, OH), 4.82 (t, 2H, Fc, J = 4.0 Hz), δ 4.62 (t, 2H, CONH), 4.31 (t, 2H, Fc, J = 4.0 Hz), 4.17 (s, 5H, Fc), 3.60 (t, 2H, $NHCH_2$), 3.56 (t, 2H, CH_2O), 3.51 (t, 2H, OCH_2), 3.42 (q, 2H, CH_2OH, J = 14.0 Hz). ^{13}C NMR (400 MHz, DMF-d_7) δ (ppm): δ 169.36 (CO), 69.94, 69.50, 68.29 (Fc), 77.13, 60.93 (CH_2NH), 72.61 (CH_2O), 69.76 (OCH_2), 39.05 (CH_2OH). FAB-MS. Calcd for $C_{15}H_{19}NO_3Fe$: m/z = 317.1. Found: m/z = 318.3 [M+H].

Preparation of bare silica nanoparticles, 1. Bare silica nanoparticles were synthesized following a literature procedure.[39] Briefly, 3.8 ml of tetraethyl orthosilicate was added to a flask containing 5.7 ml of concentrated ammoniumhydroxide and 114 ml of ethanol while stirring. The stirring was continued overnight. This resulted in the formation of approximately 60 nm silica nanoparticles **1**.

Preparation of amino-functionalized silica nanoparticles, 2. Silica nanoparticles **1** were functionalized with APTES by quickly adding 2.3 ml of APTES to 120 ml of a vigorously stirred dispersion of **1** in ethanol, and the mixture was allowed to stir overnight at room temperature. The nanoparticles were purified by centrifugation and redispersion in 60 ml of DMF, which was repeated three times.

Preparation of carbamate -functionalized silica nanoparticles, 3. The amino groups of silica nanoparticles **2** were activated by slowly adding DSC (1.46 g, 5.7 mmol) in DMF to 60 ml of amino-functionalized nanoparticles **2**. The mixture was stirred for 4 h and purified by repeated centrifugation and redispersion in DMF for at least three times.

Preparation of ferrocenyl-functionalized silica nanoparticles, 6. Mixtures of 2-ferrocenyl amido ethoxy ethanol and diethylene glycol (5 ml, molar ratios 1:0, 1:10 and 1:90) were prepared prior to functionalization of **3**. Each mixture was added slowly to a 5 ml dispersion of **3** in DMF. The concentration of the silica nanoparticles was estimated to be ~2 × 10^{12} per ml.[18] Stirring was continued overnight and products (nanoparticles **6a - 6c**, respectively) were purified by repeated centrifugation and redispersion in water for at least three times. Finally, the nanoparticles were freeze-dried and kept at room temperature as a yellowish and opaque solid.

Substrate and monolayer preparation. All adsorbate solutions were prepared freshly prior to use. Round glass-supported gold substrates for SPR (2.54 cm diameter; 47.5 nm Au) were obtained from Ssens BV (Hengelo, The Netherlands). Gold substrates were cleaned by immersing the substrates in piranha (conc. H_2SO_4 and 33% H_2O_2 in a 3:1 ratio). (**Warning!** piranha should be handled with caution; it can detonate unexpectedly) for 10 s and leaving the substrates for 5 min in absolute ethanol. The substrates were subsequently immersed into a 0.1 mM CD heptathioether adsorbate solution in EtOH and $CHCl_3$ (1:2 v/v) for 16 h at 60 °C. 1-mercapto-11-undecyl-tetra(ethylene glycol) (PEG) SAMs were adsorbed from EtOH at r.t. for 24 h. The samples were removed from the solution and rinsed with substantial amounts of $CHCl_3$, EtOH and Milli-Q water.

Silicon substrates were oxidized first by immersion in piranha solution for 15 min to form SiO_x with a thickness of approximately 1.5 nm. The substrates were then sonicated in acetone and ethanol for 1 min, and blown dry with N_2. CD SAMs were obtained using a slightly modified procedure.[13] In brief, the substrates were functionalized with amino groups by gas-phase evaporation of *N*-[3-(trimethoxysilyl)propyl]ethylenediamine in a desiccator under vacuum. The samples were left several hours and then carefully rinsed with ethanol and Milli-Q water. Transformation of the amino-terminated SAMs to isothiocyanate-bearing layers was accomplished by exposure to a solution of 1,4-phenylene diisothiocyanate at 50 ^{o}C, 2 h. CD SAMs were finally obtained by reaction of the isothiocyanate-terminated monolayer with CD heptamine, at 50 ^{o}C for 2 h.

Fourier Transform Infrared spectrometry (FT-IR). Infrared spectra were recorded on a Perkin–Elmer Spectrum BX spectrometer, using KBr pellets that contained 2–5 mg of nanoparticles **2** or **6a-6c**.

X-ray photoelectron spectroscopy (XPS). XPS was performed on a PHI Quantera SXM, using a monochromated Al K alfa X-ray source with an energy of 1486.6 eV. An X-ray beam with a diameter of 100 micrometer and a power of 25 W was used. Element scans were measured at a pass energy of 140 eV and a stepsize of 0.25 eV The N1s peak was used as reference with a binding energy of 400.1 eV. Samples were neutralized with low energy Ar ions and electrons during measurement.

Elemental analysis. The weight content of iron in each sample was measured by atomic absorption spectrometry (AAS, Unicam). The organic compounds were dissolved in H_2SO_4 and HNO_3, and silica was decomposed by HF.

Dynamic light scattering (DLS). DLS experiments were performed with a Zetasizer 4000 (Malvern Instruments Ltd., U.K.) at 25 °C using a laser wavelength of 633 nm at a scattering angle of 90°. Results obtained are the averages of three measurements. The average hydrodynamic diameter

(d_{av}) of silica nanoparticles at various pH values were determined on 1.5 ml samples in corresponding buffer solutions. The dispersions were gently shaken before the measurements for proper mixing.

Zeta potential. Zeta potentials of the silica nanoparticles were obtained with a Zetasizer 2000 (Malvern Instruments Ltd., U.K.) using the Laser Doppler velocimetry technique in which the velocity of the particles in a fluid that results from an applied electrical field is measured. Measurements were performed at 25 °C using a 1000 Hz modulator frequency and a cell drive voltage of 120 V. The values reported are the averages of ten measurements.

Electrochemistry. Electrochemical measurements were performed with an AUTOLAB PGSTAT10 in a custom built three-electrode setup with bare Au substrates as the working electrode (area exposed to the solution = 0.44 cm^2), a Ag/AgCl reference electrode, and a platinum wire as counter electrode.

Surface plasmon resonance (SPR). The SPR setup was obtained from Resonant Probes GmBH. The instrument consists of a HeNe laser (JDS Uniphase, 10 mW, λ=632.8 nm) whose light passes through a chopper that is connected to a lock-in amplifier (EG&G 7256). The modulated beam is directed through two polarizers (OWIS) to control the intensity and the plane of polarization of the light. The light is coupled via a high-index prism (Scott, LaSFN9) in the Kretschmann configuration to the backside of the gold-coated substrate, which is optically matched through a refractive-index-matching oil (Cargille; series B; n_D^{25}=1.700 ± 0.002) at the prism, mounted on a θ - 2θ goniometer in contact with a Teflon cell with a volume of 113 mm^3 and a diameter of 6 mm. The light that leaves the prism passes through a beam splitter; subsequently, the s-polarized light is directed to a reference detector, and the p-polarized light passes through a lens which focuses the light onto a photodiode detector. Laser fluctuations are filtered out by dividing the intensity of the p-polarized light (I_p) by the intensity of the s-polarized light (I_s). The SPR experiments were performed in a flow cell system.

Scanning and transmission electron microscopy (SEM, TEM). All SEM images were taken with a HR-LEO 1550 FEF SEM. TEM was performed on a Philips CM 30 Twin STEM fitted Kevex delta plus X-ray disperse electron spectroscopy (EDX) and Gatan model 666 PEELs operating at 300 kV. Samples for imaging were deposited onto a 200 mesh copper grid, and the liquid was allowed to dry in air at room temperature.

3.5 ACKNOWLEDGEMENTS

Dr. C.W. Lim is acknowledged for fruitful discussions on the functionalization of SiO_2-Fc, Dr. E.A. Speets for XPS measurements, and Dr. O. Crespo-Biel for providing the Au-CD nanoparticles.

3.6 REFERENCES AND NOTES

1. Daniel, M.-C.; Astruc, D. *Chem. Rev.* **2004**, *104*, 293.
2. Paraschiv, V.; Zapotoczny, S.; De Jong, M. R.; Vancso, G. J.; Huskens, J.; Reinhoudt, D. N. *Adv. Mater.* **2002**, *14*, 722.
3. Decher, G.; Hong, J. D.; Schmitt, J. *Thin Solid Films* **1992**, *210 & 211*, 831.
4. Crespo-Biel, O.; Juković, A.; Karlsson, M.; Reinhoudt, D. N.; Huskens, J. *Isr. J. Chem*. **2005**, *45*, 353.
5. Kotov, N. A.; Dékány, I.; Fendler, J. H. *J. Phys. Chem.* **1995**, *99*, 13065.

6. Nakanishi, T.; Ohtani, B.; Shimazu, K.; Uosaki, K. *Chem. Phys. Lett.* **1997**, *278*, 233.
7. Chen, K. M.; Jiang, X.; Kimerling, L. C.; Hammond, P. T. *Langmuir* **2000**, *16*, 7825.
8. Maury, P.; Péter, M.; Mahalingam, V.; Reinhoudt, D. N.; Huskens. *J. Adv. Funct. Mater.* **2005**, *15*, 451.
9. Kiely, C. J.; Fink, J.; Zheng, J. G.; Brust, M.; Bethell, D.; Schiffrin, D. J. *Adv. Mater.* **2000**, *12*, 640.
10. Whitesides, G. M.; Boncheva, M. *Proc. Natl. Acad. Sci. USA* **2002**, *99*, 4769.
11. Reinhoudt, D. N.; Crego-Calama, M. *Science* **2002**, *295*, 2403.
12. Beulen, M. W. J.; Bügler, J.; Lammerink, B.; Geurts, F. A. J.; Biemond, E. M. E. F.; Van Leerdam, K. G. C.; Van Veggel, F. C. J. M.; Engbersen, J. F. J.; Reinhoudt, D. N. *Langmuir* **1998**, *14*, 6424.
13. Onclin, S.; Mulder, A.; Huskens, J.; Ravoo, B. J.; Reinhoudt, D. N. *Langmuir* **2004**, *20*, 5460.
14. Huskens, J.; Deij, M. A.; Reinhoudt, D. N. *Angew. Chem. Int. Ed.* **2002**, *41*, 4467.
15. Auletta, T.; Dordi, B.; Mulder, A.; Sartori, A.; Onclin, S.; Bruinink, C. M.; Péter, M.; Nijhuis, C. A.; Beijleveld, H.; Schönherr, H.; Vancso, G. J.; Casnati, A.; Ungaro, R.; Ravoo, B. J.; Huskens, J.; Reinhoudt, D. N. *Angew. Chem. Int. Ed.* **2004**, *43*, 369.
16. Nijhuis, C. A.; Huskens, J.; Reinhoudt, D. N. *J. Am. Chem. Soc.* **2004**, *126*, 12266.
17. Nijhuis, C. A.; Yu, F.; Knoll, W.; Huskens, J.; Reinhoudt, D. N. *Langmuir* **2005**, *21*, 7866.
18. Mahalingam, V.; Onclin, S.; Péter, M.; Ravoo, B. J.; Huskens, J.; Reinhoudt, D. N. *Langmuir* **2004**, *20*, 11756.
19. Ingram, R. S.; Hostetler, M. J.; Murray, R. W. *J. Am. Chem. Soc.* **1997**, *119*, 9175.
20. Chen, S. *Langmuir* **2001**, *17*, 6664.
21. Labande, A.; Ruiz, J.; Astruc, D. *J. Am. Chem. Soc.* **2002**, *124*, 1782.
22. Xu, C.; Aoki, K. *Langmuir* **2004**, *20*, 10194.
23. Stöber, W.; Fink, A.; Bohn, E. *J. Colloid Interf. Sci.* **1968**, *26*, 62.
24. Considering the ferrocene headgroup as a hard sphere with a diameter of 6.6 Å. The total surface area of an amino group and a ferrocene moieties are therefore approximately 0.20 and 0.34 nm^2, respectively. Considering the steric hindrance and geometry available on surface of nanoparticle, only ~50 % of the amino groups will react with **4** to form **6**.
25. Chidsey, C. E. D.; Bertozzi, C. R.; Putvinski, T. M.; Mujsce, A. M. *J. Am. Chem. Soc.* **1990**, *112*, 4301.
26. Ulman, *A. Introduction to Thin Organic Films: From Langmuir-Blodgett to Self-Assembly*, Academic Press, Boston, MA, **1991**.
27. Assuming the density of SiO_2 nanoparticles is similar to bulk silica, each nanoparticle of 60 nm weighs 2.3 x 10^{-16}g.

28. Schemitz, K. S. *An Introduction to Dynamic Light Scattering by Macromolecules*, Academic Press, Boston, **1990**.
29. Jesionowski, J. *Coll. Surf. A* **2003**, *222*, 87.
30. Wilhelm, P.; Stephan, D. *J. Coll. Interface Sci.* **2006**, *293*, 88.
31. Li, D.; Zhang, Y.; Jiang, J.; Li, J. *J. Coll. Interface Sci.* **2003**, *264*, 109.
32. Gosser, D. V. Jr., *Cyclic voltammetry: Simulation and analysis of reaction mechanisms,* VCH, New York, **1993**.
33. The anodic peak current ($I_{p,A*}$) is measured by extrapolating the preceding baseline current. For details, see ref. 32.
34. DLS data showed that the diffusion constant of **6b**, in pH 2 water or carbonate buffer, is $2 - 3 \times 10^{-8}$ cm^2/s.
35. Mulder, A.; Huskens, J.; Reinhoudt, D. N. *Org. Biomol. Chem.* **2004**, *23*, 3409.
36. Guillo, F.; Jullien, L.; Hamelin, B.; Lehn, J.-M.; De Robertis, L.; Driguez, H. *Bull. Soc. Chim. Fr*. **1995**, *132*, 857.
37. Pale-Grosdemange, C.; Simon, E. S.; Prime, K. L.; Whitesides, G. M. *J. Am. Chem. Soc.* **1991**, *113*, 12.
38. Cuardo, I.; Morán, M.; Casado, C. M.; Alonso, B.; Lobete, F.; García, B.; Ibisate, M.; Losada, J. *Organometallics* **1996**, *15*, 5278.
39. Hiramatsu, H.; Osterloh, F. E. *Langmuir* **2003,** *19,* 7003.

Chapter 4

An *in situ* study of the adsorption behavior of functionalized particles on self-assembled monolayers *via* different chemical interactions*

ABSTRACT. The formation of particle monolayers by convective assembly was studied *in situ* with three different kinds of particle-surface interactions: adsorption onto native surfaces, with additional electrostatic interactions, and with supramolecular host-guest interactions. In the first case carboxylate-functionalized polystyrene (PS-COOH) particles were assembled onto native silicon oxide surfaces, in the second PS-COOH onto protonated amino-functionalized (NH_3^+) self-assembled monolayers (SAMs), and in the third β-cyclodextrin-functionalized polystyrene (PS-CD) particles onto CD SAMs with pre-adsorbed ferrocenyl-functionalized dendrimers. The adsorption and desorption behavior of particles onto and from these surfaces was observed *in situ* on a horizontal deposition setup, and the packing density and order of the adsorbed particle lattices were compared. The desorption behavior of particles from surfaces was evaluated by reducing the temperature below the dew point, thus initiating water condensation. Particle lattices on native oxide surfaces formed the best hexagonal close packed (hcp) order, and could be easily desorbed by reducing the temperature to below dew point. The electrostatically modified assembly resulted in densely packed, but disordered particle lattices. The specificity and selectivity of the supramolecular assembly process were optimized using ferrocenyl-functionalized dendrimers of low generation and by the introduction of competitive interaction by native CD molecules during the assembly. The fine-tuned supramolecularly formed particle lattices were nearly hcp packed. Both electrostatically and supramolecularly formed lattices of particles were strongly attached to the surfaces and could not be removed by condensation.

---

* This chapter has been published in X. Y. Ling, L. Malaquin, D. N. Reinhoudt, H. Wolf, J. Huskens, An *in situ* study of the adsorption behavior of functionalized nanoparticles on self-assembled monolayers *via* different chemical interactions, *Langmuir* **2007,** *23*, 9990.

4.1 INTRODUCTION

Building up ordered nanostructures from particles has attracted a lot of interest due to the need for miniaturization.[1] The intriguing chemical, electronic, and surface properties that arise from such individual or organized nanometer-sized objects makes them suitable for electronic, optical, and biological applications.[2] In general, there are two approaches to assemble nanostructured materials, namely, physical assembly and chemical assembly (see Chapter 2). The physical assembly technique is based on 'let nature do its work',[3] which includes methods like convective or capillary assembly,[4,5] spin coating,[6] and colloidal epitaxy[7]. In particular, convective assembly is a simple technique that has been frequently employed to integrate non-functionalized particles into hexagonally ordered and close packed single or multilayered particle lattices.[8] The mechanism of convective assembly has been extensively studied by Nagayama *et al*.[9] The major driving force for the assembly is the evaporation of water from the particle suspension. Mobile particles in a thin liquid film are convectively assembled, as a result of the hydrodynamic forces induced by the influx of water close to the drying edge. In general, the particles and surfaces are non-functionalized and hydrophilic, which enable the formation of a stable thin liquid layer at the drying edge with a thickness comparable to the particle diameter. The assembly process starts when the thickness of the solvent layer becomes smaller than the particle diameter.[10] The combined effects of the convective flow and the attractive capillary forces arise when the top of the particles protrude from the solvent layer, leading to the formation of extended layers or multilayers of closely packed particles, by which the local or global free energy reaches a minimum.[11] However, this technique provides limited control over the structure of the particle lattices and the dimensions and complexity of the final assemblies.

Chemical assembly, in particular supramolecular assembly utilizes chemical strategies to precisely direct and control the deposition of functionalized particles onto the substrate, possibly in more complex patterns, where physical assembly of non-functionalized particles is not possible. Typical supramolecular approaches are electrostatic interactions,[12] host-guest interactions,[13] and thiol-based self-assembly[14] In supramolecular assembly, the organization of the particle lattice will no longer solely depend on surface tension and long-range attractive forces that act in lateral direction, but rather on the competition between *lateral* attractive forces and *vertical* supramolecular interactions between functionalized particles and the surface. Electrostatics, owing to its simplicity, has been widely used to assemble chemically functionalized particles onto a surface via the attractive force between two oppositely charged surfaces. Jonas *et al.*, Hammond *et al.*, and our group have independently

reported the selective adsorption (by drop casting) of negatively charged particles onto chemically patterned surfaces.[15-17] The parameters of the adsorption of particles into patterns, *e.g.* pH, drying conditions, ionic strength, and surfactant concentration, were extensively studied. In all cases, the ordering of the particle lattice was imperfect owing to strong binding affinity of the particles for the surface.

Supramolecular host-guest interactions have been exploited for the assembly of receptor-functionalized molecules or particles onto interfaces with molecular recognition abilities. Similar to biomolecules in nature, the 'host' molecules are to interact specifically with complementary 'guest' molecules to form noncovalent host-guest pairs, for instance, crown ether complexation by ammonium SAMs,[18] His-tagged proteins by a Ni-nitrilotriacetic acid-presenting surface.[19] Multivalency is used to enhance the binding affinities and specificities between host and guest as these noncovalent interactions are kinetically labile and are continuously broken and formed.[20,21] Recently, our group introduced the concept of 'molecular printboards', i.e. β-cyclodextrin (CD) SAMs on gold or silicon oxide substrates that possess supramolecular host properties.[22,23] On these CD SAMs, complementary multivalent guest-functionalized dendrimer molecules were adsorbed, resulting in the formation of kinetically stable supramolecular assemblies.[24-26] With the aid of adamantyl- or ferrocenyl-functionalized dendrimers as a noncovalent supramolecular glue, CD-functionalized gold and silica nanoparticles were assembled onto CD SAMs.[13,27,28]Apart from the formation of multivalent and stable assemblies, the supramolecular interaction is also appealing for its highly tunable binding strength. Different guest molecules (e.g., ferrocene and adamantane) with different binding strength can be selected to bind to the CD SAMs with different binding strength.[29] The total number of interactions involved in the assembly can be easily varied by using dendrimers of different generations, therefore altering the total binding strength during the assembly. Competition can be introduced when native CD molecules are added to the particle suspension so that CD hosts on particle surfaces have to compete with the native CD to couple to the surface of the preadsorbed guest-functionalized dendrimers on the CD SAM.

In this chapter, an *in-situ* study of the adsorption and desorption behavior of particles onto and from surfaces for three different kinds of particle-surface interactions, i.e. convective assembly on surfaces, with additional electrostatic interactions and with supramolecular host-guest interactions, is described. The aim was to compare the packing order and density of the particle lattices as a result of different binding affinities between the particles and the surfaces. For the ease of visualization, poly(styrene-co-acrylic acid)

particles with or without CD functionality of about 450 nm in diameter were synthesized and employed in all experiments. The desorption behavior of the particles from the surfaces was evaluated by reducing the temperature to below the condensation temperature.[30] In particular, the supramolecular particle assembly was further fine-tuned by using ferrocenyl dendrimers of different generations and by introducing competition by adding native CD molecules into the particle suspension. Furthermore, the influences of these different assembly schemes on the creation of particle stripes on patterned substrates were studied.

4.2 RESULTS AND DISCUSSION

4.2.1 Preparation and characterization of PS-COOH and PS-CD particles

Core-shell particles of poly(styrene-co-acrylic acid) (PS-COOH) were prepared by seeded emulsifier-free emulsion polymerization (Scheme 4.1).[46,47] Polystyrene core particles (**2**, PS) were prepared using divinylbenzene as a cross-linker. When the conversion of styrene to polystyrene was nearly complete, acrylic acid was grafted subsequently onto the surface of polystyrene, forming poly(styrene-co-acrylic acid) (**3**, PS-COOH) core-shell particles. The carboxylic acid groups of PS-COOH were then converted to activated ester groups by using EDC/NHS to form **4**. The attachment of CD was performed by reacting **4** with CD heptamine, forming **5** (PS-CD).[27]

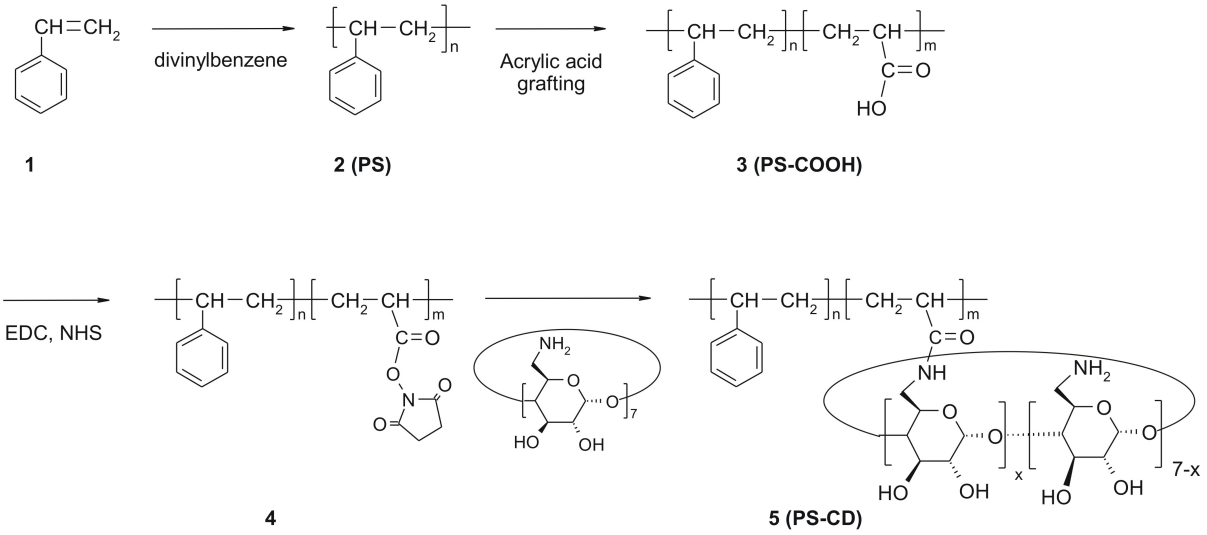

Scheme 4.1. Preparation of carboxylate- and β-cyclodextrin-functionalized poly(styrene-co-acrylic acid) particles.

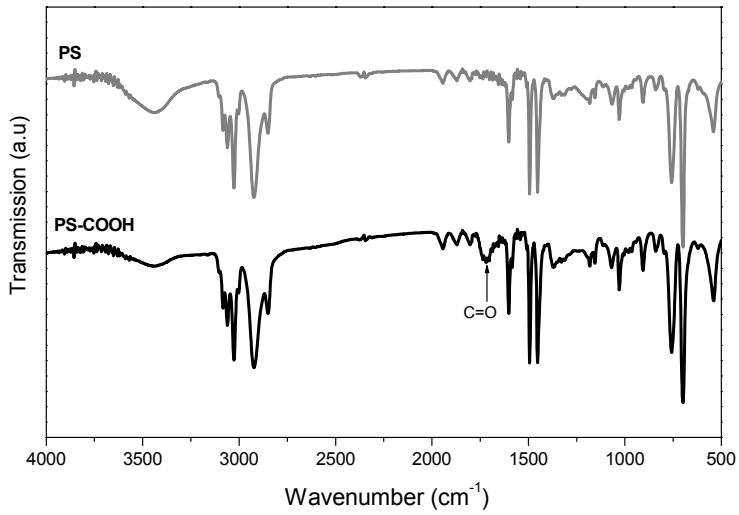

Figure 4.1. FTIR spectra of PS and PS-COOH nanoparticles.

The conversion of styrene and acrylic acid to polystyrene and subsequently to poly(styrene-co-acrylic acid) was followed by gravimetry, which showed ~ 98 % and 100 % conversion, respectively.[31] Samples of PS and PS-COOH particles were collected before and after the grafting of acrylic acid, respectively, and made into KBr pellets for FTIR measurements. The spectrum of PS-COOH was similar to PS, with aromatic CH stretching bands at 1493 and 3010 cm^{-1}; aromatic C=C stretch at 1599 cm^{-1}, and C-C vibrational bands observed at 700, 760, 1030, 1080 cm^{-1} (Figure 4.1).[32,47] CH_2 stretching was also seen at 2920 cm^{-1} for both samples. A distinctive peak at 1710 cm^{-1} was only observed for PS-COOH, clearly indicating the presence of C=O groups.

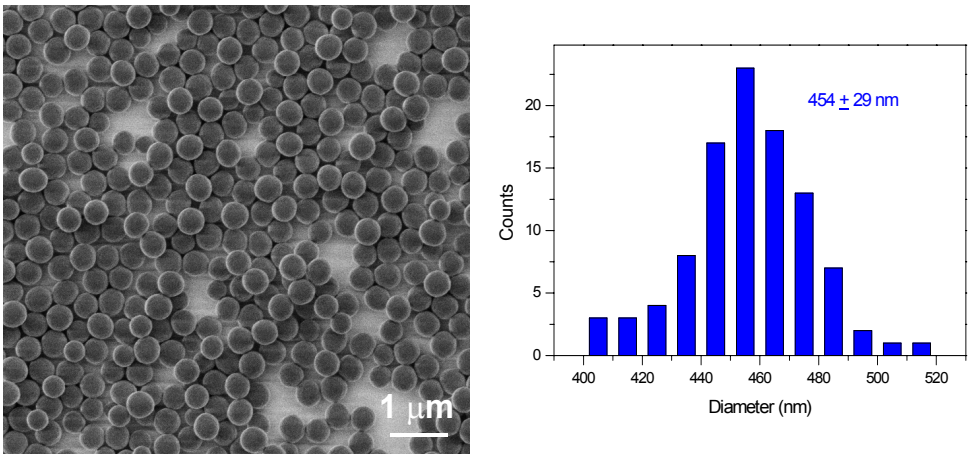

Figure 4.2. SEM image (left) and size distribution histogram (right) of the PS-COOH nanoparticles.

As PS-COOH and PS-CD were prepared from the same batch of reaction, their size and size distribution are not expected to differ. The average particle diameter distribution of PS-COOH was 450 ± 30 nm, as determined by SEM (Figure 4.2).

The host-guest complexation ability of PS-CD in solution in the presence of multivalent guest molecules was determined by DLS. The concept is that a known amount of multivalent guest molecules is added to the measuring particle suspension (concentration of ~4 × 10^{11} particles/mL),[33] such that the multiple binding sites on a guest molecule simultaneously bind two or more adjacent particles. As a result, aggregation occurs which leads to an increase of the hydrodynamic diameter. We used the adamantyl-terminated poly(propylene imine) dendrimer of generation 5 (G5-PPI-$(Ad)_{64}$), which has 64 adamantyl groups for the complexation with CD in solution.[44] The change in average hydrodynamic diameter of particle dispersions of PS-COOH and PS-CD in carbonate buffer as a function of the concentration of G5-PPI-$(Ad)_{64}$ is shown in Figure 4.3. When the amount of multivalent guest molecules was slowly increased, a drastic increase in hydrodynamic diameter of the PS-CD particle suspension was observed, indicative of supramolecular aggregation. In contrast, only a small increase in hydrodynamic radius for PS-COOH was observed, possibly due to electrostatic interactions between the positively charged dendrimers and negatively charged particles in carbonate buffer. This experiment indirectly confirms the presence of β-cyclodextrin on the surface of PS-CD.

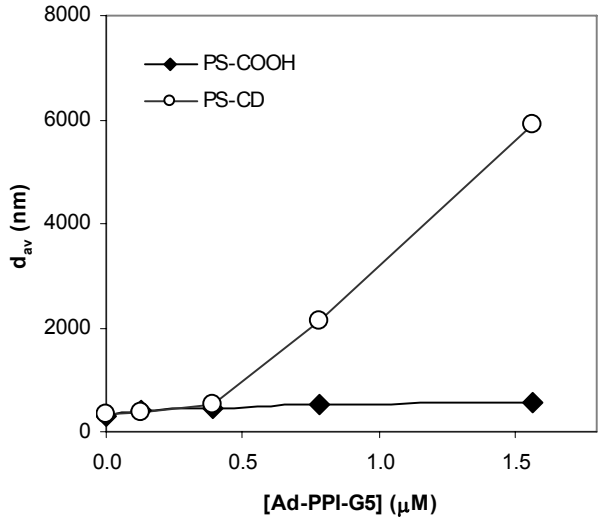

Figure 4.3. The average hydrodynamic diameter (d_{av}) of PS-COOH (♦) and PS-CD (o) particles as a function of the concentration of G5-PPI-$(Ad)_{64}$.

The concentration of CD in the PS-CD particle suspension can be estimated from this aggregation experiment.[27] From Figure 4.3, the aggregation starts when [G5-PPI-$(Ad)_{64}$] > 0.5 μM, which is equivalent to an adamantyl concentration of 32 μM. The aggregation becomes more distinguished with increase of G5-PPI-$(Ad)_{64}$ concentration. Assuming the aggregation sets off when the [Ad]/[CD] molar ratio is greater than 1,[34] the concentration of CD in the PS-CD particle suspension can be estimated to be ~ 32 μM, *i.e.* 48,000 CD molecules occupying on the surface of each particle. These observations suggest that the concentration of CD on the PS-CD particles is lower than of CD heptathioether SAMs on gold,[26] but still sufficiently high for effective multivalent host-guest interactions.

The surface charges of PS-COOH and PS-CD were examined by using zeta potential measurements (Figure 4.4). Buffers from pH 4.0 to 9.0 were used in this study. Both PS-COOH and PS-CD exhibited nearly similar negative charges at all pHs. For pH 5-9, ζ values between -40 and -50 mV were recorded. Only when lowering the pH to 4, a ζ of about -25 mV was observed, which is attributed to partial protonation of the acrylic acid groups (pK_a ~4.5). The similarity between PS-COOH and PS-CD is justified by the core-shell nature of the poly(styrene-co-acrylic acid) particles, and by noting that an excess of unreacted carboxylic acid groups remains on the surface of PS-CD, because only the outer groups react with CD heptamine.

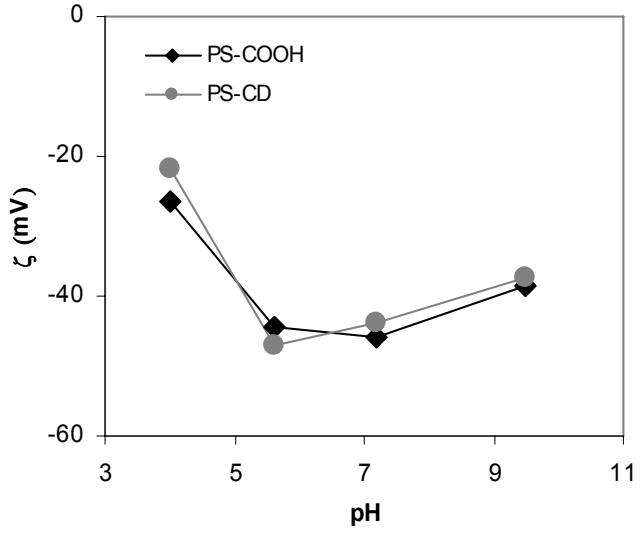

Figure 4.4. Zeta potentials of dispersions of PS-COOH (♦) and PS-CD (●) as a function of the pH of the buffer solution.

4.2.2 Assembly of particles on non-patterned flat surfaces

The adsorption and desorption behavior of the functionalized particles on various substrates was observed *in situ* by optical microscopy. We focused our studies on three basic assembly schemes, *i.e.* convective assembly onto native oxide substrates, with additional electrostatic interactions and with supramolecular (host-guest) interactions. As shown in Scheme 4.2, these interaction systems are represented by adsorption of carboxylate-functionalized polystyrene (PS-COOH) particles onto the native SiO_2 surfaces of piranha-cleaned silicon, PS-COOH onto protonated amino-functionalized (NH_3^+) SAMs and CD-functionalized polystyrene (PS-CD) particles onto CD SAMs with pre-adsorbed ferrocenyl-functionalized dendrimers as a supramolecular glue (Chart 4.1).

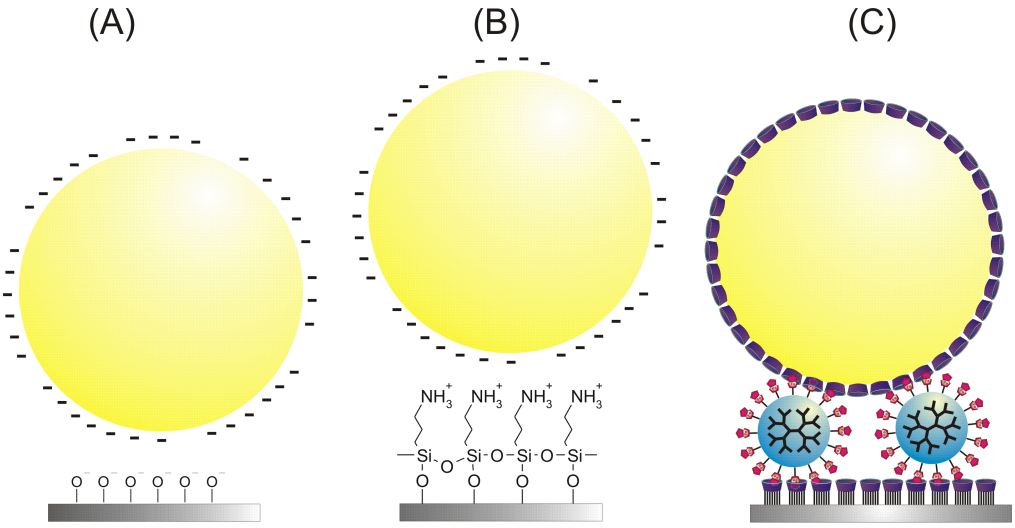

Scheme 4.2. Schematic illustrations (not to scale) of three particle assembly schemes, i.e. convective assembly of PS-COOH on the native SiO_2 surface of silicon (A), convective assembly with additional electrostatic interactions of PS-COOH on an NH_3^+ SAM (B), and convective assembly with additional supramolecular interactions of PS-CD with complementary pre-adsorbed ferrocenyl-functionalized dendrimers on a CD SAM.

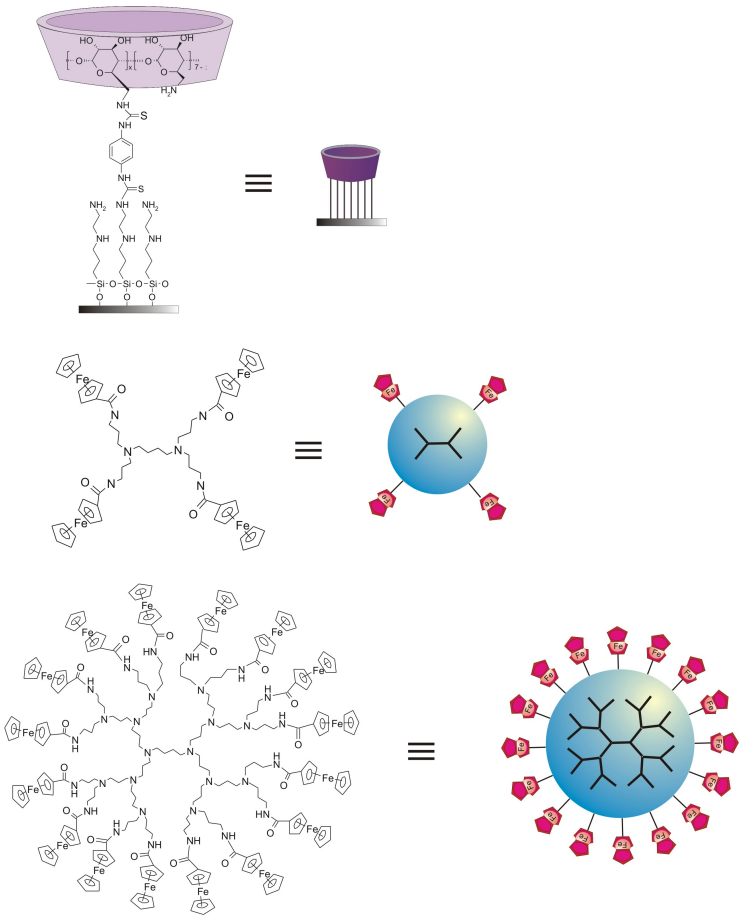

Chart 4.1. Chemical structures and representations (from top to bottom) of a CD SAM on silicon and ferrocenyl-functionalized poly(propylene imine) dendrimers of generations 1 and 3.

The polarity of the surface groups of self-assembled monolayers (SAMs) was examined by contact angle goniometry. The contact angle of each monolayer plays a crucial role in the adsorption of particles at the liquid-air-solid boundary. Table 4.1 summarizes the advancing contact angles (θ_a) of water on different SAMs. The native SiO_2 substrate exhibited a high wettability with an advancing angle of less than 20^o, due to the presence of silanol groups on the surface. The APTES (NH_2) monolayer has an advancing angle of 60^o. The advancing angle was reduced to 30^o upon protonation of the NH_2 groups to NH_3^+ by dipping the SAM in a 0.1 M aqueous HCl for 1 min. The CD monolayer on silicon was prepared as described before, with a θ_a of 50^o.[23] Complementary guest molecules, G1-PPI-$(Fc)_4$ and G3-PPI-$(Fc)_{16}$ were adsorbed onto the CD SAM by immersing the CD SAMs in the respective dendrimer solutions for 30 min, followed by rinsing with 10 mM CD solution and water to remove any physisorbed material. Due to the hydrophobic nature of the ferrocenyl moieties, θ_a increased to 60^o and 63^o for G1-PPI-$(Fc)_4$ and G3-PPI-$(Fc)_{16}$, respectively.

Table 4.1. Advancing water contact angles (θ_a) on various substrates.

Substrate	θ_a (^{o})
Native SiO_2 on Si	< 20
NH_2 SAM	60
NH_3^+ SAM	30
CD SAM	50
G1-PPI-$(Fc)_4$ on CD SAM	60
G3-PPI-$(Fc)_{16}$ on CD SAM	63

In order to quantify the amount of ferrocenyl dendrimers on the CD SAM, G1-PPI-$(Fc)_4$ and G3-PPI-$(Fc)_{16}$ were adsorbed onto CD SAMs on gold, and the cyclic voltammograms (CV) of both substrates were recorded (Figure 4.5). By integrating the areas under the peaks, the total charges of the first oxidation cycle were obtained. The total charges can be converted to surface coverage of ferrocene moieties (Fc), which were 8.7×10^{-11} mol/cm^2 and 3.7×10^{-10} mol/cm^2 for G1-PPI-$(Fc)_4$ and G3-PPI-$(Fc)_{16}$, respectively.[28] Considering the numbers of Fc endgroups and binding stoichiometries of G1-PPI-$(Fc)_4$ and G3-PPI-$(Fc)_{16}$, 50 % and 100 % of the CDs on the SAMs were coupled with G1-PPI-$(Fc)_4$ and G3-PPI-$(Fc)_{16}$, respectively.[35] The lower coverage of G1-PPI-$(Fc)_4$ is attributed to partial desorption of G1-PPI-$(Fc)_4$ from the host surface by competitive interaction with native CD solution during the rinsing procedure, in line with the relatively weak interaction of this dendrimer.[36] It should be noted that not all available Fc moieties on a dendrimer will bind to the CD host surface. Only 2 Fc endgroups of G1-PPI-$(Fc)_4$ (total 4 Fc moieties) and 4 Fc endgroups of G3-PPI-$(Fc)_{16}$ (total 16 Fc moieties) will couple to the CD SAM at each time.[28] For these ferrocenyl dendrimers sized between 2 and 4 nm, the surface of PS-CD particle of 450 nm can be considered as a flat CD SAM. Hence, the numbers of interactions for a single G1-PPI-$(Fc)_4$ and G3-PPI-$(Fc)_{16}$ dendrimer with a particle is expected to be 2 and 4 per dendrimer, respectively.

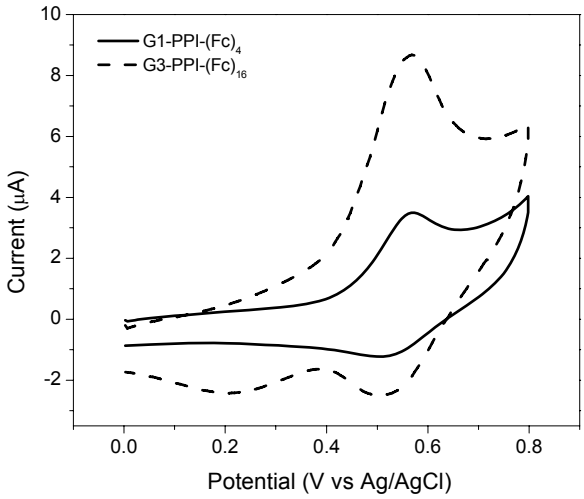

Figure 4.5. Cyclic voltammograms of G1-PPI-$(Fc)_4$ and G3-PPI-$(Fc)_{16}$ dendrimers preadsorbed on CD SAMs on gold at scan rate of 0.5 V/s in 0.1 M K_2SO_4 aqueous solution between 0 – 0.8 V vs Ag/AgCl.

The adsorption and desorption behavior of the functionalized particles on various substrates were observed *in situ* under the optical microscope with convective assembly as the driving assembly scheme. Figure 4.6 illustrates the experimental setup used for the particle assembly. A droplet of 0.2 wt % of particle suspension was added into the gap between a mobile substrate and a fixed glass slide while the temperature was controlled between 4 - 20 ^{o}C. The substrate was then shifted to the left at a constant velocity (0.1 – 1 μm/s). For ease of discussion, the substrate was categorized into two sections, i.e., the assembly and bulk suspension zones. Particles assemble on the surface in the assembly zone as a result of the convective flow of particles induced by the evaporation solvent at the assembly zone. In the suspension zone, the particle suspension is like in bulk. Depending on the particle-substrate interaction, adsorption from the suspension onto the substrate may also occur in the suspension zone when specific interactions occur.

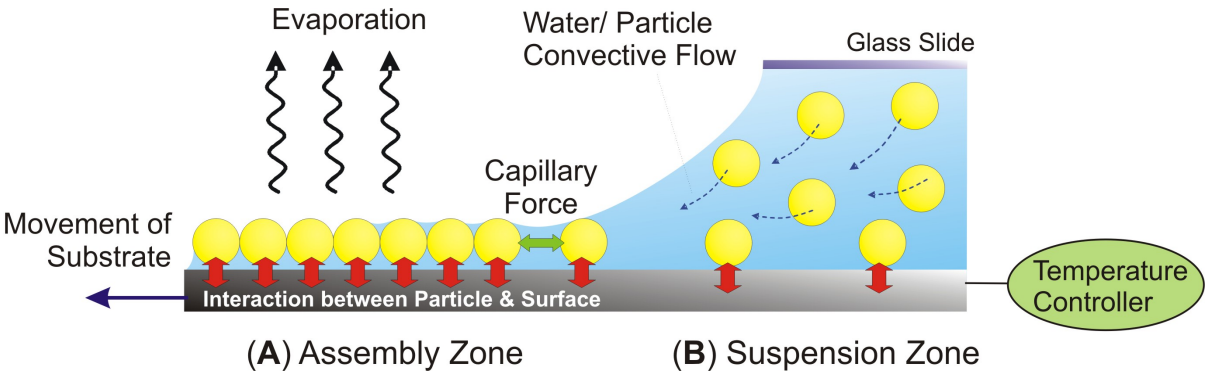

Figure 4.6. Schematic illustration of the adsorption and assembly of particles on a substrate. On the left, the assembly zone (A) refers to the area where assembly of the particles occurs. The particle assembly is caused by the evaporation of the water meniscus in this area. Between the glass slide and the substrate is the suspension zone (B). Convective flow delivers the particles from the bulk suspension zone to the assembly zone. Additional vertical interactions between the functionalized particles and the substrate may result in adsorption of particles in the suspension zone.

Figure 4.7 shows the SEM micrographs of particle lattices obtained by convective assembly and electrostatic assembly. For the pure convective assembly, the particle solution was adjusted to pH 7 to eliminate any possibility of electrostatic interaction between PS-COOH particles and the SiO_2 substrates (pK_a 4-5). The convective assembly of PS-COOH particles (Figure 4.7A) started when the SiO_2 substrate was wetted by the particle suspension, forming a very thin meniscus in the front of the assembly zone. A single layer of highly ordered particles with hexagonal close packing (hcp) was formed. No particles were found on the surface of suspension zone. After the assembly, the temperature of the substrate was gradually reduced from 18 ^{o}C to below dew point (about 6 ^{o}C). When condensation of water occurred, the particle lattice started to disintegrate and the particles regained their mobility, and finally the particle flux was reversed and all particles returned to the suspension zone. An analogous observation was made for the assembly of PS-CD particles onto SiO_2 (Figure 4.7B).

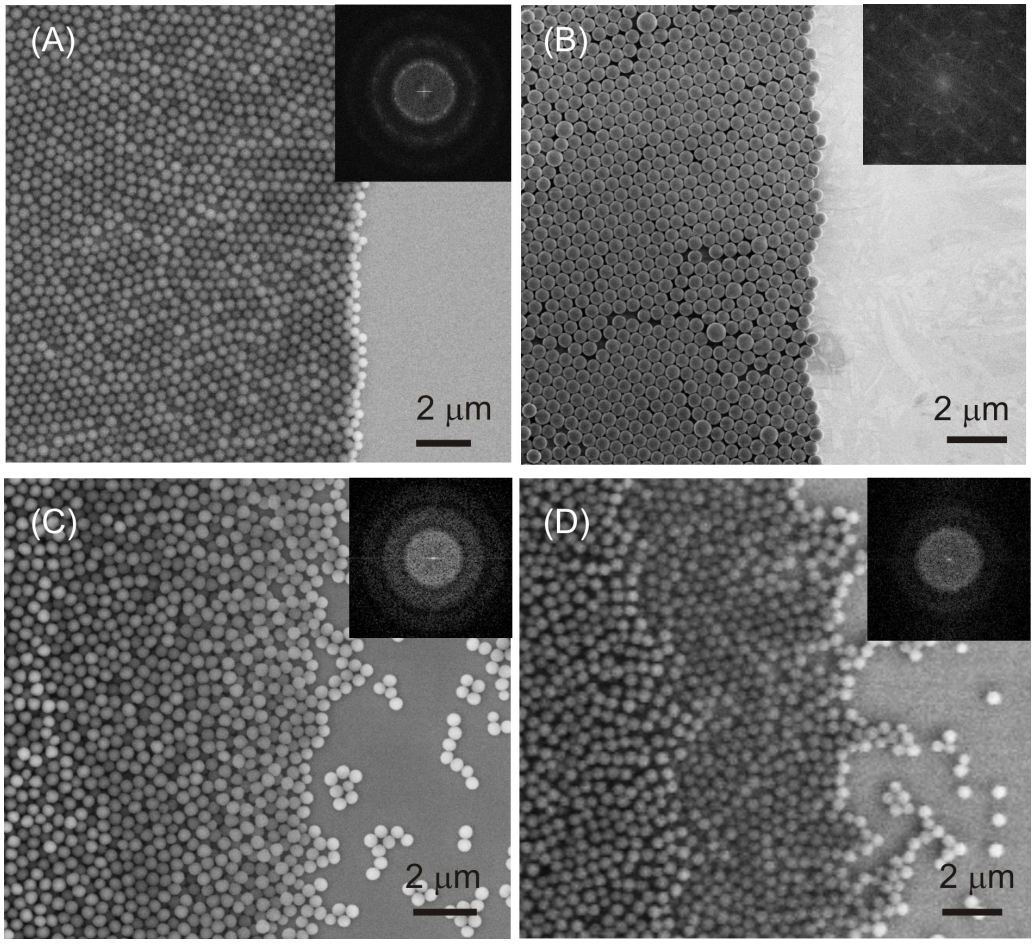

Figure 4.7. SEM micrographs of the assembled particles formed by adsorption of PS-COOH on native SiO_2 on Si (A), PS-CD on native SiO_2 on Si (B), PS-COOH on NH_3^+ SAM (C), and PS-CD on CD SAM (D). The inset at the upper right of each pictures shows the 2D Fourier transform the respective images.

In the case of the electrostatic interactions, the pH of the PS-COOH particle suspension was adjusted to 7.0. At this pH, the acrylic acid groups on the surface of PS-COOH are deprotonated ($pK_a \sim 4.5$) while the NH_2 SAM is protonated ($pK_a \sim 9.0$), which should give rise to a strong electrostatic interaction.[15] A densely occupied and disordered multilayered PS-COOH particle lattice was formed on the NH_3^+ SAM (Figure 4.7C). As observed *in situ*, particles adsorbed on the surface in the suspension zone as soon as they contacted the substrate, and they remained immobile on the surface. When decreasing the substrate temperature to below dew point, the particles with no direct contact with the surface desorbed from the surface. A single layer of particles remained at the surface because of strong electrostatic interactions. These observations contrast the assembly of PS-COOH on native SiO_2 substrates, where the particles are mobile enough to be reorganized to achieve the dense hcp packings and no adsorption occurred in the suspension zone.

The assembly of PS-CD particles onto a CD SAM in the absence of a 'supramolecular glue' (ferrocenyl-functionalized dendrimer) was examined. PS-CD particles were dispersed in carbonate buffer in the absence or presence of 5 mM CD. The assembly was initiated by wetting of the particle suspension on the moderately hydrophilic CD SAM surface. The particle lattice formed in the absence of CD showed a disordered packing similar to that observed for PS-COOH on an NH_3^+ SAM (not shown). In the presence of CD, the particle lattice appeared to have a higher degree of order, though it was not in perfect hcp organization (Figure 4.7D). The adsorption of particles in the suspension zone was also observed in both cases once the particle suspension was added, but less so in the case of added CD.

Presumably, the assembly of PS-CD on a CD SAM was merely caused by electrostatic interaction. This is because PS-CD particles are negatively charged and a CD SAM on silicon is slightly positively charged, as not all NH_2 groups of the SAM react with diisothiocyanate and CD heptamine.[23] The tendency to form multilayered particle lattices was most likely due to the low substrate's withdrawing velocity, but in part also due to electrostatics.[16] During the desorption by condensation, the particles that had no physical contact with the surface desorbed, possibly because the attractive forces exerted on these particles are weaker.

In order to quantify the degree of ordering of the particle lattice, Voronoi diagrams were created to determine the densities of the particle lattices and the number of non-hexagonally packed particles (defects) over 80 - 100 μm^2 of a single-layer particle lattice (see Table 4.2).[37,38] A simple sphere-finding algorithm was used to identify the sphere centers, enabling the construction of a Voronoi diagram which was superimposed on the original image. A particle in a perfect hexagonally packed lattice, is surrounded by 6 neighbors, and they appear as hexagons. While the non-hexagonally packed particles consist of 5- and 7-fold-coordinated sites (not shown).

The particle densities in the assembly zones of PS-COOH on SiO_2 and PS-CD on SiO_2 are between 5.1 - 5.5 particles/μm^2, which fall in the range of perfect hcp packing order.[39] In contrast, the densities of the electrostatically assembled particle lattices (PS-COOH on NH_3^+ SAM and PS-CD on CD SAM) are 3.9 – 4.8 particle/μm^2, indicating the formation of disordered particle lattices. Approximately 0.7 and 0.8 defects/μm^2 were found for PS-COOH and PS-CD lattices formed on SiO_2, respectively (see Table 4.2), possibly due to the relatively wide size distribution of particles. The defects of the electrostatically induced particle assemblies were 1.5 – 2.0 defects/μm^2, which is due to the strong adsorption

and lack of mobility of these particles once in contact with the surface, which inhibits better ordering.

The adsorption of particles in the suspension zone was observed both in Figure 4.7C and 3D. For easy comparison, the densities of particles adsorbed in the suspension zone were calculated over a suspension zone area of 1600 μm^2. The particle densities for PS-COOH on an NH_3^+ SAM, and for PS-CD on a CD SAM in absence and presence of 5 mM CD in the suspension zone were 0.5, 0.8, and 0.2 particles/μm^2, respectively, indicating strong interactions between the particles and the surfaces.

Table 4.2. Comparison of the densities of particles adsorbed onto the substrate in the suspension zone and assembly zone, and the number of defects (non-hexagonally packed particles) per μm^2.

Assembly type	Sample	Density in assembly zone (particles/ μm^2)	Defects in assembly zone (defects/μm^2)	Density in suspension zone (particles/ μm^2)
Convective	PS-COOH on SiO_2	5.1	0.7	0.0
	PS-CD on SiO_2	5.5	0.8	0.0
Convective & Electrostatic	PS-COOH on NH_3^+ SAM	4.8	2.0	0.5
	PS-CD on CD SAM	3.9	1.8	0.8
	PS-CD on CD SAM[a]	4.3	1.5	0.2
Convective & Supra-molecular	PS-CD on G1-PPI-$(Fc)_4$ on CD SAM	4.8	1.4	0.4
	PS-CD on G3-PPI-$(Fc)_{16}$ on CD SAM	4.8	1.5	1.6
	PS-CD on G1-PPI-$(Fc)_4$ on CD SAM[a]	5.0	1.1	0.1
	PS-CD on G3-PPI-$(Fc)_{16}$ on CD SAM[a]	5.3	1.2	0.4

[a] Particle suspension dispersed in the presence of 5 mM native CD (molecules).

Figure 4.8 shows particle lattices formed by utilizing the specific supramolecular host-guest interactions between CD SAMs and ferrocenyl-functionalized dendrimers. To avoid involvement of electrostatic interaction in the assembly, PS-CD were dispersed in pH 9.0 carbonate buffer, in order to deprotonate both the dendrimers and the COOH groups on the particles' surface, and to increase the ionic strength in the particle suspension, such that the electrostatic interactions can be shielded. Figure 4.8A was obtained by assembling PS-CD particles on the larger G3-PPI-$(Fc)_{16}$ dendrimer pre-adsorbed on a CD SAM. The CD SAM became somewhat less hydrophilic upon adsorption of G3-PPI-$(Fc)_{16}$ onto the substrate (see Table 4.1), but still feasible for convective assembly. The particle assembly with supramolecular interaction was distinctly different from the assembly on native SiO_2 or with electrostatic interaction. Once the particle suspension was added, huge numbers of particles adsorbed instantaneously onto the dendrimer-CD SAM surface. This phenomenon hindered the formation of a dense particle lattice in the assembly zone. In fact, the adsorbed particles act as an obstacle for the convective flow of particles toward to assembly zone. As seen *in situ* by the optical microscope, the freely suspended particles had to travel in a twisted path before reaching the boundary of the assembly zone. At some point, the density of the adsorbed particles in the suspension zone was so high that the assembly was inhibited altogether, and that a new assembly zone started to form elsewhere. The order of the resulting particle lattice was very poor (Figure 4.8A). When the temperature was reduced below the dew point, most particles remained at their original position, and desorption of the particles by condensation was negligible.

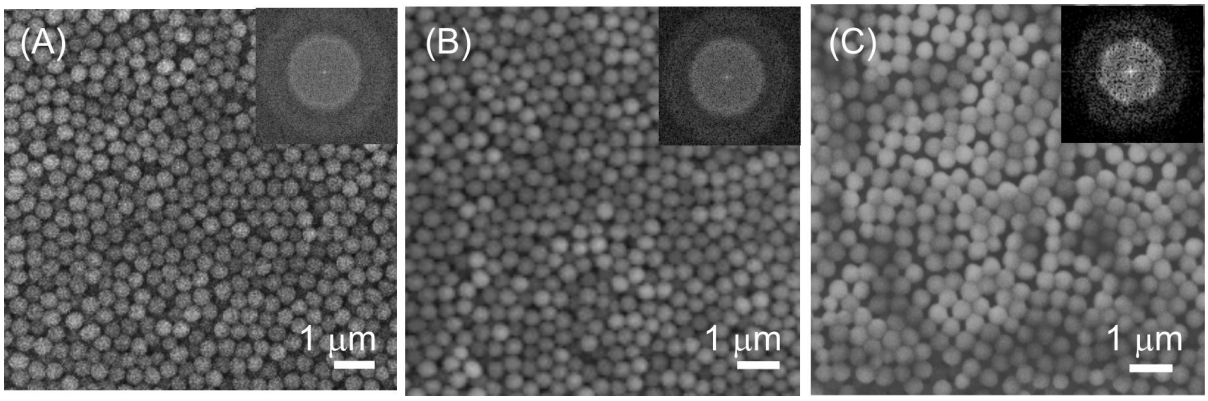

Figure 4.8. SEM micrographs of particle lattices formed by PS-CD on G3-PPI-$(Fc)_{16}$ pre-adsorbed on a CD SAM (A), and PS-CD on G1-PPI-$(Fc)_4$ pre-adsorbed on a CD SAM in the absence (B) and presence of 5 mM native CD (C). The inset at the upper right of each pictures shows the 2D Fourier transform the respective images.

The results obtained so far suggest that the particle lattices formed by additional electrostatic and/or supramolecular interaction, though very stable on the surface, fail to form perfect closely packed particle lattices as a result of strong interaction between the particles and its surface. In order to form not only a stable but also a closed packed particle lattices, a few considerations have to be taken into account, (i) the adsorption of particles in the suspension zone should be sufficiently low such that the influx of particles to the assembly zone will not be disturbed, and (ii) the mobility of the particles at the boundary between assembly and suspension zones has to be preserved to allow reorganization of particles into perfect hexagonal close packing.

Hence, further fine-tuning of supramolecular assembly was carried by first using ferrocenyl dendrimer of generation 1 (G1-PPI-$(Fc)_4$). The wettability of the surface (θ_a= 60^o) was similar to that of G3-PPI-$(Fc)_{16}$ on a CD SAM. As observed during the assembly, some particles already adsorbed onto the substrate in the suspension zone. As shown in Figure 4.8B, the PS-CD particle lattice formed on pre-adsorbed G1-PPI-$(Fc)_4$ on CD SAM was disordered. Further attempts on achieving an ordered supramolecular particle lattice were carried out by adding 5 mM native CD to the particle suspension. The assembly was performed on pre-adsorbed G1-PPI-$(Fc)_4$ on a CD SAM. The number of particles adsorbed on the surface in the suspension zone was reduced considerably (Table 4.2). As shown in Figure 4.8C, the packing of the particle lattice was nearly hexagonal which constitutes a drastic change from the disordered packing shown in Figure 4.8A and 4B. The desorption of particles by condensation was negligible for the assemblies on pre-adsorbed G1-PPI-$(Fc)_4$ on CD SAMs, as already observed previously for G3-PPI-$(Fc)_{16}$.

As shown in Table 4.2, there are differences in packing order between the supramolecular particle lattices formed in the absence and presence of competitive interaction by native CD (molecules). The particle lattices formed in the absence of CD were disordered (and random), with packing densities of 4.5 - 4.8 particle/μm^2, and defects of 1.4 defects/μm^2. In contrast, assemblies formed in the presence of CD were hexagonally closed packed, with 5.0 - 5.3 particles/μm^2 and defect densities of 1.1 - 1.2 defects/μm^2 (Table 4.2). A reduction in adsorption of particles in the suspension zone was observed. The densities of the particles in the suspension zone were reduced from 1.6 to 0.4 and 0.4 to 0.1 particles/μm^2 for G3-PPI-$(Fc)_{16}$ and G1-PPI-$(Fc)_4$ surfaces, respectively, when 5 mM native CD was added to the particle suspension.

The use of G3-PPI-$(Fc)_{16}$ resulted in the highest adsorption density in the suspension zone, indicating a strong binding affinity between the particles and the surface as a result of

spontaneous and strong multivalent supramolecular interactions, which makes reorganization and ordering of the particles very difficult. In comparison, G1-PPI-$(Fc)_4$, with a 50 % lower Fc surface coverage than that of G3-PPI-$(Fc)_{16}$ (Figure 4.5) caused less particle adsorption in the suspension zone, suggesting a weaker and more dynamic host-guest interaction. Nevertheless, the interaction force of the simultaneous binding of multiple CD sites on a single particle to multiple Fc sites on the surface is probably still larger than the lateral capillary force between the neighboring particles, which prevents the ordering of particles.[40] With addition of native CD to the particle suspension, competition was initiated. Thus, after reducing the total number of interactions and inducing competition in the assembly, a nearly hexagonally close packed supramolecular particle lattice was obtained by using G1-PPI-$(Fc)_4$ with native CD present in the particle suspension. To our knowledge, this is the first time that supramolecular competition is shown to result in fine-tuning of interactions and ordering of materials.

4.2.3 Assembly of particles on nanoimprint lithography (NIL) patterned substrates

As an extension to the fabrication of nanostructures, substrates patterned by nanoimprint lithography (NIL) were employed to assemble the particles into micrometer lines. A piranha-cleaned silicon substrate with a 500 nm thick layer of PMMA was pressed against a hard stamp at high temperature to form patterned substrates with 3.5 μm wide polymer lines. The residual layer in the imprinted areas was removed by acetone. The NH_2 and CD SAMs were subsequently formed on the native SiO_2 according to previously described procedures.[41] Figure 4.9 shows the patterned particle lattices formed on nanoimprinted patterns assembled via convective assembly, with electrostatic interactions and with supramolecular host-guest interactions. For the convective assembly (Figure 4.9A), the particles were physically confined by the PMMA polymer barriers into the 3.5 μm wide silicon oxide areas, which resulted in the formation of highly hcp-ordered particle lines. The selective particle assembly was driven by the large chemical contrast between PMMA (θ_a = 80^o) and silicon oxide.

In the beginning of the assembly with additional electrostatic interactions (Figure 4.9B), the particles bound preferentially to the NH_3^+ SAM. The particle lines were disordered and multilayered, as a result of the strong electrostatic interactions of the particles with the substrate. As the wetting contrast between the NH_3^+ SAM and PMMA is relatively low, we observed that after a few seconds of assembly, the particles started to assemble on the polymer lines too. In the end, nearly all the polymer figures were covered with particles. This

is particularly observed when the withdrawing speed was 0.5 – 1.0 μm/s, in agreement with observations made by Jonas *et al*.[42] Nevertheless, rinsing the substrate in agitated MilliQ water was sufficient to remove the particles that were physisorbed onto the PMMA, or in this case, PMMA and particles on PMMA can be easily 'lifted off' from the substrate by rinsing with acetone.

In the case of supramolecular interaction using G1-PPI-$(Fc)_4$ and a particle suspension of high pH buffer in the absence of CD, a random particle lattice was formed with nonspecifically adsorbed particles everywhere (Figure 4.9C). The lack of specificity of the assembly is attributed to the adsorption of dendrimers onto the PMMA structures as a result of hydrophobic interactions.[43]

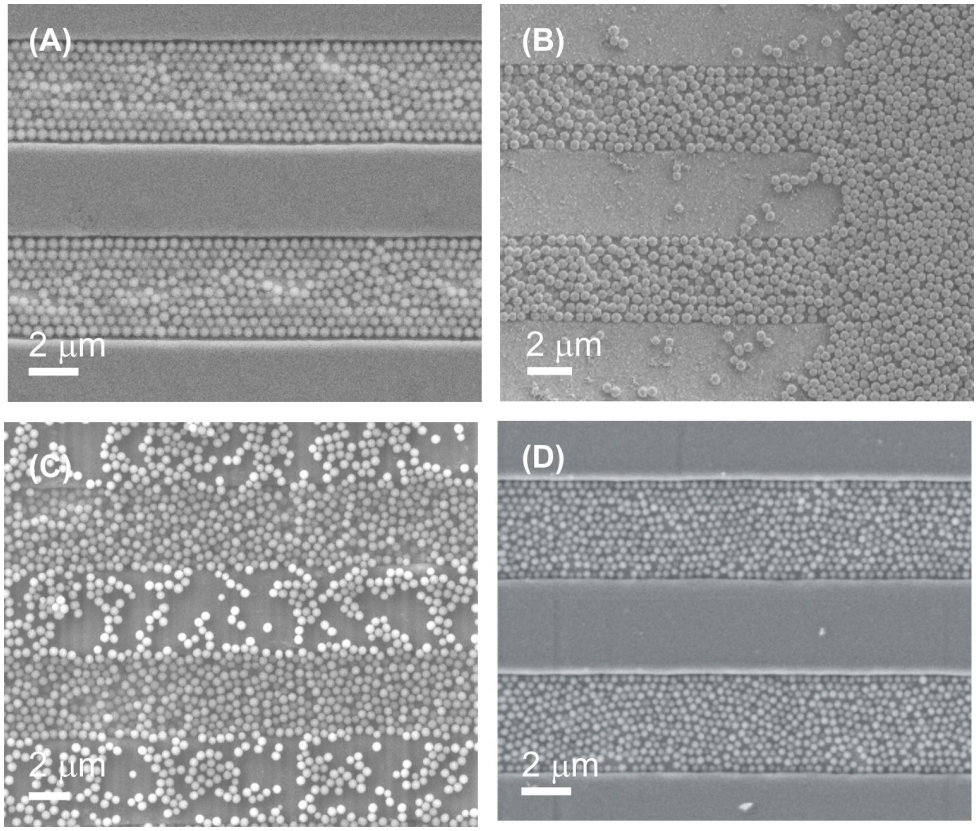

Figure 4.9. SEM micrographs of NIL-patterned particle lattices formed by adsorption of PS-COOH on native SiO_2 on Si (A), PS-COOH on an NH_3^+ SAM (B), and PS-CD on CD SAM with preadsorbed G1-PPI-$(Fc)_4$ in the absence (C) and presence (D) of 5 mM native CD.

To fine-tune and improve the specificity of the assembly, a particle suspension with 5 mM native CD was used (Figure 4.9D). Periodic changes in hydrophilic properties and the shape of the water meniscus were clearly observed as a result of alternating dewetting and wetting effects by the PMMA and CD SAM areas, respectively. The nonspecific adsorption

of dendrimers on PMMA was reduced as a result of competition by CD in solution. Hence, a well controlled, stable and single layer of particles was formed in the assembly process with a better degree of order than without CD. Potentially, this method can also yield multilayered nanostructures by repeating the adsorption of the ferrocenyl dendrimers and CD particle, as shown before in a layer-by-layer process for 5 nm gold particles.[13]

4.3 CONCLUSIONS

The *in-situ* observation of the adsorption and desorption of particles during convective assembly on native oxide surfaces, with additional electrostatic interactions and with supramolecular interactions has been presented. PS-COOH particles on native SiO_2 surfaces displayed the best hcp packing among all, but these lattices can be easily desorbed by reducing the temperature below dew point. The electrostatically induced assembly led to disordered lattices. The highly tunable supramolecular assembly, driven by multivalent host-guest interactions between PS-CD and G1-PPI-$(Fc)_4$ or G3-PPI-$(Fc)_{16}$ on CD SAMs resulted in a nearly hcp packing in the presence of a competing interaction by native CD, also providing good specificity and selectivity on NIL-patterned substrates. We envision, with the use of these specific, yet highly tunable supramolecular interactions, the generation of more sophisticated and more complex nanostructures that cannot be achieved by physical assembly becomes within reach. In particular, the combination of top-down surface patterning and bottom-up material, assembly that involves multivalent supramolecular interactions is anticipated to lead to well-defined 3D nanostructures.

4.4 EXPERIMENTAL

Chemicals. Styrene, divinylbenzene, acrylic acid, *N*-(3-dimethylaminopropyl)-*N*-ethylcarbodiimide hydrochloride (EDC), *N*-hydroxysuccinimide (NHS), 3-aminopropyl triethoxysilane (APTES), *N*-[3-(trimethoxysilyl)propyl]ethylenediamine and 1,4-phenylene diisothiocyanate were obtained from commercial sources (Sigma Aldrich, Germany). Buffer solutions of all pHs were prepared as described previously, unless otherwise stated.[27] β-Cyclodextrin (CD) heptamine, adamantyl-terminated poly(propylene imine) dendrimer of generation 5 (G5-PPI-$(Ad)_{64}$), ferrocenyl-functionalized poly(propylene imine) dendrimer of generations 1 and 3 (G1-PPI-$(Fc)_4$ and G3-PPI-$(Fc)_{16}$) were synthesized as described before.[28,44,45] Milli-Q water with a resistivity higher than 18 MΩ·cm was used in all experiments.

Preparation of carboxylate-functionalized polystyrene particles (3, PS-COOH). The core-shell particles of poly(styrene-co-acrylic acid) (PS-COOH) were prepared as described before.[46,47] Milli-Q water (100 mL) was stirred and heated to 80 ^oC under N_2 atmosphere. 11 mL of styrene and 1 mL of divinylbenzene were then added quickly into the solution. The mixture was stirred for another 20 min before adding 5 mL of 0.1 M aqueous potassium persulfate. The mixture was stirred for another 4 h

under N_2 atmosphere. 1 mL of distilled acrylic acid and 2.6 mL of 0.1 M potassium persulfate were added, and the reaction was continued for another 75 min. The reaction product was centrifuged and redispersed in water (pH 7.0) for at least three times.

Preparation of β-cyclodextrin-functionalized polystyrene particles (5, PS-CD). The attachment of β-cyclodextrin onto the surface of PS-COOH particles was based on a functionalization strategy for β-cyclodextrin-functionalized silica particles, as described in Chapter 3.[27] PS-COOH (24 mL, 11 wt%) was redispersed in MES buffer (pH 5.6) and was added to 10 mL of 5 mM EDC/NHS mixture. After 1 h stirring, the particles **3** were centrifuged and redispersed in a carbonate buffer (pH 9.6). This suspension was added dropwise to 5 mL of 5 mM aqueous CD heptamine. Stirring was continued overnight at room temperature. The final product, CD-functionalized poly(styrene-co-acrylic acid) (**4**, PS-CD) particles were centrifuged and redispersed in 10 mM carbonate buffer (pH 9.6) for at least three times to remove unreacted CD heptamine from the mixture.

Substrate and monolayer preparation. Cleaned silicon substrates were prepared by immersion in piranha solution (conc. H_2SO_4 and 33% H_2O_2 in a 3:1 volume ratio). (**Warning!** piranha should be handled with caution; it can detonate unexpectedly) for 15 min to form a SiO_2 layer on the surface. The substrates were then sonicated in Milli-Q water and ethanol for 1 min, and dried with N_2. Amino-terminated SAMs were obtained by gas-phase evaporation of APTES in a desiccator under vacuum. The samples were left several hours and then carefully rinsed with ethanol and Milli-Q water. CD SAMs were obtained according to a published procedure.[23,48] In brief, the substrates were functionalized *N*-[3-(trimethoxysilyl)propyl]ethylenediamine by gas-phase evaporation. Transformation of the amino-terminated SAMs to isothiocyanate-bearing layers was accomplished by exposure to an ethanol solution of 1,4-phenylene diisothiocyanate at 50 ^oC for 2 h. CD SAMs were finally obtained by reaction of the isothiocyanate-terminated monolayer with CD heptamine in pH 7.5 water, at 50 ^oC for 2 h. The adsorption of G1-PPI-$(Fc)_4$ or G3-PPI-$(Fc)_{16}$ was achieved by immersing the CD SAM substrates in a aqueous solution of G1-PPI-$(Fc)_4$ and/or G3-PPI-$(Fc)_{16}$ (1 mM Fc functionality) for 30 min, followed by rinsing with 10 mM aqueous CD at pH 2 and Milli-Q water.

Particle assembly. A defined volume (40 μL) of 0.2 wt% of particle suspension in was injected between the SAM and a glass slide (Figure 4.6). The liquid meniscus was moved over the SAM at a constant velocity of 1 μm/s. The entire setup was installed on the stage of an optical microscope for direct observation and control of the assembly process. A Peltier element allowed the temperature of template to be controlled.[30] Typically, the adsorption of particles was performed at temperature of about 18 ^oC, whereas the desorption was attempted at a temperature below 6 ^oC.

Nanoimprint lithography (NIL). Silicon stamps were made by photolithography followed by reactive ion etching (RIE, Elektrotech Twin system PF 340). A stamp consisted of 3.5 μm lines at 7.5 μm period with a height of 500 nm. A piranha-cleaned silicon substrate was first spin-coated with a 500 nm thick layer of PMMA. Stamp and substrate were put in contact and a pressure of 40 bar was applied at a temperature of 180 ºC using a hydraulic press (Specac). The residual layer was removed by dipping the samples in acetone during 30 s.

Fourier Transform Infrared (FT-IR) Spectroscopy. Infrared spectra were recorded on a Perkin–Elmer Spectrum BX spectrometer, using KBr pellets that contained 2 – 5 mg of particles.

Dynamic Light Scattering (DLS). DLS experiments were performed with a Zetasizer 4000 (Malvern Instruments Ltd., U.K.) at 25 °C using a laser wavelength of 633 nm at a scattering angle of 90°. Results obtained are the averages of three measurements. The average hydrodynamic diameter

(d_{av}) of the particles was determined on 1.5 mL samples in corresponding solutions. The dispersions were gently shaken before the measurements for proper mixing. The (attempted) aggregation of PS-COOH and PS-CD with the adamantyl-terminated PPI dendrimer, generation 5 (Ad-PPI-G5) was performed by measuring d_{av} for a 1 mL sample before and after subsequent additions of 40, 130, 250, and 500 μL of a 0.2 mM solution of Ad-PPI-G5.[24,27] The dispersions were gently shaken before the measurements for proper mixing.

Zeta Potential. Zeta potentials of the silica particles were obtained with a Zetasizer 2000 (Malvern Instruments Ltd., U.K.) using the Laser Doppler velocimetry technique. In this technique, the velocity of suspended particles is measured as function of an applied electrical field, which correlates to the particle motion. Measurements were performed at 25 °C using a 1000 Hz modulator frequency and a cell drive voltage of 120 V. The values reported are the averages of ten measurements.

Contact Angle Goniometry. Contact angles were measured on a Krüss G10 contact angle measuring instrument, equipped with a CCD camera. Advancing contact angles were determined automatically during growth of the droplet of Milli-Q water by a drop shape analysis routine.

Scanning Electron Microscopy (SEM). All SEM images were taken with a HR-LEO 1550 FEF SEM.

4.5 ACKNOWLEDGEMENTS

Dr. Laurent Malaquin and Dr Heiko Wolf are gratefully acknowledged for the collaboration of this work. Mr. Mark Smithers is thanked for the SEM measurements. Mr. Thomas van Zanten and Dr Monique Roerdink are acknowledged for the construction of Voronoi diagrams.

4.6 REFERENCES AND NOTES

1. Arsenault, A.; Fournier-Bidoz, S.; Hatton, B.; Míguez, H.; Tétreault, N.; Vekris, E.; Wong, S.; Yang, S. M.; Kitaev, V.; Ozin, G. A. *J. Mater. Chem.* **2004**, *14*, 781.
2. Shipway, A. N.; Katz, E.; Willner, I. *ChemPhysChem.* **2000**, *1*, 18.
3. Wang, D.; Möhwald, H. *J. Mater. Chem.* **2004**, *14*, 459.
4. Murray, C. B.; Kagan, C. R.; Bawendi, M. G. *Science* **1995**, *270*, 1335.
5. Gates, B.; Qin, D.; Xia, Y. *Adv. Mater.* **1999**, *11*, 466.
6. Ozin, G. A.; Yang, S. M. *Adv. Funct. Mater.* **2001**, *11*, 95.
7. Van Blaaderen, A.; Ruel, R.; Wiltzius, P. *Nature* **1997**, *385*, 321.
8. Zhang, J.; Alsayed, A.; Lin, K. H.; Sanyal, S.; Zhang, F.; Pao, W.-J.; Balagurusamy, V. S. K.; Heiney, P. A.; Yodha, A. G. *Appl. Phys. Lett.* **2002**, *81*, 3176.
9. Denkov, N. D.; Velev, O. D.; Kralchevsky, P. A.; Ivanov, I. B.; Yoshimura, H.; Nagayama, K. *Nature* **1993**, *361*, 26.
10. Paunov, V. N.; Kralchevsky, P. A.; Denkov, N. D.; Nagayama, K. *J. Coll.Interf. Sci.* **1993**, *157*, 100.
11. Nagayama, K. *Coll. Surf. A.* **1996**, *109*, 363.

12. Decher, G.; Hong, J. D.; Schmitt, J. *Thin Solids Films* **1992**, *210 & 211*, 831.
13. Crespo-Biel, O.; Dordi, B.; Reinhoudt, D. N.; Huskens J. *J. Am. Chem. Soc.* **2005**, *127*, 7594.
14. Kiely, C. J.; Fink, J.; Brust, M.; Bethell, D.; Schiffrin, D. J. *Nature* **1998**, *396*, 444.
15. Jonas, U.; del Campo, A.; Kruger, C.; Glasser, G.; Boos, D. *Proc. Natl. Acad. Sci. USA* **2002**, *99*, 5034.
16. Chen, K. M.; Jiang, X.; Kimerling, L. C.; Hammond, P. T. *Langmuir* **2000**, *16*, 7825.
17. Maury, P.; Escalante, M.; Reinhoudt, D. N.; Huskens, J. *Adv. Mater.* **2005**, *17*, 2718.
18. Arias, F.; Godinez, L. A.; Wilson, S. R.; Kaifer, A. E.; Echegoyen, L. *J. Am. Chem. Soc.* **1996**, *118*, 6086.
19. Dietrich, C.; Schmitt, L.; Tample, R. *Proc. Natl. Acad. Sci. USA* **1995**, *92*, 9014.
20. Mulder, A.; Huskens, J.; Reinhoudt, D.N. *Org. Biomol. Chem.* **2004**, *2*, 3409.
21. Reinhoudt, D. N.; Crego-Calama, M. *Science* **2002**, *295*, 2403.
22. Beulen, M. W. J.; Bügler, J.; Lammerink, B.; Geurts, F. A. J.; Biemond, E. M. E. F.; Van Leerdam, K. G. C.; Van Veggel, F. C. J. M.; Engbersen, J. F. J.; Reinhoudt, D. N. *Langmuir* **1998**, *14*, 6424.
23. Onclin, S.; Mulder, A.; Huskens, J.; Ravoo, B. J.; Reinhoudt, D. N. *Langmuir* **2004**, *20*, 5460.
24. Huskens, J.; Deij, M.A.; Reinhoudt, D.N. *Angew. Chem. Int. Ed.* **2002**, *41*, 4467.
25. Auletta, T.; Dordi, B.; Mulder, A.; Sartori, A.; Onclin, S.; Bruinink, C.M.; Péter, M.; Nijhuis, C.A.; Beijleveld, H.; Schönherr, H.; Vancso, G.J.; Casnati, A.; Ungaro, R.; Ravoo, B.J.; Huskens, J.; Reinhoudt, D.N. *Angew. Chem. Int. Ed.* **2004**, *43*, 369.
26. Nijhuis, C. A.; Huskens, J.; Reinhoudt, D. N. *J. Am. Chem. Soc.* **2004**, *126*, 12266.
27. Mahalingam, V.; Onclin, S.; Péter, M.; Ravoo, B. J.; Huskens, J.; Reinhoudt, D. N. *Langmuir* **2004**, *20*, 11756.
28. Nijhuis, C. A.; Huskens, J.; Reinhoudt, D. N. *J. Am. Chem. Soc.* **2004**, *126*, 12266.
29. Rekharsky, M. V.; Inoue, Y. *Chem. Rev.* **1998**, *98*, 1875.
30. Malaquin, L.; Kraus, T.; Schmid, H.; Delamarche, E.; Wolf, H. *Langmuir* **2007**, 23, 11513.
31. Shim, S.-E.; Cha, Y.-J.; Byun, J.-M.; Choe, S. *J. Appl. Polym. Sci.* **1999**, *71*, 2259.
32. Bhutto, A.A.; Vesely, D.; Gabrys, B.J. *Polymer* **2003**, *44*, 6627.
33. Based on 2 wt% solution of particles, with a polystyrene density of 1.05 kg/dm^3.
34. Crespo-Biel, O.; Juković, A.; Karlsson, M.; Reinhoudt, D. N.; Huskens, J. *Isr. J. Chem*. **2005**, *45*, 353.
35. The coverage of a CD SAM is 8×10^{-11} mol/cm^2. For details, see: Beulen, M. J. W.; Bügler, J.; De Jong, M. R.; Lammerink, B.; Huskens, J.; Schönherr, H.; Vancso, G. J.; Boukamp, B. A.; Wieder, H.; Offenhauser, Knoll, W.; Van Veggel, F. C. J. M.; Reinhoudt, D. N. *Chem. Eur. J.* **2000**, *6*, 1176.

36. Nijhuis, C. A.; Yu, F.; Knoll, W.; Huskens, J.; Reinhoudt, D. N. *Langmuir* **2005**, *21*, 7866.
37. Allen, S. M.; Thomas, E. L. *The Structure of Materials*, Wiley, New York, **1999**.
38. Roerdink, M.; Hempenius, M. A.; Vancso, G. J. *Chem. Mater.* **2005**, *17*, 1275.
39. A perfectly hexagonal close packed particle lattice has a density of 5.4 particles/μm^2, considering particle size of 450 nm.
40. Huskens, J.; Mulder, A.; Auletta, T.; Nijhuis, C. A.; Ludden, M. J. W.; Reinhoudt, D. N. *J. Am. Chem. Soc.* **2004**, *126*, 6784.
41. Maury, P.; Péter, M.; Crespo-Biel, O.; Ling, X. Y.; Reinhoudt, D. N.; Huskens, J. *Nanotechnology* **2007**, *18*, 044007.
42. Fustin, C.-A.; Glasser, G.; Spiess, H.W.; Jonas, U. *Langmuir* **2004**, *20*, 9114.
43. Crespo-Biel, O.; Dordi, B.; Maury, P.; Péter, M.; Reinhoudt, D.N.; Huskens, J. *Chem. Mater.* **2006**, *18*, 2545.
44. Michels, J. J.; Baars, M. W. P. L.; Meijer, E. W.; Huskens, J.; Reinhoudt, D. N. *J. Chem. Soc., Perkin Trans. 2* **2000**, 1914.
45. Guillo, F.; Jullien, L.; Hamelin, B.; Lehn, J.-M.; De Robertis, L.; Driguez, H. *Bull. Soc. Chim. Fr*. **1995**, *132*, 857.
46. Greci, M. T.; Pathak, S.; Mercado, K.; Prakash, G. K. S.; Thompson, M. E.; Olah, G. A. *J. Nanosci. Nanotech.* **2001**, *1*, 3.
47. Wang, Y.; Wang, Y.; Feng, L. *J. Appl. Polym. Sci.* **1997**, *64*, 1843.
48. Ling, X. Y.; Reinhoudt, D. N.; Huskens, J. *Langmuir* **2006**, *22*, 8777.

Chapter 5

Reversible attachment of nanostructures at molecular printboards through supramolecular glue*

ABSTRACT. Regenerable surfaces and reversible attachment of nanostructures onto them is an important aim in nanotechnology. Reversible attachment of nanostructures at molecular printboards was illustrated by the adsorption and desorption of β-cyclodextrin- (CD-) functionalized nanoparticles onto and from stimuli-responsive, pre-adsorbed, ferrocenyl-functionalized poly(propylene imine) dendrimers at a CD self-assembled monolayer (SAM). Electrochemical oxidation of the ferrocenyl endgroups was employed to induce desorption of nanostructures from the CD SAMs. A combined surface plasmon resonance (SPR) spectroscopy and electrochemistry setup was used to monitor the *in situ* adsorption and desorption of ferrocenyl dendrimers and CD-functionalized Au nanoparticles (Au-CD, $d \sim 3$ nm) onto and from the molecular printboard. In the case of the larger CD-functionalized silica nanoparticles (SiO_2-CD, $d \sim 60$ nm), ultrasonication was used to reduce the desorption time. By electrochemical oxidation applied to a specific area of a nanoparticle layer, local desorption of nanoparticles was observed. In the non-oxidized area, nanoparticles remained robustly attached to the surface, whereas nanoparticles on the electrochemically oxidized area were completely removed.

---

* This chapter has been published in X. Y. Ling, D. N. Reinhoudt, J. Huskens, Reversible attachment of nanostructures at molecular printboards through supramolecular glue, *Chem. Mater.* **2008**, *20*, 3574.

5.1 INTRODUCTION

Assembly of nanostructures on surfaces is an active research field owing to the increasing demand for miniaturization of microelectronic and optical devices. In addition, the ability to reversibly adsorb and desorb nanostructures from the surface is crucial,[1] as structural manipulation or modifications are often needed on a specific area of a nanostructure. General coupling chemistries, *e.g.*, electrostatic interactions,[2] covalent bonding[3] and thiol-based[4] self-assembly result in strong but irreversible functionalized nanostructures on (patterned) surfaces. Hence, biomolecular and supramolecular systems involving DNA,[5,6] biotin-streptavidin,[7] supramolecular hydrogen bonding,[8] and ligand-receptor[9,10] interactions have beed described, as they offer highly specific and/or reversible binding of nanoparticles. Supramolecular chemistry is particularly attractive as it possesses controllable molecular recognition abilities with the possibility for error correction.[9] The concept of the 'molecular printboard', i.e., β-cyclodextrin (CD) self-assembled monolayers (SAMs) on gold or glass that possess receptor properties has been developed.[11] Complementary adamantyl-functionalized dendrimers were employed as 'non-reversible molecular glue' to construct self-assembled organic/inorganic multilayers with CD-functionalized gold and silica nanoparticles (Au-CD and SiO_2-CD) at the molecular printboard employing multivalent supramolecular interactions.[12,13]

The redox behavior of ferrocene is well-known for its reversibility in host-guest systems.[14-16] Kaifer and Stoddart *et al.* have described the interfacial monovalent ferrocenyl (Fc) complexation at a per-6-thio-β-cyclodextrin monolayer.[17] Our group has demonstrated that multivalent Fc dendrimers can be reversibly adsorbed and removed from CD SAMs by electrochemical oxidization of the redox-active Fc end groups.[17-20]

In this chapter, it is demonstrated that, by using Fc dendrimers as supramolecular reversible glue, CD-functionalized nanoparticles can be reversibly adsorbed and desorbed from the molecular printboard (Scheme 1). Our aim is to practically realize the concept of reversible immobilization of nanostructures, with the focus on: (i) the electrochemical addressability of the reversible glue, when sandwiched between the SAM and nanoparticle interfaces, (ii) optimization of the conditions for disassembly of the reversible glue and the nanoparticles off the interface, and (iii) possible size effects of the nanoparticles on the reversibility. The repeated adsorption and desorption of CD functionalized gold (Au-CD) nanoparticles onto and from the surface were monitored in situ by a combined surface plasmon resonance spectroscopy (SPR) and electrochemistry setup.[19] For easy visualization

and for studying potential size effects on reversibility, experiments were repeated by using larger CD functionalized silica (SiO_2-CD) nanoparticles of 60 nm in diameter.

5.2 RESULTS AND DISCUSSION

Scheme 5.1 describes the build-up and breakdown of nanoparticle assemblies on a molecular printboard via a reversible supramolecular glue. A monolayer of nanoparticles was formed by stepwise adsorption of aqueous ferrocenyl (Fc) dendrimers and CD-functionalized nanoparticles onto the CD SAM via multivalent supramolecular host-guest interactions (Chart 5.1). Ferrocenyl poly(propylene imine) dendrimer of generation 3 (G3-PPI-$(Fc)_{16}$) serves as a 'reversible supramolecular glue' for the binding and unbinding of nanoparticles or nano-objects to and from the molecular printboard.[19] Intentional desorption of the nanoparticles from the surface can be achieved by electrochemical oxidation of the Fc groups of the dendrimers to ferrocenium cations, such that the assembled nanostructures are removed from the surface.

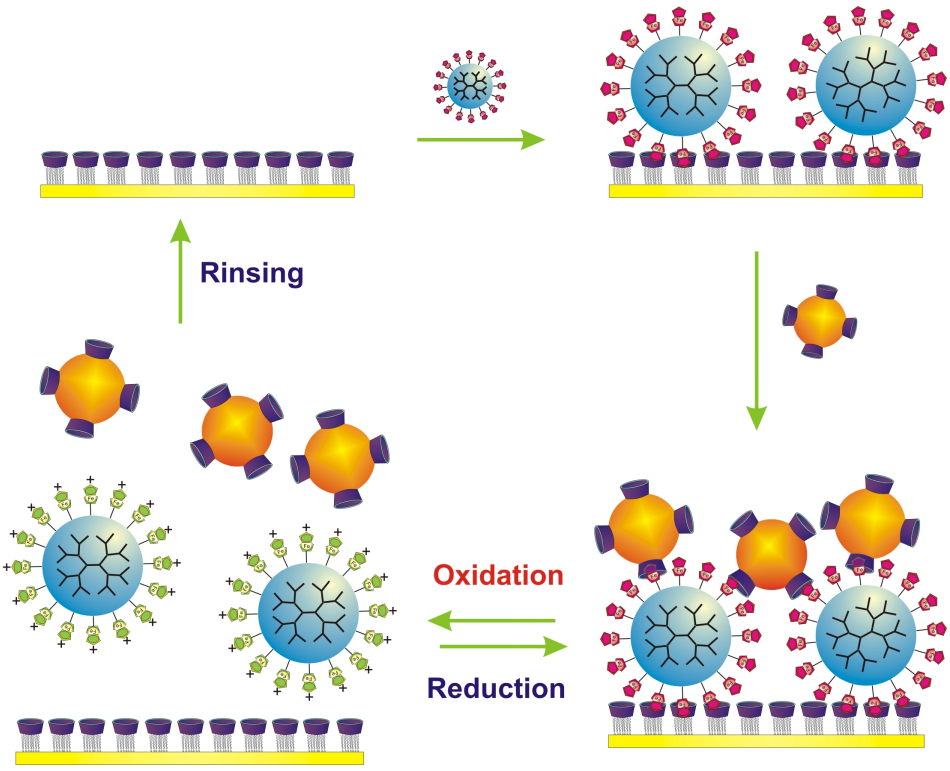

Scheme 5.1. Illustration of the adsorption and desorption of CD-functionalized nanoparticles onto and from CD SAMs with Fc dendrimers as reversible supramolecular glue.

A combined SPR and electrochemistry setup[21] was used to monitor in situ the adsorption and desorption of G3-PPI-$(Fc)_{16}$ and Au-CD nanoparticles onto and from a CD

SAM on gold, while monitoring the SPR and I/V responses simultaneously. Cyclic voltammetry (CV) was performed on a bare CD SAM, showing that the SPR signal remained unchanged during CV in the absence of electroactive dendrimers (data not shown), indicating that the SPR intensity can be completely attributed to the adsorption and desorption processes.[18,19] The adsorption of G3-PPI-$(Fc)_{16}$ in 10 mM CD in pH 2 water and Au-CD nanoparticles in 10 mM CD in HEPES buffer were adsorbed at a flow rate of 0.5 mL/min. In order to assist desorption of the nanostructures from the surface, the flow rate was increased to 4.0 mL/min during desorption. After the experiment, the flow rate was adjusted back to 0.5 mL/min for proper comparison of the SPR intensities before adsorption and after desorption.

Chart 5.1. Structures of the chemical compounds and particles that are used in this chapter: CD heptathioether, ferrocenyl poly(propylene imine) dendrimer of generation 3, CD-functionalized Au and silica nanoparticles.

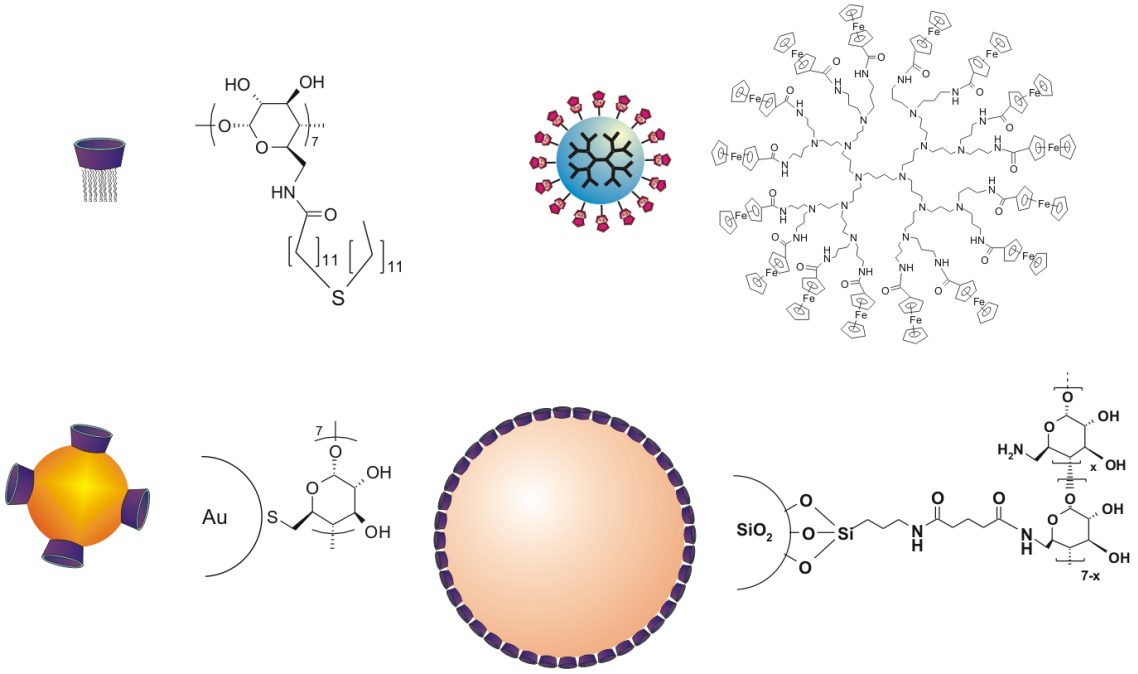

Figure 5.1 shows the sequential adsorption and electrochemically induced desorption of G3-PPI-$(Fc)_{16}$ and Au-CD (d~ 3 nm) onto and from the molecular printboard, as studied by surface plasmon resonance (SPR) spectroscopy. G3-PPI-$(Fc)_{16}$ was used because it yields thermodynamically and kinetically stable complexes at the CD SAM, even when rinsing with 10 mM CD.[19] G3-PPI-$(Fc)_{16}$ was applied in a pH 2 solution, while the Au-CD nanoparticles were applied in a HEPES buffer, both for stability reasons.[12] In order to evaluate the SPR signal changes accurately, the SPR flow cell was flushed with the corresponding buffer

before the introduction of the respective adsorbing component, and rinsed afterwards with the same buffer.[12] After adsorption of G3-PPI-$(Fc)_{16}$ (0.1 mM in Fc functionality), a Au-CD nanoparticle solution (5.8 μM in CD functionality) was introduced, and rinsing led to removal of physisorbed nanoparticles. When the adsorption of dendrimers is omitted, the Au-CD nanoparticles do not adsorb at the CD SAM.[12] Increase of the flow rate (Figure 5.1A) led to some additional removal of dendrimers and/or nanoparticles.

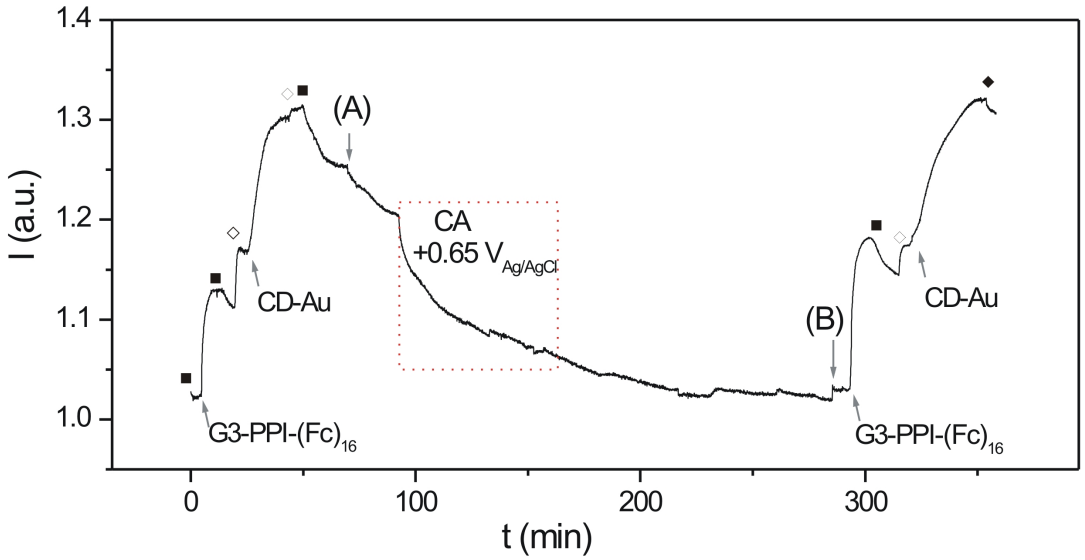

Figure 5.1. SPR sensogram of the sequential adsorption of 0.1 mM G3-PPI-$(Fc)_{16}$ dendrimers and Au-CD nanoparticles (5.8 μM in CD functionality) onto a CD SAM, followed by rinsing and chronoamperometry (CA-)induced desorption. The substrate was then reused for another buildup of G3-PPI-$(Fc)_{16}$ dendrimers and Au-CD nanoparticles. (A) change of flowrate to 4.0 mL/min; (B) change of flow rate to 0.5 mL/min. Symbols (■) and (◊) represent rinsing with 10 mM CD in pH 2 water and with HEPES buffer, respectively.

The oxidation of the Fc groups was induced by chronoamperometry (CA) at a potential of +0.65 $V_{Ag/AgCl}$ for 1 h. CA is used for the complete desorption of the nanoparticles (and dendrimers) from the molecular printboards because it allows control over the oxidation potential and duration. Cyclic voltammetry (CV) appeared to be not beneficial here because it involves repeated oxidation and reduction cycles which led to reformation of the supramolecular bonds before detectable desorption occurred (data not shown). Upon CA, a reduction in SPR intensity was observed once oxidation started. Although desorption occurred, the desorption rate was rather small, in particular when compared to the desorption

of the dendrimers in absence of nanoparticles.[18,19] The desorption rate appeared to be dependent on the flow rate through the SPR flow cell. The desorption rate observed here (Figure 5.1; about 50% coverage decrease per h) was obtained at a fairly high flow rate; at lower flow rates, desorption was (much) slower (data not shown). Nonetheless, the SPR intensity was restored to its original starting intensity at point (B), indicating a (near) complete removal of dendrimers and nanoparticles.

In order to assess the reusability of a CD SAM after prolonged electrochemistry, another stepwise adsorption of G3-PPI-$(Fc)_{16}$ and Au-CD was performed after the desorption process on the same substrate (Figure 5.1), at t =300 min. The increase in intensity was similar to the previous adsorption process, proving the robustness of the CD SAM after prolonged electrochemistry.[7] This is important, as it indicates that the CD SAM can be reused. Considering desorption assisted by flow is time-consuming, in the next experiment, desorption was performed by ultrasonicating the substrates in water for 2 min after electrochemistry, as 2 min ultrasonication appeared sufficient to assist the removal of the nanoparticle layer from the surface.

To determine possible nanoparticle size effects on the reversibility of the nanostructure attachment, larger nanoparticles, i.e., CD-functionalized silica nanoparticles (SiO_2-CD) of 60 nm were used.[9] Figure 5.2A shows a densely packed SiO_2-CD layer on G3-PPI-$(Fc)_{16}$ at the molecular printboard. The layer was repeatedly oxidized and reduced during 50 CV cycles between –0.35 and +0.30 V_{MSE} at a scan rate of 500 mV/s. The sample was sonicated in water to remove any physisorbed particles. Figure 5.2B shows that the SiO_2 nanoparticle layer remained nearly unchanged after electrochemistry, indicating robust attachment as a result of strong multivalent supramolecular interactions. The CVs show highly reversible oxidation and reduction scans (Figure 5.2C). The total coverage of Fc moieties of G3-PPI-$(Fc)_{16}$ sandwiched between the CD SAM and the SiO_2-CD nanoparticles was comparable to the coverage of G3-PPI-$(Fc)_{16}$ on a CD SAM, without the nanoparticles attached,[18] indicating that all Fc moieties were electrochemically addressable. However, the system with only dendrimers on the CD SAM showed a gradual decrease in intensity of oxidation current with increasing scan number, which indicates a gradual desorption and diffusion of dendrimers from the CD SAM.[18,19] With addition of SiO_2-CD nanoparticles onto the surfaces of G3-PPI-$(Fc)_{16}$ on CD SAMs, the current reduction was nearly negligible, probably due to the inhibited diffusion of oxidized dendrimers from the interface as a result of slow mass transport of the SiO_2-CD from the interface at the electrochemical timescale. During the subsequent reduction sweep, the dendrimers remain close to the substrate to be

reduced back to their neutral form leading to rebinding to the host surface and the SiO_2-CD nanoparticles.

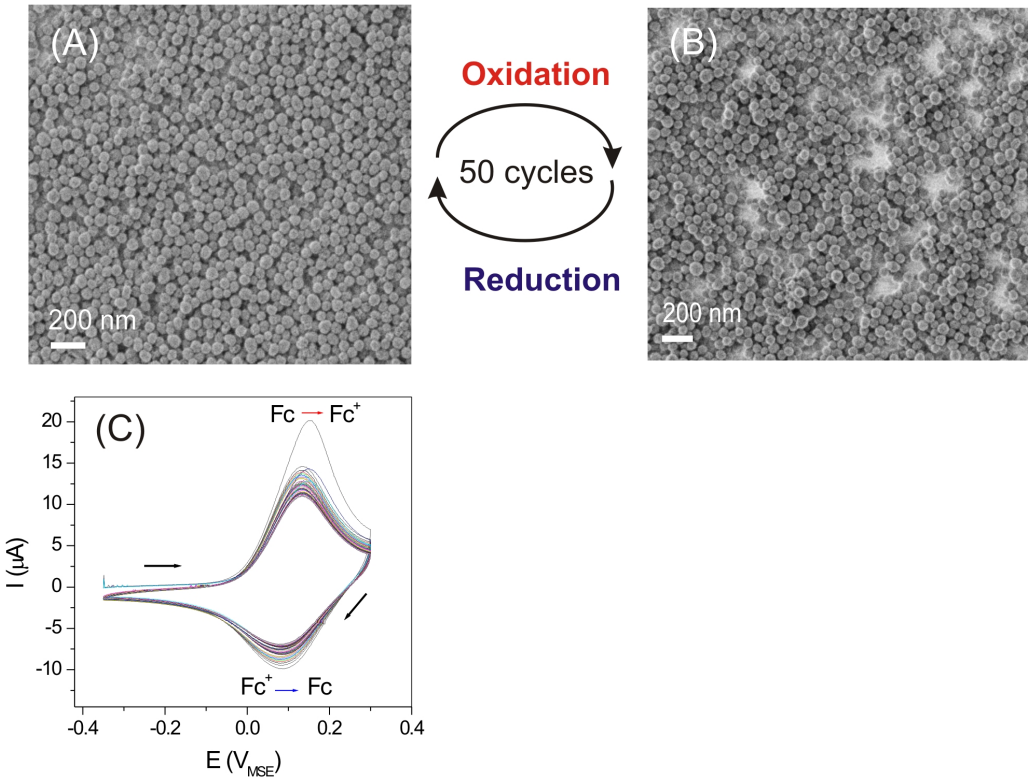

Figure 5.2. SEM images of SiO_2-CD nanoparticle layer on CD SAM with preadsorbed G3-PPI-$(Fc)_{16}$ (A) and after 50 CV scans and 2 min sonication in water (B), and cyclic voltammograms in an aqueous solution 0.1 M K_2SO_4, between –0.35 V_{MSE} and +0.30 V_{MSE}, at scan rates of 500 mV/s (C).

The removal of a complete nanoparticle layer from the surface has been shown to be feasible in Figure 5.1. In reality, one may not need to regenerate the entire substrate, but only a small area. Hence, an individually addressable electrode is essential such that a certain area of a substrate can be selectively oxidized, and error correction can be made on that specific area. As a proof of principle, an intended desorption area was defined by an O-ring. The area within the O-ring was exposed to the electrolyte with the counter electrode, whereas the area outside the O-ring remained dry. The substrate was electrochemically biased at +0.15 V_{MSE} (CA) until the oxidation current had decreased, indicating the complete oxidation of Fc endgroups to ferrocenium cations (Figure 5.3C). This result was further supported by CVs after CA (Figure 5.3D), which showed the absence of Fc oxidation and reduction peaks between -0.35 and +0.30 V_{MSE}, indicating a clean desorption of dendrimers and

nanoparticles. The SEM image in Figure 5.3A corresponds to the area exposed to electrochemistry after CA. The SiO_2-CD nanoparticle layer had been completely removed in the area inside the O-ring. The coverage of SiO_2-CD nanoparticles in the area outside the O-ring remained unchanged (Figure 5.3B).

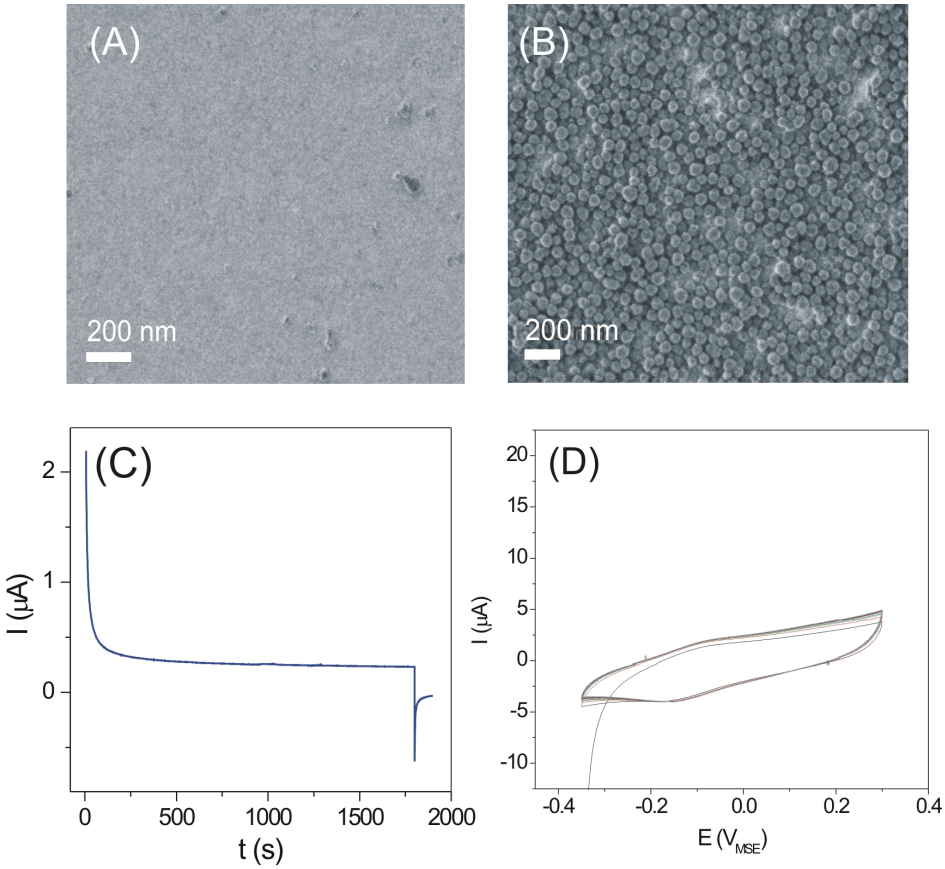

Figure 5.3. SEM images of a SiO_2-CD nanoparticle layer on a CD SAM with preadsorbed G3-PPI-$(Fc)_{16}$ after 1800 s chronoamperometry (CA) and 2 min ultrasonication inside (A) and outside (B) the electrochemically addressed area. CA scan in 0.1 M K_2SO_4 at +0.15 V_{MSE} for 1800 s (C), CVs after 1800 s CA scan (D). CV was performed in an aqueous solution 0.1 M K_2SO_4, between –0.35 V_{MSE} and 0.35 V_{MSE}, at a scan rate of 500 mV/s.

The concept of using ferrocenyl dendrimers as a reversible glue for building up nanostructures is not only limited to homogeneous substrates. The specific and directed assembly of nanostructures was achieved by selectively printing G3-PPI-$(Fc)_{16}$ onto a CD SAM by microcontact printing,[22] followed by selective deposition of SiO_2-CD nanoparticles onto the dendrimer areas of the surface, forming nanoparticle lines (Figure 5.4A). The nanoparticle lines could be 'erased' by electrochemically biasing the substrate at +0.15 V_{MSE}

(Figure 5.4B), followed by ultrasonication of the substrate in water. This led to complete particle removal, similar to that shown in Figure 5.4A.

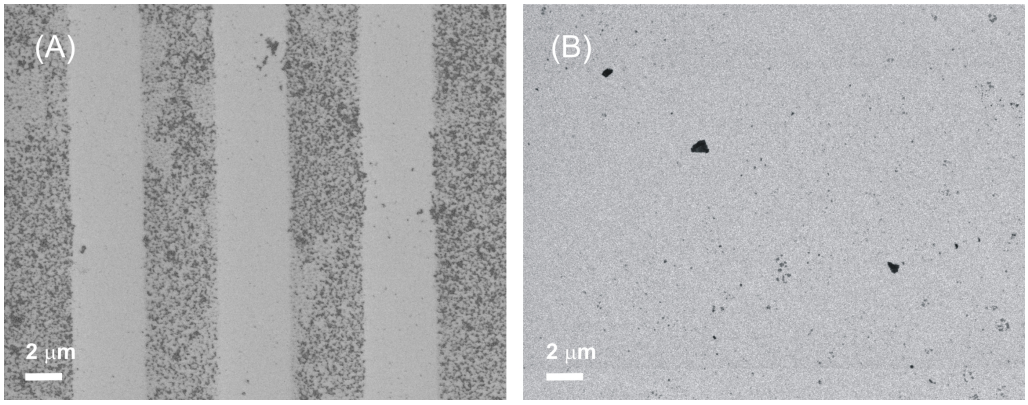

Figure 5.4. Selective deposition of SiO_2-CD nanoparticles onto microcontact printed lines of G3-PPI-$(Fc)_{16}$ at a CD SAM (A), followed by CA at 0.65 V, 20 min and 2 min sonication in water (B).

5.3 CONCLUSIONS

Reversible nanostructure attachment was demonstrated by using ferrocenyl dendrimers as multivalent 'reversible supramolecular glue' for the association and (electrochemical) dissociation of CD-functionalized nanoparticles at the molecular printboard. It is a valid method for nanoparticles of different core materials and sizes, the only requirement being the surface functionalization of the nanoparticles with CD receptors. The actual rate of desorption of the nanoparticles after electrochemical oxidation of the supramolecular glue is governed by the inertia of the nanoparticles as witnessed by the flow rate dependence and the accelerated desorption upon ultrasonic agitation.

The use of electroactive dendrimers as 'reversible supramolecular glue' for building up and (electrochemically induced) breaking down nanostructures at molecular printboards may become generally applicable to the assembly of (bio)molecules and/or nanostructures onto CD SAMs via strong, specific and tunable multivalent host-guest interactions. Local surface modification may be achieved by individually addressed electrodes on a substrate, while the integrity and molecular recognition properties of the SAMs remain unchanged after modification. The limits regarding nanostructure size depend on the accuracy with which such electrode arrays, or the positioning of the electroactive dendrimers onto them, can be controlled. The concept holds potential for the construction and local modification of nanostructures, especially for multi-electrode steered arrays.

5.4 EXPERIMENTAL

Materials. CD heptathioether,[11] and ferrocenyl poly(propylene imine) dendrimers of generation 3 (G3-PPI-$(Fc)_{16}$)[18] were synthesized as described before. CD-functionalized Au (Au-CD, $d \sim 3$ nm) and silica nanoparticles (SiO_2-CD, $d \sim 60$ nm) were prepared according to published procedures.[12,13] Poly(dimethylsiloxane) Sylgard 184 and curing agent were obtained from Dow Corning. Milli-Q water with a resistivity greater than 18 MΩ·cm was used in all our experiments.

Substrate and monolayer preparation. All adsorbate solutions were prepared freshly prior to use. Round glass-supported gold substrates for SPR and electrochemistry (2.54 cm diameter; 50 or 200 nm Au) were obtained from Ssens BV (Hengelo, The Netherlands). Gold substrates were cleaned by immersing the substrates in piranha (conc. H_2SO_4 and 33% H_2O_2 in a 3:1 ratio; **Warning!** piranha should be handled with caution; it is a highly corrosive oxidizing agent) for 10 s and leaving the substrates for 5 min in absolute ethanol. The substrates were subsequently immersed into a 0.1 mM CD heptathioether adsorbate solution in EtOH and $CHCl_3$ (1:2 v/v) for 16 h at 60 °C. The samples were then rinsed with substantial amounts of $CHCl_3$, EtOH and Milli-Q water. The adsorption of G3-PPI-$(Fc)_{16}$ was achieved by immersing the CD SAM substrates in a solution of 1 mM G3-PPI-$(Fc)_{16}$ for 30 min, followed by rinsing with 10 mM aqueous CD at pH 2 and Milli-Q water.

Microcontact Printing. Poly(dimethylsiloxane) (PDMS) stamps were prepared by casting a 10:1 (v/v) mixture of Sylgard 184 elastomer and curing agent against a patterned silicon master. After curing of the stamps overnight, they were mildly oxidized in an ozone plasma reactor (Ultra-Violet Products Inc., model PR-100) for 60 min to render their surfaces hydrophilic. Subsequently, they were inked by soaking them in a 1 mM aqueous solution of the G3-PPI-$(Fc)_{16}$ for 20 min. The stamps were blown dry in a stream of N_2 before printing. The stamps were brought in conformal contact with CD SAM for 10 min and then carefully removed. The substrates were thoroughly rinsed with water.

Assembly of a Dendrimer-Au Nanoparticle Structure. The assembly of a Au nanoparticle sandwich layer was performed in an SPR flow cell setup by first flowing 0.1 mM G3-PPI-$(Fc)_{16}$ (0.1 mM Fc functionality) dendrimers in 10 mM CD, pH 2 solution through the SPR cell, followed by introducing Au-CD (5.8 μM in CD functionality) nanoparticles in a background solution of 10 mM CD in HEPES buffer. Between the adsorption steps, the substrate was rinsed with the respective background solution to remove any physisorbed material. All adsorptions were performed at a flow rate of 0.5 mL/min.

Preparation of a Dendrimer-SiO_2 Nanoparticle Structure. A monolayer of SiO_2-CD nanoparticles was deposited onto a CD SAM with preadsorbed (from solution) or microcontact printed G3-PPI-$(Fc)_{16}$ by using a convective assembly setup.[21] The nanoparticle layer was then ultrasonicated for 20 s, rinsed with Milli-Q water of pH2, and Milli-Q water, and gently blown dry with N_2 before electrochemical testing.

Combined Surface Plasmon Resonance (SPR) Spectroscopy and Electrochemistry Setup. The SPR setup was obtained from Resonant Probes GmBH. The instrument consists of a HeNe laser (JDS Uniphase, 10 mW, λ=632.8 nm) whose light passes through a chopper that is connected to a lock-in amplifier (EG&G 7256). The modulated beam is directed through two polarizers (OWIS) to control the intensity and the plane of polarization of the light. The light is coupled via a high-index prism (Scott, LaSFN9) in the Kretschmann configuration to the backside of the gold-coated substrate, which is optically matched through a refractive-index-matching oil (Cargille; series B; n_D^{25}=1.700 ± 0.002) at the prism, mounted on a θ - 2θ goniometer in contact with a Teflon cell with a volume of 113 mm^3

and a diameter of 6 mm. The light that leaves the prism passes through a beam splitter; subsequently, the s-polarized light is directed to a reference detector, and the p-polarized light passes through a lens which focuses the light onto a photodiode detector. Laser fluctuations are filtered out by dividing the intensity of the p-polarized light (I_p) by the intensity of the s-polarized light (I_s). The SPR experiments were performed in a flow cell system. Rates of 0.5 mL/min and 4.0 mL/min were set as typical flow rates for adsorption and desorption, respectively. Upon completion of an experiment, the flow rate was adjusted back to 0.5 mL/min, such that a proper comparison of SPR intensity changes can be made between before adsorption and after desorption.

Electrochemistry was performed with an AUTOLAB PGSTAT10 in a three-electrode setup with the Au SPR substrates at the prism as the working electrode, a Ag/AgCl ($V_{Ag/AgCl}$ = +0.21 V_{NHE}) reference electrode and a platinum wire as counter electrode. The cyclic voltammetry- (CV-)induced desorption processes on gold were detected by monitoring reflectivity changes as a function of time at a fixed incidence angle, θ. CV was performed on a bare CD SAM, showing the SPR signal remained unchanged during CV, indicating that all SPR intensity changes can be attributed fully to adsorption and desorption processes. Chronoamperometry (CA) was performed by holding the potential at +0.65 $V_{Ag/AgCl}$.

Electrochemistry. Electrochemical measurements were performed in a three-electrode setup equipped with a platinum counter electrode, a mercury sulfate reference electrode (V_{MSE} = +0.61 V_{NHE}) and a screw cap holding the gold working electrode with surface area of 0.44 cm^2. Cyclic voltammetric tests were performed in an aqueous solution 0.1 M K_2SO_4, between –0.35 V_{MSE} and +0.30 V_{MSE}, at the given scan rate. Chronoamperometry (CA) was performed by holding the potential at +0.15 V_{MSE}, and the changes in the oxidation current with time were recorded. The samples after electrochemistry were sonicated for 100 s, rinsed with pH 2 Milli-Q water and blown dry with N_2.

Scanning electron microscopy (SEM). All SEM images were taken with a HR-LEO 1550 FEF SEM.

5.5 ACKNOWLEDGEMENTS

Mr. Mark Smithers is thanked for the SEM measurements. Dr. O. Crespo-Biel is acknowledged for providing the Au-CD nanoparticles.

5.6 REFERENCES

1. Tang, C. S.; Schmutz, P.; Petronis, S.; Textor, M.; Keller, B.; Voros, J. *Biotechnol. Bioeng.* **2005,** *91*, 285.
2. Decher, G. *Science* **1997,** *277*, 1232.
3. Paraschiv, V.; Zapotoczny, S.; de Jong, M. R.; Vancso, G. J.; Huskens, J.; Reinhoudt, D. N. *Adv. Mater.* **2002,** *14*, 722.
4. Kiely, C. J.; Fink, J.; Zheng, J. G.; Brust, M.; Bethell, D.; Schiffrin, D. J. *Adv. Mater.* **2000,** *12*, 640.
5. Alivisatos, A. P.; Johnsson, K. P.; Peng, X. G.; Wilson, T. E.; Loweth, C. J.; Bruchez, M. P.; Schultz, P. G. *Nature* **1996,** *382*, 609.
6. Mirkin, C. A.; Letsinger, R. L.; Mucic, R. C.; Storhoff, J. J. *Nature* **1996,** *382*, 607.

7. Haes, A. J.; Van Duyne, R. P. *J. Am. Chem. Soc.* **2002,** *124*, 10596.
8. Labande, A.; Ruiz, J.; Astruc, D. *J. Am. Chem. Soc.* **2002,** *124*, 1782.
9. Reinhoudt, D. N.; Crego-Calama, M. *Science* **2002,** *295*, 2403.
10. Lahav, M.; Shipway, A. N.; Willner, I.; Nielsen, M. B.; Stoddart, J. F. *J. Electroanal. Chem.* **2000,** *482*, 217.
11. Beulen, M. W. J.; Bügler, J.; Lammerink, B.; Geurts, F. A. J.; Biemond, E.; van Leerdam, K. G. C.; van Veggel, F.; Engbersen, J. F. J.; Reinhoudt, D. N. *Langmuir* **1998,** *14*, 6424.
12. Crespo-Biel, O.; Dordi, B.; Reinhoudt, D. N.; Huskens, J. *J. Am. Chem. Soc.* **2005,** *127*, 7594.
13. Mahalingam, V.; Onclin, S.; Peter, M.; Ravoo, B. J.; Huskens, J.; Reinhoudt, D. N. *Langmuir* **2004,** *20*, 11756.
14. Beer, P. D.; Tite, E. L.; Ibbotson, A. *Dalton Trans.* **1991**, 1691.
15. Plenio, H.; Aberle, C. *Chem. Eur. J.* **2001,** *7*, 4438.
16. Willner, I.; Doron, A.; Katz, E.; Levi, S.; Frank, A. J. *Langmuir* **1996,** *12*, 946.
17. Rojas, M. T.; Koniger, R.; Stoddart, J. F.; Kaifer, A. E. *J. Am. Chem. Soc.* **1995,** *117*, 336.
18. Nijhuis, C. A.; Huskens, J.; Reinhoudt, D. N. *J. Am. Chem. Soc.* **2004,** *126*, 12266.
19. Nijhuis, C. A.; Yu, F.; Knoll, W.; Huskens, J.; Reinhoudt, D. N. *Langmuir* **2005,** *21*, 7866.
20. Valerio, C.; Fillaut, J. L.; Ruiz, J.; Guittard, J.; Blais, J. C.; Astruc, D. *J. Am. Chem. Soc.* **1997,** *119*, 2588.
21. Nijhuis, C. A.; Sinha, J. K.; Wittstock, G.; Huskens, J.; Ravoo, B. J.; Reinhoudt, D. N. *Langmuir* **2006,** *22*, 9770.
22. Bruinink, C. M.; Nijhuis, C. A.; Peter, M.; Dordi, B.; Crespo-Biel, O.; Auletta, T.; Mulder, A.; Schonherr, H.; Vancso, G. J.; Huskens, J.; Reinhoudt, D. N. *Chem. Eur. J.* **2005,** *11*, 3988.

Chapter 6

Supramolecular layer-by-layer assembly of 3D multicomponent nanostructures *via* multivalent molecular recognition interactions*

ABSTRACT. The supramolecular layer-by-layer assembly of 3D multicomponent nanostructures of nanoparticles is demonstrated. Nanoimprint lithography (NIL) was used as the patterning tool for making patterned β-cyclodextrin (CD) self-assembled monolayers (SAMs) and for the confinement of nanoparticles on the substrate. A densely packed and multilayered nanoparticle structure was constructed by alternating assembly steps of complementary guest- (SiO_2-Fc, 60 nm) and host-functionalized (Au-CD, 3 nm) nanoparticles. The effects of order of the nanoparticle assembly steps from large to small nanoparticles and small to large nanoparticles by using SiO_2-Fc, Au-CD, and SiO_2-CD (350 nm) nanoparticles were compared. AFM height profiles revealed that the specific supramolecular assembly of nanoparticles was self-limited, *i.e.* one nanoparticle layer per assembly step, allowing the control over the thickness of the supramolecular hybrid nanostructure by choosing the size of the nanoparticles, irrespective of the core material of the nanoparticles. The roughness of structure was directly influenced by the size of the underlying nanoparticles.

---

* This chapter has been published in X. Y. Ling, I. Y. Phang, D. N. Reinhoudt, G. J. Vancso, J. Huskens, Supramolecular layer-by-layer assembly of 3D multicomponent nanostructures *via* multivalent molecular recognition interactions, *Int. J. Mol. Sci.* **2008,** *9*, 486. (Invited article)

6.1 INTRODUCTION

The assembly of three-dimensional composite nanomaterials has attracted a lot of interest owing to their fascinating optical, electrical and chemical properties that are different from the respective bulk materials,[1-4] and to the need for the development of functional and miniaturized particle-based devices. The control over the lateral dimensions, thickness and composition of the nanomaterials at the nanometer range is particularly crucial. Several assembly techniques have been studied in order to direct nanoparticles into single or multicomponent 3D nanomaterials on surfaces. These are grouped in physical assembly, *e.g.* convective assembly,[5,6] spin coating[7], and spraying[8] and chemical assembly, *e.g.* electrostatic interactions,[7,9-12] thiol-based self-assembly,[13,14] supramolecular chemistry[7,15,16] and coordination chemistry.[17] These techniques are commonly combined with layer-by-layer (LbL) assembly schemes,[18] which involve the alternating adsorption of species with complementary interacting groups to construct multilayered and/or multicomponent nanomaterials.

By combining assembly techniques with top-down lithography, nanostructures with accurate spatial confinement can be fabricated.[19] One of the most commonly used techniques is microcontact printing.[20] Hammond *et al.* demonstrated the selective fabrication of multilayered and multicomponent nanoparticle arrays on microcontact-printed surfaces *via* electrostatic LbL, with the underlying polyelectrolyte layers as adhesive.[21,22] Tsukruk *et al.* reported freely suspended polymeric monolayers with a metal nanoparticle intralayer fabricated by spin-assisted LbL, which thus resulted in a nanocomposite membrane suitable for application in sensors.[7] Recently, our group reported the use of nanoimprint lithography (NIL) as a tool to pattern SAMs and nanoparticles on silicon substrates, which allows patterning of 3D features.[23] An aminoalkylsilane monolayer was first formed on the uncovered regions of the NIL-patterned substrates, which resulted in selective attachment of carboxylate-functionalized polystyrene and silica nanoparticles onto the patterned surfaces by electrostatic interactions.

Supramolecular host-guest interactions, owing to their highly tunable binding strength and reversibility,[7] have been exploited for the assembly of receptor-functionalized molecules and nanoparticles onto interfaces with molecular recognition abilities. Our group has introduced the concept of 'molecular printboards',[24] *i.e.* β-cyclodextrin (CD) SAMs on gold or silicon oxide substrates that possess supramolecular host properties.[25,26] By using adamantyl- or ferrocenyl-functionalized dendrimers as a noncovalent supramolecular glue,[27,28] CD-functionalized gold (Au-CD) and silica (SiO_2-CD) nanoparticles were

assembled onto CD SAMs.[15,29] In Chapter 3, ferrocenyl-functionalized silica (SiO_2-Fc) nanoparticles that can be directly adsorbed onto molecular printboards *via* host-guest recognition are introduced.[7] All of these host- or guest- functionalized nanoparticle layers bind strongly at the interface owing to the formation of multivalent host-guest interactions.[24]

In this chapter, the attachment of alternating host- and guest-functionalized nanoparticles onto NIL-patterned molecular printboards, using nanoparticles of different sizes and core materials, is described. The supramolecular LbL methodology is further extended to the buildup of multicomponent hybrid (organic-metallic-inorganic) nanoobjects by using specific supramolecular nanoparticles that adsorb onto surfaces with complementary recognition properties. We used three types of nanoparticles of different sizes were used, *i.e.*, CD-functionalized Au (Au-CD, d ~ 3 nm), ferrocenyl-functionalized silica nanoparticles (SiO_2-Fc, d ~ 60 nm), and CD-functionalized silica nanoparticles (SiO_2-CD, d ~350 nm). Guest- and host-functionalized nanoparticles were alternatingly assembled in a LbL scheme. The effects of order of the nanoparticle assembly steps from large to small nanoparticles and small to large nanoparticles were compared. The results underline the flexibility of this methodology, *i.e.* the control over the thickness of the nanoobject is dependent on the size of the nanoparticles and independent of the core material of nanoparticles.

6.2 RESULTS & DISCUSSION

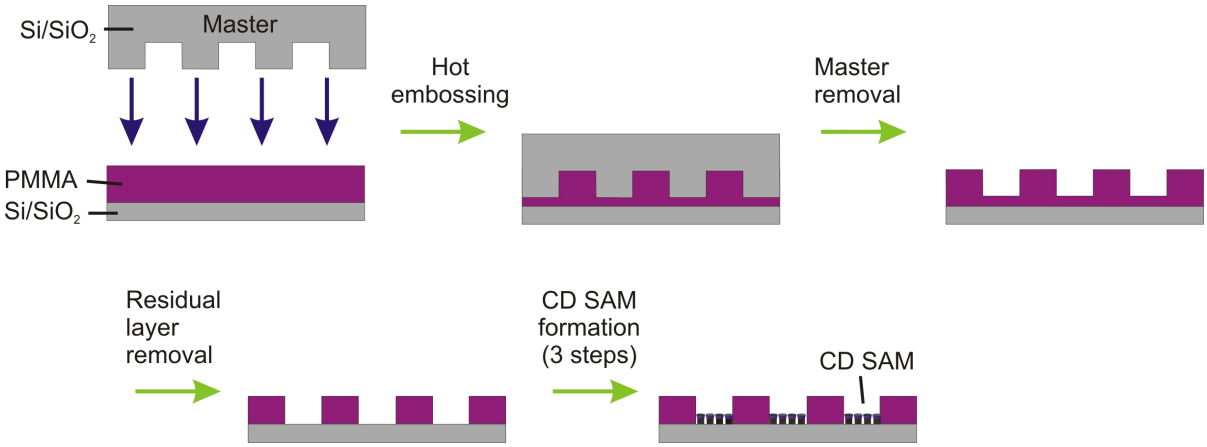

Scheme 6.1. The fabrication process of NIL-patterned CD SAMs.

The aim of this study is to chemically direct the assembly of different types of functionalized nanoparticles onto a patterned substrate, such that a nanoscale 3D architecture constructed from different materials is obtained. Scheme 6.1 illustrates the fabrication process of a NIL-patterned CD SAM. NIL was used as the patterning technique for making patterned CD self-assembled monolayers (SAMs) and to provide physical confinement for

the assembly of nanoparticles on the substrate. To fabricate a patterned substrate, a piranha-cleaned silicon substrate spin-coated with a 500 nm thick layer of PMMA was pressed against a hard stamp at high temperature to form patterned substrates with 3.5 μm wide polymer lines. The residual layer in the imprinted areas was removed sonicating the substrate in acetone for 30 s. The CD SAMs were subsequently formed on the native SiO_2 areas according to a previously described procedure.[16]

Scheme 6.2 shows the preparation of multilayered and multicomponent nanostructures constructed from the layer-by-layer assembly of host- and guest-functionalized nanoparticles at NIL-patterned molecular printboards. Combinations of organic molecules, metallic and inorganic nanoparticles were used for the buildup of multilayered and multicomponent nanoparticle arrays, *i.e.*, generation 1 adamantyl-functionalized poly(propylene imine) dendrimers (G1-PPI-$(Ad)_4$), ferrocenyl-functionalized silica nanoparticles (SiO_2-Fc, d ~ 60 nm), CD-functionalized gold (Au-CD, d ~ 3 nm) and silica nanoparticles (SiO_2-CD, d ~ 350 nm).

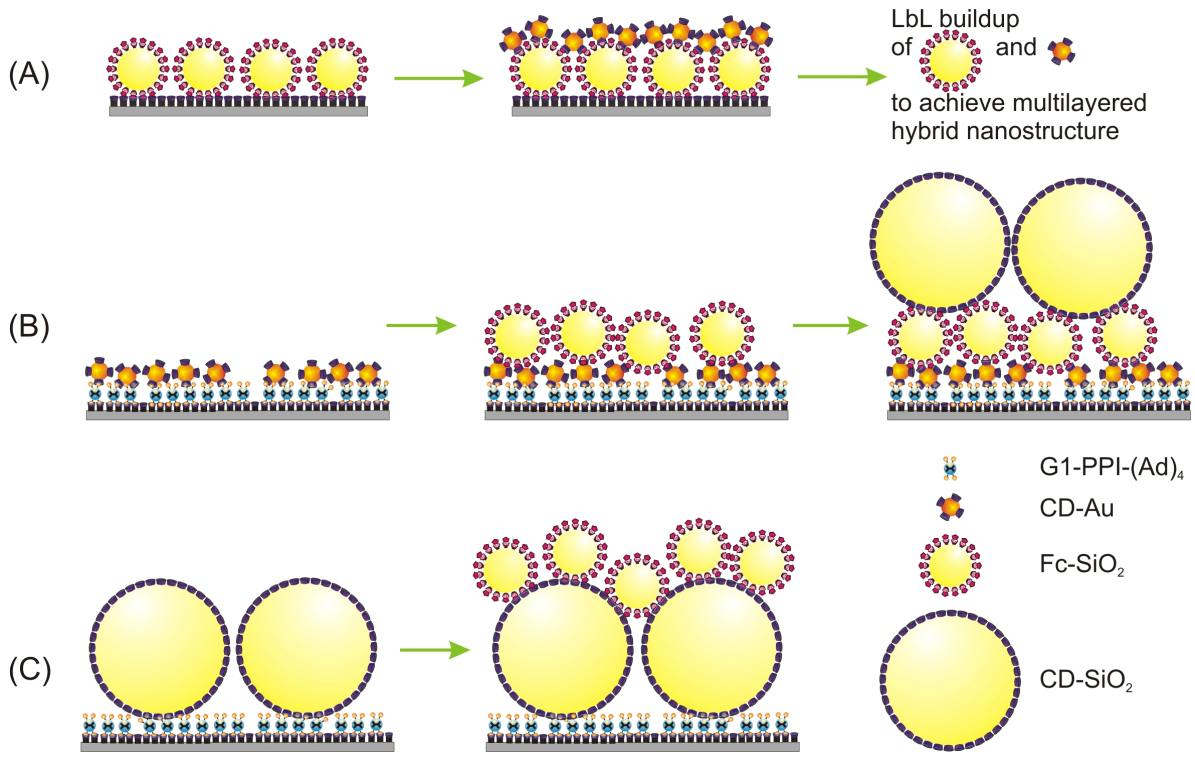

Scheme 6.2. Assembly of multicomponent nanostructures using host- and guest-functionalized nanoparticles: LbL assembly of SiO_2-Fc and Au-CD (A); the nanoparticle assembly from small to large (B) and large to small nanoparticles (C).

In order to demonstrate the suitability of supramolecular LbL assembly in the control over the thickness of a 3D nanostructure, LbL supramolecular assembly of alternate host- and guest- functionalized nanoparticles on NIL patterns was performed. The complementary SiO_2-Fc (60 nm) and Au-CD (2.6 nm) were used as the specific guest- and host-functionalized building blocks to achieve an inorganic-metallic hybrid nanostructure at the molecular printboard with controllable height.

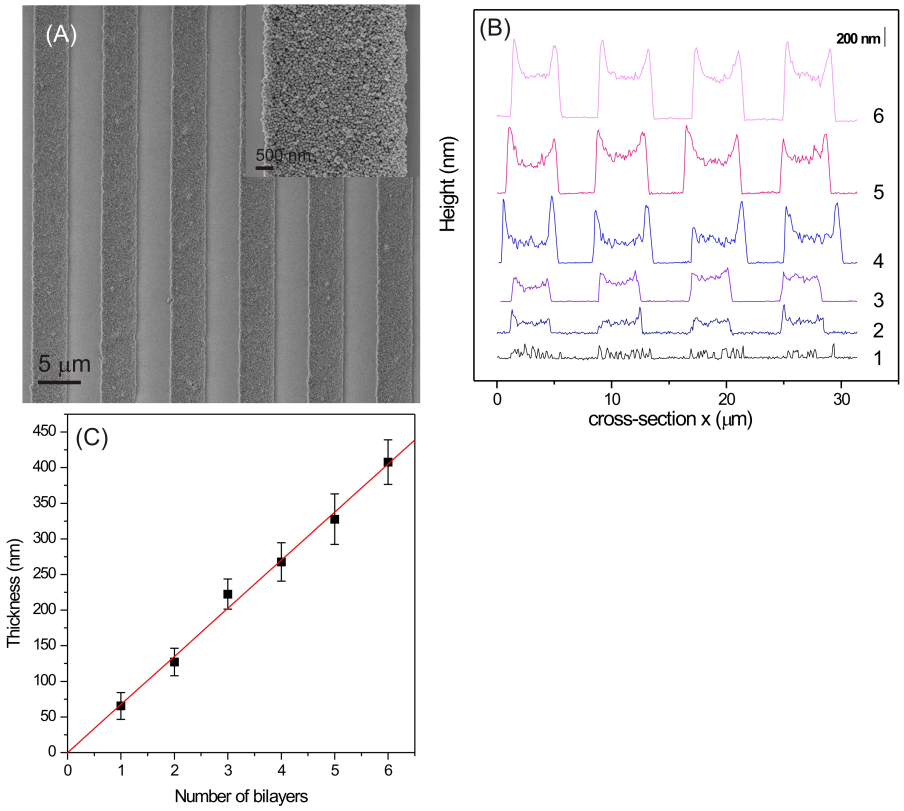

Figure 6.1. SEM image of nanoparticle lines formed after assembly of 6 bilayers of SiO_2-Fc and Au-CD nanoparticles on a NIL-patterned CD SAMs (A). Cross-sectional profiles of the buildup of 1 - 6 bilayers of nanoparticles, as determined by AFM (B). The plot of the height vs. the number of bilayers, as measured by AFM in the centers of the lines (C). A trendline was plotted crossing over origin to serve as a reference.

Figure 6.1A shows a typical image of the nanoparticle lines formed by the assembly of 6 bilayers of SiO_2-Fc and Au-CD on a NIL-patterned CD monolayer, as shown in Scheme 6.2A. For ease of imaging and height measurement, the polymer lines were removed in all cases in acetone using ultrasonication after completion of nanoparticle adsorption, unless otherwise stated. The hybrid nanostructures were constructed by first assembling SiO_2-Fc

onto NIL-patterned CD SAMs by capillary assisted assembly, followed by rinsing with pH 2 water. The complementary Au-CD nanoparticles were subsequently assembled onto the SiO_2-Fc layer by dipping the substrate in a Au-CD nanoparticle suspension, followed by rinsing with HEPES buffer. The buildup of a multilayered structure was achieved subsequently by alternating assembly steps of SiO_2-Fc and Au-CD. The resulting structure was densely packed. Only single layers of complementary nanoparticles were attached in each step, providing good specificity and control over the number of layers of nanoparticles. Figure 6.1B shows the atomic force microscopy (AFM) height profiles of the nanostructures up to 6 bilayers. In the centers of the lines, the heights correspond to the thicknesses expected from the number of bilayers. However, at the edges, the heights of the nanoparticle lines are higher, as observed before.[16] This is attributed to non-specific attachment of nanoparticles at the NIL-imprinted polymer line patterns during the assembly. Figure 6.1C shows the linear relationship of the thickness of the nanostructure (taken at the center of the nanoparticle lines) as a function of the number of bilayers of alternate host- and guest-functionalized nanoparticles. The average roughness of the nanostructures (taken at the center of the nanoparticle lines), defined as the height variation on the physical surface of the nanoparticle lines, is in the range of 17 - 32 nm, irrespective of the number of bilayers.

Figure 6.2 shows the sequential buildup of multilayered and multicomponent nanoparticle arrays with increasing nanoparticle sizes (Scheme 2B). The layer of G1-PPI-$(Ad)_4$ on NIL-patterned CD SAMs was prepared by immersing the substrate in an aqueous solution of G1-PPI-$(Ad)_4$ for 30 min, followed by rinsing with 10 mM aqueous β-CD at pH 2 and Milli-Q water. As shown in Figure 6.2A, Au-CD nanoparticles were subsequently adsorbed onto the substrate *via* specific multivalent host-guest interactions to G1-PPI-$(Ad)_4$. Complementary guest-functionalized SiO_2-Fc nanoparticles were attached to the Au-CD nanoparticle layer (on a separate sample) by capillary assisted assembly,[16] forming a hybrid nanostructure at the surface (Figure 6.2B). Further growth of the nanostructure was achieved by adsorption of SiO_2-CD of 350 nm (Figure 6.2C).

The assembly of G1-PPI-$(Ad)_4$ and Au-CD nanoparticles resulted in an average cross-section height of 4 - 5 nm (Figure 6.2A and D (i)). The height corresponds well to the summed sizes of the Au-CD and CD-SAM underneath.[30] The apparent absence of a contribution of G1-PPI-$(Ad)_4$ to the AFM height is attributed to flattening of the dendrimer upon interaction with the CD SAM.[31] The sequential deposition of SiO_2-Fc resulted in an average thickness of ~ 65 nm (Figure 6.2D (ii)), except at the edges of the structures, where there are a few spikes higher than 100 nm, which is be attributed to non-specifically adsorbed

nanoparticles along the polymer edges during assembly. Further adsorption of SiO_2-CD of 350 nm led to a total height of about 450 nm (Figure 6.2D (iii)). All nanostructures have good packing density, but lack order, which is attributed to the size distribution of the nanoparticles. Their resultant cross-sectional height profiles correspond well to the accumulated diameters of the deposited nanoparticles. This indicates that the control over the thickness of the supramolecular hybrid nanostructure can be obtained by selecting the sizes of the nanoparticles, irrespective of their core material.

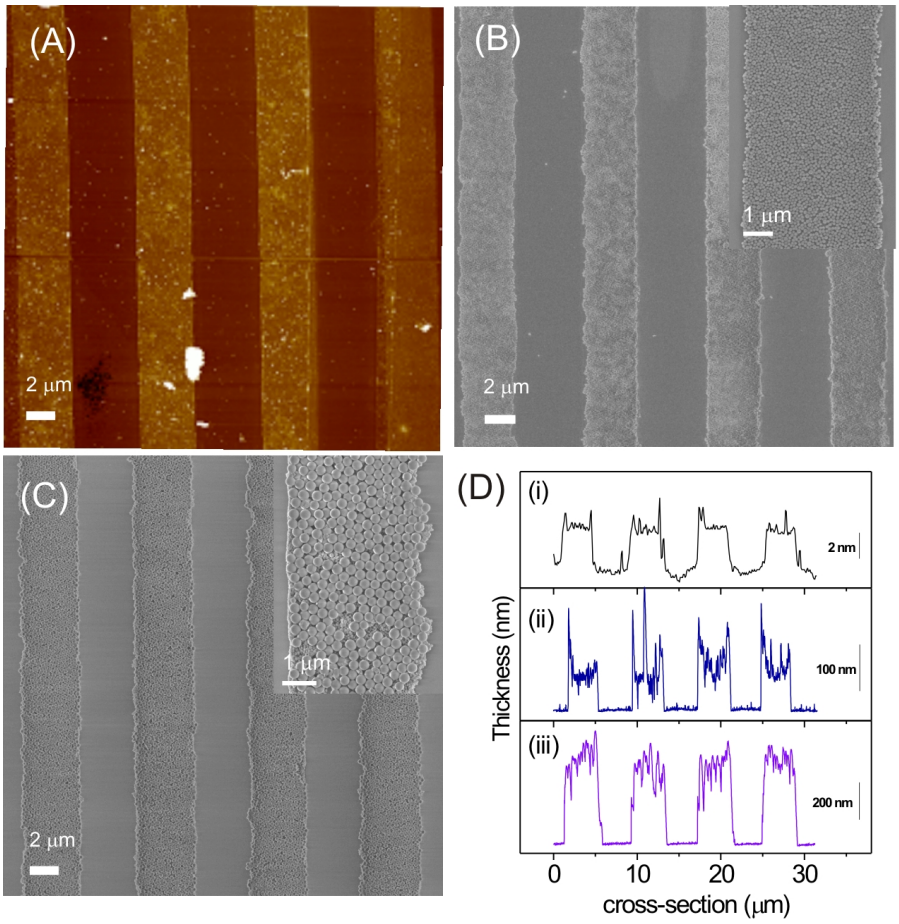

Figure 6.2. AFM image of a monolayer of Au-CD on a monolayer of G1-PPI-$(Ad)_4$ on a NIL-patterned molecular printboard (A), and SEM images of the subsequent assembly of SiO_2-Fc (60 nm) nanoparticles onto the Au-CD nanoparticle lines (B), and SiO_2-CD (350 nm) onto the SiO_2-Fc nanoparticle lines (C). In all cases, PMMA was removed in acetone using ultrasonication after completion of the adsorption steps. The cross-sectional height profiles of (i) - (iii), for samples made according to A - C, respectively, as determined by AFM is shown in (D).

In order to demonstrate the flexibility of building up nanostructures by supramolecular host-guest chemistry, the multilayer stack was reversed, *i.e.* with decreasing nanoparticle size (Scheme 6.2C). Onto a NIL-patterned CD SAMs, G1-PPI-$(Ad)_4$ and 350 nm SiO_2-CD (Figure 6.3A) were adsorbed first followed by SiO_2-Fc (Figure 6.3B). In contrast to Figure 6.2C, the SiO_2-CD layer assembled on the flat areas between the NIL patterns displayed nearly hexagonal close packing. In the subsequent assembly step, SiO_2-Fc nanoparticles were densely but unorderedly attached on the surface of SiO_2-CD. The height profiles after each assembly step correspond well to the accumulated thicknesses of nanoparticles assembled, *i.e.*, 380 nm and 480 nm for the first and second layer, respectively. The further assembly of Au-CD on the SiO_2-Fc layer is not shown here as the increase in height was negligible compared to the size distributions of the SiO_2-Fc and SiO_2-CD nanoparticles, and it was too small to be observed by SEM.

When comparing the height profiles of Figure 6.2D and Figure 6.3C, the roughness and the order of these nanostructures appear to be different. The roughness of the samples was measured by AFM. The measured 'roughness' is influenced by different factors, *e.g.* the sharpness of AFM tip, the packing density of the nanoparticle array and the size of the underlying nanoparticles. Here, the first two factors can be excluded as AFM tips used and the adsorption parameters were standardized. Hence, the roughness of nanostructure was attributed by the roughness of the underlying surfaces. For instance, the assembly of SiO_2-Fc nanoparticles on top of Au-CD, followed by SiO_2-CD (Scheme 2B) resulted in roughnesses of 17 nm and 46 nm, respectively. The size of Au-CD is 20 times smaller than of SiO_2-Fc, hence, the roughness of the Au-CD nanoparticle layer (~ 1 nm) is almost negligible compared to the SiO_2-Fc layer. The SiO_2-Fc assembled onto these smaller nanoparticles as if they were assembled on a flat surface. Thus, the roughness of the SiO_2-Fc layer has not been affected by the underlying Au-CD nanoparticle layer and is only affected by the packing of the SiO_2-Fc nanoparticles. However, in subsequent assembly of SiO_2-CD, the starting roughness inherited from the SiO_2-Fc layer induced a rougher surface (46 nm) upon adsorption of SiO_2-CD. This has also affected the packing of the SiO_2-CD layer, which was dense but without order, in contrast to the better order and smaller roughness for SiO_2-CD directly assembled to the dendrimer-covered CD SAM (15 nm). Similarly, the roughness of SiO_2-Fc adsorbed onto SiO_2-CD (63 nm) was a lot higher than when adsorbed onto the nearly flat Au-CD (17 nm).

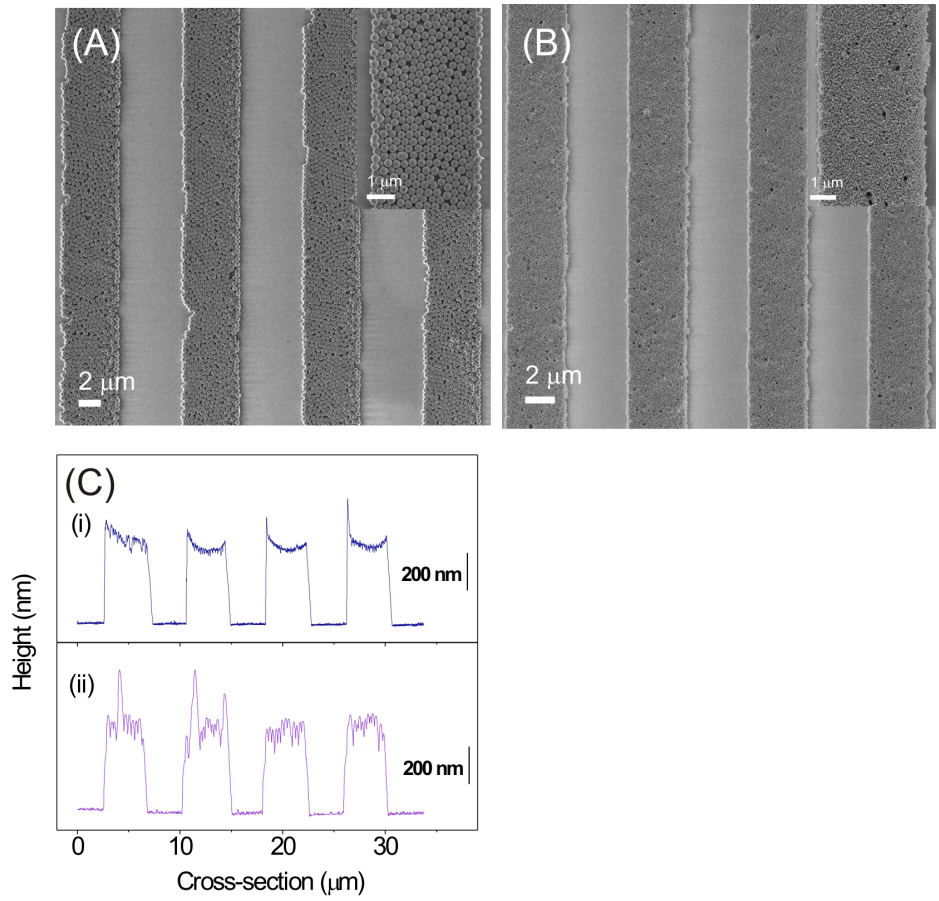

Figure 6.3. SEM images of the sequential buildup of layers of nanoparticles onto NIL-patterned molecular printboards with descending nanoparticle sizes. The first layer was formed by adsorbing SiO_2-CD (350 nm) onto G1-PPI-$(Ad)_4$ at the molecular printboard (A), followed by adsorption of SiO_2-Fc (60 nm) onto these nanoparticle lines (B). The AFM cross-sectional height profiles (i) and (ii), for samples made according to A and B, respectively, is shown in (C).

6.3 CONCLUSIONS

By combining the top-down nanoimprint lithography and bottom-up supramolecular layer-by-layer assembly, multicomponent and multilayered nanoparticle arrays have been created. NIL provides confinement in x- and y-direction to the nanostructure, while supramolecular LbL assembly provides control over of the height of the nanostructures in the nanometer range. The flexibility of the supramolecular LbL scheme has been verified by buildup of (sub-micron) multilayered and multicomponent nanoparticle nanostructures independent of core material and size. Thus, the combination of NIL and supramolecular chemistry in building up nanostructures is a powerful combination for fabricating complex

nanoparticle arrays, where tunable surface and core material properties are of high importance for future nanotechnological developments.

6.4 EXPERIMENTAL

Materials. CD heptamine[25] and generation 1 adamantyl-functionalized poly(propylene imine) dendrimer (G1-PPI-$(Ad)_4$)[27] were synthesized as described before. CD-functionalized Au (Au-CD, d ~ 3 nm), CD-functionalized silica nanoparticles (SiO_2-CD, d ~ 350 nm), and ferrocenyl-functionalized silica nanoparticles (SiO_2-Fc, d ~ 60 nm) were prepared as described previously.[15,32,29,33] Milli-Q water with a resistivity greater than 18 MΩ.cm was used in all experiments.

Substrate and monolayer preparation. Silicon substrates were cleaned by immersion in piranha solution (conc. H_2SO_4 and 33% H_2O_2 in a 3:1 ratio; **Warning!** piranha should be handled with caution; it can detonate unexpectedly) for 15 min to form a SiO_2 layer on the surface. The substrates were then sonicated in Milli-Q water and ethanol for 1 min, and dried with N_2. CD SAMs were obtained according to a published procedure.[32,26] In brief, the substrates were functionalized with *N*-[3-(trimethoxysilyl)propyl]ethylenediamine by gas-phase evaporation in a desiccator under vacuum. Transformation of the amino-terminated SAMs to isothiocyanate-bearing layers was accomplished by exposure to an ethanol solution of 1,4-phenylene diisothiocyanate at 50 ^oC for 2 h. CD SAMs were finally obtained by reaction of the isothiocyanate-terminated monolayer with CD heptamine in pH 7.5 water, at 50 ^oC for 2 h.

Nanoparticle Assembly. The assembly of a layer of Au nanoparticles was performed by first dipping a CD substrate in a 0.1 mM aqueous solution of G1-PPI-$(Ad)_4$ in 10 mM CD, pH 2, followed by dipping in a solution of Au-CD (5.8 μM in CD functionality) nanoparticles in HEPES buffer (pH 7.0). After each adsorption step, the substrate was rinsed with the corresponding buffer solution to remove any physisorbed material. The adsorptions of SiO_2-Fc and SiO_2-CD onto a CD SAM and pre-adsorbed G1-PPI-$(Ad)_4$ at a CD SAM, respectively, were performed by vertically withdrawing the substrate from a 0.2 wt% nanoparticle suspension at a constant speed of 0.1 μm/s.[34] The substrate layer was then ultrasonicated for 20 s, rinsed with pH 2 water, and MilliQ water, and gently blown dry with N_2.

Nanoimprint Lithography (NIL). Silicon stamps were made by photolithography followed by reactive ion etching (RIE, Elektrotech Twin system PF 340). A stamp consisted of 3.5 μm lines at 7.5 μm period with a height of 500 nm. A 500 nm thick layer of PMMA was spin-coated on a piranha-cleaned silicon substrate. Stamp and substrate were put in contact and a pressure of 40 bar was applied at a temperature of 180 ºC using a hydraulic press (Specac). The residual layer was removed by dipping the samples in acetone for 30 s.

Scanning electron microscopy (SEM). All SEM images were taken with a HR-LEO 1550 FEF SEM.

Atomic force microscopy (AFM). AFM measurements were carried out with a Dimension D3100 using a NanoScope IVa controller equipped with a hybrid 153 scanner (Veeco / Digital Instruments (DI), Santa Barbara, CA) under ambient conditions. Silicon cantilevers from Nanosensors (Nanosensors, Wetzlar, Germany) were used for intermittent contact (tapping) mode operation.

6.5 ACKNOWLEDGEMENTS

Mr. M. Smithers and Mr. In Yee Phang are thanked for the SEM and AFM measurements, respectively. Dr. O. Crespo-Biel is acknowledged for providing the Au-CD nanoparticles.

6.6 REFERENCES

1. Blodgett, K. B.; Langmuir, I. *Phys. Rev.* **1937,** *51*, 964.
2. Blanco, A.; Chomski, E.; Grabtchak, S.; Ibisate, M.; John, S.; Leonard, S. W.; Lopez, C.; Meseguer, F.; Miguez, H.; Mondia, J. P.; Ozin, G. A.; Toader, O.; van Driel, H. M. *Nature* **2000,** *405*, 437.
3. Lopez, C. *Adv. Mater.* **2003,** *15*, 1679.
4. Shipway, A. N.; Katz, E.; Willner, I. *ChemPhysChem* **2000,** *1*, 18.
5. Malaquin, L.; Kraus, T.; Schmid, H.; Delamarche, E.; Wolf, H. *Langmuir* **2007,** *23*, 11513.
6. Fustin, C. A.; Glasser, G.; Spiess, H. W.; Jonas, U. *Langmuir* **2004,** *20*, 9114.
7. Chen, K. M.; Jiang, X.; Kimerling, L. C.; Hammond, P. T. *Langmuir* **2000,** *16*, 7825.
8. Salata, O. V.; Dobson, P. J.; Hull, P. J.; Hutchison, J. L. *Adv. Mater.* **1994,** *6*, 772.
9. Caruso, F.; Spasova, M.; Susha, A.; Giersig, M.; Caruso, R. A. *Chem. Mater.* **2001,** *13*, 109.
10. Vossmeyer, T.; Guse, B.; Besnard, I.; Bauer, R. E.; Mullen, K.; Yasuda, A. *Adv. Mater.* **2002,** *14*, 238.
11. Hicks, J. F.; Seok-Shon, Y.; Murray, R. W. *Langmuir* **2002,** *18*, 2288.
12. Lvov, Y.; Ariga, K.; Onda, M.; Ichinose, I.; Kunitake, T. *Langmuir* **1997,** *13*, 6195.
13. Andres, R. P.; Bielefeld, J. D.; Henderson, J. I.; Janes, D. B.; Kolagunta, V. R.; Kubiak, C. P.; Mahoney, W. J.; Osifchin, R. G. *Science* **1996,** *273*, 1690.
14. Nakanishi, T.; Ohtani, B.; Uosaki, K. *J. Phys. Chem. B* **1998,** *102*, 1571.
15. Crespo-Biel, O.; Dordi, B.; Reinhoudt, D. N.; Huskens, J. *J. Am. Chem. Soc.* **2005,** *127*, 7594.
16. Maury, P. A.; Reinhoudt, D. N.; Huskens, J. *Curr. Opin. Coll. Interf. Sci.* **2008,** *13*, 74.
17. Wanunu, M.; Popovitz-Biro, R.; Cohen, H.; Vaskevich, A.; Rubinstein, I. *J. Am. Chem. Soc.* **2005,** *127*, 9207.
18. Decher, G.; Hong, J. D.; Schmitt, J. *Thin Solid Films* **1992,** *210*, 831.
19. Dziomkina, N. V.; Vancso, G. J. *Soft Matter* **2005,** *1*, 265.
20. Mrksich, M.; Whitesides, G. M. *Trends Biotechnol.* **1995,** *13*, 228.
21. C. J. Kiely, J. F., J. G. Zheng, M. Brust, D. Bethell, D. J. Schiffrin *Adv. Mater.* **2000,** *12*, 640.
22. Bae, S. S.; Lim, D. K.; Park, J. I.; Kim, S.; Cheon, J.; Lee, W. R. *J. Phys. Chem. B* **2004,** *108*, 2575.
23. Maury, P.; Escalante, M.; Reinhoudt, D. N.; Huskens, J. *Adv. Mater.* **2005,** *17*, 2718.
24. Ludden, M. J. W.; Reinhoudt, D. N.; Huskens, J. *Chem. Soc. Rev.* **2006,** *35*, 1122.

25. Beulen, M. W. J.; Bügler, J.; Lammerink, B.; Geurts, F. A. J.; Biemond, E.; van Leerdam, K. G. C.; van Veggel, F.; Engbersen, J. F. J.; Reinhoudt, D. N. *Langmuir* **1998,** *14*, 6424.
26. Onclin, S.; Mulder, A.; Huskens, J.; Ravoo, B. J.; Reinhoudt, D. N. *Langmuir* **2004,** *20*, 5460.
27. Michels, J. J.; Baars, M.; Meijer, E. W.; Huskens, J.; Reinhoudt, D. N. *J. Chem. Soc., Perkin Trans. 2* **2000**, 1914.
28. Nijhuis, C. A.; Huskens, J.; Reinhoudt, D. N. *J. Am. Chem. Soc.* **2004,** *126*, 12266.
29. Mahalingam, V.; Onclin, S.; Peter, M.; Ravoo, B. J.; Huskens, J.; Reinhoudt, D. N. *Langmuir* **2004,** *20*, 11756.
30. Crespo-Biel, O.; Dordi, B.; Maury, P.; Peter, M.; Reinhoudt, D. N.; Huskens, J. *Chem. Mater.* **2006,** *18*, 2545.
31. Bruinink, C. M.; Nijhuis, C. A.; Peter, M.; Dordi, B.; Crespo-Biel, O.; Auletta, T.; Mulder, A.; Schonherr, H.; Vancso, G. J.; Huskens, J.; Reinhoudt, D. N. *Chem. Eur. J.* **2005,** *11*, 3988.
32. Ling, X. Y.; Reinhoudt, D. N.; Huskens, J. *Langmuir* **2006,** *22*, 8777.
33. Zhang, J. H.; Zhan, P.; Wang, Z. L.; Zhang, W. Y.; Ming, N. B. *J. Mater. Res.* **2003,** *18*, 649.
34. Maury, P.; Peter, M.; Crespo-Biel, O.; Ling, X. Y.; Reinhoudt, D. N.; Huskens, J. *Nanotechnology* **2007,** *18*, 044007.

Chapter 7

The formation and transfer printing of stable and ordered 3D supramolecular nanoparticle structures

ABSTRACT. A sequential process is described to construct highly stable and crystalline supramolecular nanoparticle structures. Convective assembly was used to physically assemble and organize β-cyclodextrin (CD)-functionalized nanoparticles on a CD-functionalized surface. Subsequently, adamantyl dendrimers serve as supramolecular glue to chemically bond neighboring nanoparticles together and to couple the whole nanoparticle crystal to the CD surface. When using a patterned PDMS stamp as the substrate, the dendrimer-infiltrated nanoparticle crystals could be transfer-printed onto a target surface. By varying the geometry and size of the PDMS stamps, single nanoparticle lines, interconnected nanoparticle rings, and V-shaped nanoparticle assemblies were obtained. The nanoparticle crystals serve as 3D receptors for the binding of (multiple) complementary guest molecules, indicating that the supramolecular host functionalities of the nanoparticle crystals are retained throughout the fabrication process.

7.1 INTRODUCTION

The self-assembly of nanoparticles into integrated micro- or nanostructures on a surface is attracting a lot of attention owing to the interesting optical properties of ordered structures of nanoparticles at the 100 – 1000 nm length scale. The stability and ordering of these nanoparticle structure are the most important features of such structures so that their function can be exerted on matrices for long term application, *e.g.* in miniaturized electronic,[1] optical[2] and biological[3] devices.

Ordered nanoparticle crystals have been prepared by using physical assembly techniques, such as capillary assembly,[4-7] dewetting,[8,9] spin coating,[10-12] and sedimentation.[13,14] Such nanoparticle crystals are generally assembled by surface tension and long-range attractive forces. Therefore they lack the long-term stability required for applications. As a result, chemical nanoparticle assembly techniques employing electrostatic interactions,[6,15-18] covalent bonding,[19,20] and biomolecular[21,22] and supramolecular chemistry[23-27] have been utilized to chemically bond the nanoparticles onto surfaces, forming stable nanoparticle layers (for details, please refer to Chapter 2). In general, a high affinity of the chemically functionalized particles to the complementary surface reduces the mobility of the nanoparticles, and thus leads to less-ordered structures.[30] Hence a balance between the surface-particle interactions and the physical assembly process is needed to achieve highly stable and ordered nanoparticle crystals.

The integration of particles into devices typically requires placing them in specific positions. Top-down nanofabrication techniques, *e.g.* microcontact printing,[31] transfer printing,[4,32-34] nanoimprint lithography,[35,36] and photolithography[37] have been combined with self-assembly of nanoparticles to direct the nanoparticles into desired patterns with specified dimensions. Recently, μCP has been expanded to the transfer printing of various nanostructures.[33,38,39] Wolf *et al.* demonstrated the transfer printing of nanoparticles with single 60-nm nanoparticle resolution.[4,32] In many cases, only a single layer of nanoparticles has been transferred at each step because the transfer printing was carried out *via* conformal contact. Hence, the success of the printing strongly depends on the adhesion (e.g. van der Waals interactions) between the transferred objects and the target surface.[39]

Previously in Chapter 4, the supramolecular β-cyclodextrin (CD) host-guest chemistry for the directed and specific assembly of nanoparticle structures has been exploited. CD-functionalized nanoparticles were assembled onto (patterned) CD monolayers, with guest-functionalized dendrimers as a noncovalent supramolecular glue.[27,40-42] Fine-tuning of the supramolecular interactions is needed during the nanoparticle assembly to result

in nearly hexagonally close-packed nanoparticle arrays.[30] The supramolecular nanoparticle array is stable and reversible owing to the tunability of the binding strength of the host-guest interactions.[30,43]

In this chapter, a sequential process is presented, which leads to the formation and transfer printing of highly stable and crystalline three-dimensional functionalized nanoparticle crystals. The strategy combines the advantages of convective assembly (in ordering nanoparticles) and supramolecular chemistry (in providing stability to the nanoparticle crystal) in a serial manner. The stability of the nanoparticle crystal is assessed by sonication in water. The ability of transfer printing of nanoparticle crystals of different sizes and shapes will be demonstrated. The recognition functionality of the transfer-printed CD-functionalized nanoparticle crystals is shown by the binding of lissamine rhodamine-labeled divalent guest molecules into the nanoparticle structures.

7.2 RESULTS AND DISCUSSION

In order to create ordered and stable supramolecular three-dimensional nanoparticle crystals on surfaces, convective nanoparticle assembly and supramolecular host-guest chemistry were applied in a sequential manner (Scheme 7.1). CD-functionalized polystyrene (PS-CD) nanoparticles were assembled onto CD monolayers by using a capillary-assisted deposition setup, as introduced and described in Chapter 4.[41,44] The preformed CD-functionalized nanoparticle array was subsequently infiltrated with complementary adamantyl-terminated poly(propylene imine) dendrimers of generation 5 (G5-PPI-$(Ad)_{64}$) and rinsed with 10 mM CD solution to remove excess of dendrimers from the nanoparticle crystal.

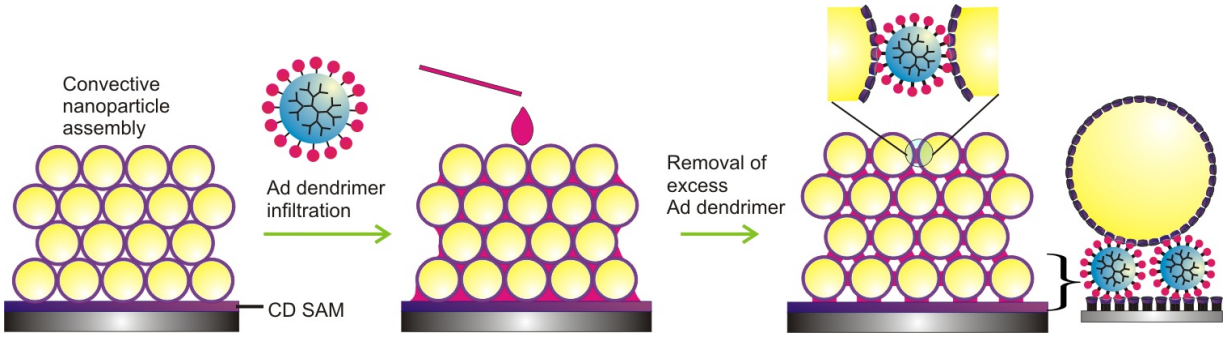

Scheme 7.1. The formation of three-dimensional supramolecular nanoparticle crystals on CD monolayers.

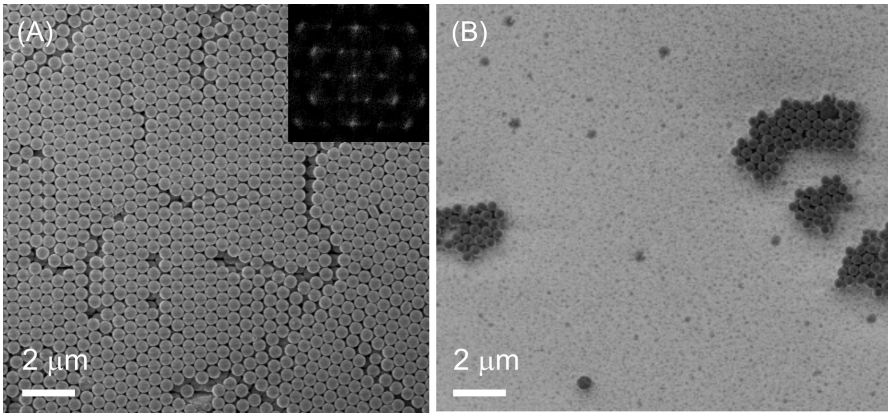

Figure 7.1. SEM images of nanoparticle crystals with (A) and without (B) infiltration with G5-PPI-$(Ad)_{64}$ after sonication in water. The inset at the upper right of (A) shows the 2D Fourier transform of (A).

In order to assess the effect of dendrimer infiltration on the stability of the nanoparticle array, 10 min sonication in water was applied. Figure 7.1 shows the SEM images of the nanoparticle crystals after sonication, where (A) was infiltrated with G5-PPI-$(Ad)_{64}$ and (B) was a sample without infiltration. The SEM image of Figure 7.1A clearly indicates that the neighboring nanoparticles were attached to each other and that the entire G5-PPI-$(Ad)_{64}$-infiltrated nanoparticle crystal was robustly attached to the surface. The crystal remained hexagonally close packed (hcp) on the CD monolayer, which is supported by a 2D Fourier transform in the inset of Figure 7.1(A). In contrast, the nanoparticle array without G5-PPI-$(Ad)_{64}$ infiltration was completely destroyed by sonication, with only a few nanoparticles remaining on the surface. These results highlight the importance of the infiltration with adamantyl-terminated dendrimers to infer stability to the nanoparticle arrays. The strong and thermodynamically stable multivalent host-guest interactions between G5-PPI-$(Ad)_{64}$ and PS-CD allow the dendrimer to function as a supramolecular glue to chemically bind neighboring nanoparticles together into a large nanoparticle structure and to adhere the nanoparticle structure to the CD monolayer. The order of the nanoparticle structures achieved here contrasts the direct assembly of CD-functionalized nanoparticles onto CD monolayers preadsorbed with adamantyl- or ferrocenyl-terminated dendrimers,[41,43,45] which typically resulted in less than perfectly packed nanoparticle arrays (see Chapter 4). The current method optimally exploits the advantages of convective assembly in ordering nanoparticles and of supramolecular interactions in binding nanoparticles into a stable entity, by applying them in sequential manner, and thus allows the formation of highly ordered and stable functionalized nanoparticle crystals.

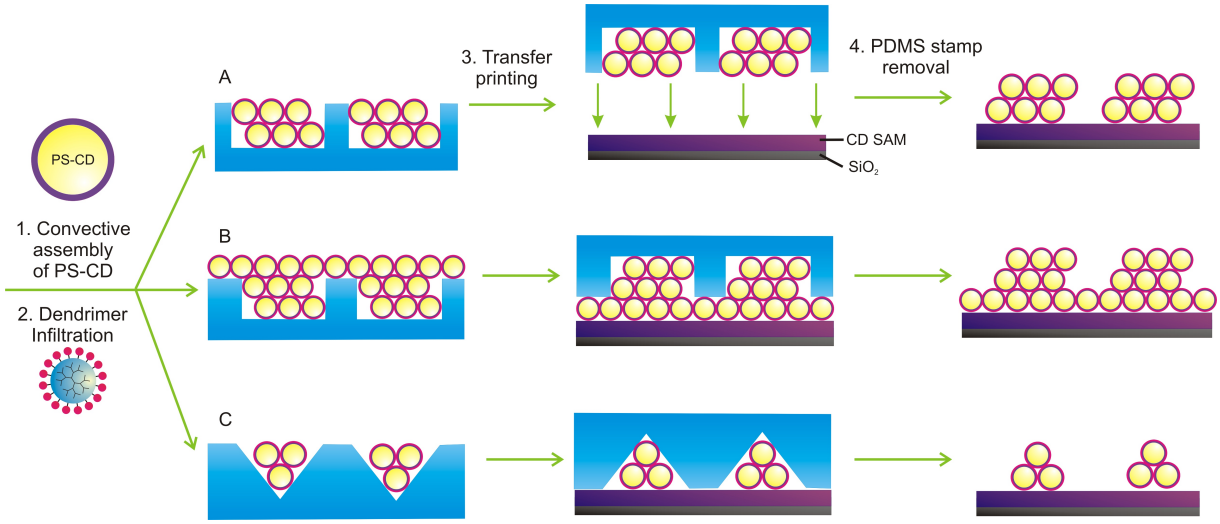

Scheme 7.2. The preparation of multilayered PS-CD nanoparticle structures on patterned PDMS stamps and transfer printing of these structures onto CD monolayer substrates. The shape and geometry of the resulting nanoparticle crystals can be varied by the choice of the shape and size of the PDMS stamps (A – C).

The assembly and integration of nanoparticles do not necessary have to be carried out directly onto the final substrate. The transfer printing of 3D nanoparticle crystals made of individual nanoparticles with supramolecular host functionalities was examined (Scheme 7.2A). A poly(dimethylsiloxane) (PDMS) stamp functions as a temporary elastomeric substrate that, after dendrimer infiltration, allows the transfer printing of the nanoparticle structures to a target surface. PS-CD nanoparticles were convectively assembled into the grooves of the oxidized PDMS stamp patterned with 3 μm grooves and 5 μm lines with a height of 750 nm (Scheme 7.2A),. The sample was dipped in a 1 mM aqueous solution of G5-PPI-$(Ad)_{64}$ for 30 min, after which it was blown dry with N_2. The PDMS stamp with G5-PPI-$(Ad)_{64}$-infiltrated PS-CD nanoparticles was brought into conformal contact with a target surface functionalized with a CD monolayer in a high-humidity environment. After stamp removal, the substrates were thoroughly rinsed with water and blown dry with N_2.

Long and continuous micrometer-sized nanoparticle lines were successfully transferred from the PDMS stamp onto the CD monolayer on silicon (Figure 7.2A). The width of the printed structures was 3 μm, which is in agreement with the width of the grooves of the PDMS stamps. The height of the printed microstructures is similar to that of the original template and corresponds to two layers of nanoparticles being transferred (Figure 7.2C, D). A zoom-in SEM image (Figure 7.2B) reveals that the packing of the transferred nanoparticle building blocks remained highly ordered and hexagonally close-packed, with a

quality similar to the nanoparticle crystal shown in Figure 7.1A. Some cracks were observed on the printed nanoparticle structures, probably resulting from the drying after the transfer printing process.

It is noted that the humidity of the printing environment is particularly vital to the success of transfer printing of the supramolecular nanoparticle structures. Under ambient conditions, the transfer was less effective, *i.e.* transfer occurred only in some areas of the sample. The efficient printing in humid environment is attributed to the fact that CD host-guest interactions are most favored in the presence of water. Similar observation was also reported by Nijhuis *et al.* in the case of supramolecular metal transfer printing.[46]

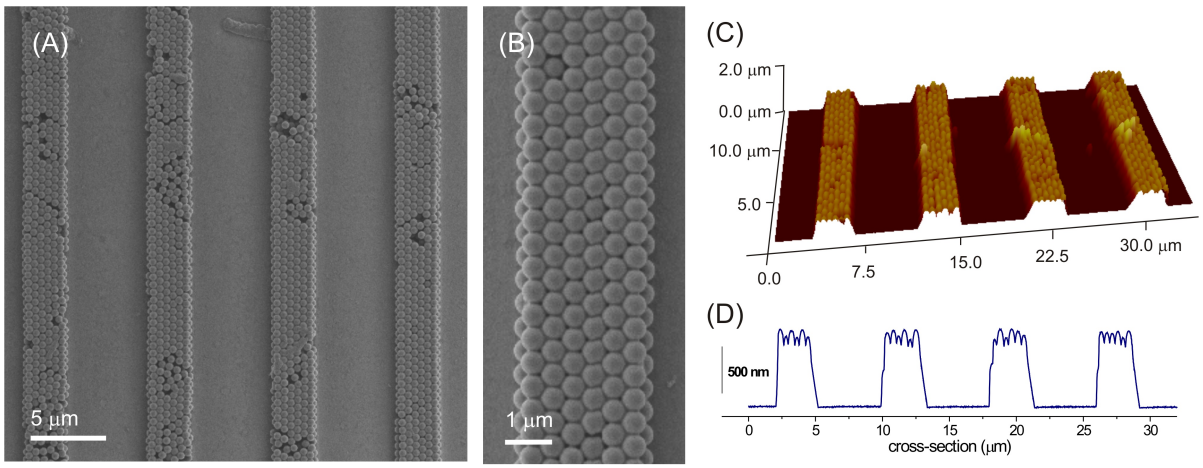

Figure 7.2. SEM (A, B), and AFM (C) images and AFM height profile (D) of the transfer-printed 3D continuous nanoparticle crystals (infiltrated with G5-PPI-$(Ad)_{64}$) on CD monolayers.

To assess the effect of infiltration by G5-PPI-$(Ad)_{64}$ in the nanoparticle transfer printing, a PS-CD array was directly printed on a CD monolayer without infiltration, which resulted in the printing of less than a layer of individual nanoparticles in the contact area (Figure 7.3A). This indicates that the use of a supramolecular glue is crucial in bonding the nanoparticles into a stable nanoparticle structure and in ensuring good adhesion to the CD monolayer *via* multiple host-guest interactions.

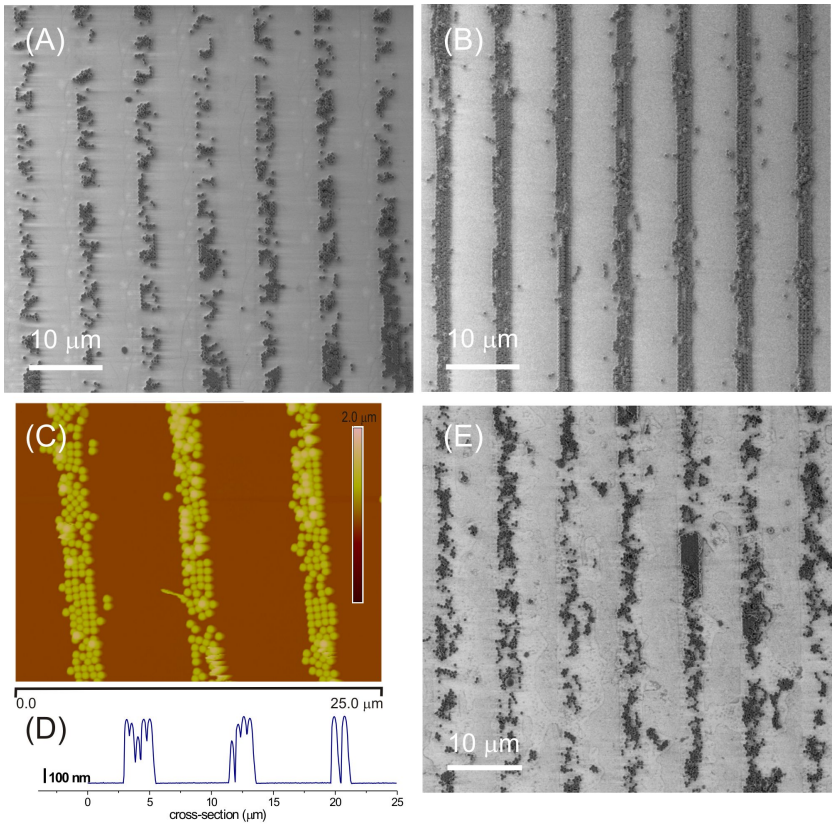

Figure 7.3. SEM image after transfer printing of a PS-CD structure without dendrimer infiltration onto a CD monolayer (A); SEM (B), AFM (C) images and an AFM height profile (D) of a PS-CD nanostructure (without dendrimer infiltration) after transfer printing onto a G5-PPI-$(Ad)_{64}$-coated CD monolayer; SEM image of a PS-CD nanoparticle structure infiltrated with G1-PPI-$(Ad)_4$ after transfer printing onto a CD monolayer (E).

In order to decouple the interactions between the particles and the substrate from the internal particle-particle cohesion, a PS-CD structure without dendrimer infiltration was transfer printed onto a G5-PPI-$(Ad)_{64}$-preadsorbed CD monolayer. Well-defined line features, but less orderly packed single layers of nanoparticles were obtained (Figure 7.3B - D). The other nanoparticles remained on the PDMS stamp, probably as a result of adhesion between the PDMS and nanoparticles.[4] The bilayer nanoparticle structures on the PDMS stamp apparently have broken apart during the printing process, so that only the nanoparticles with direct contact to the surface were successfully transferred.

One of the degrees of freedom when using supramolecular host-guest interactions is the binding strength and stoichiometry. In particular, the number of interactions and the resulting multivalent binding strength of adamantyl dendrimers binding to CD surfaces are a function of the dendrimer generation.[40] Here, adamantyl-terminated poly(propylene imine)

dendrimer of generation 1 (G1-PPI-$(Ad)_4$), which has only 4 adamantyl endgroups as compared to the 64 endgroups of G5-PPI-$(Ad)_{64}$, was used as a weaker supramolecular glue in the transfer printing of 3D nanoparticle structures. The transfer printing of G1-PPI-$(Ad)_4$-infiltrated nanoparticles onto a CD monolayer showed that mostly only a single layer of PS-CD was transferred, with occasionally a few nanoparticles stacked on top of this layer (Figure 7.3E). These results show that the binding strength of G1-PPI-$(Ad)_4$ is not strong enough to integrate the discrete nanoparticles into a stable macroscopic structure. Hence, it is important to use a supramolecular glue with a sufficiently high binding strength. In this case, G5-PPI-$(Ad)_{64}$ efficiently binds the nanoparticles into a stable crystal.

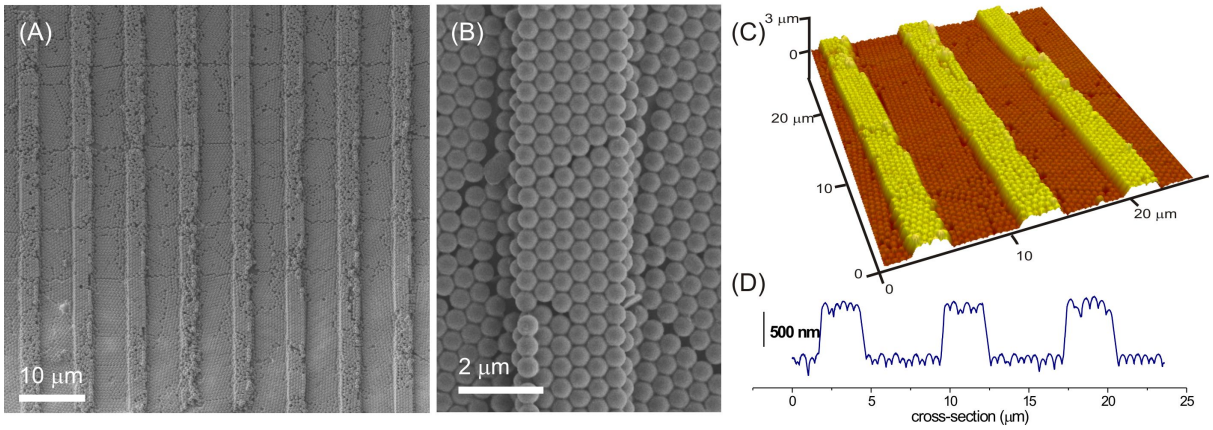

Figure 7.4. SEM images of a transfer-printed patterned continuous nanoparticle crystal (infiltrated with G5-PPI-$(Ad)_{64}$) on CD monolayers (A, B). A 3D AFM image (C) and AFM height profile (D) of the printed nanoparticle structure.

To demonstrate the versatility of the supramolecular transfer printing process, nanoparticles were assembled onto a PDMS stamp, in this case not only in the grooves, but also across the entire stamp (Scheme 7.2B). This was achieved by lowering the substrate withdrawing speed during the convective assembly step. The 3D and continuous nanoparticle array was then infiltrated with G5-PPI-$(Ad)_{64}$ and printed onto a CD monolayer. As shown in Figure 7.4, a large 3D and continuous patterned nanoparticle structure was printed on the surface. The printed structure inherited the highly hcp order (Figure 7.4B) from the initial nanoparticle array on PDMS. As dictated by the depth of the grooves on the stamp, the protruding ridges were two nanoparticle layers high (Figure 7.4C, D). As also seen in Figure 7.4, the underlying full nanoparticle layer shows domain boundaries and does not follow the crystal axes of the ridges.

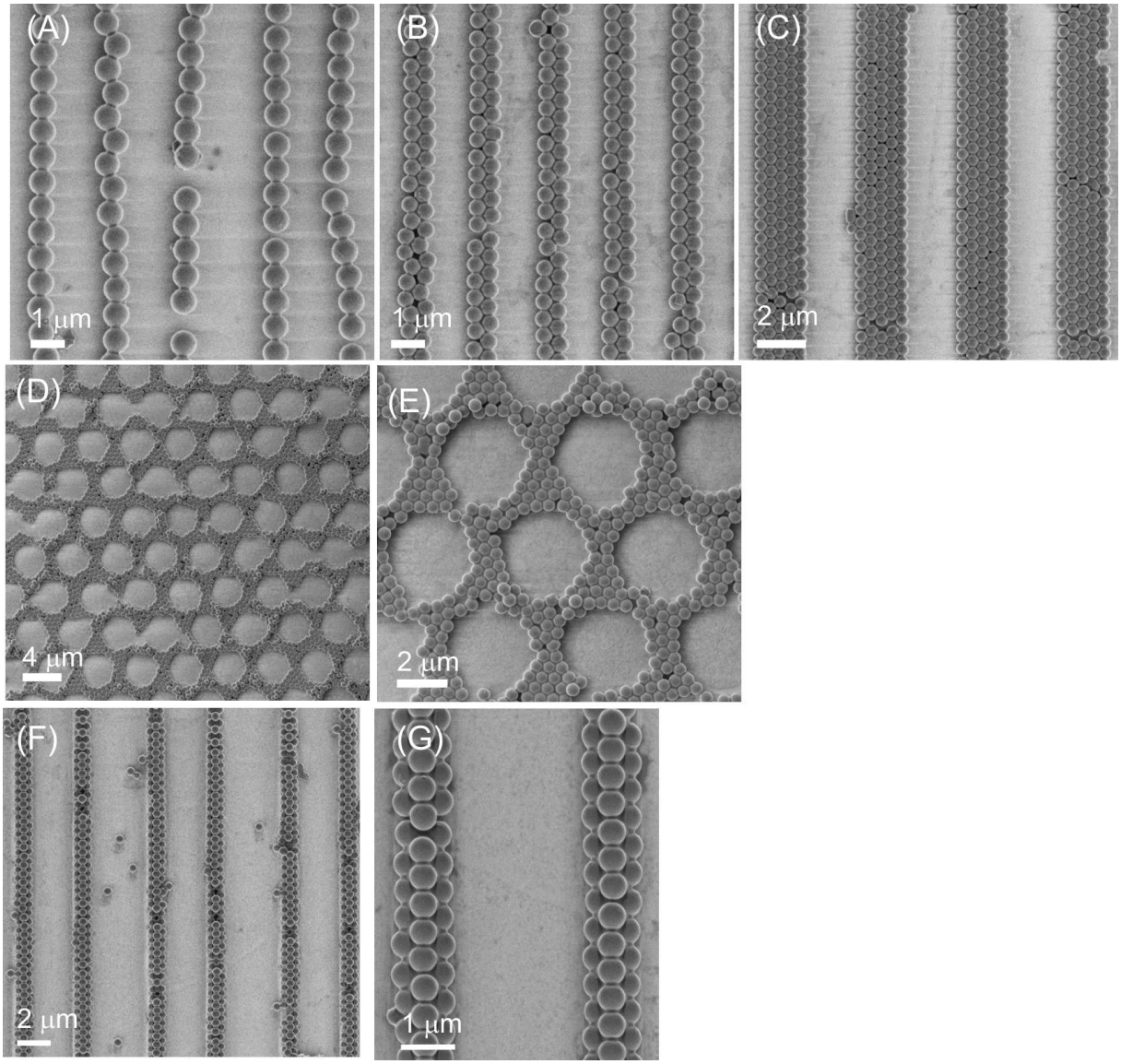

Figure 7.5. SEM images of the transfer-printed nanoparticle crystals of different shapes on CD monolayers: single-layer nanoparticle lines from a stamp of 500 nm (A), 1 μm (B) and 2 μm (C) in width, single-layer networks of interconnected PS-CD nanoparticle rings (D, E) and double-layer V-shaped nanoparticle crystals made according to Scheme 7.2c (F, G).

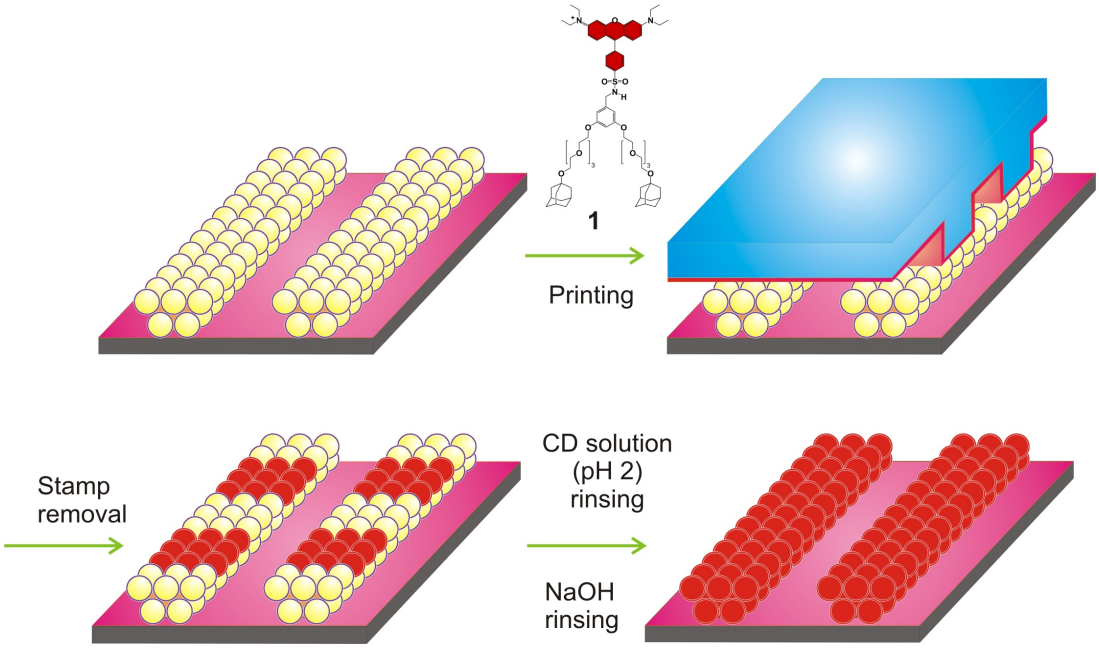

Scheme 7.3. The printing and rinsing of lissamine rhodamine-labeled divalent adamantyl guest **1** on the nanoparticle structures.

By manipulation of the sizes and shapes of the patterns on the PDMS stamp (Scheme 7.2), a broad range of transfer-printed nanoparticle structures were made (Figure 7.5). On a PDMS stamp with 500 nm, 1 μm and 2 μm wide grooves with a depth of 150 nm, single-layer nanoparticle lines were printed onto CD monolayers (Figure 7.5A - C). When using the 500-nm structures, the position of the some nanoparticle lines was slightly shifted, which is attributed to the deformation of the soft PDMS during the printing process and reduced mechanical strength of the nanoparticle structure. Nevertheless, the configurations of the nanoparticle lines are well retained. As shown in Figure 7.5(D, E), networks of interconnected PS-CD nanoparticle rings were printed onto CD monolayers. The nanoparticles remained hcp-ordered upon printing. There were occasional unoccupied spaces within the networks, which can be due to defects originating from the convective assembly step. Figure 7.5(F, G) shows V-shaped nanoparticle crystals printed on a surface, which were made using stamps with V-shaped grooves (Scheme 7.2C). Based on the results of the supramolecular transfer printing, the control over the shape and size of the nanoparticle assemblies can be elegantly provided by carefully selecting proper building blocks and stamps of desired shapes and dimensions.

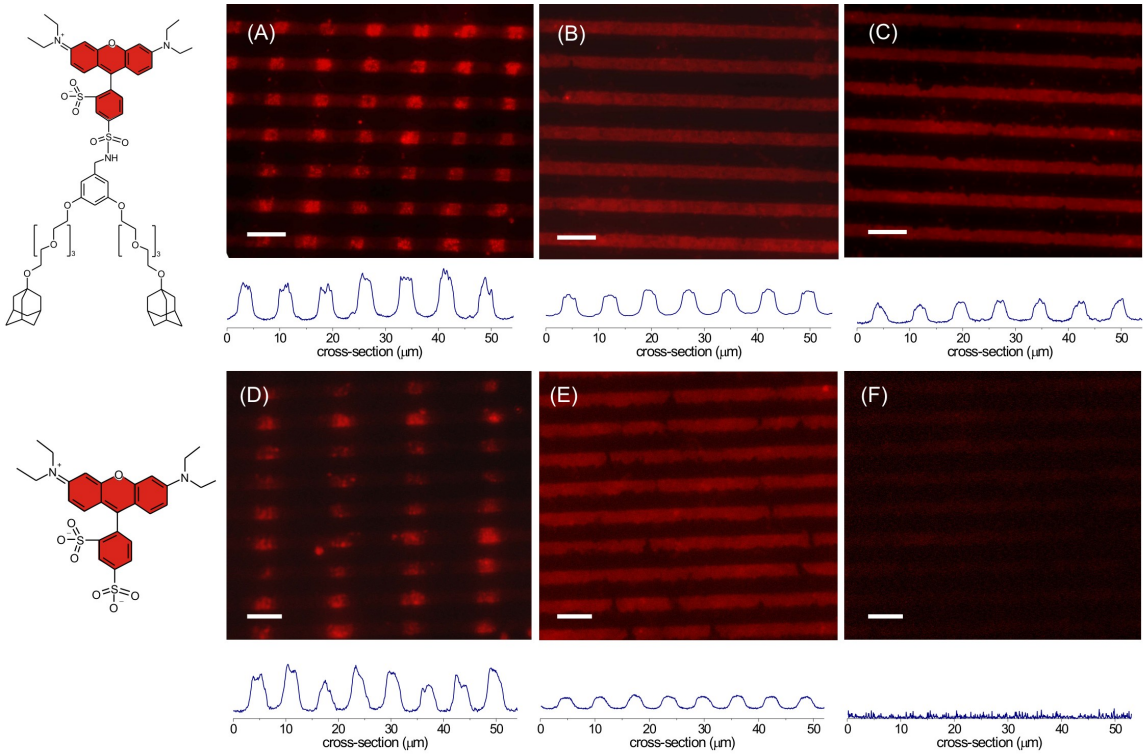

Figure 7.6. Fluorescence microscopy images and intensity profiles of the printing of divalent adamantyl guest **1** (A – C) and native lissamine rhodamine (D – F) on infiltrated and transfer-printed nanoparticle structures before (A, D), and after rinsing with a CD solution at pH 2 (B, E), and subsequent rinsing with 1 M NaOH (C, F). The images were taken at green excitation light. All scale bars indicate 10 µm. All fluorescence intensity profiles are shown at the same scale.

To investigate the host-guest functionality of the generated PS-CD microstructures, lissamine rhodamine-labeled divalent adamantyl guest molecules (**1**) were microcontact printed perpendicularly onto the continuous nanoparticle lines (Scheme 7.3). These divalent guest molecules are known to bind to the CD monolayers *via* divalent host-guest interactions.[47] A fluorescence image (Figure 7.6A) shows the substrate after printing **1** onto the nanoparticle lines. Only squares, equivalent to the size of the contact area between the nanoparticle structure and the PDMS stamp, were fluorescent. After intense rinsing with a CD solution at pH 2, the fluorescence became apparent along the complete nanoparticle lines (Figure 7.6B), while in the areas outside the nanoparticle crystals, the intensity remained negligible. The integrated fluorescence intensity along the nanoparticle lines remained constant, indicating the diffusion of **1** along the nanoparticle lines, with negligible desorption. Upon rinsing with 1 M NaOH, the fluorescence intensity (Figure 7.6C) remained similar to

Figure 7.6B. This indicates that the stability of the interaction is not resulting from electrostatic interactions, as NaOH is expected to deprotonate the dendrimer cores and to eliminate this interaction. To confirm this, native lissamine rhodamine, which is not a guest molecule for CD, was printed onto nanoparticle line structures (Figure 7.6D). The fluorescent molecules remained on the nanoparticle crystal after rinsing with a CD solution at pH 2, probably as a result of electrostatic interactions, but the fluorescence was completely removed by 1 M NaOH. This indicates that the supramolecular host properties of the nanoparticle crystals remained unchanged after the transfer printing process. The result is different from the direct printing of **1** on CD monolayers, where copious rinsing with a CD solution resulted in (near) complete reduction in fluorescence.[47] This difference may result from the three-dimensional nature of the nanoparticle crystal. It suggests that the nanoparticle crystal lines can act as a 3D receptor which allows transportation of complementary guest molecules within its structure.

The potential of the nanoparticle crystals as a building block for multiple guest molecule storage and transportation was further examined by using **1** and an analogous divalent guest **2**, labeled with fluorescein. On a nanoparticle structure freshly printed with **1** (Figure 7.7A), a drop of fluorescein-labeled divalent adamantyl guest **2** was casted, and subsequently rinsed with water. Imaging with green excitation light (Figure 7.7B) showed that the discrete fluorescent squares of **1** had become homogeneous fluorescent lines. Imaging the substrate with blue excitation (Figure 7.7E) showed that **2** was immobilized along the same nanoparticle structures, also in a homogeneous fashion. Similar to the results discussed earlier, rinsing with CD solution at pH 2 (Figure 7.7C, F) and 1 M NaOH (Figure 7.7D, G) did not reduce the fluorescence intensities in either case. The combined results show that multiple guest molecules can be stored within the CD-functionalized nanoparticle crystals simultaneously *via* the specific divalent host-guest interactions.

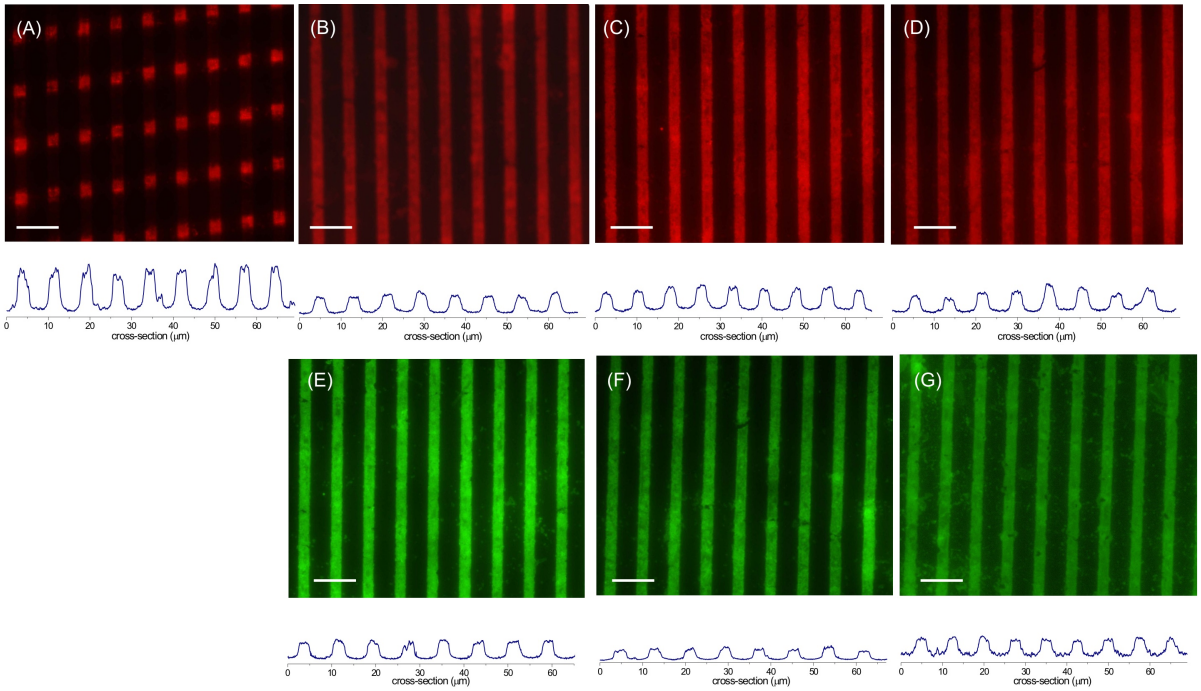

Figure 7.7. Fluorescence microscopy images and intensity profiles of the printing of lissamine rhodamine divalent guest, **1** on infiltrated and transfer-printed nanoparticle structures (A), after addition of fluorescein-labeled divalent guest **2** and rinsing with water (B, E), and after subsequent rinsing with a CD solution at pH 2 (C, F) and rinsing with 1 M NaOH (D, G). The images at top (A – D) were taken at green excitation light, whereas the images at the bottom (E – G) were taken at blue excitation. All scale bars indicate 10 μm. All fluorescence intensity profiles are shown at the same scale.

7.3 CONCLUSIONS

Stable and ordered supramolecular nanoparticle crystals were prepared by using a sequential process of convective assembly and supramolecular host-guest interactions. Highly hcp ordered nanoparticle crystals were first assembled on a CD monolayer by using convective assembly. The infiltration of adamantyl dendrimers effectively bonds the neighboring nanoparticles together and adhere the nanoparticle crystal onto the surface *via* multivalent host-guest interactions, forming a stable and ordered 3D nanoparticle structures. Nanoparticle crystals with varying shapes have been constructed by using PDMS stamps with different geometries and sizes. The molecular recognition functionality of the individual nanoparticles can be exploited for further assembly of complementary guest molecules. Such stable, ordered supramolecular nanoparticle structures with recognition properties, with highly tunable yet stable binding strength, can potentially be engineered as sensing channels for the detection, storage and transportation of complementary molecules.

7.4 EXPERIMENTAL

Materials. β-Cyclodextrin (CD) heptamine, adamantyl-terminated poly(propylene imine) dendrimers of generation 1 and 5 (G1-PPI-$(Ad)_4$ and G5-PPI-$(Ad)_{64}$), the lissamine rhodamine-labeled divalent adamantyl guest (**1**), and the fluorescein-labeled divalent adamantyl guest (**2**) were synthesized as described before.[47-49] *N*-[3-(trimethoxysilyl)propyl]ethylenediamine, 1,4-phenylene diisothiocyanate and lissamine-rhodamine B sulfonylchloride were obtained from Sigma Aldrich, Germany. Poly(dimethylsiloxane) (PDMS) Sylgard 184 prepolymer and curing agent were obtained from Dow Corning. Carboxylate-functionalized polystyrene nanoparticles of 500 nm were purchased from Polysciences Inc. CD-functionalized polystyrene nanoparticles (PS-CD) were prepared from these as described before.[30] Milli-Q water with a resistivity higher than 18 MΩ·cm was used in all experiments.

Substrate and monolayer preparation. Silicon substrates were cleaned by immersion in piranha solution (conc. H_2SO_4 and 33% H_2O_2 in a 3:1 volume ratio, **Warning!** piranha should be handled with caution; it is a highly corrosive oxidizing agent) for 15 min to form a SiO_2 layer on the surface. The substrates were then sonicated in Milli-Q water and ethanol for 1 min, and dried with N_2. CD monolayers were obtained according to a published procedure.[25,50] In brief, the substrates were functionalized with *N*-[3-(trimethoxysilyl)propyl]ethylenediamine by gas-phase evaporation. Transformation of the amino-terminated SAMs to isothiocyanate-bearing layers was accomplished by exposure to an ethanolic solution of 1,4-phenylene diisothiocyanate at 50 ^oC for 2 h. CD monolayers were finally obtained by reaction of the isothiocyanate-terminated monolayers with CD heptamine in water at pH 7.5, at 50 ^oC for 2 h.

Patterned silicon substrates were made by photolithography followed by reactive ion etching (RIE) or e-beam lithography. They consisted of gratings of 5 μm lines at 8 μm period with a height of 750 nm, a stamp consists of 1 μm, and 2 μm grooves with a height of 150 nm, of 2 μm dots with a height of 500 nm, and 2 μm v-shaped grooves with a height of 760 nm. PDMS stamps were prepared by casting a 10:1 (v/v) mixture of poly(dimethylsiloxane) (PDMS) prepolymer and curing agent against a patterned silicon master. After curing of the stamps overnight, they were mildly oxidized in an O_2 plasma etcher (Tepla 300E) for 1 min to render them hydrophilic.

Assembly of PS-CD nanoparticle layers/arrays. A nanoparticle array was prepared by vertically depositing PS-CD nanoparticles onto a CD monolayer or oxidized PDMS stamp at a withdrawing speed between 0.1 - 1 μm/s. The preformed nanoparticle array was then gently dipped in a 1 mM aqueous solution of G1-PPI-$(Ad)_4$ or G5-PPI-$(Ad)_{64}$ for 30 min, followed by rinsing with water and blowing dry with N_2.

Transfer printing of nanoparticle structures. An oxidized PDMS stamp with G5-PPI-$(Ad)_{64}$-infiltrated PS-CD nanoparticle structures was brought into conformal contact with a CD monolayer, unless otherwise stated. The printing was performed on a platform of a close-by water bath at 40 ^oC. When the nanoparticle printing was performed in ambient conditions without humidity control, the transfer of the nanoparticle structures was less effective, and took a long printing time (3 h). At high humidity, only 1 h printing time was sufficient to induce successful transfer printing with higher yields. The printing time was not further optimized. After removal of the stamp, the substrates were thoroughly rinsed with water and blown dry with N_2.

Printing of divalent guest 1 or native lissamine rhodamine on transfer-printed nanoparticle structures. A oxidized PDMS stamp with 5 μm lines at 20 μm period with a height of 2 μm was

inked by soaking in a 10 μM aqueous solution of **1** for 2 min. The stamps were blown dry in a stream of N_2 before printing. The stamps were brought in conformal contact with printed nanoparticle structures (3 or 4 μm nanoparticle line structure at 8 μm period) for 2 min and then carefully removed. The substrate was subsequently rinsed with 10 mM CD solution at pH 2, and 1 M NaOH, respectively.

Binding of divalent guest 2 to transfer-printed nanoparticle structures. A drop of 10 μM aqueous solution of **2** was casted onto nanoparticle line structures, which had been freshly printed with **1**. After 2 min, the nanoparticle structure was rinsed with water, 10 mM CD solution at pH 2, and 1 M NaOH, respectively. Fluorescence images were taken after each interval of rinsing step.

Scanning electron microscopy (SEM). All SEM images were taken with a HR-LEO 1550 FEF SEM.

Atomic force microscopy (AFM). AFM measurements were carried out with a Dimension D3100 using a NanoScope IVa controller equipped with a hybrid 153 scanner (Veeco / Digital Instruments (DI), Santa Barbara, CA) under ambient conditions. Silicon cantilevers from Nanosensors (Nanosensors, Wetzlar, Germany) were used for intermittent contact (tapping) mode operation.

Fluorescence microscopy. Fluorescence microscopy was performed using an Olympus inverted research microscope IX71 equipped with a mercury burner U-RFL-T as the light source and a digital camera Olympus DP70 (12.5 million-pixel cooled digital color camera) for image acquisition. Green excitation light and red emission light ($510 \leq \lambda_{ex} \leq 550$ nm, $\lambda_{em} \geq 590$), blue excitation and green emission light ($450 \leq \lambda_{ex} \leq 480$ nm, $\lambda_{em} \geq 515$ nm) were filtered using a U-MWG Olympus filter cube.

7.5 ACKNOWLEDGEMENTS

Mr. In Yee Phang is thanked for the AFM imaging. Ms. Janet Acikgoz, Ms. Yiping Zhao and Mr. Iwan Heskamp are gratefully acknowledged for the fabrication of lithographically patterned silicon masters.

7.6 REFERENCES

1. Yablonovitch, E. *Sci. Am.* **2001**, *285*, 46.
2. Arsenault, A.; Fournier-Bidoz, S.; Hatton, B.; Miguez, H.; Tetreault, N.; Vekris, E.; Wong, S.; Yang, S. M.; Kitaev, V.; Ozin, G. A. *J. Mater. Chem.* **2004**, *14*, 781.
3. Katz, E.; Willner, I. *Angew. Chem. Int. Ed.* **2004**, *43*, 6042.
4. Kraus, T.; Malaquin, L.; Delamarche, E.; Schmid, H.; Spencer, N. D.; Wolf, H. *Adv. Mater.* **2005**, *17*, 2438.
5. Denkov, N. D.; Velev, O. D.; Kralchevsky, P. A.; Ivanov, I. B.; Yoshimura, H.; Nagayama, K. *Nature* **1993**, *361*, 26.
6. Fustin, C. A.; Glasser, G.; Spiess, H. W.; Jonas, U. *Langmuir* **2004**, *20*, 9114.
7. Malaquin, L.; Kraus, T.; Schmid, H.; Delamarche, E.; Wolf, H. *Langmuir* **2007**, *23*, 11513.
8. Huang, J. X.; Kim, F.; Tao, A. R.; Connor, S.; Yang, P. D. *Nat. Mater.* **2005**, *4*, 896.
9. Xia, Y. N.; Yin, Y. D.; Lu, Y.; McLellan, J. *Adv. Funct. Mater.* **2003**, *13*, 907.

10. Yang, S. M.; Ozin, G. A. *Chem. Commun.* **2000**, 2507.
11. Xia, D. Y.; Biswas, A.; Li, D.; Brueck, S. R. J. *Adv. Mater.* **2004**, *16*, 1427.
12. Jiang, C. Y.; Markutsya, S.; Pikus, Y.; Tsukruk, V. V. *Nat. Mater.* **2004**, *3*, 721.
13. Wijnhoven, J.; Vos, W. L. *Science* **1998**, *281*, 802.
14. Holgado, M.; Garcia-Santamaria, F.; Blanco, A.; Ibisate, M.; Cintas, A.; Miguez, H.; Serna, C. J.; Molpeceres, C.; Requena, J.; Mifsud, A.; Meseguer, F.; Lopez, C. *Langmuir* **1999**, *15*, 4701.
15. Decher, G.; Hong, J. D.; Schmitt, J. *Thin Solid Films* **1992**, *210*, 831.
16. Blonder, R.; Sheeney, L.; Willner, I. *Chem. Commun.* **1998**, 1393.
17. Hicks, J. F.; Seok-Shon, Y.; Murray, R. W. *Langmuir* **2002**, *18*, 2288.
18. Zheng, J. W.; Zhu, Z. H.; Chen, H. F.; Liu, Z. F. *Langmuir* **2000**, *16*, 4409.
19. Li, D.; Zhang, Y. J.; Jiang, J. G.; Li, J. H. *J. Colloid Interface Sci.* **2003**, *264*, 109.
20. Granot, E.; Patolsky, F.; Willner, I. *J. Phys. Chem. B* **2004**, *108*, 5875.
21. Maye, M. M.; Nykypanchuk, D.; van der Lelie, D.; Gang, O. *J. Am. Chem. Soc.* **2006**, *128*, 14020.
22. Shenton, W.; Pum, D.; Sleytr, U. B.; Mann, S. *Nature* **1997**, *389*, 585.
23. Zirbs, R.; Kienberger, F.; Hinterdorfer, P.; Binder, W. H. *Langmuir* **2005**, *21*, 8414.
24. Boal, A. K.; Ilhan, F.; DeRouchey, J. E.; Thurn-Albrecht, T.; Russell, T. P.; Rotello, V. M. *Nature* **2000**, *404*, 746.
25. Ling, X. Y.; Reinhoudt, D. N.; Huskens, J. *Langmuir* **2006**, *22*, 8777.
26. Wanunu, M.; Popovitz-Biro, R.; Cohen, H.; Vaskevich, A.; Rubinstein, I. *J. Am. Chem. Soc.* **2005**, *127*, 9207.
27. Crespo-Biel, O.; Dordi, B.; Reinhoudt, D. N.; Huskens, J. *J. Am. Chem. Soc.* **2005**, *127*, 7594.
28. Zheng, H. P.; Lee, I.; Rubner, M. F.; Hammond, P. T. *Adv. Mater.* **2002**, *14*, 569.
29. Santhanam, V.; Andres, R. P. *Nano Lett.* **2004**, *4*, 41.
30. Ling, X. Y.; Malaquin, L.; Reinhoudt, D. N.; Wolf, H.; Huskens, J. *Langmuir* **2007**, *23*, 9990.
31. Park, J. I.; Lee, W. R.; Bae, S. S.; Kim, Y. J.; Yoo, K. H.; Cheon, J.; Kim, S. *J. Phys. Chem. B* **2005**, *109*, 13119.
32. Kraus, T.; Malaquin, L.; Schmid, H.; Riess, W.; Spencer, N. D.; Wolf, H. *Nat. Nanotechnol.* **2007**, *2*, 570.
33. Meitl, M. A.; Zhu, Z. T.; Kumar, V.; Lee, K. J.; Feng, X.; Huang, Y. Y.; Adesida, I.; Nuzzo, R. G.; Rogers, J. A. *Nat. Mater.* **2006**, *5*, 33.
34. Liao, J. H.; Bernard, L.; Langer, M.; Schonenberger, C.; Calame, M. *Adv. Mater.* **2006**, *18*, 2803.
35. Maury, P.; Pétér, M.; Crespo-Biel, O.; Ling, X. Y.; Reinhoudt, D. N.; Huskens, J. *Nanotechnology* **2007**, *18*, 044007.
36. Maury, P.; Escalante, M.; Reinhoudt, D. N.; Huskens, J. *Adv. Mater.* **2005**, *17*, 2718.

37. Yin, Y. D.; Lu, Y.; Gates, B.; Xia, Y. N. *J. Am. Chem. Soc.* **2001**, *123*, 8718.
38. Meitl, M. A.; Zhou, Y.; Gaur, A.; Jeon, S.; Usrey, M. L.; Strano, M. S.; Rogers, J. A. *Nano Lett.* **2004**, *4*, 1643.
39. Shir, D. J.; Jeon, S.; Liao, H.; Highland, M.; Cahill, D. G.; Su, M. F.; El-Kady, I. F.; Christodoulou, C. G.; Bogart, G. R.; Hamza, A. V.; Rogers, J. A. *J. Phys. Chem. B* **2007**, *111*, 12945.
40. Nijhuis, C. A.; Huskens, J.; Reinhoudt, D. N. *J. Am. Chem. Soc.* **2004**, *126*, 12266.
41. Maury, P.; Peter, M.; Crespo-Biel, O.; Ling, X. Y.; Reinhoudt, D. N.; Huskens, J. *Nanotechnology* **2007**, *18*, 044007.
42. Mahalingam, V.; Onclin, S.; Peter, M.; Ravoo, B. J.; Huskens, J.; Reinhoudt, D. N. *Langmuir* **2004**, *20*, 11756.
43. Ling, X. Y.; Reinhoudt, D. N.; Huskens, J. *Chem. Mater.* **2008**, *3574*.
44. Ling, X. Y.; Phang, I. Y.; Reinhoudt, D. N.; Vancso, G. J.; Huskens, J. *Int. J. Mol. Sci.* **2008**, *9*, 486.
45. Crespo-Biel, O.; Dordi, B.; Maury, P.; Pétér, M.; Reinhoudt, D. N.; Huskens, J. *Chem. Mater.* **2006**, *18*, 2545.
46. Nijhuis, C. A.; ter Maat, J.; Bisri, S. Z.; Weusthof, M. H. H.; Salm, C.; Schmitz, J.; Ravoo, B. J.; Huskens, J.; Reinhoudt, D. N. *New J. Chem.* **2008**, *32*, 652.
47. Mulder, A.; Onclin, S.; Pétér, M.; Hoogenboom, J. P.; Beijleveld, H.; ter Maat, J.; Garcia-Parajo, M. F.; Ravoo, B. J.; Huskens, J.; Van Hulst, N. F.; Reinhoudt, D. N. *Small* **2005**, *1*, 242.
48. Beulen, M. W. J.; Bügler, J.; Lammerink, B.; Geurts, F. A. J.; Biemond, E.; van Leerdam, K. G. C.; van Veggel, F. C. J. M.; Engbersen, J. F. J.; Reinhoudt, D. N. *Langmuir* **1998**, *14*, 6424.
49. Michels, J. J.; Baars, M.; Meijer, E. W.; Huskens, J.; Reinhoudt, D. N. *J. Chem. Soc., Perkin Trans. 2* **2000**, 1914.
50. Onclin, S.; Mulder, A.; Huskens, J.; Ravoo, B. J.; Reinhoudt, D. N. *Langmuir* **2004**, *20*, 5460.

Chapter 8

Free-standing nanoparticle bridges and hollow capsule ribbons of supramolecular materials

ABSTRACT. The formation of stable and ordered free-standing nanoparticle bridges and hollow capsule structures with controllable sizes and geometries is demonstrated by combining the directed assembly of nanoparticles, templating using transfer printing or nanoimprint lithography (NIL), and supramolecular layer-by-layer (LbL) assembly. First, 500-nm β-cyclodextrin (CD)-functionalized polystyrene (PS) nanoparticles were assembled by convective assembly onto (sacrificial) polymer templates of poly(dimethylsiloxane) (PDMS) or poly(methyl methacrylate (PMMA) patterned with predefined geometries and sizes using replica molding or NIL, resulted in the formation of a 3D nanoparticle architecture. LbL assembly of alternating supramolecular host- and guest-functionalized glues sized between 3 – 5 nm within the preformed PS nanoparticle crystals effectively bound the nanoparticles together into a nanoparticle composite. Free-standing hybrid nanoparticle bridges were formed on 3D substrates *via* transfer printing from the PDMS stamp. AFM-based bending test measurements show that these nanoparticle bridges are quite rigid, with a bending modulus of ~ 1.2 GPa. When using the PMMA template, the nanoparticle composites were released from the substrate together with the template, and transferred onto a target substrate. The nanoparticle crystal integrity, order and functionality were preserved. Rinsing the structure with dichloromethane removed the PS core material together with the polymer template, resulting in interconnected porous capsules, the sizes and shapes of which are fully determined by the PS core size and the polymer template definition. Integrity, order and shape were preserved in the rinsing step as well. Furthermore, the ability of these capsules to store organic fluorescent molecules was investigated.

8.1 INTRODUCTION

The fabrication of well-defined free-standing micro- or nano-objects with versatile structures is important to match the needs for specific applications in membranes,[1,2] sensors,[3] nanomechanical films, and nanoreactors. Nanoparticles that exhibit interesting optical, electronic, and catalytic properties are potential candidates for the fabrication of new types of functional materials. In particular, the assembly of well-defined nanoparticle-based structures is promising in the current trend of miniaturizing devices. Considerable progress has been achieved in forming self-assembled 1D or 2D nanoparticle structures in solution by means of specific chemical interactions, including linear structures of nanoparticles,[4] nanowires,[5] and spherical and network aggregates of nanoparticles.[6]

Most solution strategies to form nanoparticle structures are based on the intrinsic interparticle interactions and/or the control over kinetics of nanoparticle assembly in solution, which suffer from limited complexity of the assemblies. Moreover, the assembly of free-standing structures in solution is limited to the nanometer length scale, whereas the bottom-up assembly of the nanoparticles into nano- or microobjects with defined composition, and geometry remain experimentally challenging. Recently, the layer-by-layer (LbL) assembly technique[7] has been extended to the formation of flexible free-standing (mostly unpatterned) thin films in air, at the liquid-liquid interface, or at the air-liquid interface.[8] It generally involves the LbL growth of a polymer or polyelectrolyte[9] film with a well-defined thickness and composition on a substrate and its removal from the substrate by using a sacrificial layer, such as cellulose acetate.[3] The incorporation of fillers such as metallic nanoparticles,[2,10] clays,[11,12] and quantum dots[13] into the LbL films are essential to enhance the mechanical robustness[1] and/or to introduce additional optical properties into the thin films.[9] However, the macroscopic robustness of the free-standing structures and their potential functionalities in optics, chemical sensing, or nano- or microelectromechanical systems have to be further explored to lead to technical applications.

The self-assembly of nanoparticles can be combined with top-down nanofabrication techniques to achieve 3D nanoparticle-based structures on surfaces. Nanofabrication techniques such as soft lithography,[14,15] nanoimprint lithography (NIL),[16,17] and dip-pen nanolithography[18,19] enable the design and manipulation of the shapes and sizes of the nano- and microstructures. Microcontact printing (μCP) has been used to facilitate the direct transfer printing of patterned nanoparticle arrays onto SAMs *via* specific particle-substrate

affinity.[15,20-22] With the combination of LbL assembly, multilayers of nanocrystals and/or polyelectrolytes have been formed on (microcontact printed) SAMs.[10,23-27]

Here, a versatile approach towards the formation of stable and ordered free-standing nanoparticle and hollow capsule structures with controllable sizes and geometries is reported. The self-assembly of nanoparticles, templating, and supramolecular chemistry are combined to obtain free-standing 3D nanoparticle structures. This approach extends the use of supramolecular chemistry from the fabrication of micro- or nano-structures on surfaces to stand-alone nanoparticle structures. The self-assembly of nanoparticles was performed onto the poly(dimethylsiloxane) (PDMS) stamps and NIL-fabricated poly(methyl methacrylate) (PMMA) templates with a predefined geometry and size by the convective assembly. Nanoparticle composite was formed by LbL assembly of supramolecular host- and guest-functionalized glues within the preformed nanoparticle crystal. The transfer printing of the hybrid nanoparticle crystal, assembled on a PDMS stamp, onto the complementary topographically patterned CD monolayer substrate yields free-standing nanoparticle bridges. The mechanical stability of such nanoparticle bridges is examined by AFM-based bending tests. The hybrid nanoparticle crystals assembled on a PMMA template are released and transferred to a target substrate. Removal of the polystyrene cores of the nanoparticles in the crystal simultaneously with the NIL polymer results in ribbons of interconnected porous capsules. The potential of these structured capsules of supramolecular materials as carriers and storerooms of organic fluorescent molecules is also examined.

8.2 RESULTS AND DISCUSSION

The preparation procedure of hybrid nanoparticle crystals is shown in Scheme 8.1. CD-functionalized polystyrene nanoparticles (PS-CD, $d \sim 500$ nm), prepared as described in Chapter 4,[28] were assembled onto CD SAMs *via* convective assembly.[17,29] Adamantyl-functionalized poly(propylene imine) dendrimer of generation 5 (G5-PPI-$(Ad)_{64}$)[30] and CD-functionalized Au nanoparticles (Au-CD, $d \sim 3$ nm),[17] respectively, were used as the supramolecular guest- and host-functionalized glues to adhere the PS-CD nanoparticles within the PS-CD crystal to each other and to the substrate *via* supramolecular LbL assembly.[17] The PS-CD crystal was first infiltrated with G5-PPI-$(Ad)_{64}$, followed by the complementary Au-CD nanoparticles. These steps were repeated in a LbL fashion to reach the desired number of bilayers.[31]

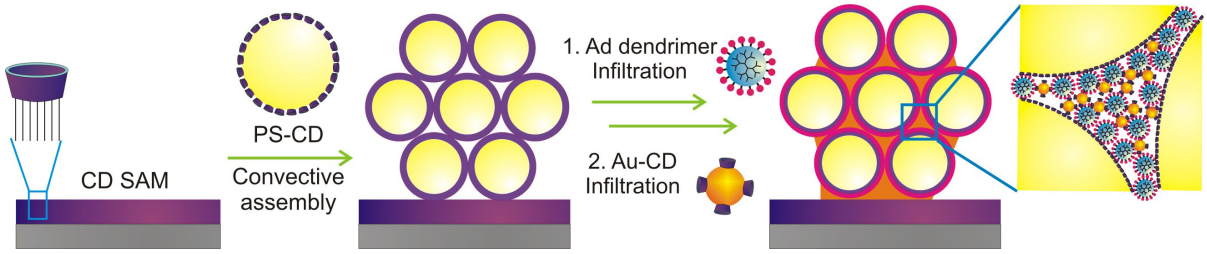

Scheme 8.1. The preparation of 3D nanoparticle composites by convective assembly of PS-CD nanoparticle (d ~ 500 nm) onto a CD SAM and supramolecular LbL assembly of G5-PPI-$(Ad)_{64}$ and Au-CD nanoparticles (d ~ 3 nm) within the PS-CD nanoparticle crystal.

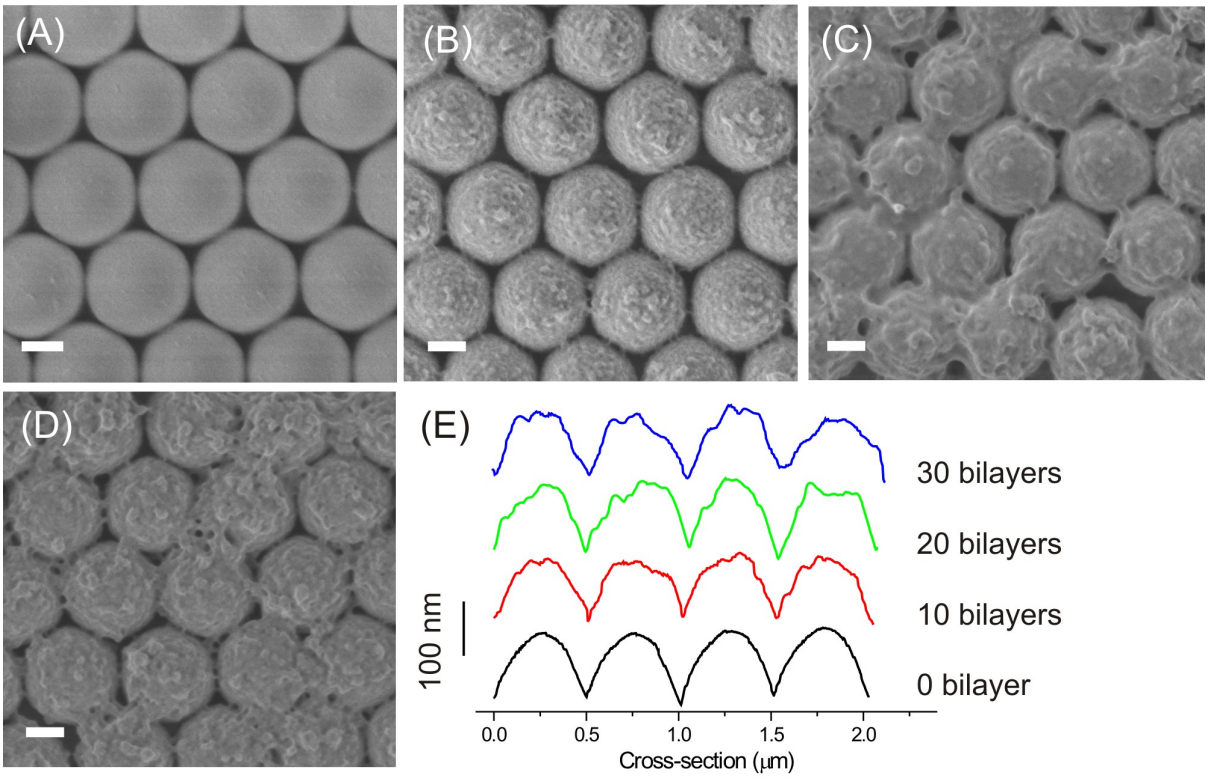

Figure 8.1. SEM images of nanoparticle crystal infiltrated with G5-PPI-$(Ad)_{64}$ only (A), and after 10 (B), 20 (C) and 30 (D) of LbL assembly cycles of G5-PPI-$(Ad)_{64}$ and Au-CD within the nanoparticle crystals. All scale bars indicate 200 nm. The AFM cross-section profiles of the nanoparticle crystals with increasing numbers of bilayers (E).

Figure 8.1(A) shows an as-prepared convectively assembled nanoparticle crystal infiltrated with G5-PPI-$(Ad)_{64}$ only, and hybrid nanoparticle crystals after 10 (B), 20 (C), and 30 (D) LbL assembly cycles. A nanoparticle crystal with a relatively smooth surface was first obtained from convective assembly and dendrimer infiltration (Figure 8.1A). With increase of the number of bilayers, more material was deposited within the crystal as well as on the

nanoparticle surface. Particularly in the case of 20 and 30 LbL assembly cycles, glue-like material was observed bridging adjacent nanoparticles (Figure 8.1C, D). The supramolecular LbL assembly of G5-PPI-$(Ad)_{64}$ and Au-CD within the PS-CD crystal has resulted in the crosslinking of individual nanoparticles into a three-dimensional stable nanoparticle crystal with full retention of the order achieved during the convective assembly. The voids between the nanoparticles have become smaller owing to the filling with the supramolecular glues. In addition, the surface of the nanoparticles became significantly rougher (Figure 8.1E), with occasional a few tens-of-nanometers agglomerates attached on the surface of the PS-CD nanoparticles. The presence of these agglomerates indicates that the assembly of Au-CD and G5-PPI-$(Ad)_{64}$ on the nanoparticle crystal might not be completely homogeneous at each adsorption cycle.

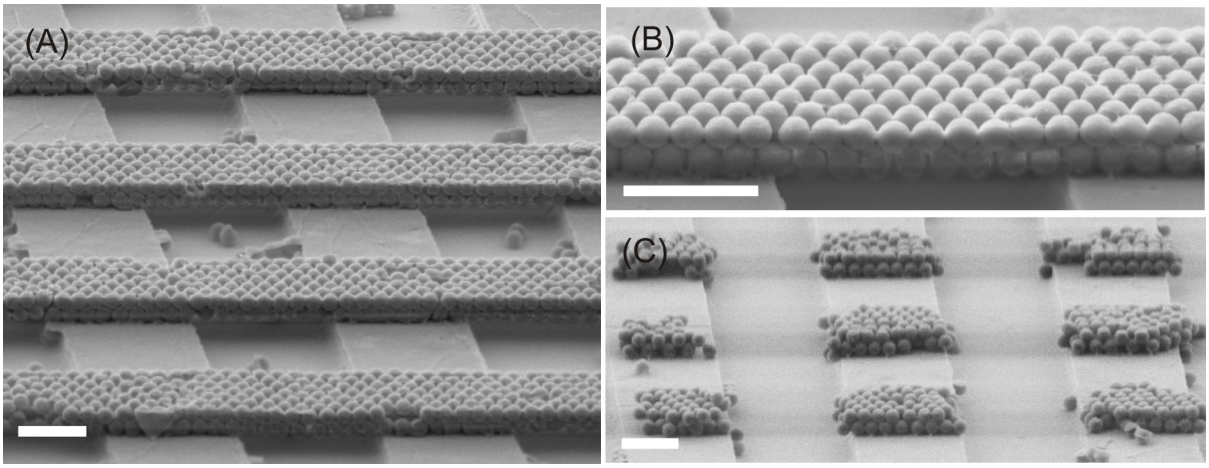

Figure 8.2. SEM images of the transfer-printed free-standing nanoparticle composite structures on topographically patterned substrates using LbL assembly (A, B), or G5-PPI-$(Ad)_{64}$-infiltration only (C). Scale bar indicates 2 μm.

The transfer printing of supramolecular nanoparticle crystals onto a topographically patterned CD monolayer was examined. A nanoparticle composite was prepared on a PDMS stamp, using 30 LbL assembly cycles, and was perpendicularly printed onto a 3D line-featured CD-functionalized substrate to yield 3D free-standing and ordered composite lines (Figure 8.2A, B). A few individual nanoparticles were observed randomly distributed over the substrate, which could originate from the convective assembly. The free-standing nanoparticle composite structures were supported by the vertical posts of the substrate. The results suggested that the discrete nanoparticles, glued by the supramolecular auxiliary building blocks, have bridged the micrometer distances between the posts to form single-span

nanoparticle microbridges. In contrast, when using only a single dendrimer infiltration step (no LbL assembly), only the sections of the nanoparticle crystals that were in direct contact with the substrate were transferred (Figure 8.2C). Apparently, the mechanical stability of the nanoparticle composites was drastically reinforced by the LbL assembly, allowing the formation of several-micrometer-long and continuous free-standing objects. To our knowledge, this is the first report on 3D and self-supported free-standing mesoscopic structures, bottom-up assembled from discrete and individual nanoparticles held together by intrinsically weak, dynamic and reversible supramolecular host-guest interactions.

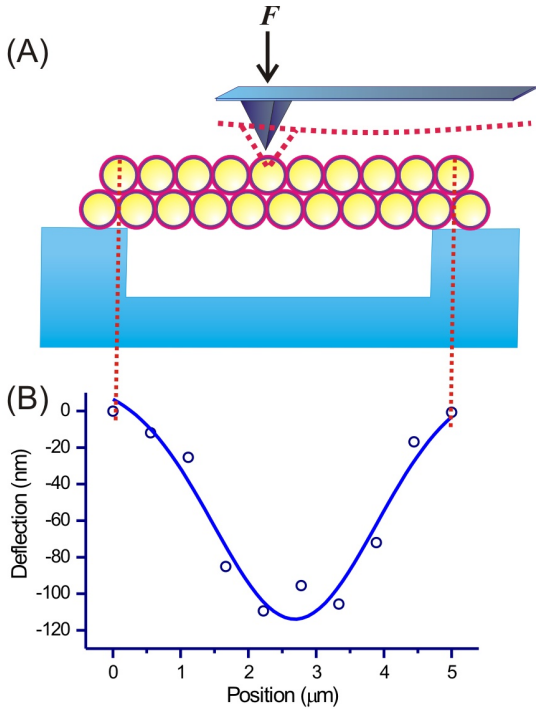

Figure 8.3. A scheme of the AFM-based bending test (A). AFM deflection-position curve of the nanoparticle composite bridge when subjected to 8 μN point loads (B).

The mechanical properties of the nanoparticle composite bridges were analyzed by AFM force spectroscopy. The deflection of each individual nanoparticle across the nanoparticle bridge was probed by an AFM tip (Figure 8.3A). A deflection-position graph of the nanoparticle bridge was obtained when loaded with a constant force of 8 μN across the bridge (Figure 8.3B). A maximum deflection was observed at the center of the nanoparticle bridge. The bending modulus of a nanomaterial can be estimated, according to classical beam theory, from the experimentally determined force-deformation relationships.[32-36] The classical beam theory is the most frequently used model to quantitatively describe the resistance of a material

toward bending. It is derived from Hooke's law ($F = k\delta$), where k = material spring constant. The relation of the maximum deflection (δ) of a rectangular beam under mid-point applied load (F) is demonstrated as below (equation 1):

$$F = \frac{48 \times I \times E}{L^3}\delta \qquad (1)$$

where E = bending modulus, $I = (wh^3)/12$ is the moment of inertia, w and h are the width and thickness of the nanoparticle bridge, respectively and L is the span length of the free-standing structure. Treating the nanoparticle bridge as a continuous material, the bending modulus, E was estimated to be 1.2 ± 0.4 GPa[34] at room temperature, which is of the same order of magnitude as bulk polystyrene.

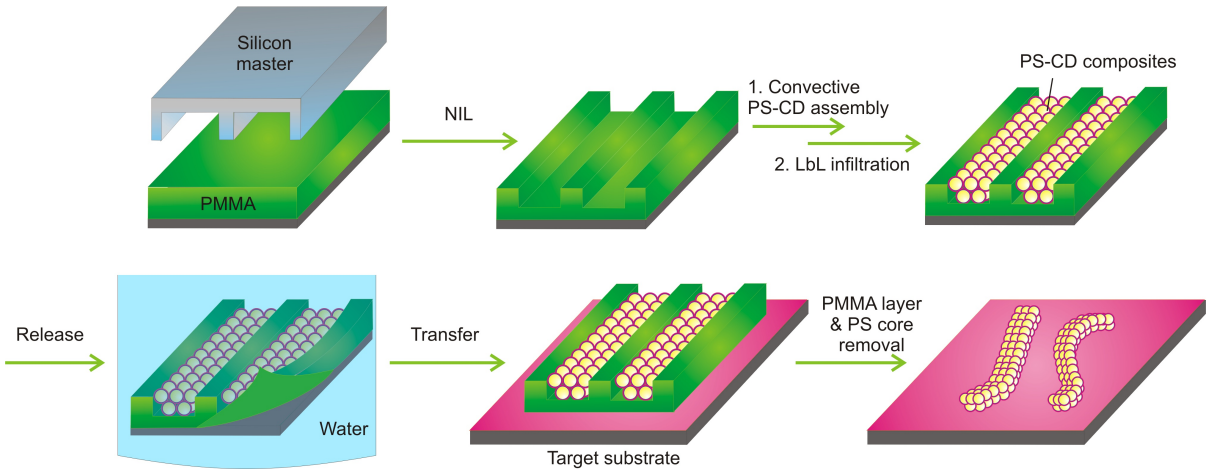

Scheme 8.2. The preparation of a PMMA template and the release-and-transfer of free-standing hydrid nanoparticle crystals, followed by template and PS core removal.

To demonstrate the versatility of the developed sequential process for a wider range of structures, self-assembly of PS-CD and supramolecular LbL assembly were used to form nanoparticle composite ribbons on a NIL-fabricated PMMA template with controlled geometry and size (Scheme 8.2). The PMMA layer was mildly oxidized in O_2 plasma to render its surface hydrophilic. Subsequently, the PS-CD nanoparticles were assembled onto the template *via* capillary-assisted assembly, with no specific affinity between the nanoparticles and the substrate. By controlling the assembly parameters,[37] nanoparticles were directed into the grooves of the PMMA template. The resulting nanoparticle crystals inherited

the overall shape from the underlying template, thus allowing the assembly of the nanoparticles into highly organized micro- or nanostructures of desired sizes and shapes. Hybrid nanoparticle crystal composites were formed by supramolecular LbL assembly of supramolecular glues (G5-PPI-$(Ad)_{64}$ and Au-CD). By using the PMMA template as a carrier, the entire nanoparticle structures were released from the silicon substrate into water, resulting in a floating PMMA template, to which the hybrid nanoparticle composites were attached, at the water-air interface. A target substrate was subsequently used to pick up the PMMA template with the nanoparticle composites for visualization.

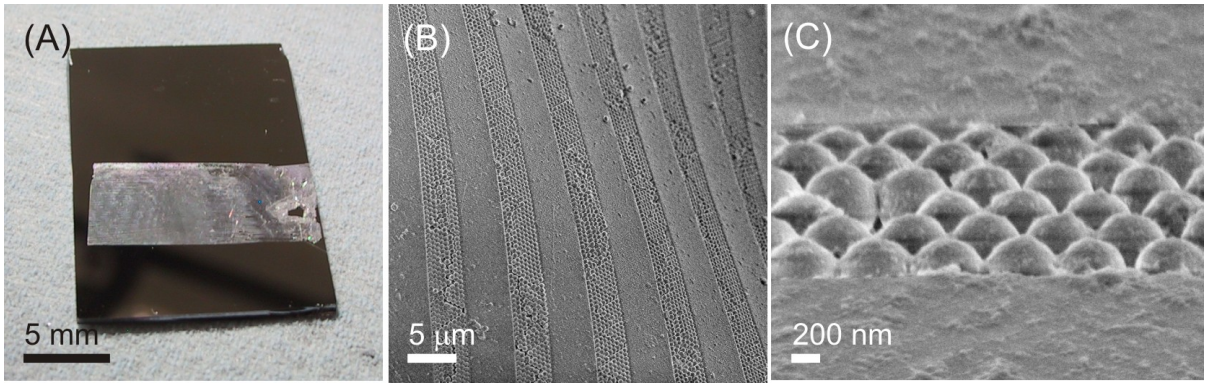

Figure 8.4. A photograph (A) and SEM images (B, C) of infiltrated nanoparticle crystals embedded in the PMMA template, after release-and-transfer onto a target SiO_2 substrate (Scheme 8.2).

Figure 8.4A shows a photograph of a hybrid nanoparticle crystal embedded in a PMMA template after transfer onto a target SiO_2 substrate. As a result of the PMMA thickness of < 1 μm, the PMMA-nanoparticle structure appeared flexible. SEM images (Figure 8.4B – C) reveal that the hybrid nanoparticle crystals in the line structures remained adhere to the PMMA template, probably as a result of Van der Waals forces[38] and electrostatic interactions between the positively charged G5-PPI-$(Ad)_{64}$ and the negatively charged oxidized PMMA surface. The polymer layer was slightly stretched during the transfer process. However, no obvious changes in the order and integrity of the nanoparticle crystals were observed, indicating the robustness and flexibility of the hybrid nanoparticle crystals during the release-and-transfer process. Only incidentally, nanoparticle vacancies were observed in the hybrid nanoparticle crystal. In contrast, when the supramolecular LbL assembly within the nanoparticle crystal was omitted, most of the nanoparticle crystals disintegrated, and the nanoparticles were removed from the polymer layer during the layer

transfer process (data not shown). Thus, the stability and integrity of the hybrid nanoparticle crystals can be attributed to the strong multivalent interactions[39] within the crystal.

TEM images (Figure 8.5A, B) reveal the nanoparticle crystal after transfer onto a copper grid. The hybrid nanoparticle crystal after 30 LbL cycles remained in a high quality hcp structure, indicating that all the nanoparticles were effectively bound together during the release-and-transfer process. At the periphery of each PS nanoparticle and at the interface between the adjacent nanoparticles (Figure 8.5B), material of high contrast is visible, indicating individual Au nanoparticles at the shell of the hybrid PS nanoparticle crystal. Energy dispersive X-ray spectroscopy (EDX) performed on a PS-CD nanoparticle and a void between nanoparticles confirmed the presence of a large amount of Au on the PS-CD nanoparticle as compared to the void area (Figure 8.5C).

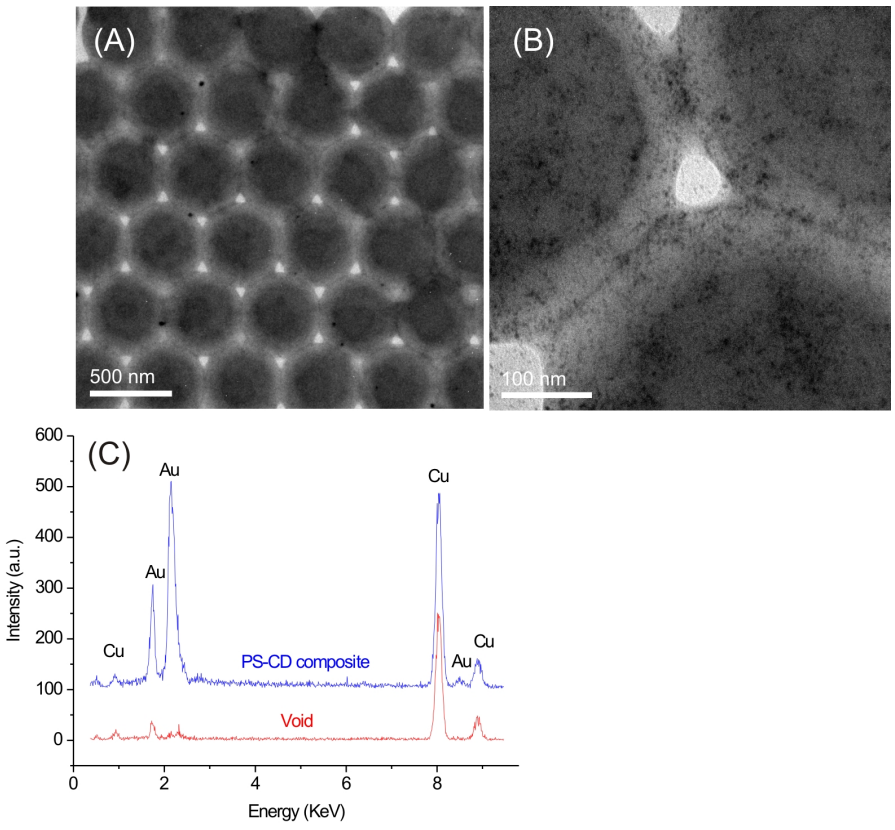

Figure 8.5. TEM images of the hybrid nanoparticle crystal after 30 LbL cycles and release-and-transfer onto a copper grid (A, B). EDX spectra (C) taken on top of a PS nanoparticle within the hybrid nanoparticle crystal and at a void between three neighboring nanoparticles.

After transferring the hybrid nanoparticle crystals onto a target substrate, the substrate was rinsed with dichloromethane to remove the PS core and the PMMA template

simultaneously. As shown in Figure 8.6, ribbons of interconnected hollow hybrid capsules, approximately 500 μm in length were formed. The hollow ribbons exhibited slight curvature in appearance, as a result of the PMMA pattern removal. A zoom-in SEM image (Figure 8.6B) shows that the internal cohesion by the supramolecular glues remained intact. The hollow nature of the capsules is confirmed by occasional defects in the LbL structure (Figure 8.6B). Even though some indented capsules were observed, the majority of the hollow capsules appeared to maintain their original spherical shape. Thus, the multilayered assemblies of G5-PPI-$(Ad)_{64}$ and Au-CD nanoparticles have formed supramolecular capsules fused together into stable macroscopic entities, which shape is governed by the PS nanoparticles and the PMMA template, both of which have been removed completely.

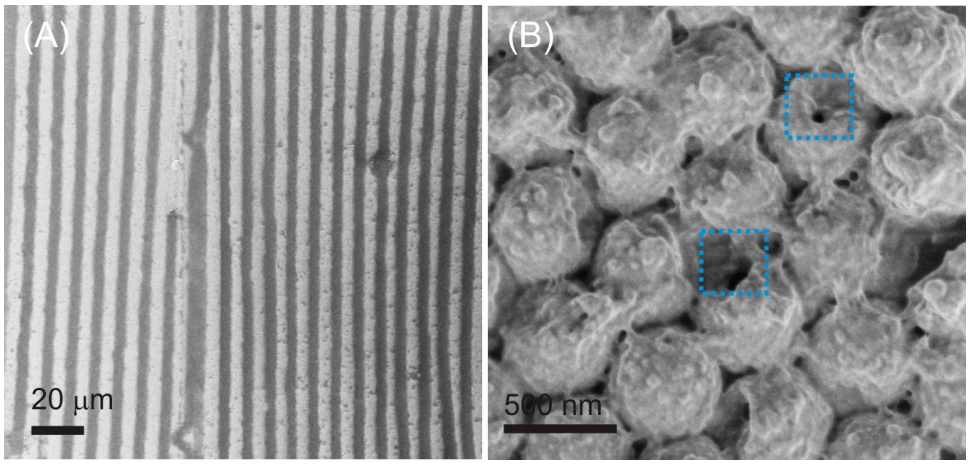

Figure 8.6. SEM images of the ribbons of hybrid hollow capsules, after which the hybrid nanoparticle crystal onto a target substrate, the PS core and the PMMA template were removed completely simultaneously.

The micromechanical properties and structural deformation of the hybrid nanoparticle structures and hollow capsule ribbons (after 30 LbL bilayers) were probed by AFM-based nanoindentation. Figure 8.7(A, D) show typical force-penetration curves obtained by applying point loads onto a hybrid nanoparticle and a hollow capsule. A sigmoidal curve was obtained when the AFM tip struck the hybrid multilayer-coated PS nanoparticle. The hybrid nanoparticle experienced a relatively low force penetration in the beginning of indentation, probably as a result of indentation of PS and/or G5-PPI-$(Ad)_{64}$ and Au-CD nanoparticles. Upon 70 - 100 nm penetration, a drastic increase in force was observed. In the retracting part of the cycle, a large hysteresis was observed. The hollow capsules obtained after dichloromethane rinsing experienced a different mechanical behavior. A larger penetration

was observed at the same 4 μN force load, suggesting a change in the material properties. The force-penetration curve was smooth with no discontinuities, indicating no cracking occurred during the indentation.[40] Compared to the hybrid nanoparticle structure, only a low force is needed to penetrate the hollow capsule. Figure 8.7(B, E) show the AFM images of the hybrid nanoparticle structure and the capsule after indentation. The indented area on the hybrid nanoparticle appears eight times smaller than on the capsule, which could be attributed to the resistance of the polystyrene nanoparticle towards indentation. The AFM cross-section profiles (Figure 8.7C, F) showed an indentation of ~ 200 nm on the capsule, as compare to < 100 nm on PS nanoparticle, confirming the hollow nature of the capsule.

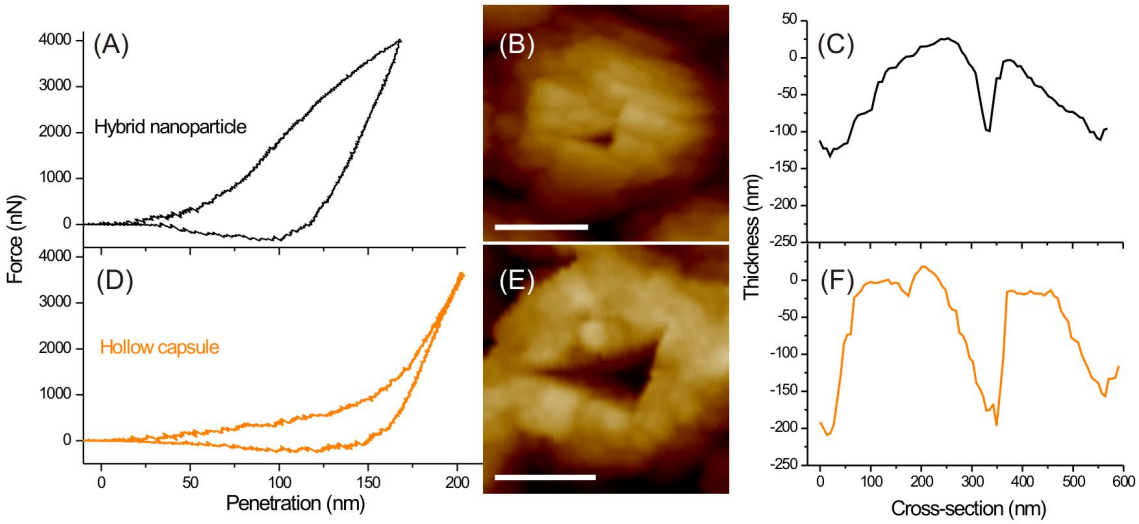

Figure 8.7. Force-penetration curves (A, D), AFM images (B, E) and cross-section profiles after indentation (C, F) of a hybrid nanoparticle (A, B, C), and a hollow capsule of 30 bilayers (D, E, F). All scale bars indicate 200 nm.

To examine the integrity of the sub-millimeter hollow capsule ribbons and the potential of these capsule ribbons in storing fluorescent molecules, the as-prepared nanoparticle composites, while still on the PMMA template, were dipped in an aqueous solution of 8-anilino-1-naphthalenesulfonic acid (ANS). ANS is a fluorescent probe that is highly sensitive toward its micro-environment.[41] The fluorescence properties of ANS depend on the polarity of the medium, and severe fluorescence quenching is observed in water. The negatively charged ANS is known to penetrate into the core of G5-PPI-$(Ad)_{64}$ *via* electrostatic interactions to restore its fluorescence intensity.[30] Here, the recognition between ANS and the

G5-PPI-$(Ad)_{64}$ is employed to observe the presence of the G5-PPI-$(Ad)_{64}$ and thus the complete capsule ribbons by fluorescence microscopy.

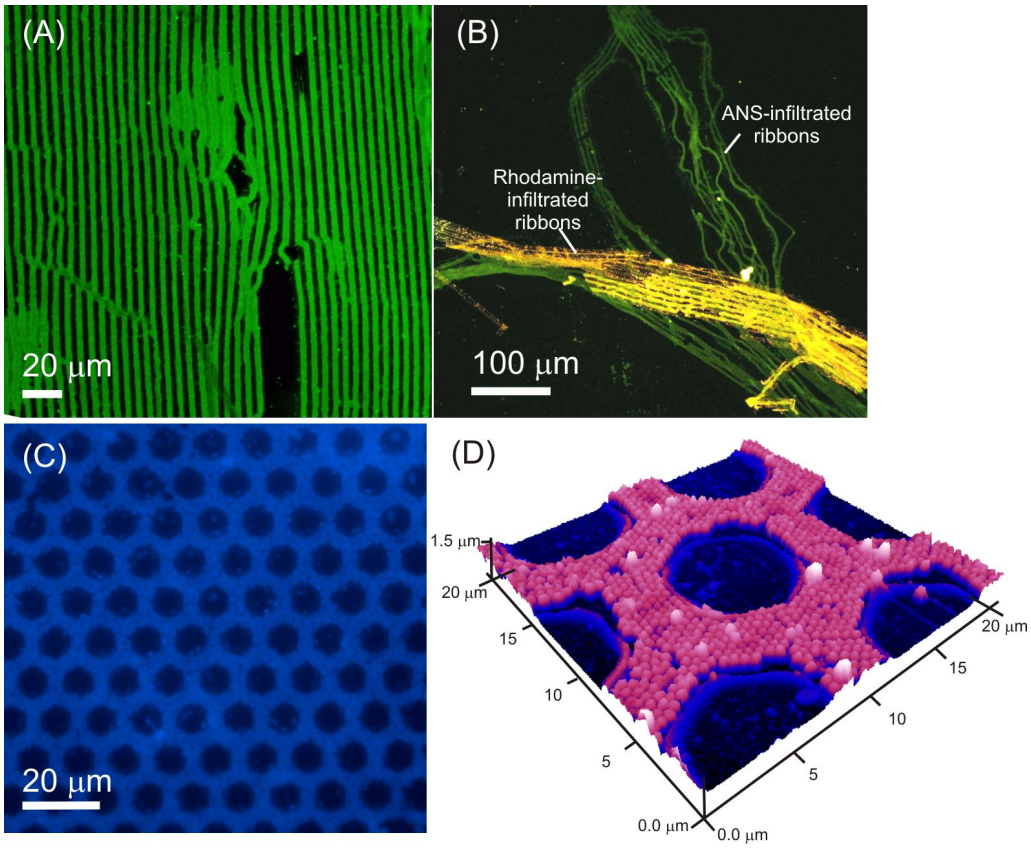

Figure 8.8. Fluorescence microscopy images of the hybrid hollow capsules infiltrated with ANS (A), overlapping structures infiltrated with lissamine rhodamine and ANS, respectively (B), and a network capsule structures infiltrated with naphthoic acid (C). 3D AFM image (D) of a network structure as shown in (C).

The ANS-infiltrated nanoparticle composites were subsequently released-and-transferred onto a target substrate. After removal of the PMMA layer and the PS cores by dichloromethane, the ribbons were monitored by fluorescence microscopy. The fluorescence image of the composites (Figure 8.8A) clearly indicates the highly fluorescent micrometer-sized ribbons. This indicates that most of the ANS molecules were stored within the shells of the hollow capsules and remained in the structure upon release, transfer, and rinsing. Besides the imaging, the results suggest the potential of the hybrid hollow capsule as an effective storeroom and carrier for molecular information. A wide variety of organic dyes can be stored within such dendrimers.[42,43] As shown in Figure 8.8B, separately made capsule ribbons pre-embedded with ANS and lissamine rhodamine molecules, respectively, were released-

and-transferred onto the same target substrate. Subsequent dichloromethane rinsing removed the PMMA templates and the PS cores of both nanoparticle crystal structures simultaneously. Despite their similar appearance, the fluorescent information embedded within each hybrid structure can be readily read out under the fluorescence microscope (upon blue excitation) to distinguish the different molecular informed stored within them. Figure 8.8C shows the shape versatility of our approach in forming capsules in a network structure, simply by changing the design of the PMMA template. Hollow capsules of ring-shaped network structures (30 LbL assemblies) were thus formed by using a PMMA template with 8 μm dots with 3 μm spacing and a height of 500 nm. The height of the network structure is similar to that of the original template and corresponds to a single layer of PS-CD nanoparticles being assembled onto the PMMA template (Figure 8.8D). The network was infiltrated with naphthoic acid, which is highly fluorescent under UV light (Figure 8.8C). The results indicate that the individual size of the hollow capsules can be manipulated by the choice of the size of the PS nanoparticles, while the overall shape and geometry of the entire capsule structures can be designed by the geometry and size of the PMMA template.

8.3 CONCLUSIONS

A versatile approach for the formation of stable and ordered free-standing nanoparticle and capsule structures with controllable size and geometry has been developed by combining the directed assembly of nanoparticles, supramolecular LbL assembly, and templating using transfer printing and NIL. This technique extends the LbL assembly of 2D flat films to 3D free-standing nanoparticle structures. The main component of the free-standing structure can be of arbitrary material provided its surface is engineered with supramolecular properties. The mechanical stability of the nanoparticle crystals was introduced by multivalent supramolecular interactions using the well-defined and highly branched dendrimers and metallic nanoparticles (of 3 – 5 nm) *via* specific host-guest interactions within the nanoparticle crystal. The resulting nanoparticle composites can be tuned from micrometer to sub-millimeter objects with pre-designed shapes and geometries. Free-standing hybrid nanoparticle bridges were demonstrated by the transfer printing of nanoparticle composites onto 3D substrates. Moreover, when using a PMMA layer as a template, the PS core and the underlying polymer template can be removed simultaneously to form hollow capsule structures. These supramolecular multilayered structures maintained the size and shape of the original 500-nm PS-CD nanoparticles to form free-standing

interconnected hollow capsule ribbons with considerable mechanical stability. Such stable and ordered hollow capsule ribbons behave as three-dimensional molecular printboards, which can potentially serve as molecular information carriers capable of storing and releasing molecular information.

8.4 EXPERIMENTAL

Materials. CD heptamine,[44] and adamantyl-terminated poly(propylene imine) dendrimer of generation 5 (G5-PPI-$(Ad)_{64}$)[30] were synthesized as described before. *N*-[3-(trimethoxysilyl)propyl]ethylenediamine and 1,4-phenylene diisothiocyanate, poly(methyl methacrylate) (PMMA, M_w: 38,000), 8-anilino-1-naphthalenesulfonic acid (ANS), lissamine rhodamine B sulfonylchloride and 6-hydroxy-2-naphthoic acid were obtained from Sigma Aldrich, Germany. Poly(dimethylsiloxane) (PDMS) Sylgard 184 prepolymer and curing agent were obtained from Dow Corning. Carboxylate-functionalized polystyrene nanoparticles of 500 nm were purchased from Polysciences Inc. CD-functionalized polystyrene nanoparticles (PS-CD), prepared from the carboxylate-functionalized nanoparticles, and gold nanoparticles (Au-CD, $d \sim 3$ nm) were prepared as described before.[31,28] Milli-Q water with a resistivity higher than 18 MΩ·cm was used in all experiments.

Substrate and monolayer preparation. Flat and topographically patterned silicon substrates were cleaned by immersion in piranha solution (conc. H_2SO_4 and 33% H_2O_2 in a 3:1 volume ratio, **Warning!** piranha should be handled with caution; it is a highly corrosive oxidizing agent) for 15 min to form a SiO_2 layer on the surface. The substrates were then sonicated in Milli-Q water and ethanol for 1 min, and dried with N_2. CD SAMs were obtained according to a published procedure.[45] In brief, the substrates were functionalized with *N*-[3-(trimethoxysilyl)propyl]ethylenediamine by gas-phase evaporation. Transformation of the amino-terminated SAMs to isothiocyanate-bearing layers was accomplished by exposure to a solution of 1,4-phenylene diisothiocyanate in ethanol at 50 ^oC for 2 h. CD SAMs were obtained by reaction of the isothiocyanate-terminated monolayers with CD heptamine in pH 7.5 water, at 50 ^oC for 2 h.

PDMS stamps were prepared by casting a 10:1 (v/v) mixture of poly(dimethylsiloxane) (PDMS) prepolymer and curing agent against a patterned silicon master (4 μm lines at 8 μm period with a height of 750 nm). After curing of the stamps overnight, they were mildly oxidized in an O_2 plasma etcher (Tepla 300E) for 1 min to render them hydrophilic.

Nanoimprint lithography (NIL) was performed by putting a silicon stamp (3 μm lines at 8 μm period with a height of 800 nm, and 8 μm holes at 3 μm spacing with a height of 500 nm) in contact with a 1 – 1.5 μm thick layer of PMMA on a SiO_2 substrate. A pressure of 40 bar was applied at a temperature of 180 ºC using a hydraulic press (Specac). The residual PMMA layer was not removed after the hot embossing process. The PMMA templates were oxidized in an O_2 plasma etcher (Tepla 300E) for 30 s to render them hydrophilic.

Assembly of PS-CD nanoparticles. On oxidized PMMA templates with 5 μm lines and 3 μm trenches with a height of 800 nm or 8 μm dots at 3 μm spacing with a height of 800 nm, 500-nm CD-functionalized polystyrene (PS-CD) nanoparticles were convectively assembled into the grooves of

the NIL substrates to form nanoparticle crystals by using a capillary-assisted deposition setup.[45] The preformed nanoparticle array was then gently dipped in a 1 mM aqueous solution of G5-PPI-$(Ad)_{64}$ for 30 min, rinsed with water, and blown dry with N_2.

Formation of hybrid nanoparticle crystals. The nanoparticle composites were prepared by layer-by-layer (LbL) assembly of Au-CD nanoparticles (d ~ 3 nm) and G5-PPI-$(Ad)_{64}$ on the pre-assembled PS-CD nanoparticle layers, according to a published procedure.[31] Up to 30 LbL cycles were performed. After each adsorption step, the substrate was blown dry with N_2.

Transfer printing of nanoparticle composite structures. An oxidized PDMS stamp with PS-CD nanoparticle composites was brought into conformal contact with a CD monolayer, unless otherwise stated. The printing was performed on a platform of a close-by water bath at 40 ^oC. The stamp was removed after 1 h. The substrates were thoroughly rinsed with water and blown dry with N_2.

Infiltration of the nanoparticle composites with fluorescent molecules. Infiltration of fluorescent molecules into the nanoparticle composites was performed prior to the release-and-transfer process. The nanoparticle composites were immersed in an aqueous solution of 1 mM ANS, lissamine rhodamine, or naphthoic acid for 10 min. The nanoparticle composites were subsequently gently rinsed with Milli-Q water and dried with N_2.

Release-and-transfer of nanoparticle composites. Oxidized NIL-patterned PMMA on a SiO_2 substrate, onto which nanoparticle composites were deposited, was gently immersed in water at 50 ^oC. The entire PMMA layer, attached to the nanoparticle composites, was slowly peeled off from the SiO_2 substrate in warm water, resulting in a floating PMMA sheet attached with nanoparticle composites at the water-air interface. A target substrate was used to pick up the PMMA layer attached with nanoparticle composites and was subsequently blown dry with N_2. Removal of the PMMA layer and PS cores was performed by gently immersing the entire substrate in dichloromethane for 1 min, followed by drying with N_2.

Scanning and transmission electron microscopy (SEM, TEM). All SEM images were taken with a HR-LEO 1550 FEF SEM. TEM was performed on a Philips CM 30 Twin STEM fitted Kevex delta and Gatan model 666 PEELs operating at 300 kV.

Atomic force microscopy (AFM). AFM measurements were carried out using a Dimension D3100 atomic force microscope equipped with a NanoScope IVa controller and a hybrid scanner (H-153) with x-, y- z- feedbacks from Veeco (Veeco / Digital Instruments (DI), Santa Barbara, CA) in ambient condition. Silicon cantilevers, PointProbe®Plus Non-Contact High resonance frequency (PPP-NCH) from Nanosensors (Nanosensors, Wetzlar, Germany) were used for intermittent contact (tapping) mode operation to obtain high resolution images of the samples and followed by indentation. Scan rates were varied from 0.35 Hz to 0.5 Hz and free amplitude (A_o) set-point value were around 1.6 V. Prior to bending test or nanoindentation, the nanostructures were imaged, and the 'point and shoot' function was used to pre-position the location of the cantilever. The AFM tip was pressed upon the sample at a preset push force. The indentation marks on the nanostructure due to the high loading force were observed and confirmed that the push force was applied at correct location. The push force applied on the sample was determined by the deflection of the cantilever multiple by the value of the spring constant of the cantilever. The spring constants of the cantilevers were assessed according to Sader's method.[46] The spring constant values were in the range of 24.7 - 31.1 N/m with a mean value of 28.3 N/m. Data conversion was carried out with Nanoscope® software version 613b.

Fluorescence microscopy. Fluorescence microscopy was performed using an Olympus inverted research microscope IX71 equipped with a mercury burner U-RFL-T as the light source and a digital camera Olympus DP70 (12.5 million-pixel cooled digital color camera) for image acquisition. The fluorescence imaging of the ANS- and rhodamine-infiltrated structures were performed at blue excitation ($450 \leq \lambda_{ex} \leq 480$ nm, $\lambda_{em} \geq 515$ nm). The images of the naphthoic acid-infiltrated structures was taken at UV excitation ($300 \leq \lambda_{ex} \leq 400$ nm, $\lambda_{em} \geq 400$ nm), which were filtered using a U-MWG Olympus filter cube.

8.5 ACKNOWLEDGEMENTS

Mr. Iwan Heskamp is acknowledged for providing the lithographically patterned silicon masters.

8.6 REFERENCES

1. Vendamme, R.; Ohzono, T.; Nakao, A.; Shimomura, M.; Kunitake, T. *Langmuir* **2007**, *23*, 2792.
2. Lu, C. H.; Donch, I.; Nolte, M.; Fery, A. *Chem. Mater.* **2006**, *18*, 6204.
3. Jiang, C. Y.; Markutsya, S.; Pikus, Y.; Tsukruk, V. V. *Nat. Mater.* **2004**, *3*, 721.
4. Li, M.; Schnablegger, H.; Mann, S. *Nature* **1999**, *402*, 393.
5. Tang, Z. Y.; Kotov, N. A.; Giersig, M. *Science* **2002**, *297*, 237.
6. Boal, A. K.; Ilhan, F.; DeRouchey, J. E.; Thurn-Albrecht, T.; Russell, T. P.; Rotello, V. M. *Nature* **2000**, *404*, 746.
7. Decher, G.; Hong, J. D.; Schmitt, J. *Thin Solid Films* **1992**, *210*, 831.
8. Jiang, C. Y.; Tsukruk, V. V. *Adv. Mater.* **2006**, *18*, 829.
9. Huck, W. T. S.; Stroock, A. D.; Whitesides, G. M. *Angew. Chem. Int. Ed.* **2000**, *39*, 1058.
10. Mamedov, A. A.; Kotov, N. A. *Langmuir* **2000**, *16*, 5530.
11. Podsiadlo, P.; Kaushik, A. K.; Arruda, E. M.; Waas, A. M.; Shim, B. S.; Xu, J. D.; Nandivada, H.; Pumplin, B. G.; Lahann, J.; Ramamoorthy, A.; Kotov, N. A. *Science* **2007**, *318*, 80.
12. Hua, F.; Cui, T.; Lvov, Y. M. *Nano Lett.* **2004**, *4*, 823.
13. Liang, Z. J.; Susha, A. S.; Yu, A. M.; Caruso, F. *Adv. Mater.* **2003**, *15*, 1849.
14. Xia, Y.; Rogers, J. A.; Paul, K. E.; Whitesides, G. M. *Chem. Rev.* **1999**, *99*, 1823.
15. Hidber, P. C.; Helbig, W.; Kim, E.; Whitesides, G. M. *Langmuir* **1996**, *12*, 1375.
16. Maury, P.; Escalante, M.; Reinhoudt, D. N.; Huskens, J. *Adv. Mater.* **2005**, *17*, 2718.
17. Ling, X. Y.; Phang, I. Y.; Reinhoudt, D. N.; Vancso, G. J.; Huskens, J. *Int. J. Mol. Sci.* **2008**, *9*, 486.
18. Rosi, N. L.; Mirkin, C. A. *Chem. Rev.* **2005**, *105*, 1547.
19. Liu, X. G.; Fu, L.; Hong, S. H.; Dravid, V. P.; Mirkin, C. A. *Adv. Mater.* **2002**, *14*, 231.

20. Musick, M. D.; Keating, C. D.; Lyon, L. A.; Botsko, S. L.; Pena, D. J.; Holliway, W. D.; McEvoy, T. M.; Richardson, J. N.; Natan, M. J. *Chem. Mater.* **2000**, *12*, 2869.
21. Zheng, J. W.; Zhu, Z. H.; Chen, H. F.; Liu, Z. F. *Langmuir* **2000**, *16*, 4409.
22. Zheng, H. P.; Lee, I.; Rubner, M. F.; Hammond, P. T. *Adv. Mater.* **2002**, *14*, 569.
23. Lvov, Y.; Decher, G.; Mohwald, H. *Langmuir* **1993**, *9*, 481.
24. Zhou, D. J.; Bruckbauer, A.; Abell, C.; Klenerman, D.; Kang, D. J. *Adv. Mater.* **2005**, *17*, 1243.
25. Jiang, C. Y.; Markutsya, S.; Tsukruk, V. V. *Langmuir* **2004**, *20*, 882.
26. Santhanam, V.; Liu, J.; Agarwal, R.; Andres, R. P. *Langmuir* **2003**, *19*, 7881.
27. Santhanam, V.; Andres, R. P. *Nano Lett.* **2004**, *4*, 41.
28. Ling, X. Y.; Malaquin, L.; Reinhoudt, D. N.; Wolf, H.; Huskens, J. *Langmuir* **2007**, *23*, 9990.
29. Maury, P.; Pétér, M.; Crespo-Biel, O.; Ling, X. Y.; Reinhoudt, D. N.; Huskens, J. *Nanotechnology* **2007**, *18*, 044007.
30. Michels, J. J.; Baars, M.; Meijer, E. W.; Huskens, J.; Reinhoudt, D. N. *J. Chem. Soc., Perkin Trans. 2* **2000**, 1914.
31. Crespo-Biel, O.; Dordi, B.; Reinhoudt, D. N.; Huskens, J. *J. Am. Chem. Soc.* **2005**, *127*, 7594.
32. Ni, H.; Li, X. D. *Nanotechnology* **2006**, *17*, 3591.
33. Roerdink, M.; Hempenius, M. A.; Gunst, U.; Arlinghaus, H. F.; Vancso, G. J. *Small* **2007**, *3*, 1415.
34. Xiong, Q.; Duarte, N.; Tadigadapa, S.; Eklund, P. C. *Nano Lett.* **2006**, *6*, 1904.
35. Yang, L.; Van der Werf, K. O.; Fitie, C. F. C.; Bennink, M. L.; Dijkstra, P. J.; Feijen, J. *Biophys. J.* **2008**, *94*, 2204.
36. Kis, A.; Kasas, S.; Babic, B.; Kulik, A. J.; Benoit, W.; Briggs, G. A. D.; Schonenberger, C.; Catsicas, S.; Forro, L. *Phys. Rev. Lett.* **2002**, *89*.
37. Malaquin, L.; Kraus, T.; Schmid, H.; Delamarche, E.; Wolf, H. *Langmuir* **2007**, *23*, 11513.
38. Meitl, M. A.; Zhu, Z. T.; Kumar, V.; Lee, K. J.; Feng, X.; Huang, Y. Y.; Adesida, I.; Nuzzo, R. G.; Rogers, J. A. *Nat. Mater.* **2006**, *5*, 33.
39. Ludden, M. J. W.; Reinhoudt, D. N.; Huskens, J. *Chem. Soc. Rev.* **2006**, *35*, 1122.
40. Li, X.; Gao, H.; Murphy, C. J.; Gou, L. *Nano Lett.* **2004**, *4*, 1903.
41. Saucier, A. C.; Mariotti, S.; Anderson, S. A.; Purich, D. L. *Biochemistry* **1985**, *24*, 7581.
42. Jansen, J. F. G. A.; de Brabander-van den Berg, E. M. M.; Meijer, E. W. *Science* **1994**, *266*, 1226.
43. Bosman, A. W.; Janssen, H. M.; Meijer, E. W. *Chem. Rev.* **1999**, *99*, 1665.

44. Beulen, M. W. J.; Bügler, J.; de Jong, M. R.; Lammerink, B.; Huskens, J.; Schönherr, H.; Vancso, G. J.; Boukamp, B. A.; Wieder, H.; Offenhauser, A.; Knoll, W.; van Veggel, F. C. J. M.; Reinhoudt, D. N. *Chem. Eur. J.* **2000**, *6*, 1176.
45. Maury, P.; Peter, M.; Crespo-Biel, O.; Ling, X. Y.; Reinhoudt, D. N.; Huskens, J. *Nanotechnology* **2007**, *18*, 044007.
46. Sader, J. E.; Larson, I.; Mulvaney, P.; White, L. R. *Rev. Sci. Instrum.* **1995**, *66*, 3789.

Summary

Fabricating well-defined and stable nanoparticle arrays and crystals in a controlled fashion receives growing attention in nanotechnology owing to the potential application in optoelectronic devices, biological sensors, and photonic structures. The research described in this thesis aims to construct stable, ordered and functional 2D and 3D nanoparticle structures. Molecular recognition abilities have been exploited by using a combination of supramolecularly directed self-assembly of receptor-functionalized nanoparticles and top-down nanofabrication techniques.

Noncovalent host-guest nanoparticle assembly is highly versatile. It involves specific multivalent interactions, in which the nanoparticle-surface or the inter-particle binding strength can be fine-tuned by introducing competitive interactions. The additional advantage is the possibility for error correction. Host or guest molecules are attached to the surface of the nanoparticles to control the assembly of functionalized nanoparticles to self-assembled monolayers (SAMs) *via* specific host-guest interactions in a layer-by-layer (LbL) assembly methodology. Top-down nanofabrication schemes were combined with supramolecular nanoparticle assembly to form stable and ordered nanoparticle architectures on surfaces, other interfaces, and as free-standing structures.

Chapter 1 provides a general introduction to this thesis. Chapter 2 reviews the recent developments on the various chemical interactions and top-down fabrication techniques to attach functionalized nanoparticles onto (patterned) SAMs.

Chapter 3 describes the synthesis of ferrocenyl-functionalized silica nanoparticles (SiO_2-Fc, $d \sim 60$ nm) with supramolecular 'guest' properties. These ferrocenyl nanoparticles disperse well in aqueous media, due to the presence of diethylene glycol at the nanoparticle surfaces that significantly increases its overall hydrophilicity. Cyclic voltammetry showed that the ferrocenyl groups are robustly attached to the nanoparticle surface within the applied potential range. The supramolecular recognition of SiO_2-Fc nanoparticles at interfaces was confirmed by their specific adsorption on β-cyclodextrin (CD) SAMs. In solution, host-guest nanoparticle complexes were formed by attaching CD-functionalized Au nanoparticles (Au-CD, $d \sim 3$ nm) to the surface of the SiO_2-Fc nanoparticles.

In Chapter 4, the adsorption and desorption of particles during the convective assembly on native oxide surfaces, with additional electrostatic interactions and with supramolecular interactions are presented. The packing density, order, and stability of the

nanoparticle lattices were compared. The convective assembly of PS-COOH particles on native SiO_2 surfaces displayed the best hcp packing. These structures can be easily desorbed from the surface by reducing the temperature below dew point. The electrostatically induced assembly led to disordered lattices because of the strong attractive particle-surface interactions. The supramolecular assembly, driven by multivalent host-guest interactions between CD-functionalized polystyrene nanoparticles (PS-CD) and ferrocenyl-terminated poly(propylene imine) dendrimers on CD SAMs resulted in a nearly perfect hcp packing. The supramolecular assembly process was optimized using ferrocenyl-functionalized dendrimers of low generation and by the introduction of competition by native CD molecules during the assembly. Substrates patterned by nanoimprint lithography (NIL) were employed to assemble the particles into micrometer lines, in which the highly specific and selective supramolecular nanoparticle assembly resulted in a well controlled, stable and single layer of particles on the NIL-patterned substrate.

Chapter 5 shows the reversible nanostructure attachment by using a stimuli-responsive ferrocenyl dendrimer as a multivalent 'reversible supramolecular glue' for the association and (electrochemical) dissociation of CD-functionalized nanoparticles at the molecular printboard. The *in situ* adsorption and desorption of ferrocenyl dendrimers and Au-CD ($d \sim 3$ nm) nanoparticles onto and from the CD SAMs was monitored by combined surface plasmon resonance (SPR) spectroscopy and electrochemistry. The regeneration of the molecular printboard after prolonged electrochemistry was confirmed by a subsequent re-adsorption of ferrocenyl dendrimers and Au-CD nanoparticles. The size effect of the nanoparticle on the reversibility of the nanostructure attachment was examined by using larger nanoparticles, i.e., CD-functionalized silica nanoparticles (SiO_2-CD) of 60 nm. Similar electrochemically induced desorption method showed the complete removal of a SiO_2-CD nanoparticle layer from the surface by using ultrasonication to accelerate the desorption. Local desorption of nanoparticles was also observed by applying electrochemical oxidation to a specific area of a nanoparticle layer.

Chapter 6 describes the construction of 3D supramolecular multicomponent nanoparticle structures on surfaces. NIL was used as the patterning tool for making patterned CD SAMs and to provide physical confinement for nanoparticles during the assembly. On these patterns, complementary guest- (SiO_2-Fc) and host-functionalized (Au-CD) nanoparticles were assembled in an alternating LbL fashion *via* multivalent molecular recognition interactions, resulting in a densely packed and multilayered inorganic-metallic hybrid nanoparticle structure. Their AFM height profiles revealed that the height of the

nanostructure corresponded well to the accumulated diameters of the deposited nanoparticles. This indicates that the specific supramolecular assembly of nanoparticles is self-limiting, *i.e.* one nanoparticle layer per assembly step. Hence, the control over the thickness of the supramolecular hybrid nanostructure can be achieved by selecting the size of the nanoparticles, irrespective of their core material. The flexibility of building up nanostructures by supramolecular host-guest chemistry was demonstrated by the buildup of (sub-micron) multilayered and multicomponent nanoparticle nanostructures from large to small nanoparticles and small to large nanoparticles by using Au-CD (d ~ 3 nm), SiO_2-Fc (d ~ 60 nm), and SiO_2-CD (d ~ 350 nm) nanoparticles.

In Chapter 7, a sequential process is introduced to construct highly stable and crystalline supramolecular nanoparticle crystals. Convective assembly was first used to physically assemble and organize CD-functionalized polystyrene (PS-CD, d ~ 500 nm) nanoparticles on a surface. The nanoparticle crystals were infiltrated with adamantyl (Ad)-functionalized dendrimers such that the neighboring nanoparticles were chemically bound together and the nanoparticle crystal was coupled to the CD surface. The spatial confinement of the nanoparticle crystals was controlled by the assembly onto a patterned elastomeric PDMS stamp. The infiltrated patterned CD-functionalized nanoparticle crystals were transferred from the elastomeric substrate to a target CD monolayer. Depending on the geometry and size of the PDMS stamps, various 3D multilayered and single-layered nanoparticle structures were prepared. The nanoparticle crystal serves as a 3D CD receptor for the subsequent assembly of (multiple) complementary guest molecules, suggesting that the supramolecular host functionality of the nanoparticle crystals remained unchanged after printing.

Chapter 8 extends the use of supramolecular chemistry from the fabrication of micro- or nano-structures on surfaces to stand-alone nanoparticle and capsule structures. Self-assembly of nanoparticles, templating, and supramolecular chemistry were combined to obtain stable and ordered free-standing 3D nanoparticle structures and capsules. Free-standing nanoparticle structures were fabricated with Ad dendrimers and Au-CD as the supramolecular glues and assembled in a LbL fashion within the PS-CD crystal to yield nanoparticle composites. Free-standing hybrid nanoparticle bridges were obtained by transfer printing of the hybrid structures onto topographically patterned substrates *via* specific host-guest interactions. The nanoparticle bridges exhibited a bending modulus of 1.2 ± 0.4 GPa at room temperature, which is of the same order of magnitude as of bulk polystyrene. A release-

and-transfer process was introduced to release the nanoparticle composites from a NIL-patterned PMMA template and to transfer them onto a target substrate while maintaining the nanoparticle crystal integrity, order and functionality. Rinsing the structure with dichloromethane removed the PS core material together with the polymer template. This resulted in interconnected porous capsules, the sizes and shapes of which are fully determined by the PS core size and the polymer template definition. AFM-based nanoindentation and SEM images confirmed that the integrity and shape of the hollow capsules were preserved. A wide variety of organic dyes, including 8-anilino-1-naphthalenesulfonic acid, lissamine rhodamine, and naphthoic acid were infiltrated in the shell of the hollow capsules even after the release, transfer and rinsing process. The flexibility of shape and geometry of our approach in forming capsules was also demonstrated by changing the design of the geometry and size of the PMMA template.

The results presented in this thesis illustrate the versatility of the combined supramolecular nanoparticle assembly and top-down fabrication techniques in creating 2D and 3D nanoparticle architectures. The incorporation of specific molecular recognition functionalities onto the surface of the nanoparticles allows the use of nanoparticles of arbitrary core material and size to form stable and ordered supramolecular nanoparticle structures, with a highly tunable and specific binding strength. In combination with the top-down fabrication techniques, 3D nanoparticle structures with well-defined geometries and sizes can be obtained. These supramolecular nanoparticle structures are ready to be used as 3D receptors for the application in sensing devices. The recognition function of the individual nanoparticles can be further engineered as a sensing tool in the subsequent assembly of complementary guest molecules or nanoobjects.

Samenvatting

Veel belangstelling gaat uit naar het vervaardigen van goed-gedefinieerde en stabiele structuren en kristallen van nanodeeltjes vanwege mogelijke interessante toepassingen op het gebied van optoelektronische apparaten, biologische sensoren en fotonische structuren. Het onderzoek dat beschreven staat in dit proefschrift heeft tot doel het construeren van stabiele, geordende en functionele 2D- en 3D-structuren van nanodeeltjes. Moleculaire herkenning is toegepast in de combinatie van de gestuurde zelf-assemblage van receptor-gefunctionaliseerde nanodeeltjes met 'top-down'-nanofabricage-technieken.

Het assembleren van nanodeeltjes met behulp van niet-covalente interacties is zeer veelzijdig. Het gaat uit van specifieke multivalente interacties waarbij de bindingssterkte tussen het nanodeeltje en het oppervlak of tussen de nanodeeltjes onderling gestuurd kan worden door competitieve interacties te introduceren. Dit heeft daarnaast het voordeel dat foutencorrectie mogelijk is. Het oppervlak van de nanodeeltjes wordt bezet met gastheer- of gastmoleculen om zo de assemblage van deze aldus gefunctionaliseerde nanodeeltjes op zelfgeassembleerde monolagen te controleren via specifieke gastheer-gast-interacties in een laagsgewijs assemblageproces. Top-down-nanofabricagetechnieken zijn gebruikt samen met deze supramoleculaire assemblage om zo stabiele en geordende structuren van nanodeeltjes te vormen op oppervlakken, andere grensvlakken, en als vrijstaande structuren.

Hoofdstuk 1 geeft een algemene inleiding tot dit proefschrift. Hoofdstuk 2 geeft een overzicht van de meest recente ontwikkelingen van de chemische interacties en de top-down-fabricagetechnieken waarmee gefunctionaliseerde nanodeeltjes gehecht kunnen worden aan al dan niet gepatroneerde monolagen.

In hoofdstuk 3 wordt de synthese beschreven van ferrocenyl-gefunctionaliseerde silica-nanodeeltjes (SiO_2-Fc, $d \sim 60$ nm) die supramoleculaire gasteigenschappen hebben. De aanwezigheid van diethyleenglycol op het oppervlak van deze nanodeeltjes doet het hydrofiele karakter van de deeltjes toenemen zodat deze nanodeeltjes goed in water gedispergeerd kunnen worden. Met cyclische voltammetrie is aangetoond dat, binnen het gebruikte potentiaalgebied, de ferrocenylgroepen sterk aan het oppervlak van de nanodeeltjes gebonden zijn. De supramoleculaire herkenning van de SiO_2-Fc-nanodeeltjes aan een grensvlak is aangetoond door middel van specifieke adsorptie aan monolagen van β-cyclodextrine (CD). Het bleek mogelijk om in oplossing gastheer-gast-structuren te vormen van CD-gefunctionaliseerde goud-nanodeeltjes (Au-CD, $d \sim 3$ nm) op SiO_2-Fc-nanodeeltjes.

Hoofdstuk 4 laat de adsorptie en desorptie van nanodeeltjes zien in een op convectie gebaseerd assemblageproces op oxidische oppervlakken, in de aan- en afwezigheid van additionele elektrostatische of supramoleculaire interacties. Er is een vergelijking gemaakt van de pakkingdichtheden, de mate van orde en de stabiliteiten van de nanodeeljesstructuren. De convectie-gedreven assemblage van carboxylaat-gefunctionaliseerde polystyreendeeltjes (PS-COOH) op ongemodificeerd SiO_2 resulteerde in de beste hexagonale pakking. Door de temperatuur tot beneden het dauwpunt te verlagen konden deze structuren gemakkelijk weer gedesorbeerd worden. Door de sterke aantrekkende interactie tussen de nanodeeltjes en het oppervlak leidde elektrostatisch gedreven assemblage tot ongeordende structuren. Daarentegen leidde supramoleculaire assemblage, gedreven door multivalente gastheer-gast-interacties tussen CD-gefunctionaliseerde PS-nanodeeltjes (PS-CD) en ferrocenyl-gefunctionaliseerde poly(propyleenimine)-dendrimeren geadsorbeerd op CD-monolagen, tot een nagenoeg perfecte pakking. Dit supramoleculaire assemblageproces is geoptimaliseerd door ferrocenyl-dendrimeren van een lagere generatie te gebruiken en d.m.v. competitie met CD-moleculen tijdens het assemblageproces. Door eerst een patroon aan te brengen op een substraat met behulp van nanoimprintlithografie (NIL) konden de nanodeeltjes geordend worden in lijnen met micrometer-afmetingen. De specifieke en selectieve eigenschappen van het supramoleculaire nanodeeltjes-assemblageproces resulteerde in een goed controleerbare, stabiele en enkelvoudige laag van nanodeeltjes op het NIL-gepatroneerde substraat.

Hoofdstuk 5 laat zien dat nanostructuren reversibel gebonden kunnen worden door gebruik te maken van ferrocenyl-dendrimeren die reageren op een externe stimulus. Deze dendrimeren functioneren als een multivalente “reversibele supramoleculaire lijm” in de associatie en (elektrochemische) dissociatie van CD-gefunctionaliseerde nanodeeltjes op een moleculaire printplaat. De adsorptie en desorptie van ferrocenyl-dendrimeren en Au-CD (d ~ 3 nm) op en van de CD-monolagen is *in situ* gevolgd m.b.v. een geïntegreerde opstelling voor oppervlakte-plasmonresonantie-spectroscopie en elektrochemie. Het herkrijgen van de lege moleculaire printplaat na langdurige elektrochemie werd bevestigd door hernieuwde adsorptie van ferrocenyl-dendrimeren en Au-CD-nanodeeltjes. Het effect van de grootte van de nanodeeltjes op de reversibiliteit van de hechting van de nanostructuren is bestudeerd door grotere nanodeeltjes te gebruiken, te weten CD-gefunctionaliseerde silica-nanodeeltjes (SiO_2-CD) van 60 nm. Een vergelijkbare elektrochemisch geïnduceerde desorptiemethode liet zien dat een laag van SiO_2-CD-nanodeeltjes volledig verwijderd kon worden van het oppervlak, waarbij ultrasone agitatie gebruikt werd om het desorptieproces te versnellen. Wanneer een

specifiek gebied van de laag van nanodeeltjes elektrochemisch geoxideerd werd, kon lokale desorptie van nanodeeltjes waargenomen worden.

In hoofdstuk 6 wordt de opbouw beschreven van 3D supramoleculaire nanodeeltjes-structuren op oppervlakken, bestaande uit meerdere componenten. NIL is gebruikt om CD-monolagen te patroneren en om tegelijk een fysieke barrière te creëren voor de nanodeeltjes gedurende het assemblageproces. Op deze patronen zijn complementaire gast- (SiO_2-Fc) en gastheer-gefunctionaliseerde (Au-CD) nanodeeltjes geassembleerd via multivalente moleculaire herkenning in een laagsgewijs assemblageproces. Dit heeft geresulteerd in een dichtgepakte nanodeeltjes-structuur opgebouwd uit meerdere hybride anorganisch-metallische lagen. De AFM-hoogteprofielen van deze nanostructuren kwamen goed overeen met de som van de diameters van de geadsorbeerde nanodeeltjes. Dit geeft aan dat deze specifieke supramoleculaire assemblage van nanodeeltjes zelfbegrenzend is, d.w.z. er wordt één laag nanodeeltjes per assemblagestap gedeponeerd. Zodoende is de dikte van deze nanostructuren te controleren door in grootte verschillende nanodeeltjes te gebruiken, onafhankelijk van het materiaal binnenin de deeltjes. De flexibiliteit waarmee nanostructuren d.m.v. supramoleculaire gastheer-gast-interacties opgebouwd kunnen worden is aangetoond door het maken van diverse (sub-micron) multilaags- en multicomponent-nanostructuren. Hierbij werden de nanostructuren opgebouwd uit meerdere lagen elk bestaande uit nanodeeltjes van een bepaalde grootte, zoals Au-CD ($d \sim 3$ nm), SiO_2-Fc ($d \sim 60$ nm), en SiO_2-CD ($d \sim 350$ nm), zowel oplopend als aflopend in grootte.

Hoofdstuk 7 beschrijft een stapsgewijs proces waarmee stabiele en kristallijne supramoleculaire structuren van nanodeeltjes gevormd kunnen worden. Eerst is convectie-gestuurde assemblage gebruikt om CD-gefunctionaliseerde (PS-CD, $d \sim 500$ nm) nanodeeltjes op een oppervlak te organiseren. Vervolgens zijn deze kristallen van nanodeeltjes geïnfiltreerd met adamantyl- (Ad) gefunctionaliseerde dendrimeren zodat de aangrenzende nanodeeltjes chemisch met elkaar verbonden worden en het geheel tevens aan de CD-monolaag. De nanodeeltjes-kristallen kunnen ruimtelijk begrensd worden door ze te assembleren in een gepatroneerde elastomere PDMS-stempel. Vervolgens zijn de geïnfiltreerde nanodeeltjes-kristallen overgebracht van de stempel op een CD-substraat. Afhankelijk van de geometrie en de grootte van de PDMS-stempel zijn diverse kristallijne 3D-structuren gemaakt bestaande uit een of meer lagen van nanodeeltjes . Zo'n nanodeeltjes-kristal kan dienen als een 3D CD-receptor voor de daaropvolgende assemblage van (meerdere) complementaire gastmoleculen. Dit geeft aan dat de supramoleculaire gastheer-eigenschappen van de nanodeeltjes-structuren bewaard blijven na de stempelstap.

In hoofdstuk 8 wordt de grens van de supramoleculaire chemie verlegd van de fabricage van micro- en nanostructuren op oppervlakken naar vrijstaande en holle structuren van nanodeeltjes. Hierbij zijn zelf-assemblage en supramoleculaire chemie toegepast in een mal om stabiele en geordende vrijstaande 3D-nanodeeltjes-structuren en -capsules te verkrijgen. Zulke vrijstaande structuren van nanodeeltjes zijn gemaakt door Ad-dendrimeren en Au-CD te gebruiken als supramoleculaire lijm door deze stapsgewijs te infiltreren in een PS-CD-kristal. Vrijstaande bruggetjes van nanodeeltjes zijn gemaakt door de desbetreffende nanodeeltjes-structuren over te dragen op een substraat met hoogteverschillen, hierbij gebruik makend van specifieke gastheer-gast-interacties. Deze bruggetjes hebben bij kamertemperatuur een buigmodulus van 1.2 ± 0.4 GPa hetgeen van dezelfde orde van grootte is als bulk-polystyreen. Een proces is ontwikkeld waarin de nanodeeltjes-composieten loslaten van de PMMA-mal, die gemaakt is m.b.v. NIL, en vervolgens overgedragen worden op een substraat, waarbij de kristallijne en functionele eigenschappen bewaard blijven. Door te wassen met dichloormethaan werden zowel het PS van de nanodeeltjes als de mal opgelost. Op deze manier zijn met elkaar verbonden poreuze capsules verkregen waarvan de grootte en vorm bepaald worden door de grootte van de PS-deeltjes en de vorm van de mal. AFM-krachtmetingen en rasterelectronen-microscopie toonden aan dat de capsules hun vorm en grootte behouden. Verschillende organische kleurstoffen, waaronder 8-anilino-1-naftaleensulfonzuur, lissamine-rhodamine en naftaleen-carbonzuur, konden in de wand van de capsules geïnfiltreerd worden zelfs na alle fabricagestappen. De flexibiliteit in de grootte en geometrie van de capsule-structuren is verder gedemonstreerd door een PMMA-mal te gebruiken met een ander ontwerp.

De resultaten die beschreven staan in dit proefschrift illustreren de veelzijdigheid van het combineren van supramoleculaire assemblage van nanodeeltjes met top-down-fabricage-technieken in het maken van 2D- en 3D-structuren van nanodeeltjes. Door het aanbrengen van functionele groepen, die moleculaire herkenning toestaan, op het oppervlak van de nanodeeltjes kunnen stabiele en geordende supramoleculaire nanodeeltjes-structuren verkregen worden met regelbare en specifieke bindingsterkte, ongeacht het materiaal en de grootte van de deeltjes. In combinatie met top-down-fabricage-technieken kunnen 3D-structuren van nanodeeltjes gemaakt worden met goed-gedefinieerde afmetingen. Deze supramoleculaire nanodeeltjes-structuren zijn geschikt om te gebruiken als 3D-receptoren in sensoren. De herkenningseigenschappen van de individuele nanodeeltjes kunnen verder ontwikkeld worden voor de hechting van complementaire gastmoleculen of nano-objecten.

Acknowledgements

At last, it is my turn to write down a few words of gratitude. The past four years has been a blessing for me. I have learnt and grown so much and have the best time of my life in this little town in the Netherlands. This would not have been possible without the people that are always there for and with me.

My first dedication goes to my dear promoter, David: Thank you David. Despite your busy schedule, you managed to have meetings with me regularly throughout my PhD, in which you challenged and stimulated me with fresh ideas or projects. You have always been very helpful and encouraging. I truly appreciate it.

Another Big THANK YOU will go to Jurriaan, my dear promoter and daily supervisor. First of all, I thank you for accepting me as your PhD student, without interviewing me. :) That was "a bit" risky, but I hope I didn't disappoint you. I will always remember the biweekly meeting, where we brainstormed and discussed my research work. You have always been very encouraging when I was in the bottleneck of the projects and always managed to come up with some brilliant and stimulating ideas. Having said that, I also enjoyed a rare freedom for a PhD student to choose my research orientation. You are the supervisor every student can dream of. In these four years, I have learnt so much from you, and there are so much efforts that you have put on to transform me into a (nearly) independent researcher. I can't thank you enough for that.

My acknowledgements also go to the CD (you know what I mean – the famous cyclodextrin) team, Christian, Olga, Manon, Andras. Christian, I like our electrochemistry talk, even though, honestly, I don't always understand what you mean, especially those complicated equations.:) Olga, thanks for sharing a lot of practical tips about CD SAMs with me! Hoi Manon, even though the CD SAM in μ-fluidics is not as easy as it seems, but at least we enjoyed the super dangerous piranha injection to the chip! Andras - many thanks for the divalent linker. I also thank Huaping, Janet, Yiping, Xuexin for being very helpful with the nanofabrication techniques.

Our SMCT/ MnF daily life will not be manageable without our supporting staffs, Marcel and Richard. I am free from the hustle of exhaustive computing and technical works thanks to them. Marcel, thank you for all the patience for finding out the weird tools or chemicals that I needed, I cannot imagine the SMCT/MNF lab without you! I also appreciated the help of Richard, who makes the life of a computer-dummy (i.e. me) so much easier with all your computing skills! And of course, thanks for organizing the unforgettable Wadlopen, for which I did my exercise of the year in the famous mud! I really appreciate that. Our secretaries, Izabel, Melissa; ex-secretaries, Danielle, Marieke are also thanked for handling most of my administrative works. I must also thank Pascal, who has just started as a staff member in the group, but immediately "chosen" to proof-read my concept thesis. ☺ I also thank Henk for spending hours to translate the summary to samenvatting.

Despite being trained as a chemical engineer, in these years in SMCT/ MnF, I have learnt a few basic tricks of organic synthetic chemistry too. I accredit this to the help of Choon Woo, my first organic synthesis teacher. Dear Choon Woo, I truly appreciate your helping hand when I did my first column. Without your help, I will never get the large amount of CD-heptathioether! :) I also thank you for many stimulating ideas we have discussed. It's unfortunate that you left UT before I kick-started my research project. Otherwise, I am sure we would have so much fun working together!

Besides the SMCT/ MNF lab, I also spent a considerable amount of time at doing SEM measurements. The SEM room is almost like my second work place. Needless to say, I owe gratitude to Mark Smithers. Dear Mark, thank you for helping me with the measurements (in the beginning) and for training me to become an independent SEM user. Besides, I also enjoyed my time there because you have made the SEM room a very friendly and lively place.

In my earlier years, I had the opportunity to work with some of the best nanoparticle scientists, Dr. Laurent Malaquin and Dr. Heiko Wolf at IBM, Zurich. Dear Laurent, thanks to your warm hospitality, I have enjoyed my visit to IBM. Your hard work and the fantastic yet home-made experimental setup have enabled the smoothness of our experiments. Chapter 4 is dedicated to you.

I am also indebted to my collaborators, In Yee (my private AFM expert), Prof. Holger Schönherr and Prof. Julius Vancso for their contribution to the AFM-related works throughout the thesis. I especially thank Holger for many fascinating discussions on the free-standing bridge project, which has made the work so interesting. Besides, I am also grateful to my master student, Gang Tian, for his contribution in the microfluidics project; and Wouter Maijenburg for his early contribution to the transfer printing work in Chapter 7.

Outside the professional life, after countless numbers of promotion, house-warming and birthday parties, pub drinking, dinners, and family-visiting, I have met a lot of friends, best friends indeed. Since then, my life is never the same again. Dear Soco & Rob, you brought me into the Spanish community. It was not easy for me, at least in the beginning, a rather "shy" person (ha ha!) to integrate into a foreign community with such a different culture. Yet, with your open arm, delicious weekly (or more often than that?) dinner, and the crazy fiesta, I feel like I am truly a member of yours! It is truly an amazing experience for me, and it will be one of the highlights in my life. I would also like to thank Antonio & Doreen. Even though my Spanish or Galician (☺) is still "a bit" shocking, your warmth make me feel like I was at home. After my third visit, I feel like I am nearly an Artes-ian now.

Dear Fernando & Lourdes, my dear Spanish-Spanish couple. You are like my brother and sister. We can always take it easy and enjoy drinks and (not to mention) 'lekker' food together, because we know this is what life is about! One of the highlights was no doubt the lunch in Roses, where we enjoyed so much – the cepe (small octopus), sardines, and the sparkling wine. Mmm… yummy! Fer, I will always remember the Christmas in Madrid where we did the pub-crawling and dinner (starting at 12 am!). In particular, I am sure you won't forget the two rationes of chopitos in the tapas bar close to your place, the crappy

cocktail bar - the fruit cocktails, chit-chats and laughs in which we enjoyed so much! ☺ Next time, we will do the same in Malaysia, promise?

Dear Janet, despite your initial impression to me as a shy and quiet Turkish girl, you have fooled us all! With your smiles and warmth, you have become one of my closest friends. I enjoyed all the girls' talk and the dinners together. Shall we have a tea? Mirko & Itxaro, we have shared so much in these four years. We have been through the stressful thesis writing period in almost the same period, thank you for passing me all the thesis printing tips. ☺ I will always remember our time in Malaysia, especially the 2-m lizard under our chalet in Perhentian. Michel & Marina (the M&M), I miss our time together in Salamanca where we had as many beers as we wanted while having the free dinner! A special thanks to Michel, for being the role model of running for IY, even though you have set an extraordinary example (for running the Enschede Marathon!), it's unfortunate that he didn't catch up with your standard (until today). Oh lello and lella! Alessio & Olga, thank you for Da Wedding, it truly opened my eyes for what is called a 'typical Spanish wedding'! All the tapas, fancy dinner and party (of course!), I hope you enjoyed it, because I really did! A special thanks to Ale's nonna and mom, for inviting us to the marvelous Christmas dinner, where we had the best Italian food ever! Of course, not to mention IY and my debut as the Italian Christmas choir duet! Henk, Marloes, shall I say the only precious Dutch couple in the group? Thanks for bringing us to the world of diving, maybe one day we can dive in Great Barrier Reef together! Dear Henk, I must say I enjoyed being your neighbor in the lab, all the chemistry talk, crazy talks, laughs, and not to mention the entertaining break.com! Eddy, thanks for all the super-late dinner at your place. Thanks to you, I now know what it takes to make authentic Italian pasta! Denis, I thank you for the real and authentic vodka, directly brought from Moscow. Martine & Sylvain, the cheese fondue, tequila, how can I forget that?! Shu-Han, I enjoyed our chats in between the experiments, which made the waiting so much fun. The families we have visited – Soco's, Alessio's, Mirko's, Michel's, Fernando's, Janet's, Rob's. I thank you for welcoming us to your place and your warm hospitality, not to mention the delicious authenthic food! ☺ Of course, many others, with whom we shared chats, laughs and drinks together, including Francesca (our yoga class was fantastic!), Lanti & Gu Hao (for all the exotic yet delicious Chinese dinner), Emiel & Monica (let's try some wine together!), Menglin, Ana (thanks for bringing us to the Gypsy party at EPFL!), Tian, Christian, Manon, Chien-Ching, Huaping (see you in Beijing!), Yiping, Elisabetta, Boon Hua & Ai Ling, Nuria (la chica de Barcelona), Deniz, Maryana, Victoria, Maria, Christiaan, Xuexin, Andras, Arancha, Alberto, Kim, Bas, Janina, Bart Jan (shall I say, Prof. Ravoo?), Mercedes (another dancing queen), Pascal, Aldrik (who is always "thirsty"), Roald, Wojtek, Melba, Jing, Dae June, Riccardo, Albert, Jealemy, Pieter, Ignacio, Deborah, Hans, Dominik, Srinidhi, Laura, Oktay, Sachin, Veera, Mustafa, Vijay, and many more……

I am also thankful to another noteworthy figure in my life, my grandmother, Madam Oh Kwi Hwa. Dear grandma, you were such an inspiration for me. Due to the environment at your time, you have missed the opportunity of being educated in school. However, that didn't perturb your eagerness to learn to write, even until your final days; you have also insisted on the education of mom and your other children even in difficult times. You are my true untold

heroine. Unfortunately you are not able to witness the day I earn my PhD degree, like you saw my degree graduation, but I hope you will see it from heaven.

My dearest aunt, BerYi, since I was a child, you have been setting a good example for me. You are independent and you prospered in school performance (or at least that's what mom told me. ☺) Despite being my aunt, you are more like a sister to me. I thank you for being there for me all the time, ups and down, supporting and encouraging me. Of course, I would also like to show my appreciation to my in-law family, uncle Tony (who can equally understand the scientific world), uncle Thian San (for our relentless conversations about the reality), uncle Thian Kiat and all my relatives.

I am also grateful to my two loving sisters, Jia Yi and Xu Yi. Despite living apart, our weekly phone calls have brought us closer together, and we have bonded stronger than ever. We share all the laughs and tears; I treasure the harmonious relationship we have.

Dear mom and dad, no words can express my gratitude to you. I remembered when I was still a child, some family friend used to tell you that "I saw your eldest daughter wandering around on the street this afternoon, AGAIN". Who can foresee the supposedly "wild child" of the family, who liked to play and cycle on the street of Jerantut after school will end up earning her PhD in a foreign land? All I have achieved today will not be possible without the unconditional love of both of you. Thank you for your unlimited love, understanding, sacrifice and support. I am who I am because of you.

Last but not least, this thesis is dedicated to my other-half, In Yee, for this thesis would not have been possible without you. You have walked into my life nine years ago and it was never the same. You fill my life with joy and satisfaction and my heart with love and happiness. For the past nine years, we have been through every good and bad moment hand-in-hand. We have grown stronger together (personally and professionally) while seeking a better future. You are my soul mate, best friend, critic, and my lover. I love you!

林歆怡

Xing Yi Ling
Enschede, the Netherlands
September 2008

About the author

Xing Yi Ling was born in 30th May 1979 in Jerantut, Pahang, Malaysia. She obtained her Bachelor degree of Chemical Engineering, 1st Class Honors from the University of Adelaide, Australia in the year 2000. After working one year as a chemical engineer in Singapore, she continued her academic study for a Master degree of Chemical Engineering at the National University of Singapore (NUS) and Institute of Materials Research & Engineering (IMRE) in Singapore in January 2001. She received her Master degree of Chemical Engineering in September 2004, with research project entitled "Platinum & Platinum-Ruthenium Nanoparticles: Synthesis, Characterization and Applications" under the supervision of Prof. Jim Yang Lee and Dr Zhaolin Liu. From September 2004, she was a PhD student under the supervision of Prof. David N. Reinhoudt and Prof. Jurriaan Huskens, in the Supramolecular Chemistry and Technology (SMCT) and Molecular Nanofabrication (MNF) groups at the University of Twente, the Netherlands, on the subject of supramolecular self-assembly of nanoparticles into 3D nanostructures. The results of this research work are described in this thesis.

List of publications

1. X. Y. Ling, D. N. Reinhoudt, J. Huskens,
Reversible attachment of nanostructures at Molecular Printboards through supramolecular glue,
Chemistry of Materials **2008,** *20*, 3574.

2. M. J. W. Ludden,* X. Y. Ling,* T. Gang, W. Bula, H. Gardeniers, D. N. Reinhoudt, J. Huskens,
Multivalent binding of small guest molecules and proteins to molecular printboards inside microchannels,
Chemistry – a European Journal **2008**, *1*, 136.
* shared first author

3. X. Y. Ling, I. Y. Phang, D. N. Reinhoudt, G. J. Vancso, J. Huskens,
Supramolecular layer-by-layer assembly of 3D multicomponent nanostructure via multivalent molecular recognition interactions,
International Journal of Molecular Sciences **2008,** *9*, 486**.** (Invited article)

4. X. Y. Ling, L. Malaquin, D. N. Reinhoudt, H. Wolf, J. Huskens,
An *in situ* study of the adsorption behavior of functionalized nanoparticles on self-assembled monolayers *via* different chemical interactions,
Langmuir **2007,** *23*, 9990.

5. Z. L. Liu, X. Y. Ling, B. Guo, L. Hong, J. Y. Lee,
Pt and PtRu nanoparticles deposited on single-wall carbon nanotubes for methanol electro-oxidation,
Journal of Power Sources **2007**, *167*, 272.

6. X. Y. Ling, D. N. Reinhoudt, J. Huskens,
Ferrocenyl-functionalized silica nanoparticles: preparation, characterization, and molecular recognition at interfaces,
Langmuir **2006**, *22*, 8777.

7. P. Maury, M. Pétér, O. Crespo-Biel, X. Y. Ling, D. N. Reinhoudt, J. Huskens,
Patterning the Molecular Printboard: patterning cyclodextrin monolayers on silicon oxide using nanoimprint lithography and its application in 3D multilayer nanostructuring,
Nanotechnology **2006,** *18*, 044007.

8. X. Y. Ling, Z. L. Liu, J.Y. Lee,
Microwave-assisted synthesis of platinum nanoparticles,
Journal of Metastable and Nanocrystalline Materials, **2005**, *23*, 199.

9. Z. L. Liu, X. Y. Ling, X. Su, J. Y. Lee, L.M. Gan,
Preparation and characterization of Pt/C and PtRu/C electrocatalysts for direct ethanol fuel cells,
Journal of Power Sources **2005**, *149*, 1.

10. Z. L. Liu, X. Y. Ling, X. Su, J. Y. Lee,
Carbon-supported Pt and PtRu nanoparticles as catalysts for a direct methanol fuel cell,
Journal of Physical Chemistry B **2004**, *108*, 8234.

11. Z. L. Liu, X. Y. Ling, J. Y. Lee, X. Su, L. M. Gan,
Nanosized Pt and PtRu colloids as precursors for direct methanol fuel cell catalysts,
Journal of Materials Chemistry **2003**, *13*, 3049.

Manuscripts submitted:

1. X. Y. Ling, I. Y. Phang, W. Maijenburg, D. N. Reinhoudt, G. J. Vancso, J. Huskens,
Stable 3D free-standing supramolecular nanoparticle composites,
Manuscript submitted, **2008.**

2. X. Y. Ling, D. N. Reinhoudt, J. Huskens,
Chemically directed self-assembly of nanoparticle structures on surfaces in *Supramolecular Chemistry of Organic-Inorganic Hybrid Materials* (Edited by K. Rurack), Wiley-VCH: Weinheim, **2008**, *submitted*.

3. H. Xu, X. Y. Ling, J. van Bennekom, X. Duan, M. Ludden, D. N. Reinhoudt, M. Wessling, R. Lammertink, J. Huskens,
Microcontact printing of heavy polar inks by porous stamps
Manuscript submitted, **2008.**

4. I Y. Phang, N. Aldred, X. Y. Ling, J. Huskens, A. S. Clare,. G. J. Vancso,
Glycoprotein "footprints" of barnacle larvae on biofouling surfaces: Morphology and mechanical behavior on the nanoscale assessed by atomic force microscopy,
Manuscript submitted, **2008.**